
Electronic Thesis and Dissertation Repository

4-25-2013 12:00 AM

Improving Acute Stroke Management with CT Perfusion Imaging: Approaches to Treatment Guidance and Brain Tissue Salvage

Christopher D. d'Esterre
The University of Western Ontario

Supervisor
Dr. Ting-Yim Lee
The University of Western Ontario

Graduate Program in Medical Biophysics
A thesis submitted in partial fulfillment of the requirements for the degree in Doctor of
Philosophy
© Christopher D. d'Esterre 2013

Follow this and additional works at: <https://ir.lib.uwo.ca/etd>



Part of the [Medical Biophysics Commons](#)

Recommended Citation

d'Esterre, Christopher D., "Improving Acute Stroke Management with CT Perfusion Imaging: Approaches to Treatment Guidance and Brain Tissue Salvage" (2013). *Electronic Thesis and Dissertation Repository*. 1239.

<https://ir.lib.uwo.ca/etd/1239>

This Dissertation/Thesis is brought to you for free and open access by Scholarship@Western. It has been accepted for inclusion in Electronic Thesis and Dissertation Repository by an authorized administrator of Scholarship@Western. For more information, please contact wlsadmin@uwo.ca.

**IMPROVING ACUTE STROKE MANAGEMENT WITH
CT PERFUSION IMAGING:
APPROACHES TO TREATMENT GUIDANCE AND BRAIN TISSUE SALVAGE**

(Thesis format: Integrated-Article)

by

Christopher D. d'Esterre

Graduate Program in
Medical Biophysics

A thesis submitted in partial fulfilment
of the requirements for the degree of
Doctor of Philosophy

The School of Graduate and Postdoctoral Studies
The University of Western Ontario
London, Ontario, Canada

© Christopher D. d'Esterre 2013

ABSTRACT

CT Perfusion (CTP) provides measurement of perfusion at the capillary level which can be used to characterize tissue viability, and blood-brain-barrier (BBB) compromise. Using CTP, the goals of this research are to: 1) select patients that will benefit from acute stroke treatment, and 2) determine if pre-stroke neuroprotection reduces stroke severity.

Chapter two investigates the cerebral blood volume (CBV) parameter in a small acute ischemic stroke (AIS) patient set. Overestimation of the acute CBV defect is caused by incomplete wash-out of the CT contrast due to a shortened CTP acquisition time (“truncation artifact”).

In chapter three we examine the prognostic reliability of the acute CBV defect to predict infarct core and penumbra in AIS. We determine that hypervolemia, the “truncation artifact” and recanalization are all important variables which affect the relationship between the acute CBV defect volume and the final infarct volume.

Chapter four implements a novel porcine model of ischemic stroke using the transient vasoconstrictor, endothelin-1. Using this model, we show that the CTP-cerebral blood flow (CBF) parameter is as good as MR-DWI for acute infarct core delineation, and the CBF/CBV mismatch may not indicate penumbral tissue in the acute stroke setting.

In Chapter five, it we show that vascular integrity measured with the CTP-BBB permeability surface area product (PS) is a strong predictor of sub-acute bleeding in the brain (hemorrhagic transformation).

Chapter six shows that different rates of CT contrast extravasation exist for primary intracerebral hemorrhage (ICH) patients with/without the CTA-Spot Sign and/or

post-contrast leakage. Furthermore, early rates of extravasation are correlated with sub-acute hematoma expansion.

Chapter seven describes the development of an improved, reproducible and survivable rabbit large clot embolic model (RLCEM) of cerebral ischemia for testing treatment options for AIS. We demonstrate that pre-stroke treatment with dipyridamole provides a neurovascular advantage post stroke onset.

In summary, the current uses of CTP imaging in acute stroke include: 1) quantifying ischemia to define infarct core and penumbra in AIS, 2) predicting hemorrhagic transformation of AIS, 3) predicting hematoma expansion in primary ICH, and 4) assessing treatment response in animal models of stroke to facilitate new drug development.

Keywords:

Stroke, CT Perfusion, cerebral ischemia, primary cerebral hemorrhage, secondary hemorrhagic transformation, cerebral blood flow, cerebral blood volume, infarction, hematoma expansion, animal stroke model, primary stroke treatment, tPA

CO-AUTHORSHIP

Chapter two has been adapted from the original research manuscript entitled “The evolution of the cerebral blood volume abnormality in patients with ischemic stroke: a CT perfusion study”, published in *Acta Radiologica* 53(4):461-7, May 2012, by: C.D. d’Esterre, R.I. Aviv, T.Y. Lee. I was responsible for the study design, analyzing and interpreting the data, and writing the manuscript under the supervision of T.Y. Lee. R.I. Aviv recruited the patients, collected data, and helped with editing the manuscript.

The contents of chapter three have been adapted from the original research manuscript entitled “Reliability of the cerebral blood volume parameter in ischemic stroke”, reviewed and re-submitted to the journal *Neuroradiology* by: C.D. d’Esterre, T.Y. Lee, S. Ceruti, G. Roversi, A. Saletti, E. Fainardi. T.Y. Lee and E. Fainardi were responsible for the study design and editing the manuscript. I was responsible for analyzing and interpreting the data, and writing the manuscript under the supervision of T.Y. Lee. The remaining authors helped with recruiting patients, collecting data, and editing the manuscript.

Chapter four has been adapted from the original research manuscript submitted to *Stroke* in April 2013. The manuscript is entitled “Multi-modality neuroimaging in a porcine model of endothelin-1 induced cerebral ischemia: defining the acute infarct core”, by: C.D. d’Esterre, U. Anazodo, K. St. Lawrence, L. Morrison, T.Y. Lee, E. Fainardi. I designed the study with T.Y. Lee and E. Fainardi. I was responsible for performing the experiments, with help from U. Anazodo, L. Morrison and K. St. Lawrence. I also

collected and analyzed all data and wrote the manuscript under the supervision of T.Y. Lee. T. Y. Lee and E. Fainardi reviewed and edited the manuscript.

Chapter five has been adapted from the original research manuscript entitled “Hemorrhagic transformation of ischemic stroke: prediction with CT perfusion” published in *Radiology* 250(3):867-77, in March 2009, by: R.I Aviv, C.D. d’Esterre, B.D. Murphy, J.J. Hopyan B. Buck, G. Mallia, V. Li, L. Zhang, S.P. Symons, T.Y. Lee. T.Y. R.I. Aviv and I contributed equally to this manuscript. Lee and R.I Aviv were responsible for the study design and manuscript editing. I was responsible for analyzing all data, under the supervision of R.I Aviv and T.Y. Lee. G. Mallia helped with the statistical analysis and manuscript writing, while the remaining authors helped with patient recruitment, collecting data, and provided assistance with manuscript preparation.

Chapter six has been adapted from the original research manuscript entitled “Early rate of contrast extravasation in patients with intracerebral hemorrhage” published in the *American Journal of Neuroradiology*, 32(10):1879-84, November 2011 by: C.D. d’Esterre, T. Chia, A. Jairath, T.Y. Lee, S.P. Symons, R.I. Aviv. T.Y. Lee and R.I. Aviv were responsible for the study design and manuscript editing. I was responsible for analyzing the data and writing the manuscript, under the supervision of T.Y. Lee and R.I Aviv. The remaining authors helped with the design of the study, recruited patients, collected data, and provided assistance with the manuscript preparation.

Chapter seven has been adapted from the original research manuscript entitled “Dipyridamole treatment prior to stroke onset: examining post-stroke cerebral circulation and outcome in rabbits”, published in *Translational Stroke Research*, 2: 186-194, January 2011, by: C.D. d’Esterre, K.M. Tichauer, R.I. Aviv, L. Morrison, W. Eisert, T.Y.. Lee. T.Y. Lee and W. Eisert were responsible for designing the study and reviewing the

manuscript. I developed the experimental procedures for the stroke model and collected all data, with the help from L. Morrison. I was responsible for data analysis and interpretation and manuscript writing and editing. The remaining authors helped with the design of the study and provided assistance with the manuscript preparation.

EPIGRAPH

“Sometimes life's so much cooler when you just don't know any better and all the painful lessons haven't hammered your head open yet.”

-Anthony Kiedis

DEDICATION

To my Mother,
I couldn't have done this without you.

ACKNOWLEDGEMENTS

The work contained within this thesis was accomplished with the help of a number of individuals. I would like to thank my supervisor, Dr. Ting-Yim Lee, for his leadership, support and friendship throughout my graduate school career. His passion for research and experimental creativity and prowess has truly been an inspiration. I would also like to thank the members of my advisory committee, Dr. Keith St. Lawrence and Dr. David Cechetto.

I would like to thank my collaborators, Dr. Richard Aviv of Sunnybrook Health Science Centre and Dr. Enrico Fainardi from the University of Ferrara. Despite their busy clinical schedules, they were always available for valued discussions and guidance. Their friendship, professional and personal, will have a lasting impression on my career.

My utmost gratitude goes out to Anne Leaist – her tireless work-ethic and meticulous devotion to the group has truly been appreciated. Special thanks to the “Lee Lab Ladies” – Jennifer Hadway, Laura Morrison, and Lise Desjardins. Their dedication and enthusiasm was the key to my successful experiments.

I would like to thank my friends, especially my roommates at “The 172”, and also my teammates from the UWO cross country and track teams. Finally, I would like to thank my mother and brother for their encouragement.

TABLE OF CONTENTS

Abstract	ii
Co-Authorship	iv
Epigraph	vii
Dedication	viii
Acknowledgements	ix
List of Tables	xvi
List of Figures	xviii
List of Appendices	xx
List of Abbreviations	xxii
1. Chapter 1 – Introduction	1
1.1 Introduction.....	1
1.2 Stroke Pathophysiology	1
1.2.1 Cerebral ischemia	2
1.2.2 Hemorrhagic transformation of cerebral ischemia	6
1.2.3 Primary intra-cerebral hemorrhage.....	7
1.3 Stroke Treatment.....	8
1.3.1 Ischemic stroke	8
1.3.2 Primary intracerebral hemorrhage	12
1.4 Medical Imaging in Stroke	14
1.4.1 Positron emission tomography	14

1.4.2 Magnetic resonance imaging	16
1.4.3 Computed tomography imaging	18
1.4.3.1 Non-contrast CT	18
1.4.3.2 CT angiography	19
1.4.3.3 CT perfusion	20
1.5 Animal Models of Stroke.....	27
1.5.1 Global ischemia	28
1.5.2 Focal ischemia	29
1.5.3 Intracerebral hemorrhage.....	30
1.6 Future Stroke Diagnosis and Treatment	31
1.7 Research Objectives.....	32
1.8 References.....	33

2. Chapter 2 – The Evolution of the Cerebral Blood Volume Abnormality in Patients with Ischemic Stroke.....	51
2.1 Introduction.....	52
2.2 Methods & Materials	53
2.2.1 Participants and study design	53
2.2.2 CT imaging procedures	54
2.2.3 CTP image analysis	55
2.2.3.1 The 5-7 day evolution of CBV within tissue destined to infarct .	55
2.2.3.2 Determining CBV defect overestimation.....	58
2.2.4 Statistical analysis.....	62
2.3 Results.....	62

2.3.1	The 5-7 day evolution of CBV within tissue destined to infarct	62
2.3.2	Determining acute CBV defect overestimation.....	65
2.4	Discussion.....	67
2.5	Conclusion.....	70
2.6	References.....	70
3.	Chapter 3 – Reliability of the CT perfusion Cerebral Blood Volume	
	Parameter in Ischemic Stroke.....	76
3.1	Introduction.....	76
3.2	Materials & Methods	78
3.2.1	Patient selection.....	78
3.2.2	Imaging protocol.....	79
3.2.3	CTP functional maps	80
3.2.4	CTP, CTA, and NCCT image analysis.....	80
3.2.5	Patient groupings and statistical analysis	82
3.3	Results.....	84
3.4	Discussion.....	99
3.5	References.....	109
4.	Chapter 4 – Multi-modality Neuroimaging in a Porcine Model of	
	Endothelin-1 Induced Cerebral Ischemia: Defining the Acute	
	Infarct Core	116
4.1	Introduction.....	116
4.2	Materials & Methods	118

4.2.1 Study design	118
4.2.2 Computed tomography perfusion imaging	121
4.2.3 Magnetic resonance imaging	121
4.2.4 ¹⁸ F-FDG Positron emission tomography imaging	122
4.2.5 Histology	123
4.2.6 Image analysis	123
4.2.7 Statistical analysis.....	127
4.3 Results.....	127
4.4 Discussion.....	134
4.5 Conclusion	140
4.6 References.....	141

5. Chapter 5 – Hemorrhagic Transformation of Ischemic Stroke:

Prediction with CT Perfusion	146
5.1 Introduction.....	146
5.2 Materials & Methods	147
5.2.1 Study design and patient cohort.....	147
5.2.2 CT and MR imaging protocols	149
5.2.3 Image analysis	150
5.2.4 Statistical analysis.....	154
5.3 Results.....	154
5.4 Discussion.....	165
5.5 Conclusion	169
5.6 References.....	170

6. Chapter 6 – Early Rate of Contrast Extravasation in ICH Patients.....	175
6.1 Introduction.....	175
6.2 Materials & methods.....	177
6.2.1 Patient cohort.....	177
6.2.2 Image acquisition.....	177
6.2.3 Image analysis	178
6.2.4 Statistical analysis.....	182
6.3 Results.....	182
6.4 Discussion.....	187
6.5 Conclusion.....	190
6.6 References.....	191
7. Chapter 7 – Development and Implementation of a Rabbit Model of Middle Cerebral Artery Embolic Occlusion: Pre-morbid Cerebrovascular Conditioning with Dipyridamole	194
7.1 Introduction.....	194
7.2 Materials & methods.....	197
7.2.1 Surgical procedures	197
7.2.2 CT perfusion imaging.....	200
7.2.3 CTP data analysis	201
7.2.4 Neurological testing.....	203
7.2.5 Post-mortem analysis.....	203
7.2.6 Statistical analysis.....	206
7.3 Results.....	206

7.4 Discussion.....	215
7.5 Conclusion.....	218
7.6 References.....	219
8. Chapter 8 – Conclusion and Future Work.....	223
8.1 Summary.....	223
8.1.1 Prediction of acute tissue viability for ischemic stroke.....	224
8.1.2 Role of the CTP-PS parameter in acute stroke.....	223
8.1.3 Reducing stroke severity with secondary prevention drugs.....	226
8.2 Experimental and Clinical Relevance.....	227
8.3 Future Work.....	229
8.3.1 Improved calculation of CTP functional maps.....	229
8.3.2 Multi-variate prospective study to determine secondary ICH.....	230
8.3.3 Minor stroke and transient ischemic attack.....	230
8.3.4 Voxel based classification.....	231
8.3.5 Comparing AIS therapeutics.....	231
8.3.6 ¹⁸ F-Flumazenil imaging in porcine AIS model.....	231
8.4 Conclusion.....	233
8.5 References.....	234
Curriculum Vitae.....	255

LIST OF TABLES

Table 2.1 – Demographics for N=13 AIS patients (Group A)	57
Table 2.2 – Demographics for N=13 AIS patients (Group B)	59
Table 3.1 – Demographics for patients with ITDC truncation.....	85
Table 3.2 – Demographics for patients without ITDC truncation.....	86
Table 3.3 – Bland-Altman and linear regression results for the admission CBV defect volume versus the final infarct volume at 3 months	88
Table 3.4 – All patients (n=55): CBF and CBV values at four time points from within superimposed final infarct volumes. Also shown are the fractions of patients with hypervolemia and hyperperfusion, along with change in NIHSS	90
Table 3.5 – Recanalization positive group (n=32): CBF and CBV values at four time points from within superimposed final infarct volumes. Also shown are the fractions of patients with hypervolemia and hyperperfusion, along with change in NIHSS	90
Table 3.6 – Table 3.6 Recanalization negative group (n=23): CBF and CBV values at four time points from within superimposed final infarct volumes. Also shown are the fractions of patients with hypervolemia and hyperperfusion, along with change in NIHSS.....	90
Table 3.7 – Clinical outcome and hemorrhage rates for patients with/without admission hypervolemia	92

Table 3.8 – Model to describe the relationship between admission CBV_D and final infarct size from 3 month NCCT	94
Table 3.9 – Predicted baseline CBV_D size relative to final infarct size among the four cases of TDCi truncation and recanalization status when prevalence of hypervolemia is 50%	94
Table 3.10 – Measured baseline CBV defect size as a percentage of the final infarct size among the four cases of TDCi truncation and recanalization status when prevalence of hypervolemia is 50%.	94
Table 4.1 – Infarct volumes from MRI, CTP and histology	132
Table 4.2 – CT perfusion values from within superimposed true infarct volume and corresponding glucose metabolism	133
Table 5.1 – Baseline and follow-up patient data dichotomized according to presence of HT	156
Table 5.2 – Mean PS, CBF and CBV values for ischemic ROIs in patients dichotomized according to HT type and presence.....	158
Table 5.3 – Baseline and follow-up patient data dichotomized according to tPA treatment status.	160
Table 6.1 – Demographics for extravasation positive and negative groups.....	183
Table 6.2 – PS values for extravasation positive and negative patients.....	185
Table 6.3 – Hematoma expansion data for extravasation positive/negative patients.....	186

LIST OF FIGURES

Figure 1.1 – Sample CTP functional maps for AIS patient	23
Figure 1.2 – Sample IRF	25
Figure 2.1 – Study design flow chart	61
Figure 2.2 – CBV within tissue destined to infarct	64
Figure 2.3 – Truncation artifact and CBV defect overestimation	66
Figure 3.1 – Admission gray matter CBV and CBF from within the superimposed final infarct ROI.....	96
Figure 3.2 – Admission white matter CBV and CBF from within the superimposed final infarct ROI.....	97
Figure 3.3 – CBV defect volume for non-HT and HT sub-groups	98
Figure 3.4 – Example of acute matched decrease in CBF and CBV, and sub-acute hypervolemia and hyperperfusion.....	103
Figure 3.5 – Example of acute mismatch CBF/CBV, and sub-acute hypervolemia and hyperperfusion.....	105
Figure 3.6 – Example of arteriovenous shunting	107
Figure 4.1 – Timeline for the experimental protocol	120
Figure 4.2 – Assesement of glucose metabolism with ¹⁸ FDG-PET.....	126
Figure 4.3 – Regression of imaging defined PIV versus TTC defined TIV	128

Figure 4.4 – Bland-Altman plots.....	130
Figure 4.5 – Examples of imaging and TTC stained brains.....	137
Figure 5.1 – CT images for patient with small leakage in ischemic region.....	152
Figure 5.2 – CT images for patient with large leakage in ischemic defect.....	153
Figure 5.3 – PS values for patients with/without HT, and HT sub-types	162
Figure 5.4 – Distribution of PS values for tPA treated/non-treated.....	163
Figure 5.5 – Receiver operator characteristic curve for PS	164
Figure 6.1 – Patient with a spot sign and post-contrast leakage	179
Figure 6.2 – Patient without contrast extravasation.....	180
Figure 7.1 – Methodology for blood clot induction with extracranial perfusion preservation.....	199
Figure 7.2 – CT perfusion study and corresponding excised brain slices.....	202
Figure 7.3 – Examples of histology	205
Figure 7.4 – Neurological scoring.....	208
Figure 7.5 – CTP-ischemia versus TTC infarction	210
Figure 7.6 – Ipsilateral CBF and CBV values	211
Figure 7.7 – Hemorrhage and apoptosis indices	214
Figure A1 – Thresholds for infarction for gray matter	242
Figure A1 – Thresholds for infarction for white matter.....	243

LIST OF APPENDICES

Appendix A – Human Ethics Approval for the work contained within chapter two entitled: “The evolution of the cerebral blood volume abnormality in patients with ischemic stroke”	236
Appendix B – Human Ethics approval for the work contained within chapter three entitled “Reliability of the CT perfusion cerebral blood volume parameter in ischemic stroke”	237
Appendix C – Animal Ethics approval for the work contained within chapter four entitled “Multi-modality neuroimaging in a porcine model of endothelin-1 induced cerebral ischemia: defining the acute infarct core”	238
Appendix D – Method to determine the optimal CT perfusion hemodynamic thresholds for gray and white matter in the setting of acute stroke.....	239
Appendix E – Human Ethics approval for the work contained within chapter five entitled “Hemorrhagic transformation of ischemic stroke: prediction with CT perfusion”	245

Appendix F – Tracer kinetic modeling for the CTP permeability surface area product.....	246
Appendix G – Human Ethics approval for the work contained within chapter six entitled “Early rate of contrast extravasation in ICH patients”	249
Appendix H – Human Ethics approval for the work contained within chapter seven entitled “Development and implementation of a rabbit model of middle cerebral artery embolic occlusion: pre-morbid cerebrovascular conditioning with dipyridamole	250
Appendix I – Copyright Agreements.....	251

LIST OF ABBREVIATIONS

ADC	Apparent Diffusion Coefficient
AIS	Acute Ischemic Stroke
AIF	Arterial Input Function
AP	Antiplatelet
ASPECTS	The Alberta Stroke Program Early CT Score
BBB	Blood-Brain Barrier
BP	Blood Pressure
CASES	Canadian Alteplase for Stroke Effectiveness Study
CBF	Cerebral Blood Flow
CBV	Cerebral Blood Volume
CBV _I	CBV Within Tissue that Progresses to Infarction
CBV _D	CBV Defect
CCA	Common Carotid Artery
CIN	Contrast Induced Nephrotoxicity
CMR _{glu}	Cerebral Metabolic Rate of Glucose
CMRO ₂	Cerebral Metabolic Rate of Oxygen
CT	Computed Tomography
CTA	Computed Tomography Angiography
CTP	Computed Tomography Perfusion
DIP	Dipyridamole
DWI	Diffusion-Weighted Imaging

ECA	External Carotid Artery
ECASS	European Cooperative Acute Stroke Study
EEG	Electroencephalography
EIC	Early Ischemic Changes
ENACT	Evaluating Neuroprotection in Aneurysm Coiling Therapy
ET-1	Endothelin-1
¹⁸ F-FMZ	F-18 labeled Flumazenil
¹⁸ F-FDG	F-18 labeled 2-fluoro-2-deoxy-d-glucose
¹⁸ F-MISO	F-18 labeled Fluoromisonidazole
GRE	Gradient-recalled echo
HI	Hemorrhagic Infarction
HT	Hemorrhagic Transformation
HU	Hounsfield Units
IA	Intra-arterial
ICA	Internal Carotid Artery
ICH	Intracerebral Hemorrhage
ICP	Intracranial Pressure
IRF	Impulse Residue Function
ISTR	International Stroke Thrombolysis Registry
IV	Intra-venous
FDA	Food and Drug Administration
MCA	Middle Cerebral Artery
MERCI	Mechanical Embolus Removal in Cerebral Ischemia
MIP	Maximum Intensity Projection

MRA	Magnetic Resonance Angiography
MRI	Magnetic Resonance Imaging
mRS	modified Rankin Score
MTT	Mean Transit Time
NCCT	Non-Contrast Computed Tomography
NCCT _D	NCCT Hypodensity Defect
NIHSS	National Institutes of Health Stroke Scale
NINDS	National Institute of Neurological Disorders and Stroke
PCCT	Post-contrast CT
PCL	Post-contrast Leakage
PET	Positron Emission Tomography
PH	Parenchymal Hematoma
PIV	Predicted Infarct Volume
PS	Permeability Surface Area Product
PVA	Partial Volume Averaging
PWI	Perfusion-Weighted Imaging
rCBF	relative Cerebral Blood Flow
RLCEM	Rabbit Large Clot Embolic Stroke Model
ROI	Region of Interest
ROS	Reactive Oxygen Species
SITS	Safe Implementation of Treatments in Stroke
SMART	Simplified Management of Acute Stroke Using Revised Treatment
STICH	Surgical Trial in Lobar Intracerebral Hemorrhage
TDC	Time-Density Curve

TDCi	TDC from Ischemic Defect
TIV	True Infarct Volume
TOAST	Trial of Org 10172 in Acute Stroke Treatment
Tmax	Time-to-maximum of IRF
tPA	Tissue Plasminogen Activator
TTC	2,3,5-Triphenyltetrazolium Chloride
TTP	Time to Peak
VOF	Venous Output Function
WHO	World Health Organization

CHAPTER 1

1.1 INTRODUCTION

According to the World Health Organization (WHO), stroke is the world leading cause of long-term morbidity, and the third leading cause of death in developed countries¹. Over the past two decades, there has been an overall reduction in stroke-related deaths in North America; however, within certain racial groups and gender cohorts, stroke incidence and severity has worsened during this time²⁻⁶. Over the next 40 years, the number of incident strokes will more than double, with the majority of the increase occurring in individuals age 75 and older⁷. Although prevention is the most effective method for mitigating stroke burden, acute treatment and long-term care remains the current focus for improving stroke outcome. The expected number of stroke survivors living with permanent disability will rise dramatically if acute treatment strategies are not improved; the degree of disability is linked to early treatment response. Further, as long term care remains the dominant cost for all stroke patients, effective acute treatment could minimize the social and economic burden of cerebrovascular disease in the future⁸.

1.2 STROKE PATHOPHYSIOLOGY

Stroke is caused by variable disturbances in blood flow to intracranial brain tissue due to blockage of supplying vessels and/or leakage of blood from damaged vessels. These cerebrovascular accidents can result in transient or long term neurological deficit, depending on the ictus duration and the area of affected brain. The WHO determined that the global incidence of stroke is ~200 per 100,000 people⁹. Ischemic stroke accounts for

~87% of strokes in North American, while primary intracerebral hemorrhage (ICH) accounts for ~13%¹⁰. Of the people who suffer an ischemic stroke, approximately 20% will die, and 55% will be left with some form of disability that does not permit independent living¹¹. For patients with primary ICH, the 30 day mortality rate ranges from 40% to 50%, with some form of long term morbidity present in almost all survivors¹².

1.2.1 Cerebral ischemia

Cerebral ischemia is a sudden decrease in brain blood flow, resulting in the alteration of cellular function. With interruption of oxygen and glucose rich arterial flow, electrically active neurons and supporting glial cells are unable to maintain basal functions needed to stay alive¹³.

Cerebral ischemia has various arterial etiologies. The most common of which is thrombosis, the formation of a blood clot secondary to general endothelial injury or rupture of an atherosclerotic plaque¹⁴. Occasionally breaking away from the site of thrombosis, single or multiple thromboemboli can travel to the brain causing focal ischemia; clot consistency (variations of fibrin-platelet bridging and red blood cell adherence) will affect response to acute treatment and overall stroke severity¹⁵. The heart is also a major source of cerebral emboli, produced by the left atrium in patients with atrial-fibrillation (blood becomes static due to weak, irregular heartbeats) or recent cardiac surgery (clots may form via the external coagulation cascade around the surgical site). Moreover, systemic hypoperfusion, as a result of a general decrease in mean arterial pressure caused by any myocardial dysfunction, can lead to ischemia in the distal territories of the cerebral arterial tree, known as watershed stroke¹⁶. The Trial of Org

10172 in Acute Stroke Treatment (TOAST) criteria allows investigators to report responses to treatment among important sub-groups of patients with ischemic stroke. The TOAST classification denotes four subtypes of ischemic stroke: large-artery atherosclerosis, cardio-embolism, small-vessel occlusion, and stroke of other determined/undetermined etiology¹⁷. Regardless of the cause, a reduction in blood supply to the brain creates a homeostatic imbalance in pH, temperature, overall nutrition, and waste removal, the first steps towards cellular dysfunction¹⁸.

More than 70% of all energy use in the brain is to maintain the neuronal membrane voltage gradient via active, facilitated transport of Na^+/K^+ . This gradient is fundamental for electrical and chemical signaling via action potential propagation. During ischemia, if cellular respiration is no longer capable of adequate ATP production, intracellular ATP is depleted within minutes due to this energy-consuming process. This first stage of the “ischemic cascade” causes neuronal depolarization, due to the influx of Ca^{2+} and Na^+ ions, and the efflux of K^+ ions¹⁹. The increase in intracellular Ca^{2+} triggers the release of glutamate, an excitatory neurotransmitter, which activates several enzymes involved in the lysis of proteins, lipids and nucleic acids. Moreover, sustained depolarization of neighbouring neurons, called spreading depression, is enhanced with the failure of glutamate re-uptake, and further Ca^{2+} influx²⁰. This state of cellular excitation leads to neuronal apoptosis or necrosis, which depends on the damage intensity caused by an onslaught of increasing inflammatory, oxidative and nitrate stressors²¹.

The understanding of the ischemic cascade brought forth distinct definitions of tissue status during hyper-acute cerebral ischemia. Within the most hypoperfused territory, called the ischemic or infarct core, cells are irreversibly damaged; even upon reperfusion, these cells are no longer viable²². Across species, the threshold for

irreversible neuronal death has been identified as a CBF value of approximately 8-10 $\text{ml}\cdot\text{min}^{-1}\cdot(100\text{g})^{-1}$ ²³⁻²⁷. The infarct core, consisting of apoptotic/necrotic tissue, is surrounded by a variably sized tissue region with blood flow above the threshold to induce immediate infarction – the ischemic penumbra. The original definition of this tissue state is based on the absence of electroencephalography (EEG) signals and sensory evoked potentials with maintenance of membrane pump function and ionic gradients retained at near normal levels^{28, 29}. Due to this electrical silence (neurons are unable to transmit signals), clinical symptoms relating to the affected tissue region are apparent; therefore, it is impossible to discern the amount of viable penumbral tissue based on clinical symptoms alone. The survival of penumbral tissue on the border zone of infarction is largely dependent on leptomeningeal collateral supply, as well the degree of peri-infarct depolarization³⁰. If blood flow is not restored promptly, the viable ischemic penumbra invariably progresses to infarction; however, with reperfusion in a timely manner, this tissue will fully recover, along with clinical function – the so-called “time is brain” paradigm³¹. Depending on the technique for measuring CBF, the upper threshold for electrical silence and neuronal dysfunction occurs at a CBF of 22-25 $\text{ml}\cdot\text{min}^{-1}\cdot(100\text{g})^{-1}$ ²⁶. The duration of ischemia will determine tissue fate below this threshold³². A third tissue state is described as having a CBF above the upper threshold for neuronal dysfunction, but lower than normal CBF values, called benign oligemia. Regardless of the duration of ischemia, this tissue does not progress to infarction and maintains normal cellular function, in spite of slight hypoperfusion³³.

The cerebrum is composed of two distinct tissue types, gray and white matter³⁴. Gray matter predominates in the cortex and deep nuclei of the brain, composed of unmyelinated axons, neuronal cell bodies, dendrites and glial cells³⁵. White matter

consists of mainly of glial cells and myelinated axonal tracts, which allow neural signals to travel quickly between the cerebrum and other brain regions³⁴. In resting gray matter, average CBF values are approximately $50\text{-}60 \text{ ml}\cdot\text{min}^{-1}\cdot(100\text{g})^{-1}$, whereas white matter values are closer to $20\text{-}25 \text{ ml}\cdot\text{min}^{-1}\cdot(100\text{g})^{-1}$ ³⁶. This substantial discrepancy in flow values is mainly because white matter synapse activity consumes $\leq 0.5\%$ of the energy of gray matter synapses³⁴. It follows that white matter may be more tolerant to ischemia than gray matter, as there is a greater relative decrease in CBF from normal in gray matter than in white matter³⁷. Further, since gray matter has a higher metabolic demand, it can be expected that the damage would occur earlier and be more severe than white matter for a given CBF. At the cellular level, the ischemic cascade also differs between gray and white matter. Gray matter infarction is facilitated primarily through glutamate excitotoxicity, as described in the previous section. White matter is deficient in glutamate receptors, and Ca^{2+} enters the cell through a reversal of the $\text{Ca}^{2+}\text{-Na}^{+}$ ion exchanger^{25, 38}. This disparity could affect the efficacy of therapeutic strategies targeting the ischemic cascade, depending on what region of the brain is affected. A recent study has shown that ischemic vulnerability is location-specific; a 60% reduction in rCBF within highly vulnerable locations (the putamen, frontal gyri, and insular ribbon) distinguishes infarct core, whereas an 85% reduction in rCBF distinguishes infarct core in the remainder of the brain³⁹.

The first perfusion thresholds to define infarct and penumbral tissue focused mainly on gray matter because animal stroke models were used; lower rodents, typical of many stroke studies, have a much lower white/gray matter ratio compared to humans and higher primates⁴⁰. Further, thresholds originating from humans frequently use regions with combined gray and white matter, which could lead to under/overestimation of

infarcted tissue in subsequent prospective studies. Since gray and white matter have very different basal perfusion and thresholds for damage to occur, both pre-clinical and clinical studies on ischemic damage should define separate thresholds for gray and white matter.

1.2.2 Hemorrhagic transformation of cerebral ischemia

Hemorrhage occurs when blood is abnormally present in brain parenchyma or cerebral spinal fluid. This may occur due to a number of vasculopathies associated with trauma, vascular abnormalities, tumours or impaired coagulation; however, several studies have demonstrated the tendency of embolic ischemia to undergo hemorrhagic transformation⁴¹⁻⁴⁴. Hemorrhage in an area of ischemia occurs when blood extravasates through vessel walls with compromised integrity and increased permeability, commonly caused by the restoration of perfusion to the site of ischemic injury. The risk of hemorrhage secondary to acute ischemic stroke (AIS) occurs in 2.2%–44.0% of patients, and is the single most important risk factor to consider in deciding whether thrombolytic therapy should be given^{11, 45-47}. AIS-related hemorrhage is divided into parenchymal hemorrhage (PH) and hemorrhagic infarction (HI), the former increasing mortality risk by 10-fold⁴⁸. While more severe hemorrhage is undoubtedly associated with worse outcome, there is controversy whether less severe forms of hemorrhage are clinically important, indicative of successful reperfusion⁴⁸⁻⁵². Some investigators believe non-PH hemorrhagic transformation may represent a clinically irrelevant epiphenomenon, with different pathogenesis⁵³. If this is the case, the ability to predict PH, the symptomatic hemorrhage sub-type, at the acute stroke phase is critical to guide early treatment. Several groups have explored the use of biomarkers, as well as CT and MRI imaging in an attempt to predict

secondary hemorrhage; however, low sensitivity and specificity have limited their use in acute triage^{43, 54-59}.

1.2.3 Primary intra-cerebral hemorrhage

ICH is an extravasation of blood into the brain parenchyma originating from the spontaneous rupture of small vessels damaged by chronic hypertension, amyloid angiopathy, or iatrogenic causes. The primary injury occurs within minutes of bleeding and is largely the result of mechanical damage associated with edema and subsequent mass effect. After the initial rupture, the hematoma can continue to expand over several hours through the primary arterial leakage or mechanically injured surrounding vessels; there is an exponential increase in mortality when the hematoma volume exceeds 30 milliliters⁶⁰. The cause of early hematoma expansion is unknown, but secondary vessel injury and peri-hematoma ischemia have been implicated⁶¹. The degree of expansion is related to both acute hypertension and the innate coagulation efficiency⁶². Pro-thrombin cleavage, an essential step in the coagulation cascade, evokes a local inflammatory reaction responsible for brain swelling and clinical deterioration⁶³. Thrombin has been shown to be neurotoxic via glutamate-mediated excitotoxicity, causing spreading depression and overall disruption of the blood–brain barrier and neuronal death⁶⁴. Further, red blood cell breakdown products, hemoglobin and the iron constituent, are cytotoxic via the generation of free radicals causing oxidative damage to enzymes, nucleic acids, and lipids within cells of the neurovascular unit⁶⁵. During the sub-acute stage, these mechanisms may also contribute to secondary ischemic injury, leading to the development of a peri-hematoma ischemic penumbra, especially in patients with therapeutically reduced blood pressure to treat the initial ICH episode⁶⁶. Investigators

have confirmed the existence of this penumbra after ICH; however, contrary to the definition of penumbral tissue, recent imaging studies have shown that this delayed hypoperfusion is accompanied by a decrease in metabolic demand and lowered, not elevated, oxygen extraction fraction^{67, 68}. Nonetheless, peri-hematoma ischemia may still represent a therapeutic target for patients with ICH.

1.3 STROKE TREATMENT

Only in the last couple of decades, treatment of stroke has progressed from basic life support at the time of onset, to administration of advanced neuroprotective therapies. For both thromboembolic cerebral ischemia and ICH, protecting and salvaging brain tissue during the acute stroke setting is vital to regulate stroke severity. The acute imaging assessment, typically a CT scan, informs clinicians on the appropriate treatment course, depending on stroke etiology (ischemic or hemorrhagic) and whether prior stroke has occurred. Identical treatment regimens may be beneficial for one stroke sub-type, while detrimental for another. Even individuals with similar stroke etiologies may also respond differently to the same treatment. Therefore, establishing individualized approaches to acute stroke management will improve outcome.

1.3.1 Ischemic stroke

The identification of reversibly damaged tissue during the acute stroke setting has led to several early treatment strategies aimed to slow the progression of compromised tissue towards infarction. Although prompt treatment is beneficial, it is currently known that the penumbra can remain viable for up to 12 hours or more in some patients⁶⁹. Therefore,

strategies to return blood flow during the first few hours of onset, as well as to preserve neuronal integrity during the sub-acute stroke setting are imperative.

Early restoration of blood flow using thrombolytic therapy is an effective way to reverse ischemic stroke. Thrombolytic agents (mainly fibrinolytic enzymes) activate the endogenous protein plasminogen to breakdown fibrin, the structural scaffold of most blood clots. However, the negative pleiotropic effects of these agents may increase the probability of hemorrhage through the degradation of important clotting factors, and disruption of the blood-brain barrier⁷⁰. Nonetheless, evidence from the National Institute of Neurological Disorders and Stroke (NINDS) tissue plasminogen activator (tPA) study, showed that tPA administered within the first three hours after stroke significantly improved the average neurological outcomes in a large cohort of patients; this result was sufficient for the Food and Drug Administration (FDA) of the United States to approval tPA in 1996¹¹. Patients treated with intravenous (IV) tPA up to 3 hours post ictus were 30% more likely to have minimal or no disability compared to those receiving placebo. However, this strict time constraint has limited the use of tPA in less than 7% of AIS patients, as the risk of hemorrhagic transformation outweighed the clinical benefit beyond the 3-hour treatment window^{71, 72}. Several important studies have investigated the use of tPA beyond the 3 hour treatment window, namely: the 2008 European Cooperative Acute Stroke Study (ECASS) III, followed by a similar study in 2009 examining a broad range of sub-groups of patients, both comparing groups given alteplase or placebo 3 hours post ictus⁷³; observational studies investigating the Safe Implementation of Treatments in Stroke (SITS) through an internet-based audit of the International Stroke Thrombolysis Registry (ISTR), and the Canadian Alteplase for Stroke Effectiveness Study (CASES), both comparing patients receiving alteplase before and after the 3 hour window^{44, 73-75}.

Consensus was that IV-tPA has proven benefits if administered up to 4.5 hours from stroke onset. Only recently, the IV- tPA therapeutic window was extended to 4.5 hours from stroke onset^{45, 76}. Nonetheless, the ECASS III study did report a significant difference in intracranial hemorrhage for patients given alteplase, yet mortality did not differ between the treated and the placebo group⁷⁵. The Simplified Management of Acute Stroke Using Revised Treatment (SMART) criteria study is ongoing, including all stroke patients for thrombolysis in a time window up to 4.5 hours, with hemorrhage being the only exclusion criterion⁷⁷.

Intra-arterial (IA) delivery of tPA to the site of occlusion (as opposed to a systemic IV delivery) has also been shown to be beneficial⁷⁸. An advantage of IA-tPA treatment is the reduced systemic exposure, which allows for a higher concentration of tPA at the site of occlusion. Early studies showed that IA-tPA may be beneficial up to six hours after stroke onset, resulting in increased recanalization rates, and no increase in mortality, compared with controls⁷⁹. Combining IV and IA-tPA has also been tested, with moderate improvement in clinical outcome⁷⁹.

Current alternatives to thrombolysis are the Mechanical Embolus Removal in Cerebral Ischemia (MERCI) device and Penumbra clot retrieval device, which are approved to be used up to 8 hours post stroke onset, and are the only treatments available after the 4.5 hour IV-tPA treatment window^{80, 81}. These devices mechanically remove the thrombus/embolus from the involved vessel, a process known as thrombectomy or embolectomy. Both devices have high reperfusion rates and low rates of secondary intracranial hemorrhage; however, sample sizes of those trials were small⁸².

A second approach for improving neurological outcome following ischemic stroke is to use agents which interfere with the ischemic cascade, with the goal of slowing, or

even stopping the progression of penumbra to infarction. Many of these drugs were successful when applied to animal models, but failed in the clinical arena, resulting in skepticism to further research and development in this domain⁸³. Pre-clinical studies assessing possible neuroprotectants often used young, healthy animals, whereas clinical subjects are typically over the age of 60 and may present with a number of confounding conditions such as atherosclerosis, hypertension, small vessel disease, diabetes and other neurovascular disorders. Further, different proportions of gray and white matter between humans and animals may further contribute to the lack of efficacy in humans trials, as both tissue types have different responses to ischemia, as described in a previous section.

One drug which actually showed promise in the clinical setting came out of the SAINT-1 trial, which investigated the free-radical trapping agent NXY-059⁸⁴. A 72-hour infusion of NXY-059 significantly reduced disability 3 months later, and showed a reduction in the rate of secondary intracerebral hemorrhage when compared to patients given placebo. However, an attempt to repeat these promising results in a phase III trial indicated no significant benefit in neurological outcome. Another recent neuroprotectant tested in the Evaluating Neuroprotection in Aneurysm Coiling Therapy (ENACT) trial, NA-1, has been successful for reducing the volume of strokes after middle cerebral artery occlusion in non-human primates⁸⁵. In a randomized control trial of 197 patients, NA-1 reduced the number of peri-procedural ischemic strokes, as detected by MR imaging, in patients undergoing endovascular repair of intracranial aneurysms⁸⁶.

Pre-morbid use of antiplatelet drugs may also offer a neuroprotective benefit via antithrombotic and anti-inflammatory pleiotropic mechanisms during the acute stroke setting⁸⁷. Well-established in their ability to prevent impending stroke, the effectiveness of pre-morbid administration to reduce stroke severity is still debated⁸⁸. Discrepancies

between studies can be attributed to inadequate outcome measurements, small sample sizes, and variable baseline characteristics between patients, including inconsistent dosing regimens⁸⁹. Therefore, controlled experiments are needed to determine the relationship of anti-platelet drugs on stroke outcome.

Without the need to administer therapeutic agents, cooling the body by ~3-5 degrees Celsius after stroke onset has been shown to be beneficial in animal models and clinical studies^{90, 91}. Hypothermia decreases the cellular metabolic rate in both gray and white matter, which coincides in a reduction in free radical formation and suppression of elevated intracellular calcium – these mechanisms slow the cytotoxic cascade⁹⁰. Nonetheless, hypothermia in the acute stroke setting is logistically difficult to achieve and sustain. Improvements in cooling techniques continue to be made⁹².

Regardless of the potential of various ischemic stroke therapies, improved functional outcome can only be achieved if treated patients have the necessary prerequisites for improvement. That is, the presence of a substantial volume of reversibly damaged penumbra. Without a relative abundance of salvageable tissue, acute stroke treatment is futile, and may at times be more detrimental to patient outcome.

1.3.2 Primary intracerebral hemorrhage

Although the pathologic progression of primary ICH is distinct from thromboembolism induced ischemia, the “time is brain” paradigm still applies with respect to acute treatment. Systolic hypertension, greater than 140 mm Hg, and increases in intracranial pressure (ICP) after ICH may be associated with hematoma expansion and has been shown to double the risk of dependency and death⁹³. Therefore, aggressive blood pressure (BP) reduction, via the combination of hyperventilation and mannitol infusion has been

employed clinically. Hypertension, causing a decrease in blood carbon dioxide tension initiating vasoconstriction, decreases the volume of blood within the rigid cranial cavity, while mannitol elevates plasma osmolarity, pulling water (brain edema) into the vasculature for clearance – both strategies directly decrease ICP^{94, 95}. Nonetheless, clinicians are cautious not to be overaggressive with BP treatment as secondary ischemic injury caused by a global decrease in cerebral perfusion pressure is possible⁹⁶.

In 2005, a phase II study showed that treatment with a powerful hemostatic agent, recombinant factor VII, within 4 hours of ICH significantly lessened hematoma expansion, reducing mortality and improving functional outcome at 3 months; although there was a small increase in thromboembolic complications with incremental doses⁹⁷. In spite of these early positive results, the phase III trial (Factor VII for Acute Hemorrhagic Stroke) failed to show improvement in severe disability and mortality rates within the treated cohort⁹⁸.

Current research on neurosurgical interventions focuses on minimally invasive surgery and intra-ventricular clot fibrinolysis to mitigate hematoma expansion and improve clinical symptoms have been promising; however, results from studies examining the benefit of hematoma evacuation and clot aspiration were contradictory in terms of functional outcome improvement⁹⁹⁻¹⁰¹. The randomized Surgical Trial in Lobar Intracerebral Hemorrhage (STICH) trial found that early surgery is ineffective corroborating other reports which suggested craniotomy and clot evacuation lead to higher re-bleeding rates^{102, 103}. Consequently, the STICH II-trial set out to establish whether earlier surgical evacuation of the hematoma in patients with spontaneous lobar ICH would improve outcome compared to initial conservative treatment – recruitment for this trial is underway¹⁰⁰. Clearly, controlled randomized trials are needed to further

explore and develop therapies to minimize hematoma expansion, peri-hematoma edema/ischemia and secondary neuronal damage.

1.4 MEDICAL IMAGING IN STROKE

In the past 40 years, the use of medical imaging to distinguish stroke sub-types has become a mainstay at almost all medical institutions, revolutionizing acute diagnosis and treatment, as well as improving prediction of long term patient outcome. For both clinical and experimental stroke, details of the anatomical structure and function of the brain are currently possible with multi-modal imaging. Computed tomography (CT), magnetic resonance imaging (MRI), and positron emission tomography (PET) have helped guide acute stroke triage and advanced our knowledge of pathophysiological mechanisms guiding stroke treatment strategies.

1.4.1 *Positron emission tomography*

PET imaging provides functional, metabolic and molecular information at the cellular level, and is the current clinical gold standard for measurement of cerebral hemodynamics and metabolism. As a highly sensitive imaging modality, localization of nanomolar concentrations of a radioactively labeled biological molecule, called tracers, is achieved through the coincident detection of gamma rays resulting from positron annihilation. These tracers can be used to measure various hemodynamic and metabolic processes of interest to diagnosis of stroke, including cerebral blood flow (CBF), cerebral blood volume (CBV), and cerebral metabolic rate of oxygen (CMRO₂). Acute tissue states defined by these PET parameters have been well established. A matched decrease in CBF

and CMRO₂, measured with ¹⁵O-labeled water and oxygen, respectively, represents non-viable tissue¹⁰⁴. Penumbra is tissue with maintained CMRO₂, with CBF below the threshold needed for basal neuronal function, a phenomenon termed ‘misery perfusion’¹⁰⁵. Measuring the cerebral metabolic rate of glucose with ¹⁸F-2-fluoro-2-deoxy-d-glucose (¹⁸F-FDG) has been shown to discern between viable and non-viable tissue during the acute stroke setting¹⁰⁶. Moreover, monitoring glucose metabolism yields information about the degree of glycolysis, discerning between aerobic and anaerobic cell states. Even with these well-established definitions for tissue status, several drawbacks exist when using these PET parameters, mainly the need for a PET scanner with a cyclotron close by (the half-life of ¹⁵O is ~2 minutes), rapid arterial sampling to obtain accurate quantitative values, and the overall poor resolution which affects infarct volume measures and tissue segmentation. These requirements make it difficult to compare CBF and CMRO₂ values, derived from PET, with values from other imaging modalities.

More recently, tracers have been developed to target cell surface receptors on neurons, inflammatory cells, and the blood-brain-barrier allowing for specific pathways and physiological states to be examined. One such tracer, ¹⁸F-labeled Flumazenil (¹⁸F-FMZ), binds to a subunit of the central benzodiazepine GABA receptor on healthy neurons; however, these receptors are only present in cortical gray matter, limiting its effectiveness to discriminate white matter lesions. Another tracer, ¹⁸F-labeled fluoromisonidazole (¹⁸F-MISO), has been shown to identify hypoxic tissue, and independently delineate ischemic penumbra¹⁰⁷. Inflammation during the sub-acute stroke setting can also be observed using ¹¹C-PK11195, which binds to activated microglial cells within the brain¹⁰⁸. A possible relationship between neuroinflammatory reaction and

integrity of white matter tracts has recently been investigated by combining microglia PET with diffusion tensor imaging¹⁰⁹.

PET imaging in acute stroke remains limited to research studies in academic centers due to its cost, and logistical/technical complexities. PET tracers and scanners will continue to evolve, but it is unlikely that PET will see widespread clinical use for acute stroke patients in the near future. Nonetheless, PET will remain instrumental in the validation of other imaging techniques and the understanding of the pathophysiology of stroke.

1.4.2 Magnetic resonance imaging

MRI is a multi-faceted imaging modality used frequently for acute stroke diagnosis and prognosis. Recent studies indicate that MRI, particularly diffusion-weighted imaging (DWI) and gradient-recalled echo (GRE) sequences are as sensitive as CT for detecting ICH in the acute setting¹¹⁰. The DWI sequence has also been shown to have a greater sensitivity for detecting acute ischemic changes, especially in patients with transient ischemic attack¹¹¹. Further, magnetic resonance angiography (MRA) can be used to assess intra- and extra-cranial vessel patency, while perfusion-weighted imaging (PWI) can describe the cerebral hemodynamics in all stroke sub-types¹¹².

DWI is one of the most sensitive methods for identifying very early ischemic changes. The hyperintense lesion is caused by reduced brownian motion (diffusion restriction) of water molecules as a result of swollen, edematous cells caused by cytotoxicity¹¹³. This defect is a downstream effect of hemodynamic dysfunction, and cellular ion pump failure, one of the final steps towards irreversible tissue damage. Nonetheless, recent reports have shown complete reversal and recovery of tissue that was

initially hyperintense on acute DWI^{114, 115}. Moreover, DWI abnormalities have been shown to disappear then recur within hours and days following an ischemic episode in both animal and clinical studies^{113, 114, 116}. In spite of these inconsistencies, the DWI sequence remains an important imaging modality to define hyper-acute and sub-acute ischemic changes.

To complement the DWI sequence, the PWI acquisition requires the intravenous injection of the paramagnetic contrast agent, gadolinium-DTPA. This dynamic sequence provides functional maps for relative cerebral blood flow (rCBF), cerebral blood volume (CBV), and time to peak (TTP)^{117, 118}. PWI cannot provide accurate absolute CBF values due to the non-linear relationship between signal intensity and contrast concentration and difficulties in obtaining accurate artery input function¹¹⁹. Thresholds of TTP and rCBF have been shown to discriminate tissue at risk of infarction, though there is no consensus on the optimal parameter or threshold^{27, 37, 117, 120-123}. By combining the PWI and DWI images, the PWI/DWI mismatch is also a commonly used working definition of the ischemic penumbra by identifying the difference between viable tissue at risk and tissue that is irreversibly damaged, given by the DWI lesion; however, recent studies have shown that milder perfusion defects are experiencing benign oligemia, insufficient to produce infarction¹²⁴.

MR imaging of blood-brain-barrier permeability has also become an important tool for prediction of hemorrhagic transformation of ischemic stroke. Several MR-permeability studies have shown that increased permeability at admission is associated with hemorrhage at later times secondary to ischemia^{118, 125, 126}.

Compared to PET imaging, MRI is more readily available in the setting of acute stroke and does not require a radioactive substance to be injected. Further, most

sequences, unlike CT, are able to cover both supra- and infra-tentorial brain regions, allowing a more robust diagnostic imaging window and increased prognostic sensitivity. In terms of patient throughput, individuals who are claustrophobic, or have metal implants and pacemakers are excluded from MR imaging. Further, MRI scanners have limited availability, primarily accessible at large city hospitals or academic centers. Nonetheless, the absence of harmful ionizing radiation and the ability to discern very early ischemic changes makes the MR imaging an important modality in acute stroke triage.

1.4.3 Computed tomography imaging

CT imaging is a diagnostic tool that is widely available, relatively inexpensive compared to its MRI counterpart, non-invasive and fast. The acute CT imaging stroke series generally consists of a non-contrast CT (NCCT), followed by CT angiography (CTA), for patients with stroke symptoms.

1.4.3.1 Non-contrast CT

Improvements in the quality of the CT images and further experience in NCCT images currently allow for a number of subtle changes to be appreciated prior to complete infarction, as well as reliable diagnosis of ICH. Petechial hemorrhage, the loss of gray-white matter differentiation, cortical swelling, and obscuration of the insular ribbon, basal ganglia, and internal capsule can be seen within a few hours of stroke onset^{127, 128}. Hypoattenuation, including loss of gray-white differentiation and delineation of brain structures on NCCT have also been recognized as specific for irreversible infarction¹²⁹.¹³⁰ Further, the change in hypoattenuation over time could be used to indicate time of

stroke onset¹³¹. In patients with ICH, a single NCCT scan at onset has been shown to predict morbidity and mortality at 30 days¹³².

Currently, the NCCT acquisition is the most common imaging modality used to make tPA administration decisions for patients with ischemic stroke. Contraindications for tPA, as observed on NCCT, are: 1) ICH, and 2) any region of hypointensity, which likely reflects non-viable tissue, greater than 1/3 of the middle cerebral artery (MCA) territory^{133, 134}. Notwithstanding general acceptance of the above criteria, inter-observer agreement for the criterion of 1/3 MCA territory involvement is rather poor¹³³. A more recent scoring system, The Alberta Stroke Program Early CT Score (ASPECTS) is a ten point rating system for assessing the extent of early ischemic changes on NCCT¹³⁵. It is easy to implement, using two representative slices from the admission NCCT, and provides valuable information for predicting patient outcome after thrombolysis. When compared with the 1/3 MCA rule, ASPECTS has been shown to have an improved reliability and inter-observer concurrence in identifying stroke patients unlikely to make an independent recovery despite thrombolytic treatment¹³⁴⁻¹³⁶.

1.4.3.1 CT angiography

CTA requires the intravenous injection of iodinated contrast agent followed by rapid helical scanning during the peak intravascular contrast enhancement. Various techniques can be applied to interpret the acquired images, including direct viewing of source images, three-dimensional reconstructions, and maximum intensity projections (MIP). Although all three techniques are utilized, MIPs are the most common, with three-dimensional reconstructions requiring extra post-processing time. Source images are

important for examining the information in detail, and are often used to confirm occlusion or stenosis seen on the reformatted MIP images.

For patients with ICH, 40-50% has contrast extravasation on acute CTA and post-contrast CT (PCCT), which is associated with hematoma expansion and increased mortality¹³⁷⁻¹⁴¹.

For patients with ischemic stroke, the CTA based Clot Burden Score and the Boston Acute Stroke Imaging Scale are also used for the successful assessment of EIC, and can determine radiological and clinical outcomes^{142, 143}.

1.4.4.2 CT Perfusion

In a few added minutes, further assessment of cerebral hemodynamics with CT perfusion (CTP) can give insight into early ischemic changes (EIC), tissue states, and blood-brain barrier disturbances, unseen on NCCT/CTA. Moreover, due to optimized scanning protocols, the added radiation dose is minimized.

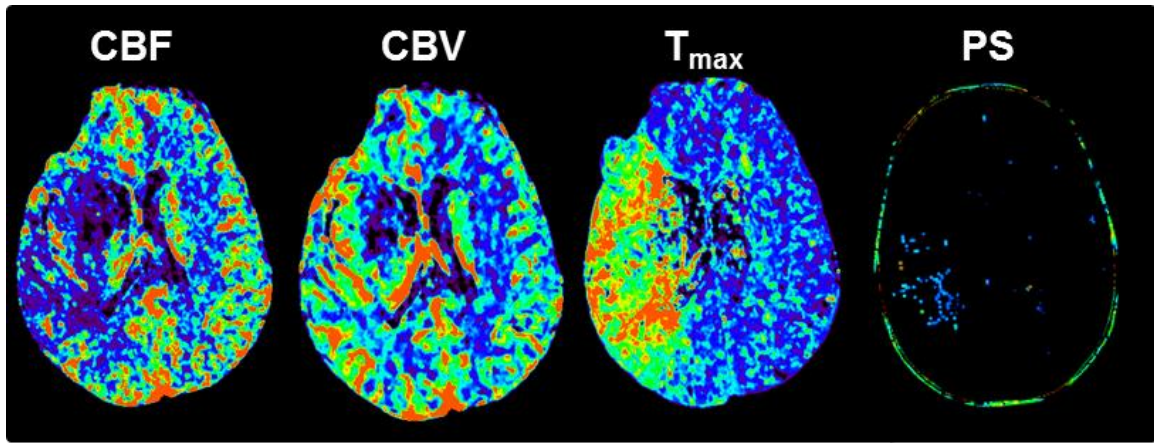
Although CTP imaging is rarely used for acute diagnosis of ICH, recent perfusion studies have attempted to find secondary ischemic changes in surrounding tissue, leading to edema and possibly worsening clinical outcome^{96, 144-146}. Briefly, Rosand et al. (2002) revealed a gradient of peri-hematoma hypoperfusion, which may have been associated with ischemic changes¹⁴⁵. Subsequent findings by Fainardi et al. (2008) demonstrated that this centrifugal CBF distribution around the hematoma was not suggestive of ischemic penumbra destined to survive, but rather indicative of edema formation, a potential confounding factor in hematoma growth¹⁴⁴. During the first 3 hours of symptom onset, early hematoma growth is seen in 18-38% of patients with ICH, reducing to 11% thereafter^{62, 65}. Mitigating secondary bleeding is imperative when dealing with ICH.

In the setting of ischemic stroke, hemodynamic thresholds from multiple parameters could be utilized to define the acute infarct core¹⁴⁷. Since absolute CTP parameter values may depend on the details of the processing algorithm, using relative thresholds have been proposed as an alternative. Schaefer et al. (2006) had success with defining infarction using normalized (to contralateral hemisphere) CTP-CBF values¹⁴⁸. It is critical that the contralateral region of interest (ROI) contains a similar distribution of gray and white matter, as both tissue types have different CBF and CBV values¹⁴⁹. Similarly, absolute thresholds obtained from ROIs with a mix of gray and white matter tissue may present a problem, as both tissue types have different CBF and CBV, as described in a previous section. To circumvent this issue, efforts to determine individual gray and white matter threshold values for infarct core and penumbra have been carried out, with varying results¹⁵⁰⁻¹⁵⁴.

Depending on the clinical symptoms, the imaged volume is selected at the level of the basal ganglia, which includes posterior, anterior, and middle cerebral arteries. CTP derived CBF and CBV describes hemodynamics within the entire vasculature including large arteries, arterioles, capillary beds, venules, and veins. As an intravascular contrast bolus passes through a mass of brain tissue, the signal intensity of each voxel within a CT image will change over time. The intensity of the CT image, expressed in Hounsfield Units (HU), is linearly proportional to the efficiency with which x-rays are attenuated. For each pixel, its time-density (attenuation) curve (TDC) is used to quantify several perfusion parameters: cerebral blood flow (CBF), the volume rate of blood moving through the mass of tissue [$\text{ml}\cdot\text{min}^{-1}\cdot(100\text{g})^{-1}$]; cerebral blood volume (CBV), the total volume of moving blood in the mass of tissue [$\text{ml}\cdot(100\text{g})^{-1}$]; the time-to-peak of the pixel TDC corrected for the dispersion in the artery TDC (T_{max}) or the time-to-maximum of the

tissue residue function, and a new parameter used in the acute stroke setting, the permeability surface area product (PS) of the blood-brain-barrier, the rate of contrast extravasation from intra- to extravascular compartments through a damaged barrier [$\text{ml}\cdot\text{min}^{-1}\cdot(100\text{g})^{-1}$].

Figure 1.1 – Sample CBF, CBV, T_{max} , and PS CTP functional maps for patient with ischemic stroke

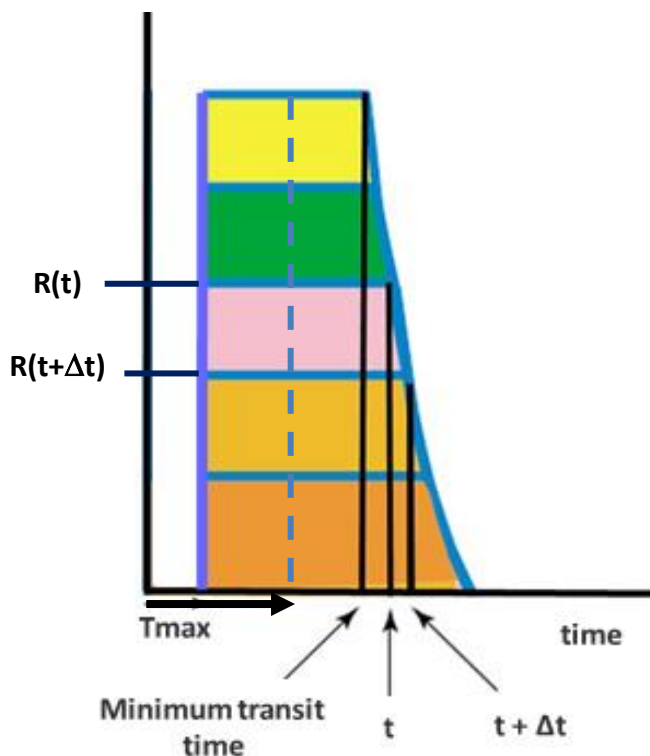


Colour coded functional maps of cerebral blood flow (CBF), cerebral blood volume (CBV), time-to-peak of tissue-residue-function (T_{max}), and permeability surface area product (PS) calculated using CT Perfusion software (GE Healthcare). CBF is expressed in units of $\text{ml}\cdot(100\text{g})^{-1}\cdot\text{min}^{-1}$, CBV in $\text{ml}\cdot(100\text{g})^{-1}$, T_{max} in seconds, and PS in $\text{ml}\cdot(100\text{g})^{-1}\cdot\text{min}^{-1}$.

With current CT perfusion software (GE Healthcare), post-processing of hemodynamic functional maps is practically automated. The operator needs only to select an arterial input function (AIF-TDC) and a venous output function (VOF-TDC). The AIF is selected from within a large artery (usually the anterior cerebral artery), preferably at a location along the artery where it is orthogonal to the scan plane to limit partial volume averaging (PVA) – this ‘dilution’ effect will become apparent when comparing the peak enhancement (increase of attenuation above baseline) of arteries of different sizes. The VOF is selected from a large vein, usually the superior sagittal sinus, to minimize the effect of PVA on its accurate measurement. As such, the underestimation of the AIF from PVA can be corrected by normalizing the area of the AIF with that of the VOF¹⁵⁵.

Deconvolution and non-deconvolution based models are used to calculate perfusion parameters. The work contained in this thesis uses the deconvolution process. Although physiologically more appropriate, deconvolution models involve complex algorithms and require more time for the calculation, whereas the simplicity of non-deconvolution models stems from their simplified assumptions about hemodynamics in the brain that may not hold true in general. Deconvolution methods correct for the inability to deliver a contrast bolus directly into the supplying artery of a tissue of interest – the bolus introduced at a peripheral vein undergoes ‘delay’ and ‘dispersion’ prior to its arrival at the artery to become the AIF or the TDC of the artery. Deconvolution corrects for this by calculating an impulse residue function [IRF or $R(t)$], which simulates the tissue TDC obtained under the ideal injection condition (Figure 1.2).

Figure 1.2 – Sample IRF



The impulse residue function (IRF) can be viewed as the fraction of contrast medium that remains in the tissue as time evolves following a bolus injection into the arterial input. Beyond the minimum transit time (the duration of the plateau), the difference of $R(t + \Delta t)$ and $R(t)$ is the fraction of contrast medium that has a transit time of t . This difference is the height of the strip with a transit time of t . Further, the area of each of the horizontal strips is the product of the transit time and the fraction of contrast medium having that transit time. It follows that the area of all the horizontal strips, that is, the area under the curve (AUC) of $R(t)$, is the mean transit time (MTT). Alternatively, as the Central Volume Principle states that the product of CBF and MTT is CBV, the AUC of $CBF \cdot R(t)$ is the CBV. The T_{max} parameter is the time to peak of the IRF. For the case when the IRF has a flat 'top' as shown, without loss of generality, T_{max} can be taken as the half-way time point of the flat 'top'.

Limited axial coverage of the whole brain and use of ionizing radiation are current limitations of CT perfusion. The volume of brain tissue which can be imaged in one CTP acquisition is limited in the craniocaudal direction (z-axis for all scanners) by the number of detector rows in a CT scanner (4-12 cm). Coverage in this direction can be doubled (to include two adjacent sections of the brain) using shuttle mode or two separate boluses^{156, 157}. The shuttle technique can have two variations, step and shoot (axial shuttle) between two sections or continuous table translation back and forth (helical shuttle). Axial shuttle mode generally has less motion artifact than helical shuttle mode as images are acquired with the patient table (brain) stationary. Also, the image interval of all slices in axial shuttle mode is uniform (2-3 seconds), while the helical shuttle mode is non-uniform for the cranial and caudal slices – the image intervals for slices in the centre of the two-section volume will be roughly uniform at 2-3 seconds, and those for the more cranial and caudal slices of that volume can vary from 1-2 to 4-5 seconds. The two injections technique requires double the dosage of iodinated contrast increasing the risk of contrast induced nephrotoxicity (CIN). However, a recent multicenter study has shown that the incidence of CIN was low ~2.6% among at-risk patients undergoing contrast enhanced CT scans in a “real world” clinical setting, where guideline-recommended strategies for CIN prevention may not be consistently followed¹⁵⁸.

Although a 60-70 second imaging protocol is sufficient for a perfusion only study, acquisitions of 90-180 second durations have been advocated for combined perfusion and blood-brain barrier permeability studies^{76, 159-161}. To minimize radiation exposure from the lengthened scan time required for blood-brain permeability measurement, temporal sampling is decreased to one image every 10-15 seconds after the first phase¹⁶⁰. The total

effective dose from a multimodal CT stroke study, for a 64-row detector CT, is ~7mSv, which is double the average annual background radiation¹⁶². Radiation-dose reduction strategies, such as the Adaptive Statistical Iterative Reconstruction, can maintain image quality while reducing effective dose by > 25%¹⁶³. Also, radiation dose could be reduced by two thirds, without compromising the accuracy of the CTP functional maps, by increasing the sampling interval from 1 second to 3 seconds in the first phase of a CTP study¹⁵⁶. Other limitations of perfusion, across all modalities, including MRI, CT and PET are: the lack of standardized image acquisition protocols; post-processing tools in the experimental and clinical settings and total perfusion imaging time, which could take up to 30 minutes from entering the imaging suite to making a treatment decision. Even with these drawbacks, the role of perfusion imaging in the setting of acute stroke continues to progress.

1.5 ANIMAL MODELS OF STROKE

Several animal models have been developed over the last four decades to explore global and focal permanent and transient cerebral ischemia, as well as primary and secondary hemorrhage. Current stroke models are divided into two categories: 1) non-induced, spontaneous vascular insults, and 2) artificially induced vascular insults. These models contribute to our overall understanding of stroke sub-type etiology, while developing primary treatment and secondary prevention strategies, in a controlled environment. Furthermore, the development of new imaging techniques and the establishment of imaging thresholds have become important research goals in the pre-clinical setting, with obvious clinical translation. Typically, rodent models of stroke have been developed due

to their cost-effectiveness, high throughput, reproducibility, and their genome is easily manipulated to form transgenic strains; however, the anatomical, and possible pathophysiological differences between the rodent and human brain remains a limitation – rat brains are lissencephalic (smooth brain surface lacking gyri and sulci), and possess very little white matter compared with humans. Therefore, rabbits, pigs, dogs and even primates have also been utilized over the years as they more closely resemble humans, including a gyrencephalic brain structure and similar proportions of gray and white matter. Disadvantages of using higher animals for stroke research are their higher cost and ethical concerns.

The use of animal models tends to eliminate confounding factors pertinent in the clinical setting (vascular cognitive impairment, small vessel disease, diabetes etc.). This is especially important when determining drug efficacies. However, no animal model completely recapitulates the complicated processes of ischemic or hemorrhagic stroke in humans, a factor which should be considered translating animal model results to the clinical arena.

1.5.1 *Global ischemia*

Global ischemia is achieved in a four vessel occlusion model where temporary ligation of two vertebral and two common carotid arteries results in a reduction in blood flow to the entire brain. These models, primarily developed in rats, are used to study the hemodynamic changes that occur during cardiac arrest, as well delayed neuronal death of the pyramidal cells in the CA1 region of the hippocampus^{164, 165}.

1.5.2 Focal ischemia

The alternative to global ischemia is focal ischemia, which attempts to mimic the majority of ischemic stroke cases, in which the occlusion of the middle cerebral artery occurs. A common model of focal ischemia is the intraluminal filament procedure, which attempts to preserve blood flow through the internal carotid artery (ICA)¹⁶⁶. This technique involves the insertion of a filament of surgical suture antegrade into the ICA, which is then advanced to block the MCA origin; however, significant mechanical abrasion may result in endothelial damage and even hemorrhage. If done correctly, this model is relatively easy to implement, produces consistent results between animals and removal of the filament can mimic a reperfusion scenario. Other models of focal ischemia are photothrombosis, endothelin-1, and the Tamura method (transection of the MCA), all of which create an occlusion of the MCA¹⁶⁷⁻¹⁶⁹.

To investigate thrombolysis and tPA therapy, an autologous blood clot can be useful. The rabbit small/large clot embolic stroke model (RCEM), which involves an injection of autologous blood clots into the internal carotid artery, causing occlusion of the MCA¹⁷⁰. This model was utilized in the original study that showed the beneficial effect of tPA and also in the development of the first neuroprotectant to show efficacy in clinical trials¹⁷¹.¹⁷² Advantages of the RCEM include a similar vascular anatomy to humans, formation of thrombus following occlusion, and the similarity of the embolic material in both the animal model and human disease. The similarities between human stroke and this embolic stroke model make it suitable for testing future therapies, especially those being tested in combination with tPA to achieve reperfusion. Nonetheless, the ligation of the

external carotid artery, prior to insertion of the clot, makes longitudinal studies difficult as extra-cranial structures, including mastication muscles, are damaged.

A number of rare forms of stroke occur in humans as a result of single gene disorders. The most common of these is cerebral autosomal dominant arteriopathy with subcortical infarcts and leucoencephalopathy, resulting from mutations in the Notch3 gene¹⁷³. With the introduction of transgenic animals, many spontaneous stroke models have been developed with small rodents to cause spontaneous vascular pathologies, as observed in the clinical setting¹⁷⁴. Though, due to inter-strain variations of the vascular territories and incomplete posterior communicating arteries, careful selection is required to minimize these effects. The spontaneously hypertensive stroke-prone rat is commonly used to mimic clinical case of hypertension, used for producing large MCA infarcts¹⁷⁵. This model closely resembles older individuals who typically have underlying vascular pathologies.

1.5.3 Intracerebral hemorrhage

Intracerebral injection of blood or bacterial collagenase, as well as mechanically induced vessel rupture mimics the pathophysiology of spontaneous primary and secondary forms of ICH in humans. These models can also be used to determine the effects of hemostatic agents on edema formation and hematoma expansion. Genetically engineered mice are valuable in determining the mechanisms of injury following ICH¹⁷⁶. Several groups have recently used transgenic mice to study the role of factors that may contribute to ICH-induced injury, identifying therapeutic targets. Furthermore, they can be used to corroborate the gene expression profile in peri-hematoma tissue after ICH in humans¹⁷⁷.

Despite the setbacks in translating experimental results to the clinical setting, animal models provide a necessary step for testing potential strategies to improve treatment of acute stroke.

1.6 FUTURE STROKE DIAGNOSIS & TREATMENT

Stroke diagnosis, prognosis and treatment planning has come a long way in the last four decades. Currently, one of the major limiting factors in the acute setting is whether treatment, either surgical or pharmacological, will improve or worsen outcome. Neuroimaging is at the forefront of establishing a more individualized approach to stroke treatment, which emphasizes the physiological condition of the brain tissue, rather than a strict reliance on time from ictus. Development of this comprehensive diagnostic work-up makes use of both MRI and CT imaging. MRI and CT can both be used to determine vessel status (MRA and CTA) while perfusion-weighted imaging (PWI) and CTP imaging can provide comparable information on the hemodynamic parameters. PWI is advantageous since it provides greater anatomical coverage than CT and does not involve ionizing radiation; however, CTP has the benefit of providing quantitative values, acquisition speed is faster, and is more frequently available at most hospitals. Further, absolute measurement of vascular integrity in terms of permeability surface area product during the first few hours of stroke onset is possible. The addition of CTA and CTP to the standard NCCT adds minimal time to the acute stroke triage, and all studies can be performed within the same scanner. Using these three CT protocols, development of a patient-specific treatment plan has the ability to significantly advance stroke treatment by assessing the relative risks and benefits of early therapy on a patient by patient basis.

Additionally, these techniques may provide the necessary information to exclude patients at high risk of hematoma expansion and hemorrhagic transformation in primary and secondary hemorrhage cases.

1.7 RESEARCH OBJECTIVES

The main objective of the work contained in this thesis is to use the CT perfusion imaging modality to reduce the average rate of neuronal loss during the acute stroke setting by guiding acute treatment and determining the efficacy of pre-stroke neuroprotective strategies.

This work is divided into the following projects:

- 1) Determine the prognostic reliability of the cerebral blood volume parameter in acute ischemic stroke.
- 2) In a porcine model of ischemic stroke, correlate the optimal CT perfusion parameter/thresholds for acute infarct core delineation in gray and white matter with the imaging and histological gold standards.
- 3) Determine whether early blood-brain-barrier integrity, as measured by the CT perfusion derived permeability surface area product, is associated with both radiological and clinical outcomes in primary and secondary intracerebral hemorrhage.

- 4) Development of a longitudinal animal model of middle cerebral artery embolic occlusion (rabbit) to explore the neuroprotective effect of dipyridamole, an anti-platelet drug, in embolic cerebral ischemia.

1.8 REFERENCES

1. Feigin VL, Lawes CM, Bennett DA, Barker-Collo SL, Parag V. Worldwide stroke incidence and early case fatality reported in 56 population-based studies: A systematic review. *Lancet neurology*. 2009;8:355-369
2. Kleindorfer DO, Khoury J, Moomaw CJ, Alwell K, Woo D, Flaherty ML, et al. Stroke incidence is decreasing in whites but not in blacks: A population-based estimate of temporal trends in stroke incidence from the greater Cincinnati/northern Kentucky stroke study. *Stroke*.41:1326-1331
3. Carandang R, Seshadri S, Beiser A, Kelly-Hayes M, Kase CS, Kannel WB, et al. Trends in incidence, lifetime risk, severity, and 30-day mortality of stroke over the past 50 years. *JAMA*. 2006;296:2939-2946
4. Xian Y, Holloway RG, Noyes K, Shah MN, Friedman B. Racial differences in mortality among patients with acute ischemic stroke: An observational study. *Ann Intern Med*.154:152-159
5. Mohan KM, Crichton SL, Grieve AP, Rudd AG, Wolfe CD, Heuschmann PU. Frequency and predictors for the risk of stroke recurrence up to 10 years after stroke: The south London stroke register. *J Neurol Neurosurg Psychiatry*. 2009;80:1012-1018
6. Minino A. Deaths: Final data for 2008. *National Vital Statistics Reports*. 2011;59
7. Howard G, Goff DC. Population shifts and the future of stroke: Forecasts of the future burden of stroke. *Annals of the New York Academy of Sciences*. 2012;1268:14-20
8. Cadilhac DA, Carter R, Thrift AG, Dewey HM. Estimating the long-term costs of ischemic and hemorrhagic stroke for Australia: New evidence derived from the north east Melbourne stroke incidence study (Nemesis). *Stroke; a journal of cerebral circulation*. 2009;40:915-921
9. Soler EP, Ruiz VC. Epidemiology and risk factors of cerebral ischemia and ischemic heart diseases: Similarities and differences. *Current cardiology reviews*. 2010;6:138-149
10. Gebel JM, Broderick JP. Intracerebral hemorrhage. *Neurologic clinics*. 2000;18:419-438
11. Tissue plasminogen activator for acute ischemic stroke. The national institute of neurological disorders and stroke rt-pa stroke study group. *The New England journal of medicine*. 1995;333:1581-1587

12. Broderick J, Connolly S, Feldmann E, Hanley D, Kase C, Krieger D, et al. Guidelines for the management of spontaneous intracerebral hemorrhage in adults: 2007 update: A guideline from the american heart association/american stroke association stroke council, high blood pressure research council, and the quality of care and outcomes in research interdisciplinary working group. *Circulation*. 2007;116:e391-413
13. Cipolla MJ, Bullinger LV. Reactivity of brain parenchymal arterioles after ischemia and reperfusion. *Microcirculation*. 2008;15:495-501
14. del Zoppo GJ, Hallenbeck JM. Advances in the vascular pathophysiology of ischemic stroke. *Thrombosis research*. 2000;98:73-81
15. Grotta J. Timing of thrombolysis for acute ischemic stroke: "Timing is everything" or "everyone is different". *Annals of the New York Academy of Sciences*. 2012;1268:141-144
16. Mangla R, Kolar B, Almast J, Ekholm SE. Border zone infarcts: Pathophysiologic and imaging characteristics. *Radiographics : a review publication of the Radiological Society of North America, Inc*. 2011;31:1201-1214
17. Wilterdink JL, Bendixen B, Adams HP, Jr., Woolson RF, Clarke WR, Hansen MD. Effect of prior aspirin use on stroke severity in the trial of org 10172 in acute stroke treatment (toast). *Stroke; a journal of cerebral circulation*. 2001;32:2836-2840
18. Berezowski V, Fukuda AM, Cecchelli R, Badaut J. Endothelial cells and astrocytes: A concerto en duo in ischemic pathophysiology. *International journal of cell biology*. 2012;2012:176287
19. Kanekar SG, Zacharia T, Roller R. Imaging of stroke: Part 2, pathophysiology at the molecular and cellular levels and corresponding imaging changes. *AJR. American journal of roentgenology*. 2012;198:63-74
20. del Zoppo GJ, Mabuchi T. Cerebral microvessel responses to focal ischemia. *Journal of cerebral blood flow and metabolism : official journal of the International Society of Cerebral Blood Flow and Metabolism*. 2003;23:879-894
21. Hossmann KA. Pathophysiology and therapy of experimental stroke. *Cell Mol Neurobiol*. 2006;26:1057-1083
22. Fisher M. The ischemic penumbra: A new opportunity for neuroprotection. *Cerebrovascular diseases*. 2006;21 Suppl 2:64-70
23. Sun Z, Zhang X, Zhang Y, Guo H, Zhang J, Yu C. Estimation of the ischemic penumbra based on ct perfusion a pilot study. *Academic radiology*. 2010;17:1535-1542

24. He ZK, Xu YK, Qiu WJ, Deng YX, Zhou ZP, Huang ZH, et al. [ct perfusion study of acute local cerebral infarction in rhesus monkeys]. *Nan fang yi ke da xue xue bao = Journal of Southern Medical University*. 2007;27:720-724
25. Arakawa S, Wright PM, Koga M, Phan TG, Reutens DC, Lim I, et al. Ischemic thresholds for gray and white matter: A diffusion and perfusion magnetic resonance study. *Stroke; a journal of cerebral circulation*. 2006;37:1211-1216
26. Hossmann KA. Viability thresholds and the penumbra of focal ischemia. *Annals of neurology*. 1994;36:557-565
27. Rohl L, Ostergaard L, Simonsen CZ, Vestergaard-Poulsen P, Andersen G, Sakoh M, et al. Viability thresholds of ischemic penumbra of hyperacute stroke defined by perfusion-weighted mri and apparent diffusion coefficient. *Stroke; a journal of cerebral circulation*. 2001;32:1140-1146
28. Symon L. The relationship between cbf, evoked potentials and the clinical features in cerebral ischaemia. *Acta neurologica Scandinavica. Supplementum*. 1980;78:175-190
29. Hossmann KA, Heiss WD, Bewermeyer H, Mies G. Eeg frequency analysis in the course of acute ischemic stroke. *Neurosurgical review*. 1980;3:31-36
30. Forster A, Szabo K, Hennerici MG. Pathophysiological concepts of stroke in hemodynamic risk zones--do hypoperfusion and embolism interact? *Nature clinical practice. Neurology*. 2008;4:216-225
31. Saver JL. Time is brain--quantified. *Stroke; a journal of cerebral circulation*. 2006;37:263-266
32. Jones TH, Morawetz RB, Crowell RM, Marcoux FW, FitzGibbon SJ, DeGirolami U, et al. Thresholds of focal cerebral ischemia in awake monkeys. *Journal of neurosurgery*. 1981;54:773-782
33. Kamalian S, Kamalian S, Konstas AA, Maas MB, Payabvash S, Pomerantz SR, et al. Ct perfusion mean transit time maps optimally distinguish benign oligemia from true "at-risk" ischemic penumbra, but thresholds vary by postprocessing technique. *AJNR. American journal of neuroradiology*. 2012;33:545-549
34. Harris JJ, Attwell D. The energetics of cns white matter. *The Journal of neuroscience : the official journal of the Society for Neuroscience*. 2012;32:356-371
35. Talos IF, Mian AZ, Zou KH, Hsu L, Goldberg-Zimring D, Haker S, et al. Magnetic resonance and the human brain: Anatomy, function and metabolism. *Cellular and molecular life sciences : CMLS*. 2006;63:1106-1124

36. Leenders KL, Perani D, Lammertsma AA, Heather JD, Buckingham P, Healy MJ, et al. Cerebral blood flow, blood volume and oxygen utilization. Normal values and effect of age. *Brain : a journal of neurology*. 1990;113 (Pt 1):27-47
37. Bristow MS, Simon JE, Brown RA, Eliasziw M, Hill MD, Coutts SB, et al. Mr perfusion and diffusion in acute ischemic stroke: Human gray and white matter have different thresholds for infarction. *Journal of cerebral blood flow and metabolism : official journal of the International Society of Cerebral Blood Flow and Metabolism*. 2005;25:1280-1287
38. Stys PK, Waxman SG, Ransom BR. Na(+)-ca²⁺ exchanger mediates ca²⁺ influx during anoxia in mammalian central nervous system white matter. *Annals of neurology*. 1991;30:375-380
39. Payabvash S, Souza LC, Wang Y, Schaefer PW, Furie KL, Halpern EF, et al. Regional ischemic vulnerability of the brain to hypoperfusion: The need for location specific computed tomography perfusion thresholds in acute stroke patients. *Stroke; a journal of cerebral circulation*. 2011;42:1255-1260
40. Lythgoe MF, Sibson NR, Harris NG. Neuroimaging of animal models of brain disease. *British medical bulletin*. 2003;65:235-257
41. Hjort N, Wu O, Ashkanian M, Solling C, Mouridsen K, Christensen S, et al. Mri detection of early blood-brain barrier disruption: Parenchymal enhancement predicts focal hemorrhagic transformation after thrombolysis. *Stroke; a journal of cerebral circulation*. 2008;39:1025-1028
42. Kim EY, Na DG, Kim SS, Lee KH, Ryoo JW, Kim HK. Prediction of hemorrhagic transformation in acute ischemic stroke: Role of diffusion-weighted imaging and early parenchymal enhancement. *AJNR. American journal of neuroradiology*. 2005;26:1050-1055
43. Montaner J, Molina CA, Monasterio J, Abilleira S, Arenillas JF, Ribo M, et al. Matrix metalloproteinase-9 pretreatment level predicts intracranial hemorrhagic complications after thrombolysis in human stroke. *Circulation*. 2003;107:598-603
44. Shobha N, Buchan AM, Hill MD. Thrombolysis at 3-4.5 hours after acute ischemic stroke onset--evidence from the canadian alteplase for stroke effectiveness study (cases) registry. *Cerebrovascular diseases*.31:223-228
45. Hacke W, Kaste M, Fieschi C, Toni D, Lesaffre E, von Kummer R, et al. Intravenous thrombolysis with recombinant tissue plasminogen activator for acute hemispheric stroke. The european cooperative acute stroke study (ecass). *JAMA : the journal of the American Medical Association*. 1995;274:1017-1025
46. Larrue V, von Kummer RR, Muller A, Bluhmki E. Risk factors for severe hemorrhagic transformation in ischemic stroke patients treated with recombinant

- tissue plasminogen activator: A secondary analysis of the european-australasian acute stroke study (ecass ii). *Stroke; a journal of cerebral circulation*. 2001;32:438-441
47. Hacke W, Albers G, Al-Rawi Y, Bogousslavsky J, Davalos A, Eliasziw M, et al. The desmoteplase in acute ischemic stroke trial (dias): A phase ii mri-based 9-hour window acute stroke thrombolysis trial with intravenous desmoteplase. *Stroke; a journal of cerebral circulation*. 2005;36:66-73
 48. Berger C, Fiorelli M, Steiner T, Schabitz WR, Bozzao L, Bluhmki E, et al. Hemorrhagic transformation of ischemic brain tissue: Asymptomatic or symptomatic? *Stroke; a journal of cerebral circulation*. 2001;32:1330-1335
 49. Molina CA, Alvarez-Sabin J, Montaner J, Abilleira S, Arenillas JF, Coscojuela P, et al. Thrombolysis-related hemorrhagic infarction: A marker of early reperfusion, reduced infarct size, and improved outcome in patients with proximal middle cerebral artery occlusion. *Stroke; a journal of cerebral circulation*. 2002;33:1551-1556
 50. Hacke W, Donnan G, Fieschi C, Kaste M, von Kummer R, Broderick JP, et al. Association of outcome with early stroke treatment: Pooled analysis of atlantis, ecass, and ninds rt-pa stroke trials. *Lancet*. 2004;363:768-774
 51. Albers GW, Thijs VN, Wechsler L, Kemp S, Schlaug G, Skalabrin E, et al. Magnetic resonance imaging profiles predict clinical response to early reperfusion: The diffusion and perfusion imaging evaluation for understanding stroke evolution (defuse) study. *Annals of neurology*. 2006;60:508-517
 52. Dzialowski I, Pexman JH, Barber PA, Demchuk AM, Buchan AM, Hill MD. Asymptomatic hemorrhage after thrombolysis may not be benign: Prognosis by hemorrhage type in the canadian alteplase for stroke effectiveness study registry. *Stroke; a journal of cerebral circulation*. 2007;38:75-79
 53. Thomalla G, Sobesky J, Kohrmann M, Fiebach JB, Fiehler J, Zaro Weber O, et al. Two tales: Hemorrhagic transformation but not parenchymal hemorrhage after thrombolysis is related to severity and duration of ischemia: Mri study of acute stroke patients treated with intravenous tissue plasminogen activator within 6 hours. *Stroke; a journal of cerebral circulation*. 2007;38:313-318
 54. Demchuk AM, Morgenstern LB, Krieger DW, Linda Chi T, Hu W, Wein TH, et al. Serum glucose level and diabetes predict tissue plasminogen activator-related intracerebral hemorrhage in acute ischemic stroke. *Stroke*. 1999;30:34-39
 55. Montaner J. Stroke biomarkers: Can they help us to guide stroke thrombolysis? *Drug News Perspect*. 2006;19:523-532

56. Selim M, Fink JN, Kumar S, Caplan LR, Horkan C, Chen Y, et al. Predictors of hemorrhagic transformation after intravenous recombinant tissue plasminogen activator: Prognostic value of the initial apparent diffusion coefficient and diffusion-weighted lesion volume. *Stroke; a journal of cerebral circulation*. 2002;33:2047-2052
57. Knauer C, Knauer K, Muller S, Ludolph AC, Bengel D, Muller HP, et al. A biochemical marker panel in mri-proven hyperacute ischemic stroke - a prospective study. *BMC Neurol*.12:14
58. Kawano H, Hirano T, Nakajima M, Inatomi Y, Yonehara T, Uchino M. Modified aspects for dwi including deep white matter lesions predicts subsequent intracranial hemorrhage. *Journal of neurology*. 2007:120-28
59. Dankbaar JW, Hom J, Schneider T, Cheng SC, Lau BC, van der Schaaf I, et al. Dynamic perfusion ct assessment of the blood-brain barrier permeability: First pass versus delayed acquisition. *AJNR. American journal of neuroradiology*. 2008;29:1671-1676
60. Tuhim S, Horowitz DR, Sacher M, Godbold JH. Validation and comparison of models predicting survival following intracerebral hemorrhage. *Critical care medicine*. 1995;23:950-954
61. Kidwell CS, Saver JL, Mattiello J, Warach S, Liebeskind DS, Starkman S, et al. Diffusion-perfusion mr evaluation of perihematomal injury in hyperacute intracerebral hemorrhage. *Neurology*. 2001;57:1611-1617
62. Kazui S, Naritomi H, Yamamoto H, Sawada T, Yamaguchi T. Enlargement of spontaneous intracerebral hemorrhage. Incidence and time course. *Stroke; a journal of cerebral circulation*. 1996;27:1783-1787
63. Aronowski J, Zhao X. Molecular pathophysiology of cerebral hemorrhage: Secondary brain injury. *Stroke; a journal of cerebral circulation*. 2011;42:1781-1786
64. Xi G, Keep RF, Hoff JT. Mechanisms of brain injury after intracerebral haemorrhage. *Lancet neurology*. 2006;5:53-63
65. Broderick JP, Diringer MN, Hill MD, Brun NC, Mayer SA, Steiner T, et al. Determinants of intracerebral hemorrhage growth: An exploratory analysis. *Stroke; a journal of cerebral circulation*. 2007;38:1072-1075
66. Warach S. Editorial comment--is there a perihematomal ischemic penumbra? More questions and an overlooked clue. *Stroke; a journal of cerebral circulation*. 2003;34:1680

67. Powers WJ, Zazulia AR, Videen TO, Adams RE, Yundt KD, Aiyagari V, et al. Autoregulation of cerebral blood flow surrounding acute (6 to 22 hours) intracerebral hemorrhage. *Neurology*. 2001;57:18-24
68. Schellinger PD, Fiebich JB, Hoffmann K, Becker K, Orakcioglu B, Kollmar R, et al. Stroke mri in intracerebral hemorrhage: Is there a perihemorrhagic penumbra? *Stroke; a journal of cerebral circulation*. 2003;34:1674-1679
69. Heiss WD, Huber M, Fink GR, Herholz K, Pietrzyk U, Wagner R, et al. Progressive derangement of periinfarct viable tissue in ischemic stroke. *Journal of cerebral blood flow and metabolism : official journal of the International Society of Cerebral Blood Flow and Metabolism*. 1992;12:193-203
70. Kaur J, Zhao Z, Klein GM, Lo EH, Buchan AM. The neurotoxicity of tissue plasminogen activator? *Journal of cerebral blood flow and metabolism : official journal of the International Society of Cerebral Blood Flow and Metabolism*. 2004;24:945-963
71. Schumacher HC, Bateman BT, Boden-Albala B, Berman MF, Mohr JP, Sacco RL, et al. Use of thrombolysis in acute ischemic stroke: Analysis of the nationwide inpatient sample 1999 to 2004. *Ann Emerg Med*. 2007;50:99-107
72. Fang MC, Cutler DM, Rosen AB. Trends in thrombolytic use for ischemic stroke in the united states. *J Hosp Med*.5:406-409
73. Bluhmki E, Chamorro A, Davalos A, Machnig T, Sauce C, Wahlgren N, et al. Stroke treatment with alteplase given 3.0-4.5 h after onset of acute ischaemic stroke (ecass iii): Additional outcomes and subgroup analysis of a randomised controlled trial. *Lancet neurology*. 2009;8:1095-1102
74. Wahlgren N, Ahmed N, Davalos A, Hacke W, Millan M, Muir K, et al. Thrombolysis with alteplase 3-4.5 h after acute ischaemic stroke (sits-istr): An observational study. *Lancet*. 2008;372:1303-1309
75. Hacke W, Kaste M, Bluhmki E, Brozman M, Davalos A, Guidetti D, et al. Thrombolysis with alteplase 3 to 4.5 hours after acute ischemic stroke. *The New England journal of medicine*. 2008;359:1317-1329
76. Aviv RI, d'Este CD, Murphy BD, Hopyan JJ, Buck B, Mallia G, et al. Hemorrhagic transformation of ischemic stroke: Prediction with ct perfusion. *Radiology*. 2009;250:867-877
77. Tong D. Are all iv thrombolysis exclusion criteria necessary? Being smart about evidence-based medicine. *Neurology*. 2011;76:1780-1781
78. Mathews MS, Sharma J, Snyder KV, Natarajan SK, Siddiqui AH, Hopkins LN, et al. Safety, effectiveness, and practicality of endovascular therapy within the first 3

- hours of acute ischemic stroke onset. *Neurosurgery*. 2009;65:860-865; discussion 865
79. Lee M, Hong KS, Saver JL. Efficacy of intra-arterial fibrinolysis for acute ischemic stroke: Meta-analysis of randomized controlled trials. *Stroke; a journal of cerebral circulation*. 2010;41:932-937
 80. Gobin YP, Starkman S, Duckwiler GR, Grobelny T, Kidwell CS, Jahan R, et al. Merci 1: A phase 1 study of mechanical embolus removal in cerebral ischemia. *Stroke; a journal of cerebral circulation*. 2004;35:2848-2854
 81. Tenser MS, Amar AP, Mack WJ. Mechanical thrombectomy for acute ischemic stroke using the merci retriever and penumbra aspiration systems. *World neurosurgery*.76:S16-23
 82. Baker WL, Colby JA, Tongbram V, Talati R, Silverman IE, White CM, et al. Neurothrombectomy devices for the treatment of acute ischemic stroke: State of the evidence. *Annals of internal medicine*.154:243-252
 83. Wahlgren NG, Ahmed N. Neuroprotection in cerebral ischaemia: Facts and fancies--the need for new approaches. *Cerebrovascular diseases*. 2004;17 Suppl 1:153-166
 84. Saver JL. Clinical impact of nxy-059 demonstrated in the saint i trial: Derivation of number needed to treat for benefit over entire range of functional disability. *Stroke; a journal of cerebral circulation*. 2007;38:1515-1518
 85. Cook DJ, Teves L, Tymianski M. A translational paradigm for the preclinical evaluation of the stroke neuroprotectant tat-nr2b9c in gyrencephalic nonhuman primates. *Science translational medicine*. 2012;4:154ra133
 86. Hill MD, Martin RH, Mikulis D, Wong JH, Silver FL, Terbrugge KG, et al. Safety and efficacy of na-1 in patients with iatrogenic stroke after endovascular aneurysm repair (enact): A phase 2, randomised, double-blind, placebo-controlled trial. *Lancet neurology*. 2012;11:942-950
 87. Sanossian N, Saver JL, Rajajee V, Selco SL, Kim D, Razinia T, et al. Premorbid antiplatelet use and ischemic stroke outcomes. *Neurology*. 2006;66:319-323
 88. Kim WJ, Ko Y, Yang MH, Im SH, Park JH, Lee J, et al. Differential effect of previous antiplatelet use on stroke severity according to stroke mechanism. *Stroke; a journal of cerebral circulation*. 2010;41:1200-1204
 89. Ovbiagele B, Buck BH, Liebeskind DS, Starkman S, Bang OY, Ali LK, et al. Prior antiplatelet use and infarct volume in ischemic stroke. *Journal of the neurological sciences*. 2008;264:140-144

90. Hoesch RE, Geocadin RG. Therapeutic hypothermia for global and focal ischemic brain injury--a cool way to improve neurologic outcomes. *The neurologist*. 2007;13:331-342
91. Kallmunzer B, Schwab S, Kollmar R. Mild hypothermia of 34 degrees c reduces side effects of rt-pa treatment after thromboembolic stroke in rats. *Experimental & translational stroke medicine*. 2012;4:3
92. Lakhan SE, Pamplona F. Application of mild therapeutic hypothermia on stroke: A systematic review and meta-analysis. *Stroke research and treatment*. 2012;2012:295906
93. Zhang Y, Reilly KH, Tong W, Xu T, Chen J, Bazzano LA, et al. Blood pressure and clinical outcome among patients with acute stroke in inner mongolia, china. *Journal of hypertension*. 2008;26:1446-1452
94. Broderick J, Connolly S, Feldmann E, Hanley D, Kase C, Krieger D, et al. Guidelines for the management of spontaneous intracerebral hemorrhage in adults: 2007 update: A guideline from the american heart association/american stroke association stroke council, high blood pressure research council, and the quality of care and outcomes in research interdisciplinary working group. *Stroke; a journal of cerebral circulation*. 2007;38:2001-2023
95. Tan G, Zhou J, Yuan D, Sun S. Formula for use of mannitol in patients with intracerebral haemorrhage and high intracranial pressure. *Clinical drug investigation*. 2008;28:81-87
96. Herweh C, Juttler E, Schellinger PD, Klotz E, Schramm P. Perfusion ct in hyperacute cerebral hemorrhage within 3 hours after symptom onset: Is there an early perihemorrhagic penumbra? *Journal of neuroimaging : official journal of the American Society of Neuroimaging*. 20:350-353
97. Mayer SA, Brun NC, Begtrup K, Broderick J, Davis S, Diringer MN, et al. Recombinant activated factor vii for acute intracerebral hemorrhage. *The New England journal of medicine*. 2005;352:777-785
98. Mayer SA, Brun NC, Begtrup K, Broderick J, Davis S, Diringer MN, et al. Efficacy and safety of recombinant activated factor vii for acute intracerebral hemorrhage. *The New England journal of medicine*. 2008;358:2127-2137
99. Sahni R, Weinberger J. Management of intracerebral hemorrhage. *Vascular health and risk management*. 2007;3:701-709
100. Gregson BA, Murray GD, Mitchell PM, Rowan EN, Gholkar AR, Mendelow AD. Update on the surgical trial in lobar intracerebral haemorrhage (stich ii): Statistical analysis plan. *Trials*. 2012;13:222

101. Lapointe M, Haines S. Fibrinolytic therapy for intraventricular hemorrhage in adults. *Cochrane database of systematic reviews (Online)*. 2002:CD003692
102. Morgenstern LB, Demchuk AM, Kim DH, Frankowski RF, Grotta JC. Rebleeding leads to poor outcome in ultra-early craniotomy for intracerebral hemorrhage. *Neurology*. 2001;56:1294-1299
103. Aguilar MI, Freeman WD. Spontaneous intracerebral hemorrhage. *Seminars in neurology*. 2010;30:555-564
104. Powers WJ, Zazulia AR. The use of positron emission tomography in cerebrovascular disease. *Neuroimaging clinics of North America*. 2003;13:741-758
105. Heiss WD, Grond M, Thiel A, von Stockhausen HM, Rudolf J, Ghaemi M, et al. Tissue at risk of infarction rescued by early reperfusion: A positron emission tomography study in systemic recombinant tissue plasminogen activator thrombolysis of acute stroke. *Journal of cerebral blood flow and metabolism : official journal of the International Society of Cerebral Blood Flow and Metabolism*. 1998;18:1298-1307
106. Walberer M, Backes H, Rueger MA, Neumaier B, Endepols H, Hoehn M, et al. Potential of early [(18)f]-2-fluoro-2-deoxy-d-glucose positron emission tomography for identifying hypoperfusion and predicting fate of tissue in a rat embolic stroke model. *Stroke; a journal of cerebral circulation*. 2012;43:193-198
107. Spratt NJ, Donnan GA, McLeod DD, Howells DW. 'Salvaged' stroke ischaemic penumbra shows significant injury: Studies with the hypoxia tracer fmiso. *Journal of cerebral blood flow and metabolism : official journal of the International Society of Cerebral Blood Flow and Metabolism*. 2011;31:934-943
108. Gerhard A, Schwarz J, Myers R, Wise R, Banati RB. Evolution of microglial activation in patients after ischemic stroke: A [11c](r)-pk11195 pet study. *NeuroImage*. 2005;24:591-595
109. Radlinska BA, Ghinani SA, Lyon P, Jolly D, Soucy JP, Minuk J, et al. Multimodal microglia imaging of fiber tracts in acute subcortical stroke. *Annals of neurology*. 2009;66:825-832
110. Rosso C, Hevia-Montiel N, Deltour S, Bardinet E, Dormont D, Crozier S, et al. Prediction of infarct growth based on apparent diffusion coefficients: Penumbra assessment without intravenous contrast material. *Radiology*. 2009;250:184-192
111. Crisostomo RA, Garcia MM, Tong DC. Detection of diffusion-weighted mri abnormalities in patients with transient ischemic attack: Correlation with clinical characteristics. *Stroke; a journal of cerebral circulation*. 2003;34:932-937

112. Edlow JA. Evidence-based guideline: The role of diffusion and perfusion mri for the diagnosis of acute ischemic stroke: Report of the therapeutics and technology subcommittee of the american academy of neurology. *Neurology*. 2011;76:2036; author reply 2038
113. Ringer TM, Neumann-Haefelin T, Sobel RA, Moseley ME, Yenari MA. Reversal of early diffusion-weighted magnetic resonance imaging abnormalities does not necessarily reflect tissue salvage in experimental cerebral ischemia. *Stroke; a journal of cerebral circulation*. 2001;32:2362-2369
114. Labeyrie MA, Turc G, Hess A, Hervo P, Mas JL, Meder JF, et al. Diffusion lesion reversal after thrombolysis: A mr correlate of early neurological improvement. *Stroke; a journal of cerebral circulation*. 2012;43:2986-2991
115. Kidwell CS, Saver JL, Mattiello J, Starkman S, Vinuela F, Duckwiler G, et al. Thrombolytic reversal of acute human cerebral ischemic injury shown by diffusion/perfusion magnetic resonance imaging. *Annals of neurology*. 2000;47:462-469
116. Kranz PG, Eastwood JD. Does diffusion-weighted imaging represent the ischemic core? An evidence-based systematic review. *AJNR. American journal of neuroradiology*. 2009;30:1206-1212
117. Shih LC, Saver JL, Alger JR, Starkman S, Leary MC, Vinuela F, et al. Perfusion-weighted magnetic resonance imaging thresholds identifying core, irreversibly infarcted tissue. *Stroke; a journal of cerebral circulation*. 2003;34:1425-1430
118. Kassner A, Mandell DM, Mikulis DJ. Measuring permeability in acute ischemic stroke. *Neuroimaging clinics of North America*. 2011;21:315-325
119. Parsons MW, Yang Q, Barber PA, Darby DG, Desmond PM, Gerraty RP, et al. Perfusion magnetic resonance imaging maps in hyperacute stroke: Relative cerebral blood flow most accurately identifies tissue destined to infarct. *Stroke; a journal of cerebral circulation*. 2001;32:1581-1587
120. Deipolyi AR, Wu O, Macklin EA, Schaefer PW, Schwamm LH, Gilberto Gonzalez R, et al. Reliability of cerebral blood volume maps as a substitute for diffusion-weighted imaging in acute ischemic stroke. *Journal of magnetic resonance imaging : JMRI*. 2012;36:1083-1087
121. Calamante F, Christensen S, Desmond PM, Ostergaard L, Davis SM, Connelly A. The physiological significance of the time-to-maximum (tmax) parameter in perfusion mri. *Stroke; a journal of cerebral circulation*. 2010;41:1169-1174
122. Olivot JM, Mlynash M, Thijs VN, Kemp S, Lansberg MG, Wechsler L, et al. Optimal tmax threshold for predicting penumbral tissue in acute stroke. *Stroke; a journal of cerebral circulation*. 2009;40:469-475

123. Heiss WD, Sobesky J, Hesselmann V. Identifying thresholds for penumbra and irreversible tissue damage. *Stroke; a journal of cerebral circulation*. 2004;35:2671-2674
124. Chen F, Ni YC. Magnetic resonance diffusion-perfusion mismatch in acute ischemic stroke: An update. *World journal of radiology*. 2012;4:63-74
125. Kassner A, Roberts T, Taylor K, Silver F, Mikulis D. Prediction of hemorrhage in acute ischemic stroke using permeability mr imaging. *AJNR. American journal of neuroradiology*. 2005;26:2213-2217
126. Bang OY, Buck BH, Saver JL, Alger JR, Yoon SR, Starkman S, et al. Prediction of hemorrhagic transformation after recanalization therapy using t2*-permeability magnetic resonance imaging. *Annals of neurology*. 2007;62:170-176
127. Muir KW, Baird-Gunning J, Walker L, Baird T, McCormick M, Coutts SB. Can the ischemic penumbra be identified on noncontrast ct of acute stroke? *Stroke; a journal of cerebral circulation*. 2007;38:2485-2490
128. Butcher KS, Lee SB, Parsons MW, Allport L, Fink J, Tress B, et al. Differential prognosis of isolated cortical swelling and hypoattenuation on ct in acute stroke. *Stroke; a journal of cerebral circulation*. 2007;38:941-947
129. Grond M, von Kummer R, Sobesky J, Schmulling S, Rudolf J, Terstegge K, et al. Early x-ray hypoattenuation of brain parenchyma indicates extended critical hypoperfusion in acute stroke. *Stroke; a journal of cerebral circulation*. 2000;31:133-139
130. Drayer BP, Dujovny M, Wolfson SK, Jr., Boehnke M, Cook EE, Rosenbaum AE. Comparative cranial ct enhancement in a primate model of cerebral infarction. *Annals of neurology*. 1979;5:48-58
131. Dzialowski I, Weber J, Doerfler A, Forsting M, von Kummer R. Brain tissue water uptake after middle cerebral artery occlusion assessed with ct. *Journal of neuroimaging : official journal of the American Society of Neuroimaging*. 2004;14:42-48
132. Nag C, Das K, Ghosh M, Khandakar MR. Prediction of clinical outcome in acute hemorrhagic stroke from a single ct scan on admission. *North American journal of medical sciences*. 2012;4:463-467
133. Kalafut MA, Schriger DL, Saver JL, Starkman S. Detection of early ct signs of >1/3 middle cerebral artery infarctions : Interrater reliability and sensitivity of ct interpretation by physicians involved in acute stroke care. *Stroke; a journal of cerebral circulation*. 2000;31:1667-1671

134. Pexman JH, Barber PA, Hill MD, Sevick RJ, Demchuk AM, Hudon ME, et al. Use of the alberta stroke program early ct score (aspects) for assessing ct scans in patients with acute stroke. *AJNR. American journal of neuroradiology*. 2001;22:1534-1542
135. Barber PA, Demchuk AM, Zhang J, Buchan AM. Validity and reliability of a quantitative computed tomography score in predicting outcome of hyperacute stroke before thrombolytic therapy. Aspects study group. Alberta stroke programme early ct score. *Lancet*. 2000;355:1670-1674
136. Dzialowski I, Hill MD, Coutts SB, Demchuk AM, Kent DM, Wunderlich O, et al. Extent of early ischemic changes on computed tomography (ct) before thrombolysis: Prognostic value of the alberta stroke program early ct score in ecass ii. *Stroke; a journal of cerebral circulation*. 2006;37:973-978
137. Kim J, Smith A, Hemphill JC, 3rd, Smith WS, Lu Y, Dillon WP, et al. Contrast extravasation on ct predicts mortality in primary intracerebral hemorrhage. *AJNR. American journal of neuroradiology*. 2008;29:520-525
138. Wada R, Aviv RI, Fox AJ, Sahlas DJ, Gladstone DJ, Tomlinson G, et al. Ct angiography "spot sign" predicts hematoma expansion in acute intracerebral hemorrhage. *Stroke; a journal of cerebral circulation*. 2007;38:1257-1262
139. Becker KJ, Baxter AB, Bybee HM, Tirschwell DL, Abouelsaad T, Cohen WA. Extravasation of radiographic contrast is an independent predictor of death in primary intracerebral hemorrhage. *Stroke; a journal of cerebral circulation*. 1999;30:2025-2032
140. Goldstein JN, Fazen LE, Snider R, Schwab K, Greenberg SM, Smith EE, et al. Contrast extravasation on ct angiography predicts hematoma expansion in intracerebral hemorrhage. *Neurology*. 2007;68:889-894
141. Delgado Almandoz JE, Yoo AJ, Stone MJ, Schaefer PW, Oleinik A, Brouwers HB, et al. The spot sign score in primary intracerebral hemorrhage identifies patients at highest risk of in-hospital mortality and poor outcome among survivors. *Stroke; a journal of cerebral circulation*. 41:54-60
142. Sillanpaa N, Saarinen JT, Rusanen H, Hakomaki J, Lahteela A, Numminen H, et al. The clot burden score, the boston acute stroke imaging scale, the cerebral blood volume aspects, and two novel imaging parameters in the prediction of clinical outcome of ischemic stroke patients receiving intravenous thrombolytic therapy. *Neuroradiology*. 2010; 23:25-31
143. Torres-Mozqueda F, He J, Yeh IB, Schwamm LH, Lev MH, Schaefer PW, et al. An acute ischemic stroke classification instrument that includes ct or mr angiography: The boston acute stroke imaging scale. *AJNR. American journal of neuroradiology*. 2008;29:1111-1117

144. Fainardi E, Borrelli M, Saletti A, Schivalocchi R, Azzini C, Cavallo M, et al. Ct perfusion mapping of hemodynamic disturbances associated to acute spontaneous intracerebral hemorrhage. *Neuroradiology*. 2008;50:729-740
145. Rosand J, Eskey C, Chang Y, Gonzalez RG, Greenberg SM, Koroshetz WJ. Dynamic single-section ct demonstrates reduced cerebral blood flow in acute intracerebral hemorrhage. *Cerebrovasc Dis*. 2002;14:214-220
146. Butcher KS, Baird T, MacGregor L, Desmond P, Tress B, Davis S. Perihematomal edema in primary intracerebral hemorrhage is plasma derived. *Stroke*. 2004;35:1879-1885
147. d'Esterre CD, Aviv RI, Lee TY. The evolution of the cerebral blood volume abnormality in patients with ischemic stroke: A ct perfusion study. *Acta radiologica*. 2012;53:461-467
148. Schaefer PW, Roccatagliata L, Ledezma C, Hoh B, Schwamm LH, Koroshetz W, et al. First-pass quantitative ct perfusion identifies thresholds for salvageable penumbra in acute stroke patients treated with intra-arterial therapy. *AJNR. American journal of neuroradiology*. 2006;27:20-25
149. Simon JE, Bristow MS, Lu H, Lauzon ML, Brown RA, Manjon JV, et al. A novel method to derive separate gray and white matter cerebral blood flow measures from mr imaging of acute ischemic stroke patients. *J Cereb Blood Flow Metab*. 2005;25:1236-1243
150. Murphy BD, Fox AJ, Lee DH, Sahlas DJ, Black SE, Hogan MJ, et al. White matter thresholds for ischemic penumbra and infarct core in patients with acute stroke: Ct perfusion study. *Radiology*. 2008;247:818-825
151. Murphy BD, Fox AJ, Lee DH, Sahlas DJ, Black SE, Hogan MJ, et al. Identification of penumbra and infarct in acute ischemic stroke using computed tomography perfusion-derived blood flow and blood volume measurements. *Stroke; a journal of cerebral circulation*. 2006;37:1771-1777
152. Kamalian S, Kamalian S, Maas MB, Goldmacher GV, Payabvash S, Akbar A, et al. Ct cerebral blood flow maps optimally correlate with admission diffusion-weighted imaging in acute stroke but thresholds vary by postprocessing platform. *Stroke; a journal of cerebral circulation*. 2011;42:1923-1928
153. Campbell BC, Christensen S, Levi CR, Desmond PM, Donnan GA, Davis SM, et al. Cerebral blood flow is the optimal ct perfusion parameter for assessing infarct core. *Stroke; a journal of cerebral circulation*. 2011;42:3435-3440

154. Wintermark M, Flanders AE, Velthuis B, Meuli R, van Leeuwen M, Goldsher D, et al. Perfusion-ct assessment of infarct core and penumbra: Receiver operating characteristic curve analysis in 130 patients suspected of acute hemispheric stroke. *Stroke; a journal of cerebral circulation*. 2006;37:979-985
155. Lee TY. Functional ct: Physiological models. *Trends in Biotechnology*. 2002;20:suppl
156. Wintermark M, Smith WS, Ko NU, Quist M, Schnyder P, Dillon WP. Dynamic perfusion ct: Optimizing the temporal resolution and contrast volume for calculation of perfusion ct parameters in stroke patients. *AJNR Am J Neuroradiol*. 2004;25:720-729
157. Wintermark M, Reichhart M, Thiran JP, Maeder P, Chalaron M, Schnyder P, et al. Prognostic accuracy of cerebral blood flow measurement by perfusion computed tomography, at the time of emergency room admission, in acute stroke patients. *Annals of neurology*. 2002;51:417-432
158. Lencioni R, Fattori R, Morana G, Stacul F. Contrast-induced nephropathy in patients undergoing computed tomography (connect) - a clinical problem in daily practice? A multicenter observational study. *Acta Radiol*.51:741-750
159. d'Esterre CD, Chia TL, Jairath A, Lee TY, Symons SP, Aviv RI. Early rate of contrast extravasation in patients with intracerebral hemorrhage. *AJNR. American journal of neuroradiology*.32:1879-1884
160. Hom J, Dankbaar JW, Soares BP, Schneider T, Cheng SC, Bredno J, et al. Blood-brain barrier permeability assessed by perfusion ct predicts symptomatic hemorrhagic transformation and malignant edema in acute ischemic stroke. *AJNR. American journal of neuroradiology*.32:41-48
161. Wintermark M, Albers GW, Alexandrov AV, Alger JR, Bammer R, Baron JC, et al. Acute stroke imaging research roadmap. *Stroke; a journal of cerebral circulation*. 2008;39:1621-1628
162. Frey GD, Rumboldt Z. Radiation effects from perfusion ct. *Radiology*. 2005;234:638
163. Rapalino O, Kamalian S, Payabvash S, Souza LC, Zhang D, Mukta J, et al. Cranial ct with adaptive statistical iterative reconstruction: Improved image quality with concomitant radiation dose reduction. *AJNR. American journal of neuroradiology*. 2009;56:98-103
164. Wang JY, Xia Q, Chu KT, Pan J, Sun LN, Zeng B, et al. Severe global cerebral ischemia-induced programmed necrosis of hippocampal cal neurons in rat is prevented by 3-methyladenine: A widely used inhibitor of autophagy. *Journal of neuropathology and experimental neurology*. 2011;70:314-322

165. Colbourne F, Li H, Buchan AM, Clemens JA. Continuing postischemic neuronal death in ca1: Influence of ischemia duration and cytoprotective doses of nbqx and snx-111 in rats. *Stroke; a journal of cerebral circulation*. 1999;30:662-668
166. Engel O, Kolodziej S, Dirnagl U, Prinz V. Modeling stroke in mice - middle cerebral artery occlusion with the filament model. *Journal of visualized experiments : JoVE*. 2011; 34-38
167. Gu W, Jiang W, Wester P. A photothrombotic ring stroke model in rats with sustained hypoperfusion followed by late spontaneous reperfusion in the region at risk. *Experimental brain research. Experimentelle Hirnforschung. Experimentation cerebrale*. 1999;125:163-170
168. Tamura A, Graham DI, McCulloch J, Teasdale GM. Focal cerebral ischaemia in the rat: 1. Description of technique and early neuropathological consequences following middle cerebral artery occlusion. *Journal of cerebral blood flow and metabolism : official journal of the International Society of Cerebral Blood Flow and Metabolism*. 1981;1:53-60
169. Zubkov AY, Rollins KS, Parent AD, Zhang J, Bryan RM, Jr. Mechanism of endothelin-1-induced contraction in rabbit basilar artery. *Stroke; a journal of cerebral circulation*. 2000;31:526-533
170. Lapchak PA, Araujo DM, Pakola S, Song D, Wei J, Zivin JA. Microplasmin: A novel thrombolytic that improves behavioral outcome after embolic strokes in rabbits. *Stroke; a journal of cerebral circulation*. 2002;33:2279-2284
171. Zivin JA, Fisher M, DeGirolami U, Hemenway CC, Stashak JA. Tissue plasminogen activator reduces neurological damage after cerebral embolism. *Science (New York, N.Y.)*. 1985;230:1289-1292
172. Lapchak PA, Araujo DM, Song D, Wei J, Purdy R, Zivin JA. Effects of the spin trap agent disodium- [tert-butylimino)methyl]benzene-1,3-disulfonate n-oxide (generic nxy-059) on intracerebral hemorrhage in a rabbit large clot embolic stroke model: Combination studies with tissue plasminogen activator. *Stroke; a journal of cerebral circulation*. 2002;33:1665-1670
173. Pavlovic AM, Dobricic V, Semnic R, Lackovic V, Novakovic I, Bajcetic M, et al. A novel notch3 gly89cys mutation in a serbian cadasil family. *Acta neurologica Belgica*. 2013;25:110-117
174. Ayata C. Cadasil: Experimental insights from animal models. *Stroke; a journal of cerebral circulation*. 2010;41:S129-134
175. Johnson RA, Belmonte A, Fan NY, Lavesa M, Nasjletti A, Stier CT, Jr. Effect of ifetroban, a thromboxane a2 receptor antagonist, in stroke-prone spontaneously hypertensive rats. *Clinical and experimental hypertension*. 1996;18:171-188

176. Chang CF, Chen SF, Lee TS, Lee HF, Chen SF, Shyue SK. Caveolin-1 deletion reduces early brain injury after experimental intracerebral hemorrhage. *The American journal of pathology*. 2011;178:1749-1761
177. MacLellan CL, Paquette R, Colbourne F. A critical appraisal of experimental intracerebral hemorrhage research. *Journal of cerebral blood flow and metabolism : official journal of the International Society of Cerebral Blood Flow and Metabolism*. 2012;32:612-627

CHAPTER 2

The Evolution of the Cerebral Blood Volume Abnormality in Patients with Ischemic Stroke

The contents of this chapter have been adapted from the paper entitled “The evolution of the cerebral blood volume abnormality in patients with ischemic stroke: a CT perfusion study”, published in *Acta Radiologica* 2012;53(4):461-7 by C.D. d’Esterre, R.I. Aviv, and T.Y. Lee.

2.1 INTRODUCTION

When a cerebrovascular accident of thromboembolic origin occurs, the primary objective is to salvage tissue at-risk (penumbra) by limiting infarct expansion. Treatment with tissue plasminogen activator (tPA) up to 4.5 hours post stroke onset has shown to be clinically effective in this regard¹. Yet, the triggering of clinically adverse events, such as hemorrhagic transformation, remains a concern anytime thrombolysis treatment is given². Recent studies have shown that hemorrhage risk post revascularization and clinical outcome are highly correlated with final infarct volume and acute (< 6 hours post ictus) infarct volume, respectively^{3, 4}. In conjunction with the admission National Institutes of Health Stroke Scale (NIHSS) score, the acute infarct core could be used to indicate the amount of tissue at-risk – presumably, a small infarct core at onset combined with a high NIHSS score suggests there is a substantial amount of electrically silent but viable tissue. Therefore, acute infarct core quantification during the acute stroke setting bears high clinical significance, potentially guiding acute stroke treatment.

Numerous attempts to identify admission imaging thresholds for delineation of non-viable cerebral tissue have been extensive, resulting in a wide range of values⁵⁻¹⁰. One modality, magnetic resonance (MR) diffusion weighted imaging (DWI), has the capability to detect cerebral infarction within hours of stroke onset with high sensitivity, and is correlated with clinical outcome days later¹¹⁻¹³. Nonetheless, there are instances where DWI hyperintensities have been shown to reverse following successful thrombolysis¹⁴⁻¹⁷. This overestimation of acute infarct volume may falsely exclude patients from receiving thrombolytic therapy^{17, 18}. Further, the limited availability of MR imaging during the acute stroke setting promotes the use of other imaging modalities.

Due to its accessibility and simplicity, computed tomography (CT) is suitable for diagnosis ischemic stroke. Although the Alberta Stroke Program Early CT Score (ASPECTS) has proven to be a reliable indicator of early ischemic change using only a standard CT examination, irreversibly damaged tissue and/or tissue at risk of progression to infarction may still exist within normal appearing regions on hyper-acute non-contrast CT (NCCT)^{19, 20}. CT perfusion (CTP) ASPECTS has been shown to provide some advantage over NCCT for clinical outcome prediction, and detecting reversible ischemia²¹. Specifically, the CBV-ASPECTS emerged as the best predictor of fatal stroke in the hyperacute state²²; however, due to high correlation between predicted infarct volumes defined by DWI- and CBV-defects, speculation concerning the evolution of CBV within critically hypoperfused tissue is vindicated^{23, 24}. Therefore, we sought to examine: (1) the temporal profile of CTP-derived CBV within tissue that progresses to infarction (CBV_I) at admission, 24 hours and 5-7 days post stroke onset to determine if CBV_I, like DWI defects, can normalize, and (2) the possible overestimation of predicted infarct volume as defined by the CBV abnormality.

2.2 MATERIALS & METHODS

2.2.1 *Participants and study design*

Ethics approval was obtained from both participating institutions⁺. Informed consent was obtained from patients and family members. Patients were eligible for inclusion in the study if they: showed signs and symptoms of middle cerebral artery occlusion, had CTA confirmed recanalization, presented at the hospital < 6 hours post symptom onset, had no previous stroke, NIHSS > 4, had a CT perfusion (CTP) scan at admission, 24 hour and 5-7 post ictus, and had a delayed non-contrast CT (NCCT) to quantify final infarct size. Exclusion criteria were as follows: evidence of brain stem infarct, prior stroke with residual deficit intracranial hemorrhage, minor stroke symptoms (NIHSS score < 4), clinically significant hyperglycemia, impaired renal function and/or known allergy to contrast media; pregnancy, and age less than 18 years. Patients were enrolled regardless of therapy, and results of the CT perfusion study performed at admission did not influence treatment decisions (patients and family members providing informed consent were aware of this).

⁺ Appendix A – Human Ethics Approval Form

2.2.2 CT imaging procedures

Imaging was performed on a Lightspeed CT scanner (GE Healthcare, Milwaukee, WI, USA) at Sunnybrook Health Sciences Center, Toronto Canada. Thirteen patients had a non-contrast CT (NCCT), CT angiography (CTA), and CT perfusion (CTP) scan at admission and 24 hours, and NCCT and CTP 5-7 days post admission. Thirty-two patients had a NCCT, CTA, and CTP scan at admission, and NCCT/CTA and 5-7 days post admission. NCCT scans were performed using the following parameters: 120 kVp, 340 mA, 4 x 5 mm collimation, 1 second/rotation. CTA scan covered from the carotid bifurcation through to the vertex and was acquired using 0.7 ml/kg contrast agent, at 120 kVp and 270 mA, 1 sec/rotation, 1.25 mm thick slices, and pitch of 0.75. Recanalization was characterized as no visible narrowing of the vessel, while occlusion was characterized by the absence of contrast material distal to the thrombus on the CTA, based on an adaptation of the thrombolysis in myocardial infarction criteria²⁵. CTP images were collected from the basal ganglia to the lateral ventricles, with 4 x 5 mm thick slices acquired at 80 kVp and 190 mAs for 60 seconds. Iodinated contrast agent, Omnipaque (300 mg iodine per milliliter; Iohexol; GE Healthcare, Mississauga, Ontario, Canada) was injected (0.5 ml/kg) at a rate of 4 ml/sec.

An overview of the CTP image processing was provided in Chapter 1. Briefly, each CTP imaging study was analyzed using commercially available CT perfusion, delay-insensitive software (version 4, GE Healthcare, Milwaukee, WI, USA). For each CTP scan, time-density curves (TDC) for the arterial input function (AIF) and venous output functions (VOF) were obtained from the anterior cerebral artery and superior sagittal sinus, respectively. The AIF was corrected for partial volume averaging by scaling its area relative to that of the VOF-TDC; partial volume averaging effects are minimal in the

sagittal sinus²⁶. Parametric maps of cerebral blood flow [CBF; $\text{ml}\cdot\text{min}^{-1}\cdot(100\text{g})^{-1}$] and cerebral blood volume [CBV; $\text{ml}\cdot(100\text{g})^{-1}$] were calculated by deconvolution of tissue TDCs and the AIF; these values have been validated by using microspheres in animal studies and positron emission tomography (PET) in humans^{27, 28}. Perfusion weighted maps were created by averaging the cine CTP images over the duration of the first pass of contrast.

2.2.3 CTP image analysis

Custom software (IDL, version 6.2, RSI, Boulder, Colorado) was used for all post processing analysis. Analysis was performed while blinded to results from imaging at each time point, as well as to clinical outcomes.

2.2.3.1 The 5-7 day evolution of CBV within tissue destined to infarct

Group A was used for this analysis (Table 2.1). Delayed NCCT images were registered with admission, 24 hour and 5-7 post admission parametric maps by adjusting for in-plane rotational changes. Final infarct regions of interest (ROI), as defined by areas of hypoattenuation, were traced onto the delayed NCCT images by an experienced neuroradiologist of 5 years. These ROIs were superimposed onto CBF and CBV parametric maps at each time point, avoiding cerebrospinal fluid, and skull bones. Perfusion weighted maps were used to produce a gray and white matter anatomical mask based on the Hounsfield Unit differences between the two tissue types. CBV values from within superimposed infarct ROIs (CBV_I) for gray and white matter were calculated from all ROIs for each patient, at each time point. These values were weighted according to the size of the ROI for each slice. Further, patients were dichotomized based on whether the

TDC, taken from the ischemic defect (TDC_i), was truncated or non-truncated; truncation was defined as the absence of the lower 50% of the TDC trailing slope (contrast wash out phase). An overall average CBV_I using all patients was calculated at each time point. Pixels with a $CBF > 100 \text{ ml}\cdot\text{min}^{-1}\cdot(100\text{g})^{-1}$ or $CBV > 8 \text{ ml}\cdot(100\text{g})^{-1}$ were excluded from the average calculation, a technique used to eliminate large vessel hemodynamic values, focusing on parenchymal perfusion²⁸.

Table 2.1 Demographics for Group A, N = 13 ischemic stroke patients.

Patient	Age	Gender	Onset to Imaging (minutes)	Admission NIHSS	tPA	Recanalization @ 24 hours	TDC _i truncation
1	54	M	73	18	IV	Partial	No
2	60	M	135	8	IV+IA	Partial	No
3	62	F	78	21	IV+IA	Partial	Yes
4	56	F	75	8	IV	Partial	Yes
5	78	M	286	25	None	No	No
6	72	M	126	13	IV	No	No
7	64	M	175	19	IV	No	No
8	90	F	427	19	None	No	No
9	72	F	394	19	None	No	No
10	67	M	169	12	IV	No	Yes
11	53	M	300	22	None	No	Yes
12	92	F	107	24	None	No	No
13	57	M	225	17	IV+IA	No	No
67±13		8M,5F	197±120	17.3±5.5	8/13		4/13

NIHSS = National Institutes of Health Stroke Scale, M = Male, F = Female, tPA = tissue plasminogen activator, IA = intra-arterial, TDC_i = time density curve from tissue destined to infarct. Data presented as mean ± standard deviation.

2.2.3.2 Determining CBV defect overestimation

In part 1 of this analysis, Group B was used to obtain admission CBV thresholds for infarction in gray and white matter, respectively. Patients were included if they had full recanalization and were classified as ITDC truncation negative. Of the 32 patients with imaging, 13 contributed data for this analysis (Table 2.2). This was carried out as follows: the perfusion weighted map was used to segment gray and white matter on the basis of Hounsfield unit thresholds to produce a gray/white matter mask. This ROI mask was then applied to the admission CBF and CBV maps. The admission perfusion-weighted, CBF, and CBV maps were automatically co-registered as they came from the same CT perfusion study. Delayed NCCT images were registered to the admission images using custom software (IDL, version 6.0, RSI, Boulder, Colorado). The final infarct was outlined by an experienced neuroradiologist of 5 years. The final infarct ROI was then superimposed onto the admission CBF and CBV functional maps, and the gray/white matter ROI mask was applied within the infarct ROI. CBV values from within the superimposed ROI were obtained for gray and white matter, respectively. These values represent the acute infarction thresholds. To be certain penumbral tissue pixels were not incorporated, we set an upper threshold for CBV for each patient using the mirror contralateral hemisphere ROI – this upper threshold was defined as the mean CBV subtract one standard deviation.

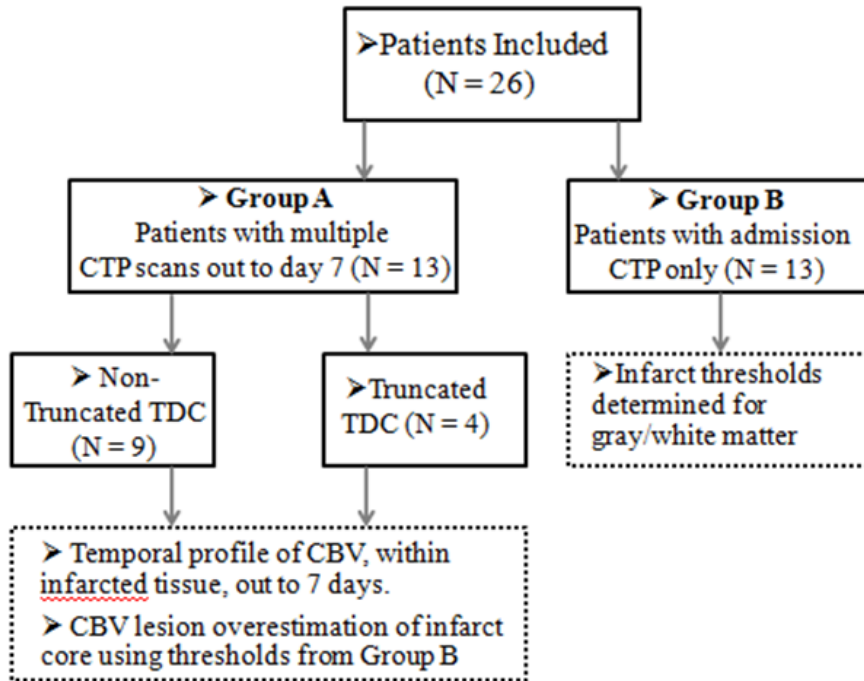
Table 2.2 Demographics for Group B, N = 13 ischemic stroke patients.

Patient	Age	Gender	Onset to Imaging (minutes)	Admission NIHSS	tPA	Recanalization @ 24 hours	TDC_i Truncation
14	44	F	280	10	IA	Complete	No
15	77	F	163	6	IA	Complete	No
16	81	F	147	26	None	Complete	No
17	75	M	168	4	None	Complete	No
18	82	F	178	23	None	Complete	No
19	89	F	133	18	None	Complete	No
20	54	F	129	9	IV	Complete	No
21	77	F	82	10	IV	Complete	No
22	78	M	157	9	None	Complete	No
23	60	F	64	11	IV+IA	Complete	No
24	67	F	130	13	IV+IA	Complete	No
25	57	F	137	14	None	Complete	No
26	82	M	122	11	IV	Complete	No
71±		3M,10F	145±51	12.3±6.3	7/13		0/13

NIHSS = National Institutes of Health Stroke Scale, M = Male, F = Female, tPA = tissue plasminogen activator, IA = intra-arterial, TDC_i = time density curve from tissue destined to infarct. Data presented as mean ± standard deviation.

In part 2 of this analysis, the CBV values obtained in part 1 were applied to all CTP time points for patients in Group A. This was carried out as follows: peri-infarct hypoperfusion was outlined at $CBF < 25 \text{ ml} \cdot \text{min}^{-1} \cdot (100\text{g})^{-1}$ ²⁹. Within this hypoperfused region, gray and white matter tissue was flooded with their respective CBV infarct thresholds obtained in part 1. Patients with peri-infarct tissue regions with a CBV below these determined thresholds were classified as having an overestimation of the CBV defect (ie. the final infarct volume at 5-7 days, defined on NCCT, was smaller than the admission and/or 24 hour infarct volume predicted by the CBV infarct thresholds).

Figure 2.1 - Study design flow chart



Number of patients assigned to each of the study groups (solid boxes), and analysis procedure performed on each group (dashed boxes).

2.2.4 Statistical analysis

Results are reported as mean \pm standard deviation, unless stated otherwise. An unpaired t-test was used to examine significant differences in overall average CBV_I between time points, for both cerebral tissue types. Within truncated and non-truncated TDC_i groups, CBV_I values were analyzed by repeated measures ANOVA to identify significance over time. All statistical analyses were performed by using software (SPSS, version 16 for Windows; SPSS, Chicago, IL, USA).

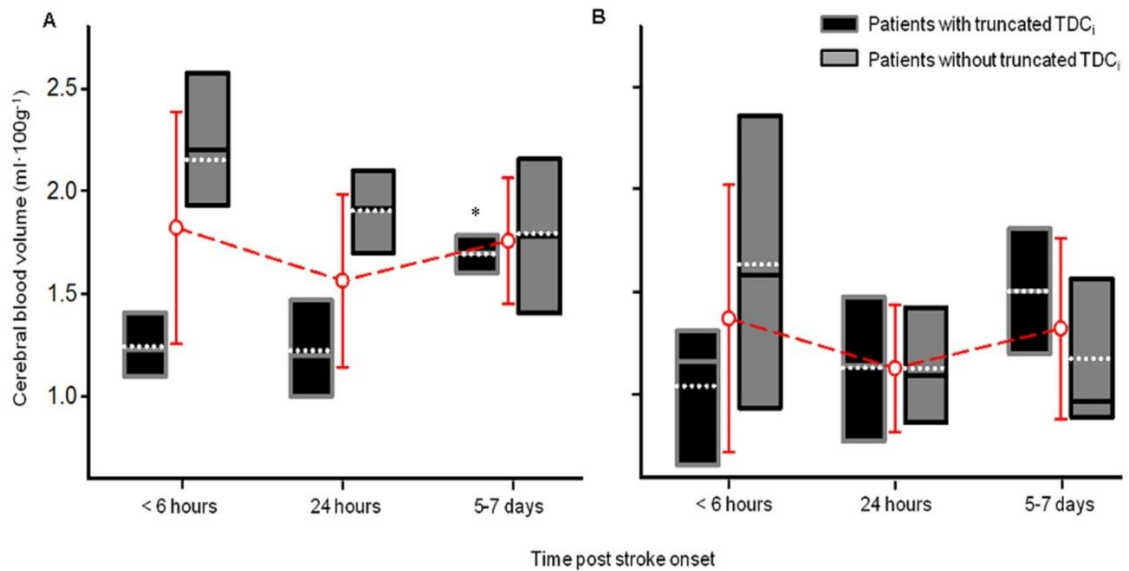
2.3 RESULTS

2.3.1 *The 5-7 day evolution of CBV within tissue destined to infarct*

Gray matter infarct regions were present in 11 patients, while white matter infarct regions were present in 9 patients. Three patients did not have CTP data at 24 hours. CBV_I [$\text{ml}\cdot(100\text{g})^{-1}$; mean \pm stdev] values for gray and white matter at admission, 24 hours and 5-7 days were 1.82 ± 0.56 , 1.56 ± 0.42 , 1.75 ± 0.31 and 1.38 ± 0.65 , 1.13 ± 0.31 , 1.32 ± 0.44 , respectively when averaged over all patients (Figure 2.2). There were no significant differences in mean CBV_I between time points for both brain tissue types ($p > 0.05$). TDC_i truncation was present in 4/13 (30%): Two patients had TDC_i truncation at admission only, while two others had TDC_i truncation at admission and 24 hours. For these four patients, mean CBV_I [$\text{ml}\cdot(100\text{g})^{-1}$; mean \pm stdev] values for gray and white matter at admission, 24 hours and 5-7 days were 1.24 ± 0.17 , 1.22 ± 0.20 , 1.70 ± 0.9 , and 1.05 ± 0.36 , 1.13 ± 0.37 , 1.51 ± 0.32 , respectively. Significant CBV_I increases occurred at the 5-7 day time point within gray matter only ($p < 0.05$); white matter values were not significant, but showed a similar trend. For patients without TDC_i truncation, 9/13 (70%),

mean CBV_I [$\text{ml} \cdot (100\text{g})^{-1}$; mean \pm stdev] values for gray and white matter at admission, 24 hours and 5-7 days were 2.15 ± 0.41 , 1.90 ± 0.21 , 1.79 ± 0.38 , and 1.64 ± 0.75 , 1.13 ± 0.28 , 1.18 ± 0.32 , respectively. There were no significant CBV_I increases at 24 hours or 5-7 days compared to admission for this group.

Figure 2.2 Cerebral blood volume within tissue destined to infarct

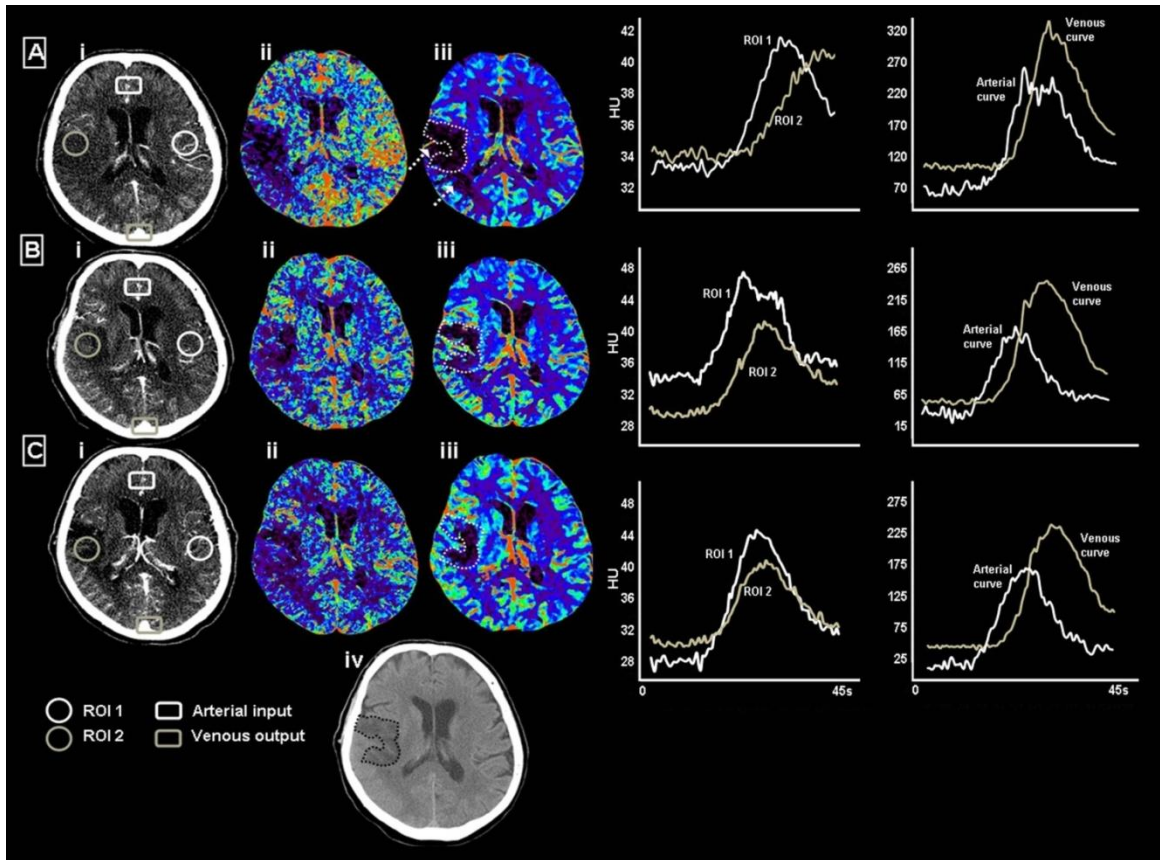


Mean \pm stdev CBV_I [ml·(100g)⁻¹] for gray matter (A) and white matter (B) at admission, 24 hours and 5-7 days post stroke onset for all patients (open circles). Box plots represent patients with and without TDC_i. In each box, median (solid line), mean (dotted line), first and third quartile values are illustrated. A significant increase in gray matter CBV_I was observed at 5-7 days for the truncated group ($*p < 0.05$).

2.3.2 Determining acute CBV defect overestimation

In part 1, CBV [$\text{ml} \cdot (100\text{g})^{-1}$; mean \pm stdev] values to define infarction, obtained from 13 patients (group B) with confirmed recanalization/reperfusion and no ITDC truncation, were 1.10 and 0.75 for gray and white matter, respectively. In part 2, overestimation of the final infarct volume, as defined by the CBV thresholds in part 1, was present at admission in 3/4 (75%) and 1/9 (11%) of patients who were TDC_i truncation positive and negative, respectively. Final infarct volume overestimation was absent at both 24 hour and 5-7 day CTP imaging time points (Figure 2.3).

Figure 2.3 Example of truncation artifact and CBV defect overestimation



Patient 10, CTP-derived contrast enhanced image, CBF [scale $0-150 \text{ ml}\cdot\text{min}^{-1}\cdot(100\text{g})^{-1}$] and CBV [scale $0-8 \text{ ml}\cdot(100\text{g})^{-1}$] functional maps (i-iii) at admission, 24 hours, and 7 days post stroke onset (A-C). NCCT from 7 days post stroke shows outlined infarct region (iv). Corresponding time-density curves (Hounsfield units versus time) were taken at each time point. Confluent areas outside of superimposed infarct ROI showing CBV defect overestimation (dashed arrows); at this time, TDC_i truncation is apparent. CBV_i reversibility is observed at 24 hours and 7 days, compared to admission, for this patient.

2.4 DISCUSSION

To our knowledge, progression of CTP-derived CBV defect has never been realized beyond the acute stroke stage. This study examines CBV changes within gray and white matter cerebral tissue destined to infarct, as well as determines the final infarct volume overestimation as defined by the CBV abnormality. Previous studies have shown the ability of acute CTP-derived CBV defects (ie. CBV close to zero) to predict non-viable ischemic tissue^{9, 30}. Briefly, a decrease in cerebral perfusion pressure leads to the eventual loss of cerebrovascular autoregulation in very hypoperfused tissue, followed by a permanent, focal decrease in CBV; however, this mechanism is not yet fully understood³¹⁻³³. We observe CBV_i reversibility out to 7 days post admission in several patients; however, this reversal is more common in patients with an incomplete (truncated) tissue TDC_i at admission and/or 24 hours post stroke ictus. We also observe CBV defect overestimation (very low CBV outside of superimposed final infarct volume) at admission in 75% and 11% of patients with and without TDC_i truncation, respectively. Figure 2.3 illustrates CBV overestimation in a patient with TDC_i truncation at admission. These findings highlight the importance of acquiring a complete tissue TDC for the accurate calculation of the impulse residue function, $H(t)$, by the CT perfusion software (GE Healthcare). This function describes the amount of contrast remaining in the tissue over time. In short, the adiabatic approximation to the Johnson and Wilson model describes the impulse residue function as³⁴:

$$H(t) = \left\{ \begin{array}{ll} 1 & 0 \leq t \leq T_c \\ Ee^{-\left[\frac{EF}{V_c}\right](t-T_c)} & t > T_c \end{array} \right\} \quad (1)$$

where T_c is the capillary mean transit time and F is CBF. Therefore, according to the central volume principle, CBV is $F \cdot T_c$. E is the contrast extraction fraction, and V_c is the contrast agent distribution volume in the extra-vascular space (EVS). The measured tissue TDC, $Q(t)$, can be calculated by the convolution of the arterial input, $C_a(t)$ and $H(t)$:

$$Q(t) = F \cdot [C_a(t) * H(t - T_0)] \quad (2)$$

where $*$ is the convolution operator and T_0 is the tracer arrival time relative to the arterial input. After measuring $Q(t)$ and $C_a(t)$ using the CTP study, CBV and CBF are calculated by iteratively changing their values until an optimum fit to $Q(t)$ is achieved by means of Equations (1)-(2). The initial height of the function $H(t)$ is equal to CBF in $\text{ml} \cdot \text{min}^{-1} \cdot (100\text{g})^{-1}$ and the area under this function gives CBV in $\text{ml} \cdot (100\text{g})^{-1}$. Therefore, when the tissue TDC is truncated, CBV is underestimated as a consequence.

In the present study, there were four instances where the admission CTP-CBV defined defect volumes extended beyond the superimposed final infarct ROI. One of these patients did not have TDC_i truncation, and was therefore considered to have ‘true CBV reversibility’. This reversibility may be caused by a failure of contrast to access the ischemic tissue even though blood filled capillaries may still be present before and/or after the short imaging time window³⁵. Endothelial swelling (cytotoxic edema) and inflammatory mechanisms, such as platelet aggregation and leukocyte adhesion in capillaries of ischemic tissue, known as capillary plugging, may play a role³⁶. Moreover, early reperfusion could allow recovery of cellular membrane ion pumps, instigating metabolic resurgence in clusters of cells within the periphery of CBV-predicted infarction – this is especially true during instances when spontaneous partial/full reperfusion occurs

around the time of image acquisition³⁷. In similar work by Silvennoinen *et al.*, 4/45(9%) of tPA treated patients had CBV defect volumes that were larger than final infarct volumes. However, the CTP software (CTP version 3, GE Healthcare) used to produce these hemodynamic parametric maps uses a singular value decomposition algorithm which does not have delay correction optimization. To help compensate for the late tracer bolus to the affected area, the newest version of CT perfusion (CTP version 4, GE Healthcare) “delay optimized” algorithm shifts the tissue TDC baseline to match the arterial input function. Making use of this optimized delay correction CTP software (CTP version 4, GE Healthcare), Schaefer *et al.* observed CBV defect reversibility in 2/11 (18%) patients post endovascular induced recanalization³⁸. The small decreases in initial defect size were also considered ‘true CBV reversibility’ as TDC_i truncation was reported not to affect CBV computation.

The use of CTP imaging to define non-viable tissue during the acute stroke setting is possible if technical aspects are considered. Several institutes continue to use a CTP acquisition less than 50 seconds when examining acute stroke³⁹⁻⁴². By incorporating a two-phase CTP imaging protocol, TDC_i truncation can be prevented. Following the initial 50-60 second cine scan, sampling every 15 seconds for an additional 90 seconds can minimize radiation dose while obtaining the data required for an accurate CBV calculation⁴³. The second phase data can also be used to evaluate blood brain barrier permeability, further guiding thrombolysis treatment⁴³. In addition to the lengthened scan time, newest versions of the CT Perfusion functional map processing software (GE Healthcare), with the delay correction algorithm, should always be utilized; however, this correction may not always be sufficient, especially when the peak contrast enhancement of the TDC is never reached during the CTP acquisition. Endogenous characteristics

which may contribute to the late arrival time of the CT contrast include: atrial fibrillation, internal carotid stenosis, inadequate blood supply from collaterals and congestive heart failure. To improve arrival time of contrast, a higher injection rate (6-8 ml/sec) is needed. In the study by Silvennoinen *et al.* a rate of 7 ml/sec was used which would shorten the contrast bolus, and thus the width of the measured TDC. They reported a much lower incidence of TDC truncation, in contrary to the results herein.

This study is not without its limitations. First, improvement on the small sample size of 13 patients with CTP imaging out to 5-7 days or more is needed. Second, defining infarcted tissue at 5-7 days post stroke could result in over/underestimation of final infarct volume as penumbral tissue remains in a transient state of viability past one week⁸. An NCCT with a DWI scan several weeks after stroke onset would be more suitable. Third, since slice location varied slightly between time points, image registration was not always exact. Accordingly, an ROI analysis comparing the entire 20 mm slab was performed (weighted average of 4 slices), instead of a pixel-by-pixel analysis. Fourth, only a 2 cm slab of tissue was imaged during the CTP acquisition, which could have missed part of the infarct volume. Also of note, the validation of CTP-CBV has yet to be demonstrated in any clinical study, and only CTP-CBF has been formally validated⁴⁴.

2.5 CONCLUSION

This study describes changes in the CBV abnormality from the first few hours of ischemic stroke onset. The acute CBV abnormality is shown to be a reliable indicator of impending infarction when the CT contrast wash out phase within ischemic tissue is

completed within the CTP imaging time frame. Further investigation is needed to determine the effects of this truncation artifact on other CTP parameters.

2.6 REFERENCES

1. Hacke W, Kaste M, Bluhmki E, Brozman M, Davalos A, Guidetti D, et al. Thrombolysis with alteplase 3 to 4.5 hours after acute ischemic stroke. *The New England journal of medicine*. 2008;359:1317-1329
2. Clark WM, Wissman S, Albers GW, Jhamandas JH, Madden KP, Hamilton S. Recombinant tissue-type plasminogen activator (alteplase) for ischemic stroke 3 to 5 hours after symptom onset. The atlantis study: A randomized controlled trial. Alteplase thrombolysis for acute noninterventional therapy in ischemic stroke. *JAMA*. 1999;282:2019-2026
3. Gasparotti R, Grassi M, Mardighian D, Frigerio M, Pavia M, Liserre R, et al. Perfusion ct in patients with acute ischemic stroke treated with intra-arterial thrombolysis: Predictive value of infarct core size on clinical outcome. *AJNR. American journal of neuroradiology*. 2009;30:722-727
4. Mayer TE, Schulte-Altdorneburg G, Droste DW, Bruckmann H. Serial ct and mri of ischaemic cerebral infarcts: Frequency and clinical impact of haemorrhagic transformation. *Neuroradiology*. 2000;42:233-239
5. Bristow MS, Simon JE, Brown RA, Eliasziw M, Hill MD, Coutts SB, et al. Mr perfusion and diffusion in acute ischemic stroke: Human gray and white matter have different thresholds for infarction. *Journal of cerebral blood flow and metabolism : official journal of the International Society of Cerebral Blood Flow and Metabolism*. 2005;25:1280-1287
6. Heiss WD, Sobesky J, Hesselmann V. Identifying thresholds for penumbra and irreversible tissue damage. *Stroke; a journal of cerebral circulation*. 2004;35:2671-2674
7. Hossmann KA. Viability thresholds and the penumbra of focal ischemia. *Annals of neurology*. 1994;36:557-565
8. Murphy BD, Fox AJ, Lee DH, Sahlas DJ, Black SE, Hogan MJ, et al. White matter thresholds for ischemic penumbra and infarct core in patients with acute stroke: Ct perfusion study. *Radiology*. 2008;247:818-825
9. Schaefer PW, Roccatagliata L, Ledezma C, Hoh B, Schwamm LH, Koroshetz W, et al. First-pass quantitative ct perfusion identifies thresholds for salvageable penumbra in acute stroke patients treated with intra-arterial therapy. *AJNR. American journal of neuroradiology*. 2006;27:20-25
10. Wintermark M, Flanders AE, Velthuis B, Meuli R, van Leeuwen M, Goldsher D, et al. Perfusion-ct assessment of infarct core and penumbra: Receiver operating characteristic curve analysis in 130 patients suspected of acute hemispheric stroke. *Stroke; a journal of cerebral circulation*. 2006;37:979-985
11. Baird AE, Lovblad KO, Dashe JF, Connor A, Burzynski C, Schlaug G, et al. Clinical correlations of diffusion and perfusion lesion volumes in acute ischemic stroke. *Cerebrovasc Dis*. 2000;10:441-448

12. Hjort N, Butcher K, Davis SM, Kidwell CS, Koroshetz WJ, Rother J, et al. Magnetic resonance imaging criteria for thrombolysis in acute cerebral infarct. *Stroke; a journal of cerebral circulation*. 2005;36:388-397
13. Gonzalez RG, Schaefer PW, Buonanno FS, Schwamm LH, Budzik RF, Rordorf G, et al. Diffusion-weighted mr imaging: Diagnostic accuracy in patients imaged within 6 hours of stroke symptom onset. *Radiology*. 1999;210:155-162
14. Kranz PG, Eastwood JD. Does diffusion-weighted imaging represent the ischemic core? An evidence-based systematic review. *AJNR. American journal of neuroradiology*. 2009;30:1206-1212
15. Marks MP, Olivot JM, Kemp S, Lansberg MG, Bammer R, Wechsler LR, et al. Patients with acute stroke treated with intravenous tpa 3-6 hours after stroke onset: Correlations between mr angiography findings and perfusion- and diffusion-weighted imaging in the defuse study. *Radiology*. 2008;249:614-623
16. Albers GW, Thijs VN, Wechsler L, Kemp S, Schlaug G, Skalabrin E, et al. Magnetic resonance imaging profiles predict clinical response to early reperfusion: The diffusion and perfusion imaging evaluation for understanding stroke evolution (defuse) study. *Annals of neurology*. 2006;60:508-517
17. Kidwell CS, Saver JL, Mattiello J, Starkman S, Vinuela F, Duckwiler G, et al. Thrombolytic reversal of acute human cerebral ischemic injury shown by diffusion/perfusion magnetic resonance imaging. *Annals of neurology*. 2000;47:462-469
18. Lutsep HL, Nesbit GM, Berger RM, Coshow WR. Does reversal of ischemia on diffusion-weighted imaging reflect higher apparent diffusion coefficient values? *Journal of neuroimaging : official journal of the American Society of Neuroimaging*. 2001;11:313-316
19. Puetz V, Dzialowski I, Hill MD, Demchuk AM. The alberta stroke program early ct score in clinical practice: What have we learned? *Int J Stroke*. 2009;4:354-364
20. Parsons MW, Pepper EM, Bateman GA, Wang Y, Levi CR. Identification of the penumbra and infarct core on hyperacute noncontrast and perfusion ct. *Neurology*. 2007;68:730-736
21. Aviv RI, Mandelcorn J, Chakraborty S, Gladstone D, Malham S, Tomlinson G, et al. Alberta stroke program early ct scoring of ct perfusion in early stroke visualization and assessment. *AJNR. American journal of neuroradiology*. 2007;28:1975-1980
22. Kim JT, Park MS, Choi KH, Nam TS, Choi SM, Lee SH, et al. The cbv-aspect score as a predictor of fatal stroke in a hyperacute state. *European neurology*. 2010;63:357-363

23. Eastwood JD, Lev MH, Wintermark M, Fitzek C, Barboriak DP, DeLong DM, et al. Correlation of early dynamic ct perfusion imaging with whole-brain mr diffusion and perfusion imaging in acute hemispheric stroke. *AJNR. American journal of neuroradiology*. 2003;24:1869-1875
24. Wintermark M, Reichhart M, Cuisenaire O, Maeder P, Thiran JP, Schnyder P, et al. Comparison of admission perfusion computed tomography and qualitative diffusion- and perfusion-weighted magnetic resonance imaging in acute stroke patients. *Stroke; a journal of cerebral circulation*. 2002;33:2025-2031
25. The thrombolysis in myocardial infarction (timi) trial. Phase i findings. Timi study group. *The New England journal of medicine*. 1985;312:932-936
26. Lee TY, Purdie TG, Stewart E. Ct imaging of angiogenesis. *Q J Nucl Med*. 2003;47:171-187
27. Cenic A, Nabavi DG, Craen RA, Gelb AW, Lee TY. Dynamic ct measurement of cerebral blood flow: A validation study. *AJNR. American journal of neuroradiology*. 1999;20:63-73
28. Kudo K, Terae S, Katoh C, Oka M, Shiga T, Tamaki N, et al. Quantitative cerebral blood flow measurement with dynamic perfusion ct using the vascular-pixel elimination method: Comparison with h2(15)o positron emission tomography. *AJNR. American journal of neuroradiology*. 2003;24:419-426
29. Murphy BD, Fox AJ, Lee DH, Sahlas DJ, Black SE, Hogan MJ, et al. Identification of penumbra and infarct in acute ischemic stroke using computed tomography perfusion-derived blood flow and blood volume measurements. *Stroke; a journal of cerebral circulation*. 2006;37:1771-1777
30. Silvennoinen HM, Hamberg LM, Lindsberg PJ, Valanne L, Hunter GJ. Ct perfusion identifies increased salvage of tissue in patients receiving intravenous recombinant tissue plasminogen activator within 3 hours of stroke onset. *AJNR. American journal of neuroradiology*. 2008;29:1118-1123
31. Sette G, Baron JC, Mazoyer B, Levasseur M, Pappata S, Cruzel C. Local brain haemodynamics and oxygen metabolism in cerebrovascular disease. Positron emission tomography. *Brain*. 1989;112 (Pt 4):931-951
32. Powers WJ, Grubb RL, Jr., Raichle ME. Physiological responses to focal cerebral ischemia in humans. *Annals of neurology*. 1984;16:546-552
33. Koenig M, Kraus M, Theek C, Klotz E, Gehlen W, Heuser L. Quantitative assessment of the ischemic brain by means of perfusion-related parameters derived from perfusion ct. *Stroke*. 2001;32:431-437
34. St Lawrence KS, Lee TY. An adiabatic approximation to the tissue homogeneity model for water exchange in the brain: I. Theoretical derivation. *Journal of cerebral blood flow and metabolism : official journal of the International Society of Cerebral Blood Flow and Metabolism*. 1998;18:1365-1377

35. Zaharchuk G, Mandeville JB, Bogdanov AA, Jr., Weissleder R, Rosen BR, Marota JJ. Cerebrovascular dynamics of autoregulation and hypoperfusion. An mri study of cbf and changes in total and microvascular cerebral blood volume during hemorrhagic hypotension. *Stroke*. 1999;30:2197-2204; discussion 2204-2195
36. Garcia JH, Liu KF, Yoshida Y, Lian J, Chen S, del Zoppo GJ. Influx of leukocytes and platelets in an evolving brain infarct (wistar rat). *Am J Pathol*. 1994;144:188-199
37. Mayer TE, Hamann GF, Baranczyk J, Rosengarten B, Klotz E, Wiesmann M, et al. Dynamic ct perfusion imaging of acute stroke. *AJNR Am J Neuroradiol*. 2000;21:1441-1449
38. Schaefer PW, Mui K, Kamalian S, Nogueira RG, Gonzalez RG, Lev MH. Avoiding "pseudo-reversibility" of ct-cbv infarct core lesions in acute stroke patients after thrombolytic therapy. The need for algorithmically "delay-corrected" ct perfusion map postprocessing software. *Stroke; a journal of cerebral circulation*. 2009; 40(8): 2875-8
39. Bivard A, McElduff P, Spratt N, Levi C, Parsons M. Defining the extent of irreversible brain ischemia using perfusion computed tomography. *Cerebrovascular diseases*. 2011;31:238-245
40. Chang CH, Chang TY, Chang YJ, Huang KL, Chin SC, Ryu SJ, et al. The role of perfusion computed tomography in the prediction of cerebral hyperperfusion syndrome. *PloS one*. 2011;6:e19886
41. Abels B, Klotz E, Tomandl BF, Kloska SP, Lell MM. Perfusion ct in acute ischemic stroke: A qualitative and quantitative comparison of deconvolution and maximum slope approach. *AJNR. American journal of neuroradiology*. 2010;31:1690-1698
42. Orrison WW, Jr., Snyder KV, Hopkins LN, Roach CJ, Ringdahl EN, Nazir R, et al. Whole-brain dynamic ct angiography and perfusion imaging. *Clin Radiol*. 2011;66:566-574
43. Aviv RI, d'Este CD, Murphy BD, Hopyan JJ, Buck B, Mallia G, et al. Hemorrhagic transformation of ischemic stroke: Prediction with ct perfusion. *Radiology*. 2009;250:867-877
44. Nabavi DG, Cenic A, Craen RA, Gelb AW, Bennett JD, Kozak R, et al. Ct assessment of cerebral perfusion: Experimental validation and initial clinical experience. *Radiology*. 1999;213:141-149

CHAPTER 3

Reliability of the CT Perfusion Cerebral Blood Volume Parameter in Ischemic Stroke

The contents of this chapter have been adapted from the paper entitled “Reliability of the cerebral blood volume parameter in ischemic stroke”, has been reviewed and re-submitted to the journal *Neuroradiology*, by C.D. d’Esterre, T.Y. Lee, S. Ceruti, G. Roversi, A. Saletti, E. Fainardi.

3.1 INTRODUCTION

Thromboembolic cerebral ischemia makes up 87% of all stroke sub-types¹. Early restoration of blood flow using thrombolytic therapy is the most effective way to reverse stroke symptoms, improving clinical outcome². The intravenous (IV) tissue plasminogen activator (tPA) therapeutic window is limited to 4.5 hours post stroke onset^{3, 4}. This time constraint has limited its use in less than 7% of acute ischemic stroke (AIS) patients as the risk of hemorrhagic transformation outweighed the clinical benefit beyond the treatment window^{5, 6}. A major goal of acute neuroimaging in AIS is to eliminate this rigid temporal criterion used to decide if thrombolytic therapy is appropriate. Instead, a patient specific approach, based on tissue viability at the time of onset, is currently being explored by many investigators, using both computed tomography (CT) and magnetic resonance (MR) imaging⁷⁻¹⁴.

CT imaging remains the modality of choice for AIS for its widespread availability, acquisition speed and limited invasiveness. The initial non-contrast CT (NCCT) scan is used for detection of stroke mimics, intracranial hemorrhage, infarct

delineation, and remains the imaging modality needed to administer tissue plasminogen activator (tPA)¹⁵. Nonetheless, a current widespread method to detect early ischemic changes (EIC), the Alberta Stroke Program Early CT Score (ASPECTS), provides only subtle indication of EIS along with broad inter-subject variability, especially during the first few hours from ictus^{16, 17}. Consequently, there have been many attempts to standardize perfusion parameters to determine cerebral tissue viability during the acute stroke setting¹⁸⁻²⁴. A complete reduction in CBV was suggested as the hemodynamic indicator to discriminate between viable and non-viable tissue states^{25, 26}. The rationale is that a decrease in cerebral perfusion pressure in severely hypoperfused tissue leads to cerebrovascular autoregulatory failure followed by a supposedly permanent, focal decrease in CBV²⁷. Conversely, an acute increase in cerebral blood volume (CBV) was proposed to have a protective effect on perfusion compromised, yet viable tissue; the so-called “penumbral hypothesis”^{10, 28}. Recently, when comparing perfusion parameters to the AIS imaging gold standard, the MR-diffusion weighted (DWI) sequence, several studies suggest that the CBV parameter is unreliable in the accurate delineation of the acute infarct core^{22, 23, 29}. Specifically, Campbell et al. (2011) and Kamalian et al. (2011) both demonstrated that absolute and relative (to contralateral hemisphere) CBF parameter approximate better the DWI-defined infarct core than CBV and MTT parameters^{22, 23}; however, both studies used shortened CT Perfusion (CTP) scan times, which may under- and overestimate CBV and MTT, respectively³⁰. Further, acute DWI defects may not be truly representative of non-viable tissue, as partial/full reversal has been shown in 7%-85% of patients^{31, 32}. Therefore, the CBV parameter may still have its place in AIS imaging triage. Accordingly, using the newest CTP software from GE Healthcare, which incorporates a delay-insensitive deconvolution algorithm, we address the physiological

and technical variables which affect the CBV parameter during the acute and sub-acute stroke period by comparing the acute CBV defect (CBV_D) with the fully evolved infarct, defined on the 3 month NCCT, and examining perfusion values, CBV and CBF, within tissue destined to infarct at admission, 24 hours, 7 days and 3 months.

3.2 MATERIALS & METHODS

3.2.1 Patient selection

The study was approved by the research ethics board of the institution⁺. Informed consents were obtained from patient and/or their legal representative. Sixty-four consecutively screened acute ischemic stroke patients were enrolled over a two year period (between February 2009 and July 2011). Patients were included if they: presented at the hospital < 6 hours post symptom onset, had no previous stroke and showed signs and symptoms of middle cerebral artery occlusion, had a CT angiography (CTA) at baseline and 24 hours for recanalization status, and were able to complete CTP studies at all four time points. Exclusion criteria included: evidence of brain stem infarct, prior stroke with residual deficit, intracranial hemorrhage, minor stroke symptoms [onset National Institutes of Health Stroke Scale (NIHSS) score < 4], clinically significant hyperglycemia, impaired renal function and/or known allergy to contrast media; pregnancy, and age less than 18 years. Of the 64 patients enrolled, 55 contributed data for this study, while 9 were excluded for the following reasons: onset NIHSS score < 4 (n=5), no perfusion deficit at onset (n=4). Results of the CTP study performed at admission did

⁺ Appendix B – Human Ethics Approval form

not influence treatment decisions (patients and/or legal representatives providing informed consent were aware of this). Patients were enrolled regardless of therapy. An experienced neurologist (G.R.) assessed clinical outcome for all patients using the NIHSS and at admission, 24 hour, one week, and 3 months, as well as modified Rankin Scoring (mRS) 3 months post stroke onset.

3.2.2 Imaging protocol

Imaging was performed at four time points post stroke onset. Patients underwent a NCCT, CTA and CTP at admission (< 6 hours post ictus), 24 hours, 7 days and at 3 months. Imaging was conducted on a 64–slice Lightspeed VCT scanner (GE Healthcare, Waukesha, WI, USA). The CTP scanning protocol consisted of a continuous 50 second scan using 80 kV, 100 mA and 1 second rotation time while the couch remained stationary. Seven-hundred ninety two 512×512 images were reconstructed with a 25 cm field-of-view at 0.5 second intervals for each of the eight 5 mm thick slice locations. Five seconds before the start of scanning, a 40 ml bolus of iodinated contrast agent (Iomeron 300 mg/ml, Bracco Imaging SpA, Milan, Italy) was injected at a rate of 4 ml/second into an antecubital vein with an automatic injector (Medrad, Indianola, PA). The gantry was tilted to parallel the supraorbito-meatal line to avoid irradiation of eye lenses. NCCT helical scans were performed from the skull base to the vertex using the following imaging parameters: 120 kV, 340 mA, 4x5-mm collimation, 1 second/rotation, and table speed of 15 mm/rotation. CTA was performed as follows: 0.7 mL/kg contrast (maximum 90 mL), 5- to 10-second delay from injection to scanning, 120 kV, 270 mA, 1

second/rotation, 1.25-mm thick slices, and table speed 3.75 mm/rotation. CTA covered from the carotid bifurcation to vertex.

3.2.3 CTP functional maps

For consistency, each CTP imaging study was analyzed using a commercially available delay-insensitive deconvolution software (CT Perfusion 4D, GE Healthcare, Waukesha, WI). For each CTP scan, time-density curves (TDC) for the arterial input function (AIF) and venous output functions (VOF) were obtained from the anterior cerebral artery and superior sagittal sinus, respectively. The AIF was corrected for partial volume averaging using the VOF-TDC. Functional maps of cerebral blood flow [CBF; $\text{ml}\cdot\text{min}^{-1}\cdot(100\text{g})^{-1}$] and cerebral blood volume [CBV; $\text{ml}\cdot(100\text{g})^{-1}$] were calculated by deconvolution of tissue TDCs and the AIF. Perfusion weighted maps were created by averaging the cine CTP images over the duration of the first pass of contrast. A functional map was also created representing the percentage of TDC truncation (incomplete imaging of the contrast wash-out phase) for each tissue voxel, defined as: the ratio of the increase in Hounsfield Unit (HU) value at the end of the CTP acquisition relative to that of the peak HU above baseline.

3.2.4 CTP, CTA, and NCCT image analysis

One author performed all analysis on CTP maps using custom software (IDL, version 6.2, RSI, Boulder, Colorado). For all perfusion studies, perfusion weighted maps were used to exclude cerebrospinal fluid (CSF) and cranium from analysis as well as to produce a gray and white matter anatomical mask based on the HU differences between the two tissue types. All CTP and NCCT scans were co-registered. The admission CBV_D volumes were

outlined on all CBV functional maps (8 x 5mm) using previously established gray and white matter CBV thresholds for infarct core, derived from maps generated by delay-insensitive deconvolution software (GE Healthcare)³⁰. This was performed separately by two observers with the final result arrived at by consensus. For each patient, the total CBV_D size (gray plus white matter volumes) was determined and compared with corresponding 3 month post ictus NCCT images. Two neuroradiologist, traced a region of interest (ROI) around the hypodense area of the 3 month NCCT (NCCT_D) as the final infarct ROI. All CBV_D and NCCT_D areas from each involved slice were multiplied by the section thickness and summed to obtain the final defect volume in cubic centimeters.

To examine perfusion states within the tissue destined to infarct over time, the final infarct ROI, from the 3 month NCCT, was superimposed onto the CBV and CBF functional maps at all four time points. This ROI was mirrored in the contralateral hemisphere. Large vessels within the infarct and contralateral ROIs were excluded from the calculation of the mean tissue perfusion parameters³³.

Recanalization was classified using CTA at 24 hours post as complete, partial, or absent by an experienced neuroradiologist based on an adaptation of the thrombolysis in myocardial infarction (TIMI) criteria³⁴. Complete occlusion was characterized by the absence of CT contrast distal to the thrombus, while full recanalization was characterized by no visible narrowing of the involved vessel seen at baseline CTA. Partial recanalization was defined as a narrowing of the vessel at the site of occlusion with contrast distal to the thrombus.

The 24 hour and 7 day NCCT was used to categorize hemorrhagic transformation (HT), if present, according to the European Cooperative Acute Stroke Study II criteria³⁵: hemorrhagic infarction (HI-1,2) or parenchymal hematoma (PH-1,2). Symptomatic

intracerebral hemorrhage (sICH) was identified as PH with worsening of neurological deficit ≥ 4 points on the NIHSS between admission and 24 hours.

3.2.5 Patient groupings and statistical analysis

One author performed all statistical analysis (SPSS, version 16 for Windows; SPSS, Chicago, IL, USA) and results were verified by all co-authors. All data sets were checked for normality with the Shapiro-Wilk test prior to analysis with the appropriate parametric or non-parametric tests.

In some CTP studies, the 50 second acquisition led to truncation of ischemic tissue time density curves (TDCi) before the washout phase was completed underestimating the area under the TDCi. Therefore, patients were divided into TDCi truncation positive (n=24) and negative (n=31) sets, based on the average (values from both gray and white matter tissue) TDCi truncation. An TDCi with an average truncation value of 50% or greater was deemed truncation positive (Table 3.1 and 3.2). For both sets, the mean and standard deviation for age, time from ictus, treatment status with tPA, recanalization status at 24-hours, NIHSS (admission, 24 hours, 7 days and 3 months), 3 month modified Rankin Score (mRS) and severity of HT were listed .

The agreement between the admission CBV_D volume and $NCCT_D$ volume was assessed with Bland-Altman analysis for recanalization positive (n=32) and negative groups (n=23), and sub-groups based on TDCi truncation and hypervolemia status at admission (Table 3.3). Agreement between CBV_D and $NCCT_D$ volume was evaluated by 95% limits of agreement, defined as the bias ± 1.96 times the standard deviation of the differences³⁶. As a secondary analysis, all CBV_D volumes were plotted against $NCCT_D$

volumes for linear regression analysis. The Pearson correlation coefficient and slope of the regression line was calculated for both groups and sub-groups as listed in table 3.3.

To examine perfusion states within gray and white matter destined to infarct over time, admission CBF and CBV were compared with 24 hour, 7 day, and 3 month perfusion values using Mann-Whitney Rank Sum Tests for all patients, recanalization positive and negative groups. Significant differences were defined as $p < 0.05$.

For this study, we define hypervolemia and hyperperfusion as CBV and CBF, from within the superimposed final infarct ROI, greater than the average plus one standard deviation of the CBV and CBF values obtained from the contralateral mirrored ROI, respectively, for each patient. The fractions of patients with hypervolemia and hyperperfusion along with the clinical improvement, as given by the average \pm standard deviation of the difference of the NIHSS from admission for all patients, were determined at admission, 24 hours, 7 days and 3 months post stroke. At each of the four time points, Fisher Exact Tests were used to investigate: 1) whether the fractions of patients with hypervolemia or hyperperfusion between the recanalization positive and negative groups and 2) the difference in clinical improvement from admission, as defined by a decrease in the NIHSS of ≥ 4 points, between the recanalization positive and negative groups were significantly different.

Patients were also dichotomized into hypervolemia positive ($n=25$) and hypervolemia unknown ($n=30$). Comparing both groups, Fisher Exact Tests were used to investigate: 1) the difference in clinical improvement from admission, as defined by a decrease in the NIHSS of ≥ 4 points and 2) the fraction of patients with HT.

Average gray and white matter admission CBV and CBF values from within tissue destined to infarct were determined for each HT type and compared with Student-t

tests. Also, for patients with a CBV_D at admission (n=30) average CBV_D volume (cm^3) for patients with HI, PH and non-HT were compared using student t-tests, to examine the effect of admission infarct core size on HT severity.

3.3 RESULTS

Fifty-five patients (23 females, 32 males) were included in this study, and their demographics are shown in tables 3.1 and 3.2. A summary for all patients is as follows [mean (range; SD)]: Age was 67 (42 to 82; 11 years), stroke onset to CTP time 155 (50 to 345; 90 minutes), NIHSS 12 (4 to 25; 6), 24 hour NIHSS 9 (1 to 22; 6), 7 day NIHSS 6 (1 to 22; 6), 3 month NIHSS 5 (1 to 21; 6), 3 month modified Rankin Score 2 (1 to 5; 1). Twenty-seven patients were treated with intra-venous (IV) tPA, 7 with intra-arterial (IA) tPA, 1 with both IV and IA tPA, and 20 were not treated with thrombolytic agents. Locations of occlusions were as follows: 27 M1 only occlusions, 6 proximal ICA + M1 occlusions, 16 M2 only occlusions, 6 M3 only occlusions.

Table 3.1 Demographics for patients with truncation of the ischemic time-density curve at admission.

Patient	Age	Gender	Recan. at 24 hrs	Onset NIHSS	24hrs NIHSS	7day NIHSS	3month NIHSS	3month mRS	HT
1	65	F	No	12	6	1	1	1	None
2	78	M	No	13	4	4	1	1	None
3	67	F	Yes	5	10	5	1	2	None
4	50	F	No	10	4	3	1	1	HI-1
5	72	F	Yes	4	3	2	1	1	None
6	73	F	No	22	8	3	2	1	None
7	43	F	No	4	4	2	2	1	None
8	73	F	Yes	20	9	4	3	1	HI-2
9	56	M	Yes	8	3	2	2	1	None
10	51	M	Yes	9	9	7	5	2	HI-1
11	57	M	No	9	6	4	2	1	None
12	74	F	Yes	14	9	9	5	2	None
13	69	F	No	24	22	22	20	4	None
14	69	M	No	13	13	10	15	4	HI-1
15	65	M	Yes	4	1	1	1	1	None
16	50	F	No	13	13	2	1	1	None
17	69	M	Yes	16	11	4	3	1	HI-1
18	42	M	Yes	13	3	1	0	0	None
19	76	M	Yes	4	4	4	6	1	None
20	66	M	Yes	7	3	3	3	1	PH-2
21	78	M	Yes	7	6	3	2	1	None
22	77	F	Yes	4	4	4	2	1	None
23	76	M	Yes	4	8	2	2	1	None
24	82	F	Yes	12	2	2	4	2	None
N=24	65±11	12F,12M		10.7±5.7	6.9±4.7	4.3±4.4	3.5±4.6	1.5±1.2	

NIHSS = National institute of health stroke scale, tPA = tissue plasminogen activator, i.v. = intra-venous, i.a. = intra-arterial, M = male, F = female, mRS = modified Rankin Score, HT = hemorrhagic, HI = hemorrhagic infarction, PH = parenchymal hematoma.

Table 3.2 Demographics for patients without truncation of the ischemic time-density curve at admission.

Patient	Age	Gender	Recan. at 24 hrs	Onset NIHSS	24hrs NIHSS	7day NIHSS	3month NIHSS	3month mRS	HT
25	70	M	No	17	17	17	3	1	HI-1
26	61	M	Yes	12	10	6	6	3	PH-1
27	55	M	No	22	16	9	18	3	None
28	55	M	Yes	9	6	3	2	1	None
29	47	F	Yes	14	7	2	1	1	None
30	56	M	Yes	20	15	15	12	4	PH-1
31	56	M	No	8	3	2	2	1	None
32	80	F	No	16	13	10	14	3	HI-1
33	69	M	No	25	21	19	12	4	HI-1
34	67	F	No	9	9	4	3	1	HI-1
35	69	M	Yes	16	11	4	3	1	HI-1
36	80	F	No	6	6	1	1	1	None
37	67	M	Yes	8	6	3	2	1	None
38	42	M	No	12	17	14	11	3	HI-2
39	65	M	Yes	13	15	8	3	2	None
40	81	M	No	4	18	18	15	3	PH-1
41	77	F	No	18	17	17	5	1	None
42	65	M	Yes	9	7	3	1	1	None
43	80	F	Yes	11	3	1	0	0	None
44	67	M	Yes	5	1	1	1	1	None
45	76	F	No	18	18	17	17	5	PH-2
46	76	M	No	8	6	5	4	2	PH-1
47	82	F	Yes	8	0	0	0	0	None
48	78	F	Yes	8	1	1	1	1	None
49	59	M	Yes	7	13	13	6	3	PH-1
50	78	M	Yes	10	3	1	1	1	None
51	81	M	Yes	10	5	2	1	1	None
52	58	F	Yes	4	1	1	1	1	None
53	70	M	No	19	17	9	4	2	HI-1
54	79	F	Yes	20	16	11	3	1	PH-2
55	80	M	No	21	21	18	21	5	HI-2
N=31	68±11	11F,20M		12.5±5.7	10.0±6.6	7.6±6.5	5.6±6.0	1.9±1.3	

NIHSS = National institute of health stroke scale, tPA = tissue plasminogen activator, i.v. = intra-venous, i.a. = intra-arterial, M = male, F = female, mRS = modified Rankin Score, HT = hemorrhagic, HI = hemorrhagic infarction, PH = parenchymal hematoma.

Table 3.3 contains the results for the Bland-Altman analysis, as well as the Pearson correlation for the CBV_D volume versus final infarct volume, measured on the 3-month NCCT. The 95% limits of agreement from the Bland-Altman analysis were widest for the recanalization negative group and its sub-groups, compared with the recanalization positive group and its sub-groups. The recanalization positive and truncation negative group had the highest Pearson correlation coefficient ($R = 0.81$) and slope of the regression line closest to unity (slope = 0.80). The regression line slopes for both hypervolemia positive sub-groups were negative and closest to zero.

Table 3.3 Bland-Altman and linear regression results for the admission CBV defect volume versus the final infarct volume at 3 months

	95% Limits of Agreement (mean difference $\pm 2*SD$)	Pearson Correlation Coefficient, R (P value)	Slope of Regression Line
<i>Recanalization Positive (n=32)</i>	[-48.3,29.1]	0.78 (0.08)	0.64
Truncation negative (n=17)	[-8.4,16.0]	0.81 (0.19)	0.80
Truncation positive (n=15)	[-40.5,30.3]	0.61 (0.11)	0.46
Hypervolemia unknown (n=17)	[-51.9,38.2]	0.80 (0.04)	0.57
Hypervolemia positive (n=15)	[-37.6,16.1]	0.22 (0.79)	-0.04
<i>Recanalization Negative (n=23)</i>	[-86.2,51.1]	0.57 (0.03)	0.42
Truncation negative (n=14)	[-85.9,68.3]	0.15 (0.74)	0.14
Truncation positive (n=9)	[-69.9,36.9]	0.71 (0.04)	0.62
Hypervolemia unknown (n=13)	[-96.9,61.3]	0.68 (0.10)	0.37
Hypervolemia positive (n=10)	[-56.9,19.2]	0.39 (0.22)	-0.13

Tables 3.4, 3.5 and 3.6 give CBF [$\text{ml}\cdot\text{min}^{-1}\cdot(100\text{g})^{-1}$] and CBV [$\text{ml}\cdot(100\text{g})^{-1}$] values from within the superimposed final infarct volume for all patients, the recanalization positive group and negative group, respectively, at each time point. CBF and CBV were highest at day 7 for both tissue types; gray matter CBF was significantly higher than the admission CBF value ($p < 0.05$). For both gray and white matter, there were no significant differences between admission and 3 month CBF and CBV values ($p > 0.05$). Also shown are the fractions of patients with hypervolemia or hyperperfusion at each time point, and the NIHSS improvement relative to the admission NIHSS. The recanalization positive group had a higher fraction of patients with hypervolemia at admission, 24 hours, 7 days, and hyperperfusion at 24 hours and 7 days than the recanalization negative group ($p = 0.054$ to 0.067). There were trends in clinical improvement from admission in patients who recanalized, but the changes in NIHSS scores were not significantly different from the non-recanalized group ($p > 0.05$).

Table 3.4 All patients (n=55): CBF and CBV values at four time points from within superimposed final infarct volumes. Also shown are the fractions of patients with hypervolemia and hyperperfusion, along with change in NIHSS.

	CBF [$\text{ml}\cdot\text{min}^{-1}\cdot 100\text{g}^{-1}$]		CBV ($\text{ml}\cdot 100\text{g}^{-1}$)		Hyper-volemia	Hyper-perfusion	NIHSS Improvement
	Gray matter	White matter	Gray matter	White matter			
Admission	10.4±8.3	8.8±5.6	1.01±0.66	1.09±0.49	25/55	0/55	-
24 hours	15.3±11.0	13.8±9.3	1.27±0.58	1.23±0.58	26/55	11/55	2.7±4.6
7 days	20.8±17.17	17.1±14.8	1.86±1.15	1.33±0.81	26/55	16/55	5.2±5.3
3 months	12.3±4.5	11.2±2.6	0.93±0.25	0.94±0.94	0/55	0/55	6.6±5.6

Table 3.5 Recanalization positive group (n=32): CBF and CBV values at four time points from within superimposed final infarct volumes. Also shown are the fractions of patients with hypervolemia and hyperperfusion, along with change in NIHSS.

	CBF ($\text{ml}\cdot\text{min}^{-1}\cdot 100\text{g}^{-1}$)		CBV ($\text{ml}\cdot 100\text{g}^{-1}$)		Hyper-volemia	Hyper-perfusion	NIHSS Improvement
	Gray matter	White matter	Gray matter	White matter			
Admission	12.2±8.0	10.7±6.5	1.15±0.60	1.34±1.00	15/32	0/32	-
24 hours	19.1±12.7	12.2±7.6	1.41±0.62	1.39±0.93	19/32	11/32	3.7±4.1
7 days	28.7±14.1 [‡]	19.4±19.9	1.95±1.18	1.39±0.11	18/32	11/32	5.9±4.5
3 months	12.7±4.1	10.9±3.1	0.99±0.28	1.23±0.59	0/32	0/32	7.2±4.6

[‡]Significantly different ($p < 0.05$) from admission gray matter CBF.

Table 3.6 Recanalization negative group (n=23): CBF and CBV values at four time points from within superimposed final infarct volumes. Also shown are the fractions of patients with hypervolemia and hyperperfusion, along with change in NIHSS.

	CBF ($\text{ml}\cdot\text{min}^{-1}\cdot 100\text{g}^{-1}$)		CBV ($\text{ml}\cdot 100\text{g}^{-1}$)		Hyper-volemia	Hyper-perfusion	NIHSS Improvement
	Gray matter	White matter	Gray matter	White matter			
Admission	10.8±7.4	6.3±2.4	1.03±0.73	0.73±0.39	10/23	0/23	-
24 hours	11.3±8.6	9.8±7.0	1.04±0.54	0.84±0.69	7/23	4/23	1.9±5.1
7 days	12.8±6.3	13.6±7.1	1.66±1.17	1.25±0.54	8/23	4/23	4.9±6.3
3 months	11.2±3.6	11.4±2.4	0.83±0.23	0.91±0.19	0/23	0/23	6.4±6.8

Table 3.7 shows the NIHSS improvement from admission throughout the 3 months in patients with/without hypervolemia at admission, and the HT percentage for both groups. Comparing the NIHSS improvement among the three time points, there were no significant differences ($p > 0.05$). However, admission hypervolemia was associated with a significantly higher incidence of HT ($p = 0.048$), but this group also had a non-significantly higher incidence of recanalization relative to hypervolemia negative patients.

Table 3.7 Clinical outcome and hemorrhage rates for patients with/without admission hypervolemia.

Hypervolemia at admission	Improvement in NIHSS from admission			HT
	24 hours	7 days	3 months	
Positive (n=25)	2.2±4.5	4.8±5.1	6.4±5.5	52%*
Unknown (n=30)	2.6±4.5	5.2±5.4	6.7±5.7	26%

* Percentage of patients with hemorrhagic transformation (HT) was significantly higher ($p = 0.0478$) when hypervolemia was confirmed at admission.

The relationship between admission CBV_D and final infarct size is affected by the following technical and physiological conditions: truncation of TDCi, recanalization status within 24 hours of the admission CTP study and hypervolemia during the admission CTP study. Using the scores 1, 0 and -1 to denote admission CBV defect is larger than, equal to and smaller than final infarct size, respectively, table 3.8 evaluates the effect of the presence or absence of each of the confounding factors on the size of admission CBV defect size relative to the final infarct size. While TDCi truncation and recanalization can be determined by analysis of the TDCi and CTA/CTP-CBF images, respectively, hypervolemia cannot be determined with certainty, except for the case when the admission CBV is higher than contralateral normal brain. In cases where ipsilateral CBV is equal to or lower than contralateral CBV, hypervolemia status is unknown because of one or more of the following reasons: the TDCi is truncated, hypervolemia is heterogeneous and does not happen uniformly throughout the CBV_D , or it may have occurred before or after the admission CTP study. In these instances, if we assume the proportion of hypervolemia positive and negative cases are equal, table 3.8 contracts to table 3.9. Therefore, this heuristic model predicts that the admission CBV_D will overestimate the final infarct size for truncation positive/recanalization positive cases, and underestimate the final infarct size for all other cases (Table 3.9). Table 3.10 shows the measured admission CBV_D as a percentage of the final infarct volume, under different conditions of TDCi truncation and recanalization. The proposed heuristic model was able to demonstrate the trend in the dis/agreement between admission CBV_D and the final infarct size, though no significance of the dis/agreement was observed in any of the groups ($p > 0.05$).

Table 3.8 Model to describe the relationship between admission CBV_D and final infarct size from 3 month NCCT.

<i>Hyper (-)</i>	0	<i>Hyper (-)</i>	0	<i>Hyper (-)</i>	0	<i>Hyper (-)</i>	0
<i>Truncat (+)</i>	1	<i>Truncat (+)</i>	1	<i>Truncat (-)</i>	0	<i>Truncat (-)</i>	0
<i>Recan(+)</i>	0	<i>Recan(-)</i>	-1	<i>Recan(+)</i>	0	<i>Recan(-)</i>	-1
Sum	1	Sum	0	Sum	0	Sum	-1
<i>Hyper (+)</i>	-1	<i>Hyper (+)</i>	-1	<i>Hyper (+)</i>	-1	<i>Hyper (+)</i>	-1
<i>Truncat (+)</i>	1	<i>Truncat (+)</i>	1	<i>Truncat (-)</i>	0	<i>Truncat (-)</i>	0
<i>Recan(+)</i>	0	<i>Recan(-)</i>	-1	<i>Recan(+)</i>	0	<i>Recan(-)</i>	-1
Sum	0	Sum	-1	Sum	-1	Sum	-2

Table 3.9. Predicted baseline CBV_D size relative to final infarct size among the four cases of TDCi truncation and recanalization status when prevalence of hypervolemia is 50%.

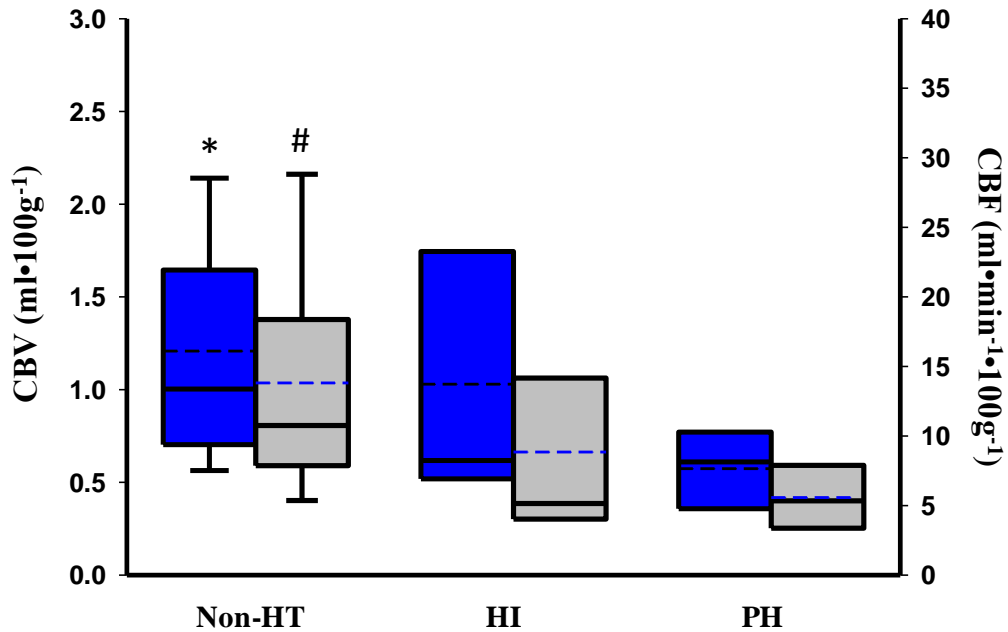
	Recanalization (+)	Recanalization (-)
Truncation (+)	0.5	-0.5
Truncation (-)	-0.5	-1.5

Table 3.10 Measured baseline CBV defect size as a percentage of the final infarct size among the four cases of TDCi truncation and recanalization status when prevalence of hypervolemia is 50%.

	Recanalization (+)	Recanalization (-)
Truncation (+)	111.1 ± 94.1	64.9 ± 50.2
Truncation (-)	83.4 ± 78.2	74.4 ± 99.2

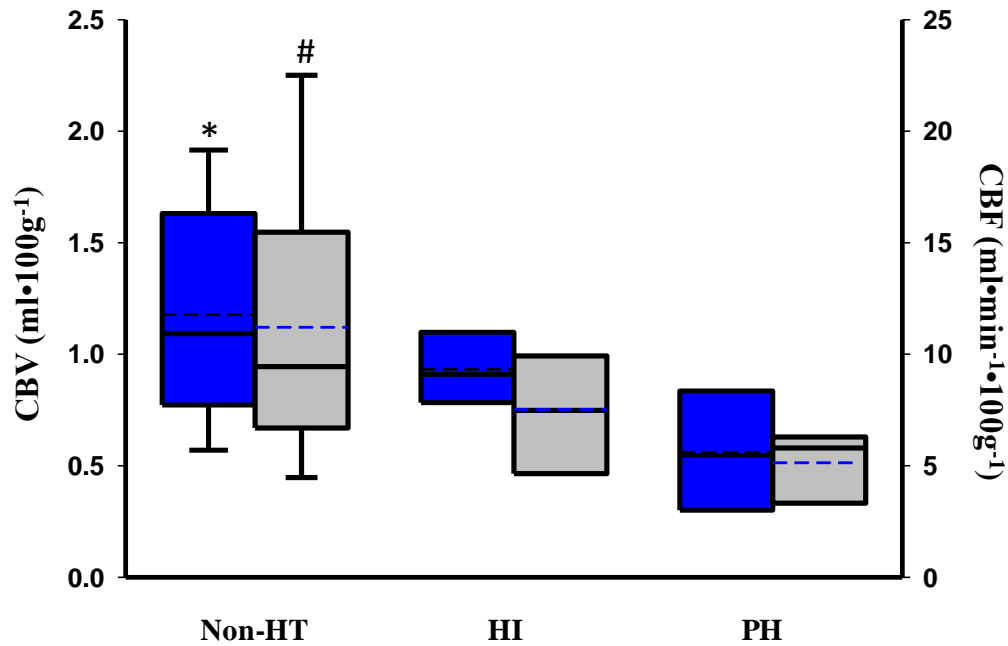
Hemorrhagic transformation (HT) was observed in 21/55 patients: 13 HI, 8 PH (Tables 3.1 and 3.2). HT was present in 10/32 and 11/23 patients in the recanalization positive and negative groups, respectively. Figure 3.1 and 3.2 depict box plots for admission gray and white matter CBV and CBF values for patients with PH, HI and without HT. For both cerebral tissue types, mean CBV and CBF values, from within tissue destined to infarct, in non-HT patients were significantly different than values from patients with PH ($p < 0.05$). Average CBV_D volumes (cm^3) for non-HT, HI, and PH and groups were 39.9 ± 32.3 , 53.1 ± 28.9 and 102.3 ± 43.0 , respectively (Figure 3.3). Average admission CBV_D volume for patients with PH was significantly higher than the CBV_D volume for patients without HT ($p < 0.05$).

Figure 3.1 Admission gray matter CBV and CBF from within the superimposed final infarct ROI



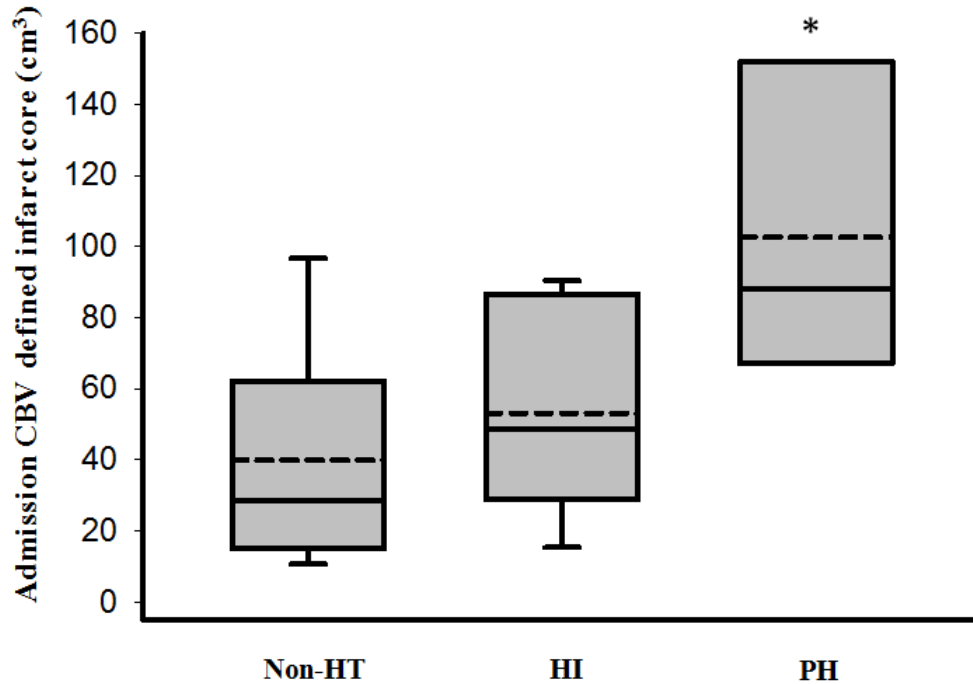
Box plots for admission gray matter CBV [$\text{ml} \cdot (100\text{g})^{-1}$; blue boxes] and CBF [$\text{ml} \cdot \text{min}^{-1} \cdot (100\text{g})^{-1}$; gray boxes] from within the superimposed final infarct ROI. Patients were separated into non-hemorrhagic transformation (HT), hemorrhagic infarction (HI), and parenchymal hematoma (PH). Median and mean are given as solid and dashed lines, respectively. Mean CBV (*) and CBF (#) values for the non-HT group were both significantly different ($p < 0.05$) than the mean CBV and CBF values for the PH group.

Figure 3.2 Admission white matter CBV and CBF from within the superimposed final infarct ROI



Box plots for admission white matter CBV [$\text{ml} \cdot (100\text{g})^{-1}$; blue boxes] and CBF [$\text{ml} \cdot \text{min}^{-1} \cdot (100\text{g})^{-1}$; gray boxes] from within the superimposed final infarct. Patients were separated into non-hemorrhagic transformation (HT), hemorrhagic infarction (HI), and parenchymal hematoma (PH). Median and mean are given as solid and dashed lines, respectively. Mean CBV (*) and CBF (#) values for the non-HT group were both significantly different ($p < 0.05$) than the mean CBV and CBF values for the PH group.

Figure 3.3 CBV defect volume for non-HT and HT sub-groups



Average \pm standard deviation admission CBV_D volume (cm^3) for patients with a CBV defect present at admission for patients with no hemorrhagic transformation (n=17), hemorrhagic infarction (HI; n=9) and parenchymal hematoma (PH; n=5). Median and mean are given as solid and dashed lines, respectively (*) denotes significantly different from non-HT patients ($p < 0.05$)

3.4 DISCUSSION

This AIS study explores technical and physiological processes which affect the CBV parameter: 1) TDCi truncation, 2) nutritive and non-nutritive hypervolemia, and 3) recanalization status. As a secondary analysis, we describe acute and sub-acute perfusion states (CBV and CBF values) within gray and white matter that progresses to infarction, and association with hemorrhagic transformation (HT). The volume of infarct core, as defined by the CBV parameter, is associated with the severity of HT. Further, very low CBF and CBV values, within tissue that progresses to infarction, were also indicative of HT severity. A three month NCCT was used to define the final infarct volume to allow for edema reduction and infarct maturation.

The CBV parameter continues to be an important parameter to distinguish tissue viability states in the setting of ischemic stroke. A substantial reduction in CBV during the acute stroke setting is presumed to be a physiological surrogate for infarction, due to the irreversible loss of vascular smooth muscle autoregulatory capacity³⁷. Conversely, an increase in CBV in an area of hypoperfusion has been suggested to represent electrically silent, yet viable tissue³⁸. Still, there remains a lack of standardization for CBV thresholds to define tissue viability, and with its poor correlation with the acute DWI hyperintensity, the reliability of the CBV parameter are increasingly being questioned²⁹. Although diffusion-weighted imaging (DWI) hyperintensities are commonly described as non-viable tissue, a recent study showed that reversal can occur in > 50% of patients³¹. PET imaging of the central benzodiazepine receptor with ¹⁸F-flumazenil, is the only method to truly define infarct core, but this technique is not practicable within the setting of acute stroke³⁹. The results herein show that the best correlation between CBV_D versus the final infarct volume occurs in patients who recanalize within 24 hours. This makes intuitive

sense, as the infarct core will minimally expand into the surrounding penumbra once recanalization is achieved. Moreover, TDCi truncation has a differing effect on recanalization positive and negative groups, as shown in table 3.3. In patients who do not recanalize and have truncation of the TDCi, the acute CBV_D volume closely matches the final infarct volume because truncation at admission artificially lowers CBV, overestimating the predicted infarct core. This could lead to an inaccurate estimate of the CBV threshold for infarction in retrospective studies. Conversely, in patients who recanalize, the overestimation of the infarct core at admission, caused by truncation of the TDCi, could lead to the paradoxical phenomenon of reversal of infarct define with CBV threshold^{30, 40}.

In determining whether truncation of the TDCi is present, it is important to note that complete wash-in and wash-out of the arterial input function and/or venous output function do not mean the ischemic tissue TDC is free of the artifact. Conditions which may lead to the late arrival time of the CT contrast and truncation of the TDCi include internal carotid artery stenosis, atrial fibrillation, insufficient blood supply from collaterals and congestive heart failure. An effective way to prevent truncation of TDCi from late arrival of contrast is to use an extended second phase perfusion imaging protocol. Following the initial 45-50 second cine scan, sampling every 15 seconds for an additional 90 seconds can minimize radiation dose while obtaining the data required for an accurate CBV calculation⁴¹. The second phase data can also be used to evaluate blood brain barrier permeability, further guiding thrombolysis administration decisions⁴¹. The total effective dose from a multimodal CT stroke study, for a 64-row detector CT, is ~7mSv, double the annual background radiation dose⁴². Radiation-dose reduction strategies, such as the Adaptive Statistical Iterative Reconstruction (ASIR) (GE

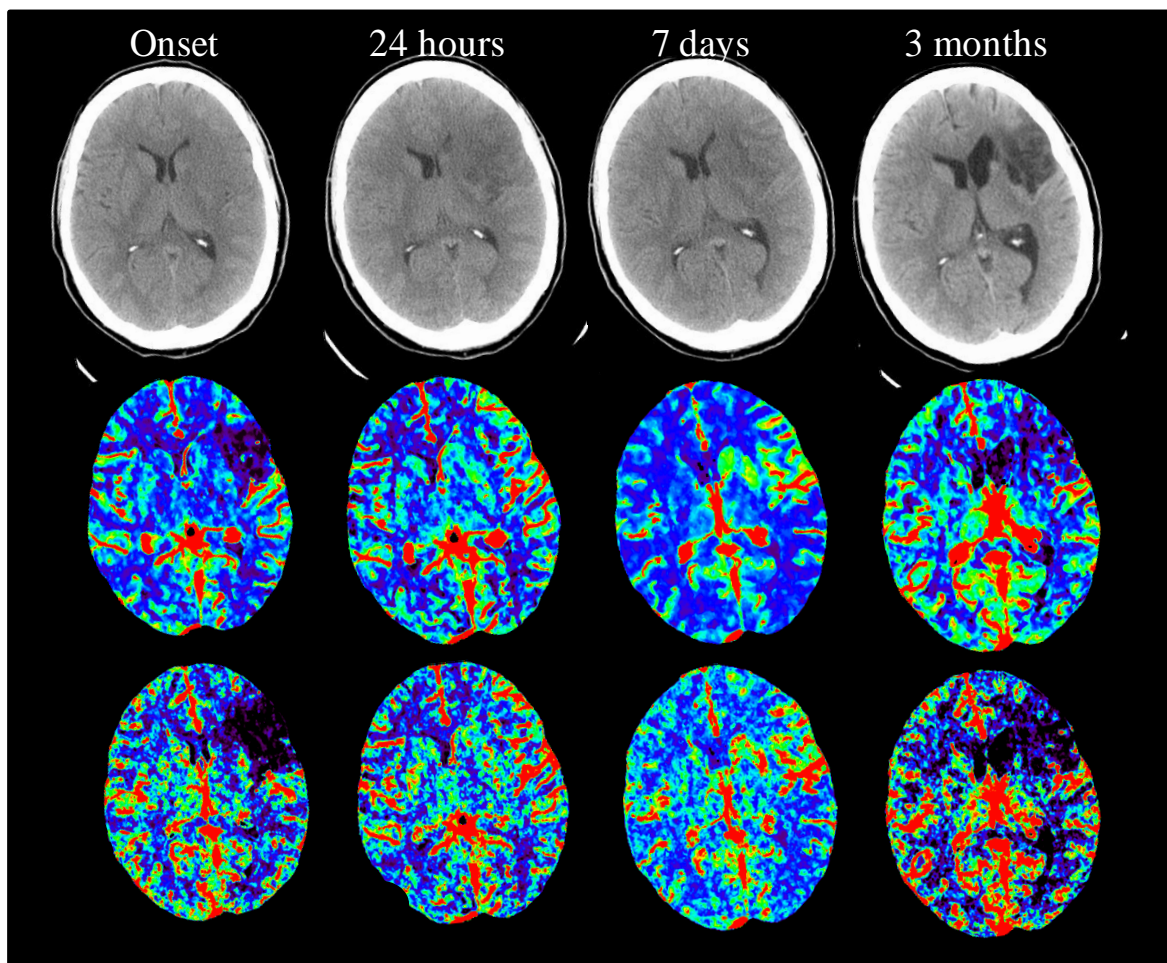
Healthcare), can maintain image quality while reducing effective dose by $> 25\%$ ⁴³. Also, radiation dose could be reduced by two thirds, without compromising the accuracy of the CTP functional maps, by increasing the sampling interval from 1 s to 3 seconds in the first phase of a CTP study⁴⁴.

The physiological state of hypervolemia, defined as an increase in CBV, or the increase in the amount of blood in tissue, relative to the mirror region of the contralateral hemisphere, may also impact both prospective clinical decisions as well as characterizing perfusion thresholds experimentally. Irrespective of recanalization, the CBV_D volume had the poorest correlation with final infarct volume in patients with admission hypervolemia. This transient perfusion state is observed in regions with increased, decreased or normal CBF at any time during infarct maturation⁴⁵. The hypervolemic response can be promoted by embolic migration, therapeutic dissolution, and/or release of vasodilatory- and inflammatory-mediators⁴⁵.

Chronic, non-nutritive hypervolemia and hyperperfusion can induce blood-brain barrier breakdown, enhancing the risk of HT, edema formation and release of inflammatory-related mediators (reperfusion injury) potentially worsening clinical outcome, as shown in figure 3.4^{45, 46}. Here, a matched decrease in CBF and CBV is apparent at onset within the hypodense region, indicative of cortical swelling, on the corresponding admission NCCT. After CTA confirmed recanalization, hyperperfusion and hypervolemia are seen at 24 hours and 7 days post stroke onset, the so-called “luxury perfusion syndrome”⁴⁷. Nonetheless, this non-nutritive hypervolemic/hyperperfusion response was associated with only a short-term decline in clinical outcome. When examining all patients at 24 hours, 7 days and 3 months, an increase in CBV was present in 33%, 40% and 0% of patients, respectively, which was not associated with an average

overall worsening of the NIHSS score at any time point, compared to the patients without hypervolemia at onset. This finding is consistent with a study by Kidwell et al. (2001) who found that hyperperfusion occurred in 50% of AIS patients by day 7; correlating perfusion images with diffusion weighted MR images, this hyperperfusion occurred mainly in regions that went on to infarction and was not associated with clinical outcome⁴⁸. Examining 9 patients with AIS, Hatazawa et al. (2011) demonstrated that variable states of hypervolemia, as shown by increased, decreased and unchanged CBV, depended on the severity of hypoperfusion. The results herein showed that early hypervolemia was associated with low CBF, and late hypervolemia was associated with low, normal or high CBF within tissue progressing to infarction.

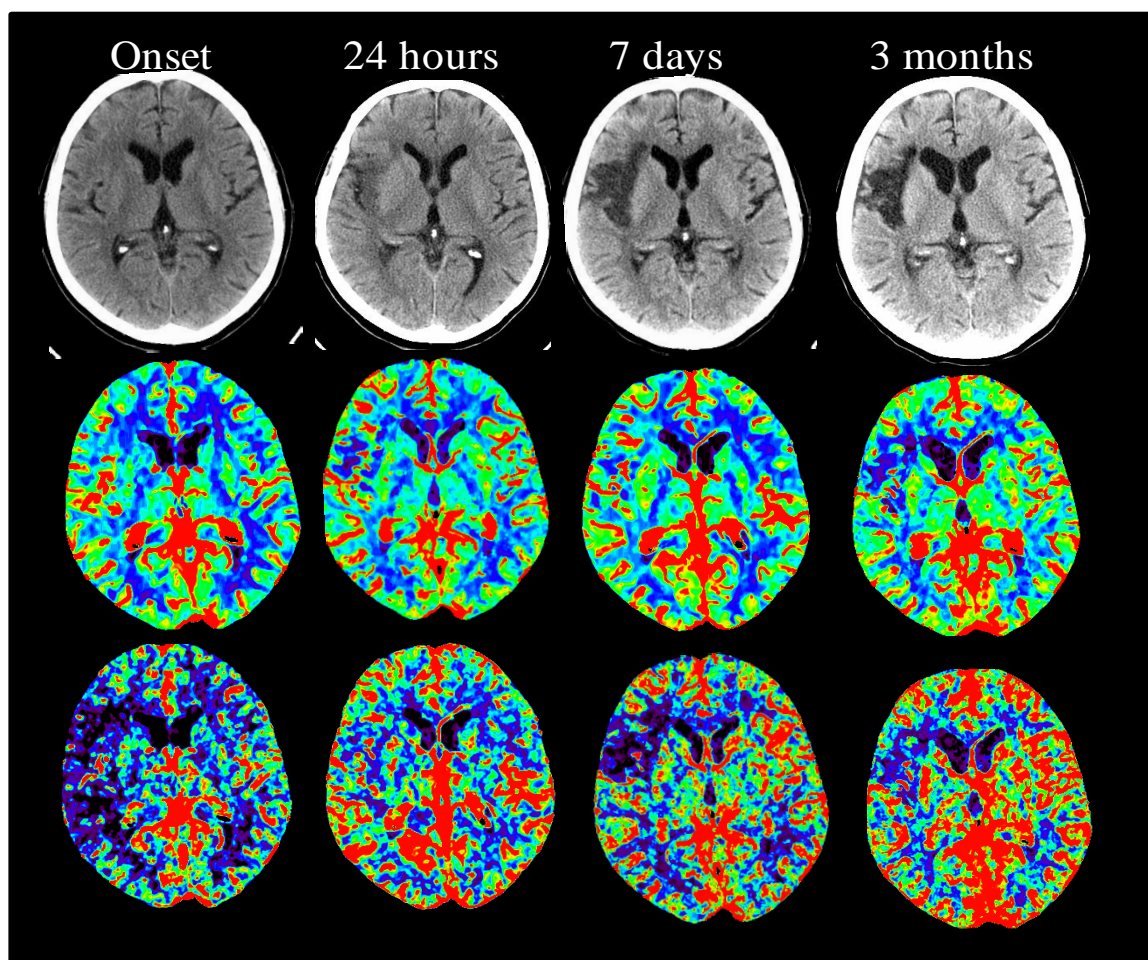
Figure 3.4 Example of acute matched decrease in CBF and CBV, and sub-acute hypervolemia and hyperperfusion



CT perfusion studies at admission, 24 hours, 7 days, and 3 months post ictus for AIS patient 3, with confirmed recanalization at 24 hours. NCCT, CBV and CBF maps are shown in rows 1, 2 and 3, respectively. A matched decrease in CBV and CBF is visible at onset, corresponding to the slightly hypodense area on the NCCT. At 24 hours and 7 days, a matched increase in CBV and CBF, within the tissue destined to infarct, is indicative of hyperperfusion and hypervolemia responses, respectively. NIHSS scores for this patient were 5, 10, 5, 1 for onset, 24 hours, 7 days and 3 months, respectively, with modified Rankin score of 2, at 3 months

Overall, incidences of hypervolemia and hyperperfusion were highest at 7 days in both gray and white matter tissue and more pronounced in patients who recanalized. During this sub-acute stroke stage, the occurrence could mask late, evolving infarction, but does not seem to have a long term effect on clinical outcome. During the hyper-acute stroke stage (< 6 hours), increased CBV within hypoperfused tissue has been used to detect potentially salvageable tissue, the so called “penumbral hypothesis”. Contrary to sub-acute hypervolemia, the hyper-acute (< 6 hours) increase in pooled blood may offer improved nutrition and act as a buffer for acid metabolites, protecting against pH changes; however these hypervolemic regions may not be distinguished from potentially malignant, non-nutritional hypervolemia within already evolving infarction. Figure 3.5 shows a patient with a CBF/CBV mismatch at admission with little evidence of early ischemic change on the corresponding NCCT. Even with confirmed recanalization/reperfusion at 24 hours, portions of the supposedly viable hypervolemic tissue at admission still progressed to infarction. For the entire patient cohort, this admission CBF/CBV mismatch within areas of little or no early ischemic change discerned on contemporaneous NCCT images was observed in 38% (12/32) of patients with confirmed recanalization at 24 hours. Of this sub-group, 83% (10/12) of patients had hypervolemic tissue at admission (the CBF/CBV mismatch) and 24 hours (either a matched increase, or mismatch in CBF/CBV), that went on to infarction. Also, the same 10/12 patients had full or partial hyperperfusion at 24 hours within areas of NCCT hypoattenuation at 3 months. Moreover, incidence of HT was higher in patients with admission hypervolemia, but this group also had a higher incidence of recanalization; however, just 17% of patients with HT had hypervolemia out to 7 days.

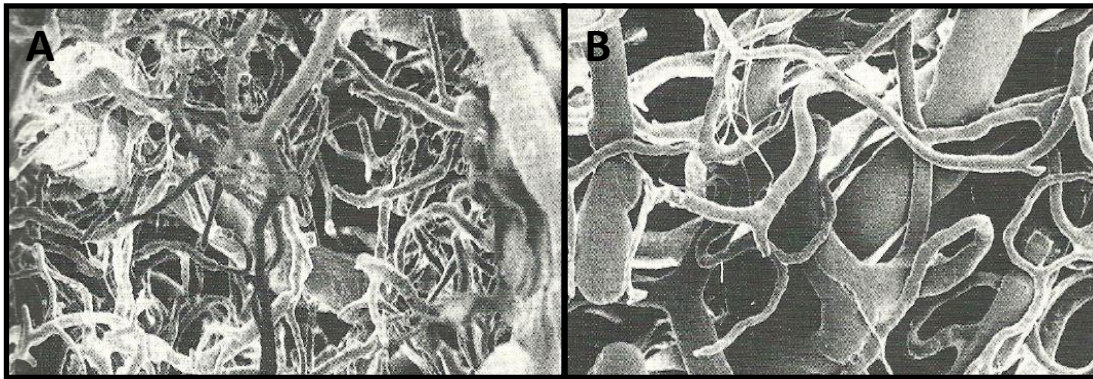
Figure 3.5 Example of acute mismatch CBF/CBV, and sub-acute hypervolemia and hyperperfusion



CT perfusion studies at admission, 24 hours, 7 days, and 3 months post ictus for AIS patient 29, with confirmed recanalization at 24 hours. NCCT, CBV and CBF maps are shown in rows 1, 2 and 3, respectively. A mismatch between CBF and CBV is apparent at onset. At 24 hours, CBF returns to normal, while a slight decrease in CBV was visible. At 7 days, the CBF defect matched the area of hypoattenuation on the NCCT, while CBV remained high within the region of hypoperfusion. At 3 months, both the CBV and CBF defects matched the final infarct volume. NIHSS scores for this patient were 14, 7, 2, 1 for onset, 24 hours, 7 days and 3 months, respectively, with modified Rankin score of 1 at 3 months.

We speculate that acute and sub-acute collateral recruitment and vasodilatory effort of relatively (compared to neurons) ischemic resistant endothelial cells is one of futility, as neurons have already begun their slow progression towards apoptotic/necrotic cell death, a process which could last out to 7 days post ictus; neurons are more vulnerable to ischemic injury than any other type of cell in the brain (except immature oligodendrocytes)⁴⁹⁻⁵¹. Hypervolemia and hyperperfusion during the acute and sub-acute stages can also result from the opening of arteriovenous shunts (anastomoses) and subsequent increase in venous volume, a feature independent of the particular injury process, within the infarct zone⁵². Figure 3.6 depicts a scanning electron micrograph of the gerbil microvascular architecture in a control animal and papaverine pre-treated animal, injected with acrylic resin causing parenchymal herniation from brain swelling. In response to the increased intra-cranial pressure, development of direct arteriovenous

Figure 3.6 Example of arteriovenous shunting



Scanning electron micrograph of the gerbil microvascular architecture in a control animal (A) and papaverine pre-treated animal (B), injected with acrylic resin causing parenchymal herniation from brain swelling. Arteriovenous shunting, venous filling, and capillary compression are evident. Adapted from *Cerebral Hyperemia and Ischemia: From the Standpoint of Cerebral Blood Volume* (p. 19), by M. Tomita et. al., 1987, Osaka, Japan: Elsevier Science Publishers. Adapted and Reprinted with permission

shunting via thoroughfare channels, venous distension, and compressed capillaries is evident. In stroke, similar pathological mechanisms, as shown in Figure 3.6, likely characterize the transition from nutritive to non-nutritive hypervolemia as cytotoxic and/or vasogenic edema increases in conjunction with the loss of endothelial cell smooth muscle regulation, and capillary compression. Therefore, we hypothesize that a hyper-acute CBF/CBV mismatch is not always indicative of viable tissue (penumbra), an important consideration when defining the infarct core. This is further validated by the fact that the degree of clinical improvement was not higher in patients with an acute CBF/CBV mismatch, compared to patients with a matched decrease in CBF/CBV (Table 3.7). Nonetheless, the transition from nutritive to malignant hypervolemia is time dependent and differs between individuals.

When implementing brain perfusion thresholds it's also important to separate gray and white matter. In resting gray matter, average CBF values are approximately 50-60 $\text{ml}\cdot\text{min}^{-1}\cdot(100\text{g})^{-1}$, whereas white matter values are closer to 20-25 $\text{ml}\cdot\text{min}^{-1}\cdot(100\text{g})^{-1}$. This substantial discrepancy in flow values is mainly because white matter synapses consume $\leq 0.5\%$ of the energy of gray matter synapses⁵³. It follows that white matter may be more tolerant to ischemia than gray matter, as there is a greater relative decrease in CBF from normal in gray matter than in white matter⁵⁴. Further, since gray matter has a greater metabolic demand for maintenance of cell structure integrity, it can be expected that the damage would occur earlier and be more severe than white matter for a given CBF. Thresholds originating from human studies frequently use regions with combined gray and white matter, which could lead to under/overestimation of infarcted tissue in follow-up prospective studies. Since we know gray and white matter have very different

basal and pathological perfusion thresholds, current studies need to define separate thresholds for gray and white matter.

This study is not without its limitations. First, use of the 3 month NCCT to determine final infarction volume could be affected by infarct shrinkage and secondary vascular injury, potentially causing under- and overestimation of final infarct volume, respectively. Second, only a 2cm slab of tissue was imaged during the CTP acquisition, which could have missed part of the infarct volume and hypervolemic states. Further, recanalization and reperfusion are defined using the 24 hour CTA and CTP-CBF images, respectively.

In summary, the reliability of the admission CBV defect to define infarct is affected by the physiological factors of recanalization and hypervolemia, and the technical factor of TDCi truncation. When determining an optimal threshold to define acute tissue viability, patients should be dichotomized into recanalization positive and negative groups, due to potential differences in infarct expansion. The truncation artifact can cause varying degrees of artificial CBV reduction, potentially overestimating the acute infarct core. We observed varying perfusion states within evolving infarction, both acutely and sub-acutely. Late hypervolemia and hyperperfusion measures were not associated with clinical decline or HT, but could mask late evolving infarction if CBV thresholds were used to define infarct size. We speculate that early hypervolemia, as seen in the CBF/CBV mismatch, could contain 'hidden infarction' due to opening of non-nutritive arteriovenous shunts, causing venous filling. This could affect both thrombolytic treatment decisions as well as the validity of CBV thresholds obtained from retrospective studies. At admission, the size of the CBV_D volume in patients without admission hypervolemia, and lower CBF and CBV values were associated with HT development.

Although use of CBV thresholds may miss infarction present in ~80% of CBF/CBV mismatch, we conclude that very low CBV, or a matched decrease in CBF/CBV, is a valuable predictor of infarct core, and potentially HT when the acquisition of TDCi data is complete and recanalization does not occur. Therefore, CBV thresholds for acute infarct core should be obtained from this sub-set of patients, and may be used to guide thrombolysis treatment.

3.5 REFERENCES

1. Rosamond W, Flegal K, Furie K, Go A, Greenlund K, Haase N, et al. Heart disease and stroke statistics--2008 update: A report from the american heart association statistics committee and stroke statistics subcommittee. *Circulation*. 2008;117:e25-146
2. Wahlgren N, Ahmed N, Davalos A, Hacke W, Millan M, Muir K, et al. Thrombolysis with alteplase 3-4.5 h after acute ischaemic stroke (sits-istr): An observational study. *Lancet*. 2008;372:1303-1309
3. Hacke W, Kaste M, Bluhmki E, Brozman M, Davalos A, Guidetti D, et al. Thrombolysis with alteplase 3 to 4.5 hours after acute ischemic stroke. *The New England journal of medicine*. 2008;359:1317-1329
4. Bluhmki E, Chamorro A, Davalos A, Machnig T, Sauce C, Wahlgren N, et al. Stroke treatment with alteplase given 3.0-4.5 h after onset of acute ischaemic stroke (ecass iii): Additional outcomes and subgroup analysis of a randomised controlled trial. *Lancet neurology*. 2009;8:1095-1102
5. Schumacher HC, Bateman BT, Boden-Albala B, Berman MF, Mohr JP, Sacco RL, et al. Use of thrombolysis in acute ischemic stroke: Analysis of the nationwide inpatient sample 1999 to 2004. *Ann Emerg Med*. 2007;50:99-107
6. Fang MC, Cutler DM, Rosen AB. Trends in thrombolytic use for ischemic stroke in the united states. *J Hosp Med*. 5:406-409
7. Albers GW, Thijs VN, Wechsler L, Kemp S, Schlaug G, Skalabrin E, et al. Magnetic resonance imaging profiles predict clinical response to early reperfusion: The diffusion and perfusion imaging evaluation for understanding stroke evolution (defuse) study. *Annals of neurology*. 2006;60:508-517
8. Bandera E, Botteri M, Minelli C, Sutton A, Abrams KR, Latronico N. Cerebral blood flow threshold of ischemic penumbra and infarct core in acute ischemic stroke: A systematic review. *Stroke; a journal of cerebral circulation*. 2006;37:1334-1339
9. Ebinger M, De Silva DA, Christensen S, Parsons MW, Markus R, Donnan GA, et al. Imaging the penumbra - strategies to detect tissue at risk after ischemic stroke. *Journal of clinical neuroscience : official journal of the Neurosurgical Society of Australasia*. 2009;16:178-187
10. Hatazawa J, Shimosegawa E, Toyoshima H, Ardekani BA, Suzuki A, Okudera T, et al. Cerebral blood volume in acute brain infarction: A combined study with dynamic susceptibility contrast mri and 99mtc-hmpao-spect. *Stroke; a journal of cerebral circulation*. 1999;30:800-806
11. Heiss WD, Sobesky J, Hesselmann V. Identifying thresholds for penumbra and irreversible tissue damage. *Stroke; a journal of cerebral circulation*. 2004;35:2671-2674

12. Hjort N, Butcher K, Davis SM, Kidwell CS, Koroshetz WJ, Rother J, et al. Magnetic resonance imaging criteria for thrombolysis in acute cerebral infarct. *Stroke; a journal of cerebral circulation*. 2005;36:388-397
13. Rohl L, Ostergaard L, Simonsen CZ, Vestergaard-Poulsen P, Andersen G, Sakoh M, et al. Viability thresholds of ischemic penumbra of hyperacute stroke defined by perfusion-weighted mri and apparent diffusion coefficient. *Stroke; a journal of cerebral circulation*. 2001;32:1140-1146
14. Zaro-Weber O, Moeller-Hartmann W, Heiss WD, Sobesky J. The performance of mri-based cerebral blood flow measurements in acute and subacute stroke compared with 15o-water positron emission tomography. Identification of penumbral flow. *Stroke; a journal of cerebral circulation*. 2009; 40(7):2413-21
15. Hacke W, Kaste M, Fieschi C, Toni D, Lesaffre E, von Kummer R, et al. Intravenous thrombolysis with recombinant tissue plasminogen activator for acute hemispheric stroke. The european cooperative acute stroke study (ecass). *JAMA : the journal of the American Medical Association*. 1995;274:1017-1025
16. Bivard A, Parsons M. Aspectasaurus (a dinosaur)? *International journal of stroke : official journal of the International Stroke Society*. 2012;7:564
17. Wardlaw JM, Dorman PJ, Lewis SC, Sandercock PA. Can stroke physicians and neuroradiologists identify signs of early cerebral infarction on ct? *Journal of neurology, neurosurgery, and psychiatry*. 1999;67:651-653
18. Turk AS, Nyberg EM, Chaudry MI, Turner RD, Magarik JA, Nicholas JS, et al. Utilization of ct perfusion patient selection for mechanical thrombectomy irrespective of time: A comparison of functional outcomes and complications. *Journal of neurointerventional surgery*. 2012, epub.
19. Turk A, Magarik JA, Chaudry I, Turner RD, Nicholas J, Holmstedt CA, et al. Ct perfusion-guided patient selection for endovascular treatment of acute ischemic stroke is safe and effective. *Journal of neurointerventional surgery*. 2012;4:261-265
20. Kamalian S, Kamalian S, Konstas AA, Maas MB, Payabvash S, Pomerantz SR, et al. Ct perfusion mean transit time maps optimally distinguish benign oligemia from true "at-risk" ischemic penumbra, but thresholds vary by postprocessing technique. *AJNR. American journal of neuroradiology*. 2012;33:545-549
21. Garcia-Bermejo P, Calleja AI, Perez-Fernandez S, Cortijo E, del Monte JM, Garcia-Porrero M, et al. Perfusion computed tomography-guided intravenous thrombolysis for acute ischemic stroke beyond 4.5 hours: A case-control study. *Cerebrovascular diseases*. 2012;34:31-37
22. Kamalian S, Kamalian S, Maas MB, Goldmacher GV, Payabvash S, Akbar A, et al. Ct cerebral blood flow maps optimally correlate with admission diffusion-weighted imaging in acute stroke but thresholds vary by postprocessing platform. *Stroke; a journal of cerebral circulation*. 2011;42:1923-1928

23. Campbell BC, Christensen S, Levi CR, Desmond PM, Donnan GA, Davis SM, et al. Cerebral blood flow is the optimal ct perfusion parameter for assessing infarct core. *Stroke; a journal of cerebral circulation*. 2011;42:3435-3440
24. Murphy BD, Fox AJ, Lee DH, Sahlas DJ, Black SE, Hogan MJ, et al. White matter thresholds for ischemic penumbra and infarct core in patients with acute stroke: Ct perfusion study. *Radiology*. 2008;247:818-825
25. Wintermark M, Flanders AE, Velthuis B, Meuli R, van Leeuwen M, Goldsher D, et al. Perfusion-ct assessment of infarct core and penumbra: Receiver operating characteristic curve analysis in 130 patients suspected of acute hemispheric stroke. *Stroke; a journal of cerebral circulation*. 2006;37:979-985
26. Hossmann KA. Viability thresholds and the penumbra of focal ischemia. *Annals of neurology*. 1994;36:557-565
27. Zaharchuk G, Mandeville JB, Bogdanov AA, Jr., Weissleder R, Rosen BR, Marota JJ. Cerebrovascular dynamics of autoregulation and hypoperfusion. An mri study of cbf and changes in total and microvascular cerebral blood volume during hemorrhagic hypotension. *Stroke*. 1999;30:2197-2204; discussion 2204-2195
28. Murphy BD, Fox AJ, Lee DH, Sahlas DJ, Black SE, Hogan MJ, et al. Identification of penumbra and infarct in acute ischemic stroke using computed tomography perfusion-derived blood flow and blood volume measurements. *Stroke; a journal of cerebral circulation*. 2006;37:1771-1777
29. Deipolyi AR, Wu O, Macklin EA, Schaefer PW, Schwamm LH, Gilberto Gonzalez R, et al. Reliability of cerebral blood volume maps as a substitute for diffusion-weighted imaging in acute ischemic stroke. *Journal of magnetic resonance imaging : JMRI*. 2012;36:1083-1087
30. d'Esterre CD, Aviv RI, Lee TY. The evolution of the cerebral blood volume abnormality in patients with ischemic stroke: A ct perfusion study. *Acta radiologica*. 2012;53:461-467
31. Labeyrie MA, Turc G, Hess A, Hervo P, Mas JL, Meder JF, et al. Diffusion lesion reversal after thrombolysis: A mr correlate of early neurological improvement. *Stroke; a journal of cerebral circulation*. 2012;43:2986-2991
32. Kidwell CS, Saver JL, Mattiello J, Starkman S, Vinuela F, Duckwiler G, et al. Thrombolytic reversal of acute human cerebral ischemic injury shown by diffusion/perfusion magnetic resonance imaging. *Annals of neurology*. 2000;47:462-469
33. Kudo K, Terae S, Katoh C, Oka M, Shiga T, Tamaki N, et al. Quantitative cerebral blood flow measurement with dynamic perfusion ct using the vascular-pixel elimination method: Comparison with h2(15)o positron emission tomography. *AJNR. American journal of neuroradiology*. 2003;24:419-426

34. The thrombolysis in myocardial infarction (timi) trial. Phase i findings. Timi study group. *The New England journal of medicine*. 1985;312:932-936
35. Larrue V, von Kummer RR, Muller A, Bluhmki E. Risk factors for severe hemorrhagic transformation in ischemic stroke patients treated with recombinant tissue plasminogen activator: A secondary analysis of the european-australasian acute stroke study (ecass ii). *Stroke; a journal of cerebral circulation*. 2001;32:438-441
36. Bland JM, Altman DG. Measuring agreement in method comparison studies. *Statistical methods in medical research*. 1999;8:135-160
37. Derdeyn CP, Videen TO, Yundt KD, Fritsch SM, Carpenter DA, Grubb RL, et al. Variability of cerebral blood volume and oxygen extraction: Stages of cerebral haemodynamic impairment revisited. *Brain : a journal of neurology*. 2002;125:595-607
38. Astrup J, Siesjo BK, Symon L. Thresholds in cerebral ischemia - the ischemic penumbra. *Stroke; a journal of cerebral circulation*. 1981;12:723-725
39. Odano I, Halldin C, Karlsson P, Varrone A, Airaksinen AJ, Krasikova RN, et al. [18f]flumazenil binding to central benzodiazepine receptor studies by pet--quantitative analysis and comparisons with [11c]flumazenil. *NeuroImage*. 2009;45:891-902
40. Schaefer PW, Mui K, Kamalian S, Nogueira RG, Gonzalez RG, Lev MH. Avoiding "pseudo-reversibility" of ct-cbv infarct core lesions in acute stroke patients after thrombolytic therapy. The need for algorithmically "delay-corrected" ct perfusion map postprocessing software. *Stroke; a journal of cerebral circulation*. 2009
41. Aviv RI, d'Esterre CD, Murphy BD, Hopyan JJ, Buck B, Mallia G, et al. Hemorrhagic transformation of ischemic stroke: Prediction with ct perfusion. *Radiology*. 2009;250:867-877
42. Frey GD, Rumboldt Z. Radiation effects from perfusion ct. *Radiology*. 2005;234:638
43. Rapalino O, Kamalian S, Kamalian S, Payabvash S, Souza LC, Zhang D, et al. Cranial ct with adaptive statistical iterative reconstruction: Improved image quality with concomitant radiation dose reduction. *AJNR. American journal of neuroradiology*. 2012;33:609-615
44. Wintermark M, Smith WS, Ko NU, Quist M, Schnyder P, Dillon WP. Dynamic perfusion ct: Optimizing the temporal resolution and contrast volume for calculation of perfusion ct parameters in stroke patients. *AJNR Am J Neuroradiol*. 2004;25:720-729
45. Olsen TS, Larsen B, Skriver EB, Herning M, Enevoldsen E, Lassen NA. Focal cerebral hyperemia in acute stroke. Incidence, pathophysiology and clinical significance. *Stroke; a journal of cerebral circulation*. 1981;12:598-607

46. del Zoppo GJ, Mabuchi T. Cerebral microvessel responses to focal ischemia. *Journal of cerebral blood flow and metabolism : official journal of the International Society of Cerebral Blood Flow and Metabolism*. 2003;23:879-894
47. Lassen NA. The luxury-perfusion syndrome and its possible relation to acute metabolic acidosis localised within the brain. *Lancet*. 1966;2:1113-1115
48. Kidwell CS, Saver JL, Mattiello J, Starkman S, Vinuela F, Duckwiler G, et al. Diffusion-perfusion mri characterization of post-recanalization hyperperfusion in humans. *Neurology*. 2001;57:2015-2021
49. Namura S, Zhu J, Fink K, Endres M, Srinivasan A, Tomaselli KJ, et al. Activation and cleavage of caspase-3 in apoptosis induced by experimental cerebral ischemia. *The Journal of neuroscience : the official journal of the Society for Neuroscience*. 1998;18:3659-3668
50. Kitagawa K. Ischemic tolerance in the brain: Endogenous adaptive machinery against ischemic stress. *Journal of neuroscience research*. 2012;90:1043-1054
51. Fern R, Moller T. Rapid ischemic cell death in immature oligodendrocytes: A fatal glutamate release feedback loop. *The Journal of neuroscience : the official journal of the Society for Neuroscience*. 2000;20:34-42
52. Rowed DW, Stark VJ, Hoffer PB, Mullan S. Cerebral arteriovenous shunts re-examined. *Stroke; a journal of cerebral circulation*. 1972;3:592-600
53. Harris JJ, Attwell D. The energetics of cns white matter. *The Journal of neuroscience : the official journal of the Society for Neuroscience*. 2012;32:356-371
54. Bristow MS, Simon JE, Brown RA, Eliasziw M, Hill MD, Coutts SB, et al. Mr perfusion and diffusion in acute ischemic stroke: Human gray and white matter have different thresholds for infarction. *Journal of cerebral blood flow and metabolism : official journal of the International Society of Cerebral Blood Flow and Metabolism*. 2005;25:1280-1287

CHAPTER 4

Multi-modality Neuroimaging in a Porcine Model of Endothelin-1

Induced Cerebral Ischemia: Defining the Acute Infarct Core

The contents of this chapter have been adapted from the paper entitled “Multi-modality neuroimaging in a porcine model of endothelin-1 induced cerebral ischemia: defining the acute infarct core”, was submitted to *Stroke* in April, 2013 by: C.D. d’Esterre, U. Anazodo, K. St. Lawrence, L. Morrison, T.Y. Lee, E. Fainardi.

4.1 INTRODUCTION

As discussed in Chapters 2 and 3, delineation of irreversibly injured tissue that cannot be salvaged, even with reperfusion, in patients with anterior large vessel occlusion has important implications for recanalization decisions, hemorrhagic transformation prognosis, and long-term clinical outcome. Patients with a small infarct core volume, confirmed with neuroimaging techniques, and a high NIHSS will likely benefit from reperfusion therapy, less than 4.5 hours post ictus; however, consensus on the optimal imaging parameter to delineate hyper-acute infarct core remains uncertain¹⁻⁴.

There remains conflicting evidence concerning the reliability of the acute MR-diffusion weighted imaging (DWI) defect, as permanent hyperintensity reversal is prevalent in both temporary artery occlusion models, and human stroke; however, the causal relationship between DWI defect reversal and improved clinical outcome remains uncertain^{5, 6}. Due to the impracticality of the MRI modality during the acute stroke setting, much effort has been put forth to determine CT perfusion (CTP)-derived

hemodynamic thresholds to define acute tissue states - CT imaging is fast, non-invasive, and with new dose-saving techniques, relatively safe^{7, 8}. Taking into account certain caveats which affect the prognostic ability of the cerebral blood volume (CBV) parameter, namely reactive hypervolemia, truncation of the ischemic time density curve, and recanalization status, reversibility of very low CBV is uncommon, as loss of vascular autoregulation likely represents non-viable tissue^{9, 10}. In contrast, normal or elevated CBV is suspected to represent either nutritive or non-nutritive hypervolemia, within electrically silent yet viable tissue (penumbra) and infarct core, respectively, as discussed in Chapter 3. As such, recent reports suggest a cerebral blood flow (CBF) threshold is optimal to separate infarct from penumbra, prior to reperfusion efforts^{1, 2, 11}. It has been shown in animal stroke studies that the threshold for pan-necrosis is between 0.17 and 0.24 ml·min⁻¹·g⁻¹ with persistent occlusion¹². This threshold decreases to 0.12 ml·min⁻¹·g⁻¹ when ischemia is limited to a few hours¹³. However, the threshold of infarction (pan-necrosis) for ischemia lasting less than an hour, which is becoming more relevant in the era of rapid revascularization, is unknown.

Due to the assortment of different perfusion post-processing algorithms, and consequent lack of standardized perfusion thresholds, CTP has yet to fully breakthrough into the clinical setting^{4, 11, 14}. Further, many CTP thresholds are commonly compared to the final infarct volume derived from delayed imaging at 24 hours or 5-7 days post ictus, which may under/overestimate the final infarct volume, depending on time of recanalization^{15, 16}. PET imaging with ¹⁸F-flumazenil, the imaging gold standard for infarction, or histology are not feasible in the clinical setting^{17, 18}. Therefore, stroke models continue to be valuable for defining and assessing perfusion thresholds for acute tissue status. The use of endothelin-1 (ET-1) to cause transient cerebral ischemia has been

well established in rodents and lower primates^{19, 20}. As a potent vasoconstrictor, ET-1 causes a dose-dependent focal CBF decrease through G-protein coupled contraction of smooth muscle, adjacent to endothelium²¹. Appearance of infarction, with minimal tissue edema, occurs within an hour of ET-1 administration, mimicking ischemic progression similar to that of humans²². This characteristic makes the ET-1 stroke model useful for tracking changes in vascular/tissue pathophysiology during the early stages of stroke onset²³.

This hyper-acute ischemic stroke study sought to determine: 1) whether the predicted infarct volume (PIV) described by CTP parameters and contemporaneous DWI imaging correlates with true infarct volume (TIV) defined by 2,3,5-tetrazolium chloride (TTC) histology; 2) the distribution of ¹⁸F-FDG uptake (glucose metabolism) within the TIV and peri-TIV; 3) CTP-CBF and CBV values within superimposed TIV regions of interest.

4.2 MATERIALS & METHODS

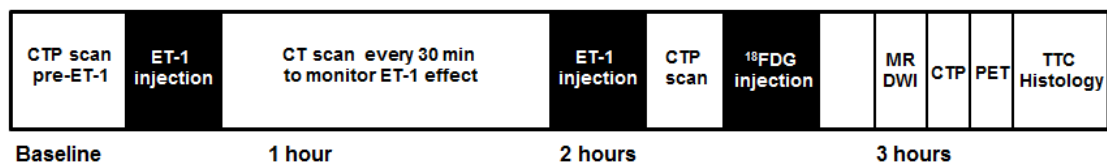
4.2.1 Study design

Animal experiments were conducted following the guidelines of the Canadian Council on Animal Care and approved by the Animal Use Subcommittee at the University of Western Ontario⁺. Duroc-cross pigs (n = 10) were obtained from a local supplier, housed and allowed to grow to a desired weight of 45 ± 10 kg. Anesthesia was induced with an intra-muscular injection of telazol (100 mg/ml, 1 ml/20 kg). A 22 gauge catheter was

⁺ Appendix C – Human Ethics Approval form

placed in the ear vein for single bolus of propofol (10 mg/ml, 2-5 mg/kg) to maintain anaesthesia during intubation. Animals were mechanically ventilated with an oxygen/medical air mixture and surgical anesthesia was maintained with inhaled isoflurane at 2-4%. A 22 gauge catheter was placed in the cephalic vein for imaging contrast injections. A femoral artery was also catheterized (24 or 22 gauge) to monitor heart rate and mean arterial blood pressure as well as to intermittently collect arterial blood samples for blood gas measurements. Heart rate, end tidal CO₂, arterial O₂ saturation, respiration rate, blood pressure and temperature were monitored continuously. Rectal temperature was maintained between 37.5 and 39.5 °C at all times throughout surgery and imaging, using a whole-body water blanket. The animals were placed in a prone position, an incision was made above the parietal bone, mid-way between the left ear and eye, and the skin and periosteum were separated from the skull bone. A 2 mm diameter hole was drilled into the parietal bone through the incision site, using a dremel rotary hand tool. A 27 gauge, 1 ¼ inch needle and PE20 polyethylene tubing was used to inject 25µg of ET-1 (human/porcine, Sigma Chemical Company, St. Louis, MO, USA) in 150 µL of sterile water, at a rate of 50µL/minute (NE-100 single syringe pump, New Era Pump Systems Inc., Farmingdale, NY). Careful placement of the needle into the left striatum, avoiding ventricles, was confirmed with a non-contrast CT (NCCT) scan prior to ET-1 infusion. Two equal doses of ET-1 were given 2 hours apart with monitoring of ischemic progression using CT perfusion imaging after each infusion. An experimental timeline is shown in figure 1. Throughout all imaging anesthesia was maintained with 2-3% isoflurane.

Figure 4.1 Timeline for the experimental protocol



Mean \pm standard deviation acquisition time for post 3 hour contemporaneous MR, CTP and PET imaging was 2hrs21min \pm 18min. CTP = CT perfusion, ET-1 = endothelin-1, ¹⁸F¹⁸FDG = glucose analog radiotracer, MR-DWI = magnetic resonance diffusion weighted imaging, PET = positron emission tomography, TTC = tetrazolium chloride stain

4.2.2 Computed tomography perfusion imaging

Each CT acquisition was performed with a Discovery LS PET/CT hybrid scanner (GE Healthcare, Waukesha, WI). A preliminary axial CT scan was used to localize 16 x 2.5 mm-thick slices in the territory of the ET-1 injection. For CT perfusion (CTP) imaging, a contrast-enhanced cine continuous scan was performed where the couch remained stationary while the gantry rotated continuously, acquiring images simultaneously from sixteen different (contiguous) slice locations. A 40 ml bolus of 370 mg·ml⁻¹ non-ionic, iodinated contrast (Iovue[®]-300, Bracco Diagnostics, Princeton, NJ) was injected (1.5 ml·s⁻¹) into a saphenous vein 5 seconds after the start of the CTP acquisition. The head was continuously scanned at 120 kVp, 200 mA and 1second rotation period for 120 seconds, to avoid any truncation artifact. From the acquired data, 512 x 512 images were reconstructed at 0.5 second intervals and 15 cm FOV. CTP scans were performed at baseline (pre-ET-1) and every 30 minutes post-ET-1 to monitor its effect on tissue perfusion. A second dose of ET-1 was given around 2 hours after the first dose – the second dose was given when the CBF defect started to normalize, as observed on the CTP-CBF functional maps (ie. any shrinkage of the initial CBF defect observed after the first ET-1 infusion). ‘Severe’ ischemia (adequate to cause infarction) was confirmed with CTP imaging immediately following the infusion. The final CTP acquisition was performed within 10 minutes of the completion of MR imaging (see below).

4.2.3 Magnetic resonance imaging

MR imaging was performed on a Siemens 3T BIOGRAPH mMR (Erlangen, Germany) with software *syngo* VB 18P. Heart rate and O₂ saturation were monitored by an MR compatible pulse oximeter (8604F0 Pulse Oximeter, Nonin Medical, Plymouth, MN).

Animals were imaged supine using a 15 channel phase array transmit/receive extremity coil. Diffusion imaging was performed parallel to collosal line as determined from acquisition of 3D high resolution anatomical scan (MPRAGE T1, 1 mm x 1 mm x 1 mm resolution). Echo Planar DWI was acquired with the following parameters: TR (repetition time) 3500 ms, TE (echo time) 95 ms, FOV (field of view) 220 mm, spectral fat saturation, 16 interleaved slices 5 mm thick with no gap, matrix 128 x 128, in-plane resolution 1.7 mm x 1.7 mm, acceleration GRAPPA 2, b-values 0 and 1000 s/mm², 20 diffusion gradient directions, 6 signal averages and bandwidth 1446 Hz/pixel. Time for DWI acquisition 7:46 min. 20 diffusion directions were applied to avoid anisotropy effects and allow signal averaging to generate high quality apparent diffusion coefficient (ADC) maps from the DWI data. Median (range) time (minutes) of MR imaging relative to the second ET-1 infusion was 57 (49-68).

4.2.4 ¹⁸F-FDG Positron emission tomography imaging

Thirty minutes after the second injection of ET-1, a dose of the glucose analog, fluorine-18 labeled fluorodeoxyglucose (¹⁸F-FDG, 300-380MBq), was administered via ear vein. PET imaging commenced within 15 minutes of completing the MR imaging (3 minutes after completion of the last CTP scan), 40-60 minutes after ¹⁸F-FDG injection. Prior to acquisition of the PET raw data, a CT-based attenuation correction was performed. PET emission data was collected on a Discovery LS PET/CT hybrid scanner (GE Healthcare) in 2D mode, with a photopeak window of 280-700keV for 20 minutes. Data were acquired in a 128 × 128 matrix with pixel widths of 0.478 mm and slice thickness of 3.3 mm. Image sets were reconstructed, using the iterative reconstruction software available

on the commercial system (GE Medical Systems software) including attenuation and random correction.

4.2.5 Histology

Following imaging, the whole brain was carefully excised and cut into coronal sections corresponding to the CT-perfusion weighted images (PWI) scan slice locations. To identify infarcted tissue, each slice was stained with TTC to quantify the extent of dead tissue, and fixed in 10% formalin. TTC, which is colorless in solution, is reduced to a deep red formazan by dehydrogenase enzymes of functioning mitochondria, while infarcted brain regions do not convert TTC and remain unstained. Digital images were acquired with a desktop colour scanner (Brother DCP-7040, Bridgewater, NJ). Image J (Image J, Bethesda, MD) software was used to determine the TIV (cm^3) as described previously²⁴. Briefly, to determine infarct volume by manual measurement, a calibration factor was derived by scanning a ruler alongside the brain slices, and determining the number of pixels per mm. For each animal, this calibration factor was entered into ImageJ to convert pixel area measures to mm^2 . The outlined infarct area for each slice was multiplied by 5 mm (thickness of each section) and the volumes summed to get the true infarct volume (cm^3).

4.2.6 Image analysis

For consistency, functional maps of cerebral blood flow [CBF; $\text{ml}\cdot\text{min}^{-1}\cdot(100\text{g})^{-1}$] cerebral blood volume [CBV; $\text{ml}\cdot(100\text{g})^{-1}$] and time-to-maximum (Tmax; seconds) were calculated by one author using a commercially available delay-insensitive deconvolution software (CT Perfusion 4D, GE Healthcare, Waukesha, WI). A 2×2 pixel region of

interest was placed in the right common carotid artery to obtain the arterial input function (AIF). The AIF was deconvolved with each tissue time density curve using a method described previously^{25, 26}. After functional map processing, a CBF•CBV product map was also calculated by multiplying matching voxels from the CBF and CBV functional maps. PWIs were created by averaging the cine CTP images over the duration of the first pass of CT contrast.

Custom software (IDL, version 6.2, RSI, Boulder, Colorado) was used for all image post processing analysis. The ~3 hour post (final CTP acquisition) CTP-PWIs were matched up with the histological slices to establish the reference slab. Using anatomical features, the MR-DWI/ADC maps, and ¹⁸FDG-PET images were registered with the CTP-PWI image set and hence the CTP functional maps as well.

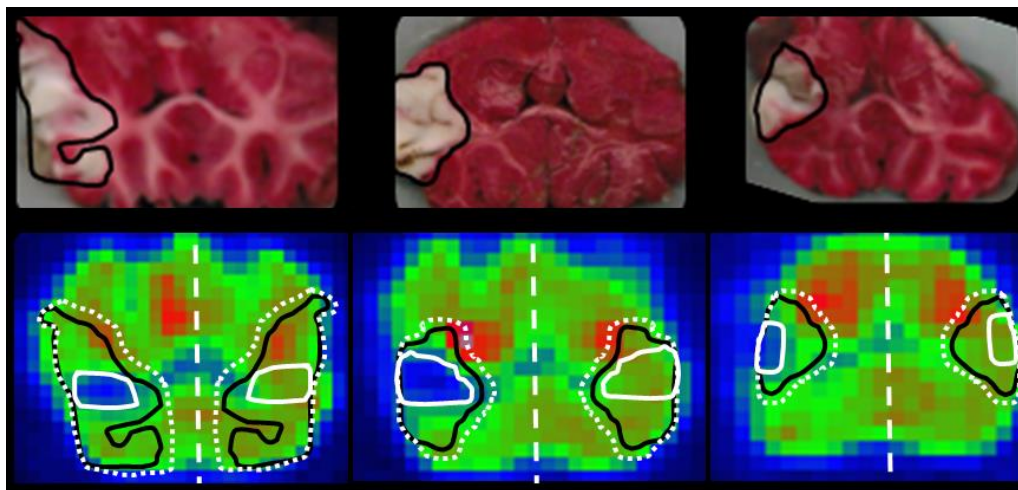
The PWIs were used to exclude cerebrospinal fluid and cranium from analysis as well as to produce a gray and white matter anatomical mask based on the Hounsfield Unit differences between the two tissue types. The critically hypoperfused area was defined as relative Tmax > 2². Gray and white matter CTP thresholds, derived from human studies (see Appendix D), were used to delineate the PIV volume on CBF, CBV and CBF•CBV functional maps, while blinded to MRI, PET, and histological results. CBF, CBV and CBF•CBV product infarct thresholds were 10.1 ml·min⁻¹·(100g)⁻¹, 1.9 ml·(100g)⁻¹, and 26.0, respectively, for gray matter and 7.4 ml·min⁻¹·(100g)⁻¹, 1.25 ml·(100g)⁻¹, and 9.9, respectively, for white matter (Appendix D). The volume of each voxel was determined as (120 mm/512 pixels)² x 5 mm. For each animal, total infarct volume (cm³) was calculated by multiplying the number of infarct positive voxels (gray plus white matter) with the voxel volume.

As a secondary analysis, the histologically defined TIV was superimposed onto CTP-CBF and CBV functional maps to determine perfusion values within gray and white, and mirrored contralateral regions. Pixels with a CBF $> 100 \text{ ml}\cdot\text{min}^{-1}\cdot(100\text{g})^{-1}$ or CBV $> 8 \text{ ml}\cdot(100\text{g})^{-1}$ were excluded from the region of interest to remove influence of large vessels on parenchymal perfusion²⁷. Animals were classified as having CBF/CBV mismatch (complete or partial) or CBF/CBV matched decrease (Table 4.2). We define mismatch as an increase in CBV, from within the superimposed TIV, greater than the average plus one standard deviation of the CBV value obtained from the contralateral mirrored region of interest (ROI) for each animal.

MR-derived PIV was defined as the abnormal hyperintense (exceeding the DWI signal intensity of the contralateral hemisphere by more than three standard deviations) and hypointense (ADC signal $< 85\%$ of contralateral hemisphere) areas on DWI and ADC maps, respectively, while blinded to CTP, PET and histological results, as described previously^{28, 29}. The volume of each voxel was determined as $(220 \text{ mm}/128 \text{ pixels})^2 \times 5 \text{ mm}$ slice thickness. Total number of voxels in all slices were determined and scaled by the voxel volume to obtain the total infarct volume (cm^3).

We visually assessed uptake of the ^{18}F -FDG semi-quantitatively within superimposed TIV as defined by TTC staining by categorizing the regional uptake as increased, decreased, or similar to uptake in the contralateral hemisphere. Core, periphery and peri-infarct uptake were assessed (Figure 4.2). Core was defined as very low uptake [Standard uptake value (SUV) $< 50\%$ of contralateral hemisphere SUV] within the superimposed TIV. Periphery-TIV is the total TIV less the core-TIV area. All ROIs were mirrored into contralateral hemisphere.

Figure 4.2 Assesement of glucose metabolism with ^{18}F FDG-PET



TTC-stained excised brain with TIV delineated and corresponding ^{18}F FDG uptake with superimposed TIV (solid black lines), core ROI (solid white), peri-TIV (dashed white).

4.2.6 Statistical analysis

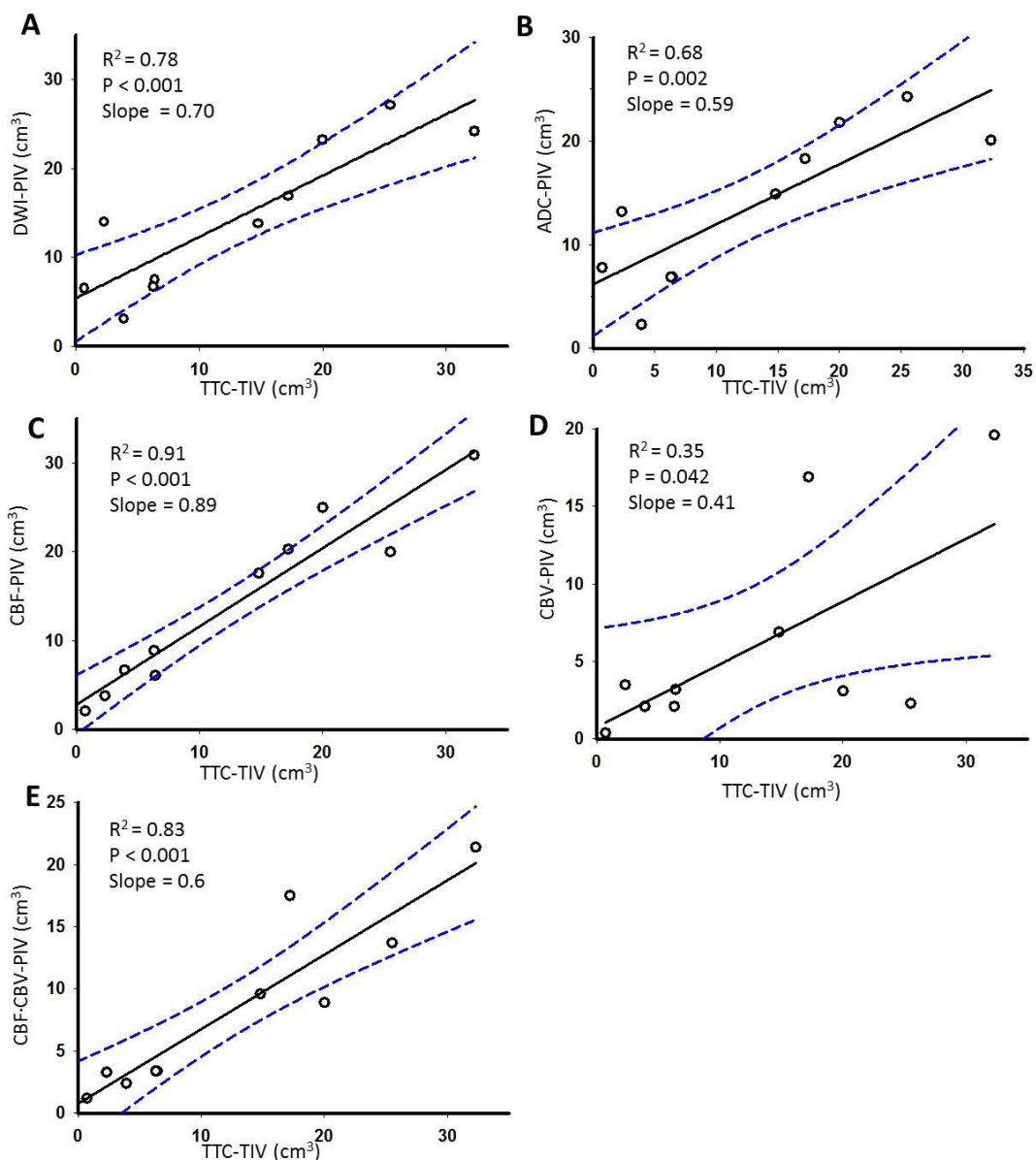
The statistical package, SPSS 15.0 (SPSS Inc., Chicago, IL), was used for all analyses. Differences were considered significant at $p < 0.05$. All data sets were checked for normality with the Shapiro-Wilk test prior to analysis with the appropriate parametric or non-parametric tests.

The relationship between the PIV as defined by CTP and MRI parameters and TIV from TTC-histology was evaluated for agreement with: 1) percent difference, 2) linear regression and 3) Bland-Altman analysis between PIV and TIV. The last analysis determined the systematic error (bias) and the 95% limits of agreement, defined as the mean and ± 1.96 times standard deviation of the individual differences respectively. Pearson correlation was applied to 2), while pairwise multiple comparisons using ANOVA with Tukey correction was applied to 1). Also, a paired student t-test was used to compare average CBF and CBV values from within superimposed TIV and mirrored contralateral TIV. Differences were considered significant at $p < 0.05$.

4.3 RESULTS

For all imaging parameters, a significant correlation ($p < 0.05$) was observed between the PIV and TIV (Figure 4.3). The CTP-CBF parameter had the highest R^2 value and slope closest to unity, while the CTP-CBV had the lowest R^2 value and slope furthest away from unity. The CTP-CBF•CBV parameter had a higher R^2 value, but lower slope than both MR parameters.

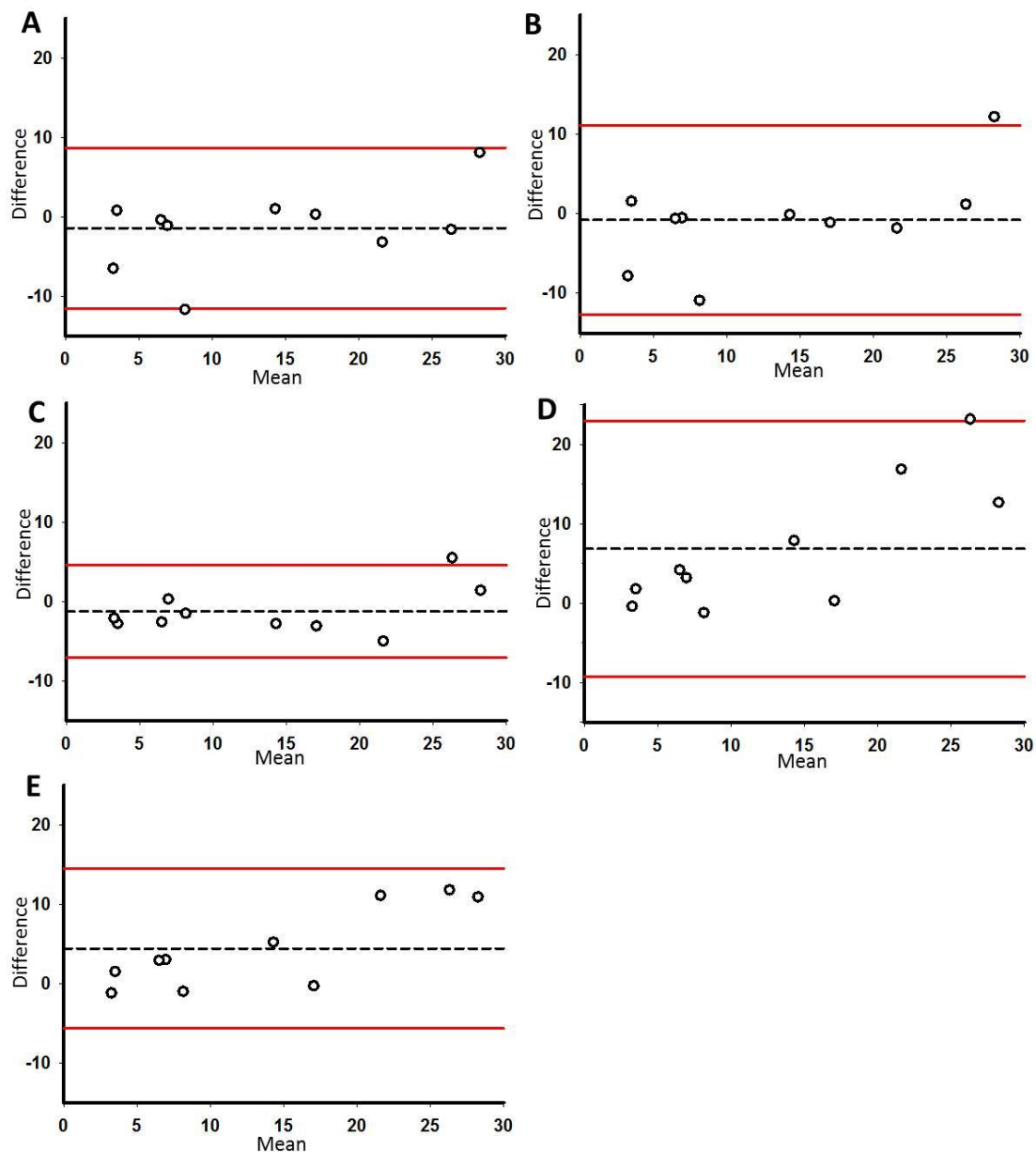
Figure 4.3 Regression of imaging defined PIV versus TTC defined TIV



Scatterplots for predicted infarct volumes (PIVs) as defined by A) MR-DWI, B) MR-ADC, C) CTP-CBF, D) CTP-CBV, E) CTP- CBF•CBV versus the true infarct volume (TIV), defined on TTC-stained excised brain (n=10). Graphs are plotted with linear regression fit (solid line) and 95% confidence intervals (dashed lines). Adjusted R^2 values, p-values and slopes of regression lines are also shown. Significance was classified as $p < 0.05$.

The 95% limits of agreement from the Bland-Altman analysis were as follows: MR-DWI = [8.7, -11.5], MR-ADC = [11.1, -12.7], CTP-CBF = [4.7, -6.8], CTP-CBV = [23.0, -9.1], CTP-CBF•CBV = [14.4, -5.6]. The best agreement was observed with CTP-CBF. The limits of agreement for MR-DWI and CTP- CBF•CBV were closely matched (Figure 4.4).

Figure 4.4 Bland-Altman plots



Bland-Altman plots for predicted infarct volumes (PIVs), as defined by A) MR-DWI, B) MR-ADC, C) CTP-CBF, D) CTP-CBV, E) CTP-CBF•CBV, and the true infarct volume (TIV), defined on TTC-stained excised brain (n=10). For all plots, the y-axis depicts the difference between the PIV and TIV, while the x-axis depicts the mean of both PIV and TIV values. Also shown are the mean differences (dotted line) \pm 95% limits of agreement (solid lines).

PIV from MR-DWI, ADC and CTP-CBF overestimated the TIV defined with histology (Table 4.1). The percent difference between CTP-CBF defined PIV and TIV was significantly lower than those for CTP-CBV and CTP-CBF•CBV defined PIVs ($p < 0.05$). Significant differences were not observed between CTP-CBF, MR-DWI or MR-ADC defined PIVs or their percent differences from TIV ($p > 0.05$). For all animals, mean CBF within superimposed TIV was decreased relative to the contralateral side ($p < 0.05$), while CBV was not ($p > 0.05$). Median (range) values for CBF [$\text{ml}\cdot\text{min}^{-1}\cdot(100\text{g})^{-1}$] and CBV [$\text{ml}\cdot\text{min}^{-1}\cdot(100\text{g})^{-1}$] within mirror contralateral TIV ROIs were 42.3 (31.5-64.1) and 2.1 (1.9-2.7) for gray matter, respectively, and 28.9 (19.4-38.0) and 1.5 (1.2-2.1) for white matter, respectively. A complete CBF/CBV mismatch (hypervolemia without a CBV defect), partial mismatch (hypervolemia with a CBV defect) and absent mismatch (no hypervolemia) was observed in 3/10 (30%), 3/10 (30%), and 4/10 (40%) of animals, respectively (Table 4.2).

A decrease in glucose metabolism (reduced uptake of ^{18}F FDG) was observed within the core TIV, peripheral TIV, and peri-TIV in 8/10 (80%), 1/10 (10%) and 0/10 (0%) of animals (Table 4.2).

Table 4.1 Infarct volumes from MR imaging, CTP imaging and histology.

Parameter	Infarct volume Median [range] (cm³)	% change between PIV & TIV Mean \pm SD (cm³)
MR-DWI	13.9 [3.1-27.1]	-31.4 \pm 98.5
MR-ADC	14.1 [2.3-24.3]	-31.6 \pm 115.4
CTP-CBF	13.3 [3.8-30.9]	-23.3 \pm 31.7*
CTP-CBV	3.2 [0.4-19.6]	42.3 \pm 44.1
CTP-CBF•CBV	6.2 [1.2-21.4]	28.5 \pm 31.5
Histology (TTC)	10.6 [0.7-32.3]	N/A

*Significantly different from the CTP-CBV and CTP-CBF•CBV parameters ($p < 0.05$).

TTC = tetrazolium chloride, PIV = predicted infarct volume, TIV = true infarct volume, N/A = not applicable

Table 4.2 CT perfusion values from within superimposed true infarct volume and corresponding glucose metabolism.

Animal	Perfusion values within TIV ROI					¹⁸ F-DG-uptake		
	Gray matter CBF	Gray matter CBV	White matter CBF	White matter CBV	CBF/CBV mismatch	Core TIV	Peripheral TIV	Peri-TIV
1	6.5	1.8	4.3	1.5	Complete	↓	↑	→
2	11.6	2.3	7.4	1.9	Complete	↓	↑	↑
3	7.6	2.0	6.9	1.1	Absent	↓	↑	↑
4	8.5	1.9	7.5	1.3	Complete	↓	↑	→
5	9.1	1.7	5.7	1.2	Partial	↓	→	↑
6	12.6	1.1	5.3	1.0	Partial	↓	↓	↑
7	4.87	1.8	7.2	0.9	Partial	→	→	↑
8	9.1	1.2	5.8	1.1	Absent	↓	↑	↑
9	5.9	1.4	6.7	0.7	Absent	↓	↑	↑
10	13.7	2.3	14.7	1.8	Absent	→	↑	↑
Mean	8.9	1.8	7.2	1.3				
Stdev	2.9	0.4	2.8	0.4				

TIV = true infarct volume, ROI = region of interest, Complete mismatch = hypervolemia without CBV defect, Partial mismatch = hypervolemia with CBV defect, Absent mismatch = no hypervolemia. ¹⁸F-FDG was categorized as increased (↑), decreased (↓), or similar (→) to the uptake in the contralateral hemisphere. Units for CBF is ml·min⁻¹·(100g)⁻¹ and CBV is ml·(100g)⁻¹

4.4 DISCUSSION

This study used a porcine model of endothelin-1 (ET-1) induced focal cerebral ischemia to compare predicted infarct volume (PIV) with true infarct volume (TIV), defined with acute neuroimaging and histology, respectively. We showed that the PIV defined with absolute gray and white matter CT-CBF thresholds correlated best with the TIV, and was similar to both MR-DWI and ADC defined PIVs. This is contrary to previous results which showed that the CBF•CBV product was the optimal parameter for infarct delineation in gray and white matter^{15, 16}. These studies by Murphy et al. used a shortened CTP acquisition of 45 seconds, delay-sensitive CTP software, and defined the final infarct volume with a 7 day NCCT, which could be larger than the acute infarct volume due to maturation and edema. Herein, we used a 2-phase 120 second CTP acquisition to eliminate data truncation, followed by functional map calculation using the newest delay-insensitive CTP software (GE Healthcare, CT Perfusion 4D), and compared our CTP-PIVs with both the imaging and histological gold standards³⁰.

Our result is consistent with the current literature which confirms that CBF is superior to CBV and CBF•CBV in defining infarct volume; although consensus on the use of relative or absolute CBF thresholds has not been established³¹. Applying an absolute CBF threshold can be problematic if CTP image acquisition protocol and processing algorithms are not optimized to calculate accurate CBF values. In this study, the average CBF gray and white matter (9.9 and $7.2 \text{ ml}\cdot\text{min}^{-1}\cdot(100\text{g})^{-1}$, respectively), from within superimposed TIV, varied only $\sim 8\%$ and $\sim 2\%$, respectively, from the described clinical CBF thresholds, obtained using similar scanning parameters with the same post-processing algorithm and image analysis. These CBF values are similar to those obtained by Jones et al. (1981) who demonstrated in a primate stroke model, that

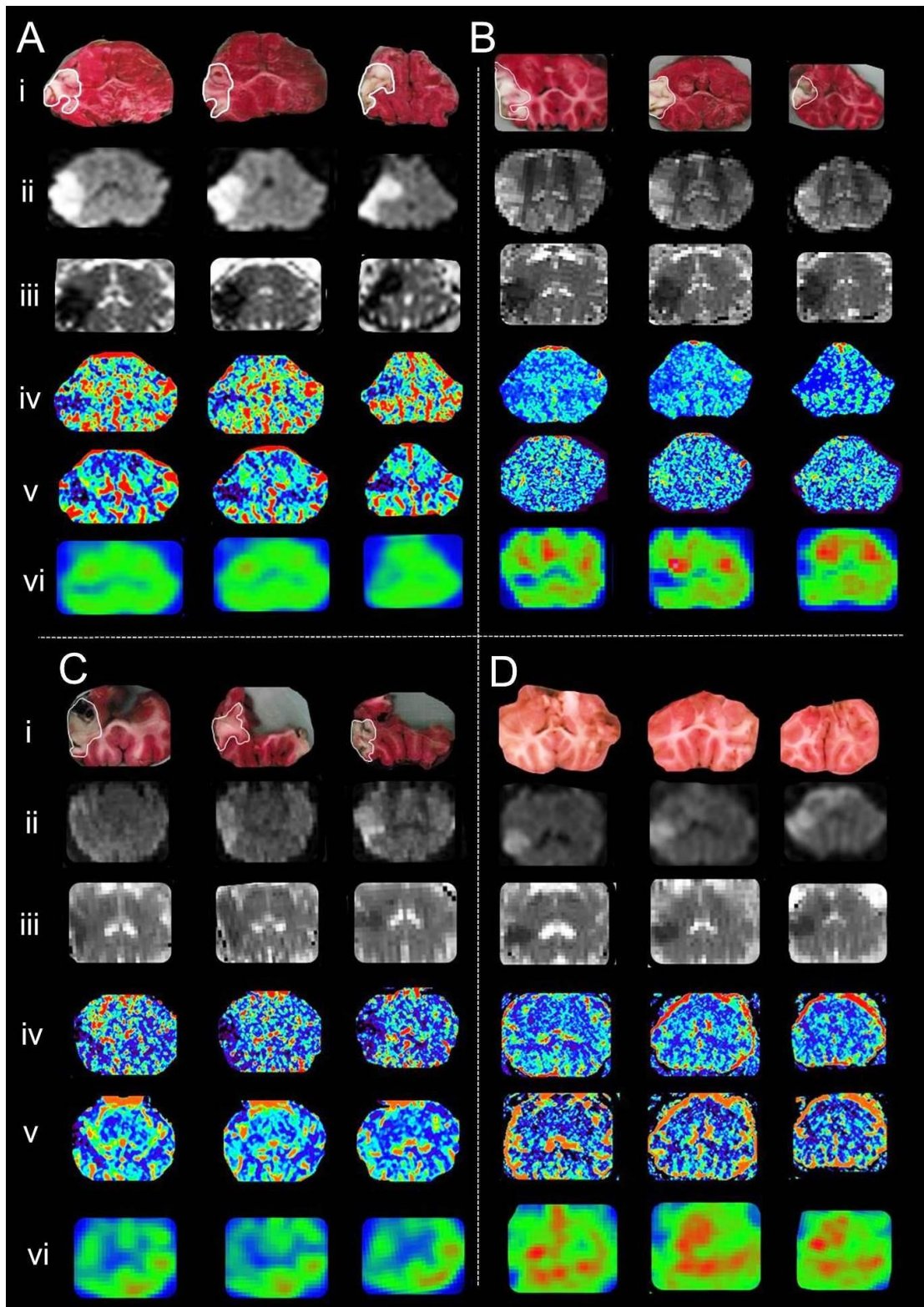
the CBF threshold for infarction was $10\text{--}12 \text{ ml}\cdot\text{min}^{-1}\cdot(100\text{g})^{-1}$ for 2–3 hours of occlusion which was similar to the time of ischemia in this study¹². Conversely, CBV values from both gray and white matter were ~17% and ~27% higher, respectively, than human thresholds, which is likely due to the varying incidence of hypervolemia at the time of CTP imaging.

As discussed in chapter 3, the prognostic reliability of the CBV parameter is affected by reactive hypervolemia, truncation of ischemic time density curve, and recanalization status, all of which will vary between study cohorts. Drawbacks for the use of relative to contralateral ‘normal’ region perfusion thresholds include variation in gray/white matter tissue distributions, potential underlying vascular pathologies, and variable/unstable central hemodynamic status of acute stroke patients at admission.

Many investigators define the penumbra as hypoperfused (low CBF) tissue with hypervolemia (high CBV, relative to the contralateral hemisphere) - the so called CBF/CBV mismatch hypothesis^{33, 34}. Complete or partial CBF/CBV mismatch was observed in 60% of animals, and in all of these cases, a portion of the mismatched area occurred within infarcted tissue, defined with histology (Figure 4.5 B & C). As described in chapter 3, we speculate that acute increases in CBV may be nutritive or non-nutritive, the latter caused by the opening of arteriovenous shunts within areas of considerable neuronal death³⁵. These mismatched regions were accompanied by varying degrees of glucose metabolism, which may indicate whether the CBV increase is futile or not; however, increased ^{18}F -FDG accumulation could also be due enhanced anaerobic glycolysis, activated repair processes (inflammatory phagocytosis and gliosis), and neuronal excitation from spreading depolarization^{36, 37}. This is one limitation besides others (see below) of this study.

Both the DWI and ADC defined PIV overestimated the TIV in 60% of animals, by as much as 350%. Nonetheless, brain tissue that stains positively for TTC may not necessarily be healthy and may yet succumb hours later. TTC staining relies on the ability of mitochondrial dehydrogenase enzyme to react with the tetrazolium salt to form the red formazan pigment¹⁸. Therefore, with mitochondrial breakdown, and subsequent dehydrogenase enzyme denaturation, the pro-apoptotic/necrotic factors are released into the cell³⁸. The DWI and ADC parameters are related to bioenergetic failure in neurons, causing cytotoxic edema and reduced water diffusion³⁹. Therefore, for tissue with a DWI -PIV/TIV mismatch, mitochondria are not producing enough ATP to maintain neuronal ionic gradients, but their structural integrity is likely maintained – a borderzone between infarct core and penumbra⁴⁰. Timely reperfusion of this tissue region is potential cause for the high incidence of DWI reversal in both clinical and experimental studies^{5, 41}. Similarly, CBF defined PIV overestimate the TIV in 60% of animals by as much as ~70%. One possible explanation is that CBF threshold for infarction was derived from a prior clinical study in which the infarct size was determined from a 5-7 days post ictus NCCT scan. The expansion of infarct between admission and follow-up imaging could contribute to a higher CBF threshold for infarct evaluated at admission.

Figure 4.5 Examples of imaging and TTC stained brains



Coronal sections of (i) TTC stained excised brain, with infarct outlined in white, (ii) MR-DWI, (iii) MR-ADC, (iv) CTP-CBF, (v) CTP-CBV, (vi) ^{18}F FDG uptake. Colour maps of CBF and CBV are $0\text{-}100\text{ ml}\cdot\text{min}^{-1}\cdot(100\text{g})^{-1}$ and $0\text{-}8\text{ ml}\cdot(100\text{g})^{-1}$, respectively. (A) Animal 3 shows matched infarct volume defects in all imaging modalities, with a decrease and increase in ^{18}F FDG uptake within core TIV and peri-TIV, respectively, relative to contralateral uptake; (B) Animal 4 shows a complete CBF/CBV mismatch in the corresponding TTC- and MR-defined infarct volumes, along with a decrease and same ^{18}F FDG uptake in the core-TIV and peri-TIV areas, respectively, relative to contralateral uptake. (C) Animal 6 shows a partial CBF/CBV mismatch, which corresponds to TTC- and MR-defined infarct volumes, with a decrease in ^{18}F FDG uptake within the entire TIV and peri-TIV, relative to contralateral uptake. (D) Animal 10, shows MR-defined DWI and ADC infarct volumes without corresponding TTC- and CTP-defined infarction, with the same and increased ^{18}F FDG uptake within the core-TIV and peri-TIV, respectively, relative to contralateral uptake.

Besides the limitation of the ^{18}F FDG-PET study, this study has several other limitations. First, ET-1 receptors are found on vascular smooth muscle cells (pericytes) and, endothelial cells. When ET-1 binds to endothelial receptors, the formation of nitric oxide (NO) is stimulated, and in the absence of smooth muscle endothelin receptor stimulation, this NO causes vasodilation^{42, 43}. Therefore, the hypervolemia, observed in the CBF/CBV mismatch of this study, may be mechanistically different than that observed in thromboembolic stroke models where presence of arteriovenous shunts causing venous filling and capillary compression are expected and can be confirmed with scanning electron microscopy. Second, false-negative errors may be caused by partial volume effects of neighbouring large blood vessels, masking regions of infarction; this may contribute to the high incidence of CBF/CBV mismatch within DWI and TTC defects. Third, as mentioned previously, glucose is used for all processes requiring energy, including acute inflammation and excitotoxic events, which may mask the reduced glucose uptake within infarcted tissue. The use of ^{18}F -flumazenil, a central benzodiazepine receptor antagonist, would be specific for neuronal death⁴⁴. Fourth, we qualitatively assessed and outlined DWI and ADC defects, which has a high level of subjectivity; applying diffusion thresholds may be an objective way to delineate infarction, and could improve accuracy in delineating infarct volume. Fifth, PIV can underestimate TIV as TTC staining occurred 20-30 minutes after the animal was euthanized as time was required to excise the brain; moreover, TIV may also be underestimated as the apoptotic cascade may already be initiated within peri-infarct tissue. Lastly, differentiation between gray and white matter is challenging due to limited resolution of the CT scanner coupled with the smaller porcine brain compared to humans.

4.5 CONCLUSION

This study determined that the CBF parameter is as good as MR diffusion imaging for acute infarct delineation, when CTP functional map calculation and image post-processing was standardized. We also show that the CBF/CBV mismatch may not indicate penumbral tissue in the acute stroke setting. These observations could have implications on patient selection for thrombolytic therapy.

4.6 REFERENCES

1. Campbell BC, Christensen S, Levi CR, Desmond PM, Donnan GA, Davis SM, et al. Cerebral blood flow is the optimal ct perfusion parameter for assessing infarct core. *Stroke; a journal of cerebral circulation*. 2011;42:3435-3440
2. Bivard A, Spratt N, Levi C, Parsons M. Perfusion computer tomography: Imaging and clinical validation in acute ischaemic stroke. *Brain : a journal of neurology*. 2011;134:3408-3416
3. Kudo K, Sasaki M, Yamada K, Momoshima S, Utsunomiya H, Shirato H, et al. Differences in ct perfusion maps generated by different commercial software: Quantitative analysis by using identical source data of acute stroke patients. *Radiology*. 2010;254:200-209
4. Konstas AA, Lev MH. Ct perfusion imaging of acute stroke: The need for arrival time, delay insensitive, and standardized postprocessing algorithms? *Radiology*. 2010;254:22-25
5. Labeyrie MA, Turc G, Hess A, Hervo P, Mas JL, Meder JF, et al. Diffusion lesion reversal after thrombolysis: A mr correlate of early neurological improvement. *Stroke; a journal of cerebral circulation*. 2012;43:2986-2991
6. Olivot JM, Mlynash M, Thijs VN, Purushotham A, Kemp S, Lansberg MG, et al. Relationships between cerebral perfusion and reversibility of acute diffusion lesions in defuse: Insights from radar. *Stroke; a journal of cerebral circulation*. 2009;40:1692-1697
7. Rapalino O, Kamalian S, Kamalian S, Payabvash S, Souza LC, Zhang D, et al. Cranial ct with adaptive statistical iterative reconstruction: Improved image quality with concomitant radiation dose reduction. *AJNR. American journal of neuroradiology*. 2012;33:609-615
8. Roberts HC, Roberts TP, Smith WS, Lee TJ, Fischbein NJ, Dillon WP. Multisection dynamic ct perfusion for acute cerebral ischemia: The "togglable" technique. *AJNR. American journal of neuroradiology*. 2001;22:1077-1080
9. d'Este CD, Aviv RI, Lee TY. The evolution of the cerebral blood volume abnormality in patients with ischemic stroke: A ct perfusion study. *Acta radiologica*. 2012;53:461-467

10. Schaefer PW, Mui K, Kamalian S, Nogueira RG, Gonzalez RG, Lev MH. Avoiding "pseudo-reversibility" of ct-cbv infarct core lesions in acute stroke patients after thrombolytic therapy. The need for algorithmically "delay-corrected" ct perfusion map postprocessing software. *Stroke; a journal of cerebral circulation*. 2009;40(8):2875-8
11. Kamalian S, Kamalian S, Maas MB, Goldmacher GV, Payabvash S, Akbar A, et al. Ct cerebral blood flow maps optimally correlate with admission diffusion-weighted imaging in acute stroke but thresholds vary by postprocessing platform. *Stroke; a journal of cerebral circulation*. 2011;42:1923-1928
12. Jones TH, Morawetz RB, Crowell RM, Marcoux FW, FitzGibbon SJ, DeGirolami U, et al. Thresholds of focal cerebral ischemia in awake monkeys. *Journal of neurosurgery*. 1981;54:773-782
13. Hossmann KA. Viability thresholds and the penumbra of focal ischemia. *Annals of neurology*. 1994;36:557-565
14. Abels B, Klotz E, Tomandl BF, Kloska SP, Lell MM. Perfusion ct in acute ischemic stroke: A qualitative and quantitative comparison of deconvolution and maximum slope approach. *AJNR. American journal of neuroradiology*. 2010;31:1690-1698
15. Murphy BD, Fox AJ, Lee DH, Sahlas DJ, Black SE, Hogan MJ, et al. White matter thresholds for ischemic penumbra and infarct core in patients with acute stroke: Ct perfusion study. *Radiology*. 2008;247:818-825
16. Murphy BD, Fox AJ, Lee DH, Sahlas DJ, Black SE, Hogan MJ, et al. Identification of penumbra and infarct in acute ischemic stroke using computed tomography perfusion-derived blood flow and blood volume measurements. *Stroke; a journal of cerebral circulation*. 2006;37:1771-1777
17. Odano I, Halldin C, Karlsson P, Varrone A, Airaksinen AJ, Krasikova RN, et al. [18f]flumazenil binding to central benzodiazepine receptor studies by pet--quantitative analysis and comparisons with [11c]flumazenil. *NeuroImage*. 2009;45:891-902
18. Isayama K, Pitts LH, Nishimura MC. Evaluation of 2,3,5-triphenyltetrazolium chloride staining to delineate rat brain infarcts. *Stroke; a journal of cerebral circulation*. 1991;22:1394-1398
19. Nikolova S, Moyanova S, Hughes S, Bellyou-Camilleri M, Lee TY, Bartha R. Endothelin-1 induced mcao: Dose dependency of cerebral blood flow. *Journal of neuroscience methods*. 2009;179:22-28

20. Virley D, Hadingham SJ, Roberts JC, Farnfield B, Elliott H, Whelan G, et al. A new primate model of focal stroke: Endothelin-1-induced middle cerebral artery occlusion and reperfusion in the common marmoset. *Journal of cerebral blood flow and metabolism : official journal of the International Society of Cerebral Blood Flow and Metabolism*. 2004;24:24-41
21. Hughes PM, Anthony DC, Ruddin M, Botham MS, Rankine EL, Sablone M, et al. Focal lesions in the rat central nervous system induced by endothelin-1. *Journal of neuropathology and experimental neurology*. 2003;62:1276-1286
22. Reid JL, Dawson D, Macrae IM. Endothelin, cerebral ischaemia and infarction. *Clinical and experimental hypertension*. 1995;17:399-407
23. Fuxe K, Bjelke B, Andbjør B, Grahn H, Rimondini R, Agnati LF. Endothelin-1 induced lesions of the frontoparietal cortex of the rat. A possible model of focal cortical ischemia. *Neuroreport*. 1997;8:2623-2629
24. Zhang F, Chen J. Infarct measurement in focal cerebral ischemia: Ttc staining #. *T animal models of acute neurological injuries ii*.93-98.
25. St Lawrence KS, Lee TY. An adiabatic approximation to the tissue homogeneity model for water exchange in the brain: I. Theoretical derivation. *Journal of cerebral blood flow and metabolism : official journal of the International Society of Cerebral Blood Flow and Metabolism*. 1998;18:1365-1377
26. Konstas AA, Goldmakher GV, Lee TY, Lev MH. Theoretic basis and technical implementations of ct perfusion in acute ischemic stroke, part 2: Technical implementations. *AJNR. American journal of neuroradiology*. 2009;30:885-892
27. Kudo K, Terae S, Katoh C, Oka M, Shiga T, Tamaki N, et al. Quantitative cerebral blood flow measurement with dynamic perfusion ct using the vascular-pixel elimination method: Comparison with h2(15)o positron emission tomography. *AJNR. American journal of neuroradiology*. 2003;24:419-426
28. Albers GW, Thijs VN, Wechsler L, Kemp S, Schlaug G, Skalabrin E, et al. Magnetic resonance imaging profiles predict clinical response to early reperfusion: The diffusion and perfusion imaging evaluation for understanding stroke evolution (defuse) study. *Annals of neurology*. 2006;60:508-517
29. Drier A, Tourdias T, Attal Y, Sibon I, Mutlu G, Lehericy S, et al. Prediction of subacute infarct size in acute middle cerebral artery stroke: Comparison of perfusion-weighted imaging and apparent diffusion coefficient maps. *Radiology*. 2012;265:511-517

30. Bederson JB, Pitts LH, Germano SM, Nishimura MC, Davis RL, Bartkowski HM. Evaluation of 2,3,5-triphenyltetrazolium chloride as a stain for detection and quantification of experimental cerebral infarction in rats. *Stroke; a journal of cerebral circulation*. 1986;17:1304-1308
31. Engelhorn T, Doerfler A, Forsting M, Heusch G, Schulz R. Does a relative perfusion measure predict cerebral infarct size? *AJNR. American journal of neuroradiology*. 2005;26:2218-2223
32. Kitagawa K, Matsumoto M, Kuwabara K, Tagaya M, Ohtsuki T, Hata R, et al. 'Ischemic tolerance' phenomenon detected in various brain regions. *Brain research*. 1991;561:203-211
33. Wang XC, Gao PY, Xue J, Liu GR, Ma L. Identification of infarct core and penumbra in acute stroke using ct perfusion source images. *AJNR. American journal of neuroradiology*. 2010;31:34-39
34. de Lucas EM, Sanchez E, Gutierrez A, Mandly AG, Ruiz E, Florez AF, et al. Ct protocol for acute stroke: Tips and tricks for general radiologists. *Radiographics : a review publication of the Radiological Society of North America, Inc*. 2008;28:1673-1687
35. Rowed DW, Stark VJ, Hoffer PB, Mullan S. Cerebral arteriovenous shunts re-examined. *Stroke; a journal of cerebral circulation*. 1972;3:592-600
36. Paik JY, Lee KH, Choe YS, Choi Y, Kim BT. Augmented 18f-fdg uptake in activated monocytes occurs during the priming process and involves tyrosine kinases and protein kinase c. *Journal of nuclear medicine : official publication, Society of Nuclear Medicine*. 2004;45:124-128
37. Nasu S, Hata T, Nakajima T, Suzuki Y. [evaluation of 18f-fdg pet in acute ischemic stroke: Assessment of hyper accumulation around the lesion]. *Kaku igaku. The Japanese journal of nuclear medicine*. 2002;39:103-110
38. Kroemer G, Dallaporta B, Resche-Rigon M. The mitochondrial death/life regulator in apoptosis and necrosis. *Annual review of physiology*. 1998;60:619-642
39. Oppenheim C, Grandin C, Samson Y, Smith A, Duprez T, Marsault C, et al. Is there an apparent diffusion coefficient threshold in predicting tissue viability in hyperacute stroke? *Stroke; a journal of cerebral circulation*. 2001;32:2486-2491
40. Goyal M, Menon BK, Derdeyn CP. Perfusion imaging in acute ischemic stroke: Let us improve the science before changing clinical practice. *Radiology*. 2013;266:16-21

41. Kidwell CS, Saver JL, Mattiello J, Starkman S, Vinuela F, Duckwiler G, et al. Thrombolytic reversal of acute human cerebral ischemic injury shown by diffusion/perfusion magnetic resonance imaging. *Annals of neurology*. 2000;47:462-469
42. Tawa M, Fukumoto T, Ohkita M, Yamashita N, Geddawy A, Imamura T, et al. Contribution of nitric oxide in big endothelin-1-induced cardioprotective effects on ischemia/reperfusion injury in rat hearts. *Journal of cardiovascular pharmacology*. 2011;57:575-578
43. Schinelli S. Pharmacology and physiopathology of the brain endothelin system: An overview. *Current medicinal chemistry*. 2006;13:627-638
44. Powers WJ, Zazulia AR. The use of positron emission tomography in cerebrovascular disease. *Neuroimaging clinics of North America*. 2003;13:741-758

CHAPTER 5

Hemorrhagic Transformation of Ischemic Stroke:

Prediction with CT Perfusion

The contents of this chapter have been adapted from the paper entitled “Hemorrhagic transformation of ischemic stroke: prediction with CT perfusion” published in *Radiology* 2009;250(3):867-77 by R.I Aviv, C.D. d’Esterre, B.D. Murphy, J.J. Hopyan B. Buck, G. Mallia, V. Li, L. Zhang, S.P. Symons, T.Y. Lee.

5.1 INTRODUCTION

Hemorrhagic transformation (extravasation of red blood cells through a damaged BBB; HT) of acute ischemic stroke is an undesirable complication that occurs with rates between 2.2% and 44% in clinical studies and increasing to 70% in pathological studies¹⁻⁵. Several radiological and clinical parameters including baseline stroke severity, time to reperfusion, thrombolytic protocol violations, tissue plasminogen activator (tPA), white matter disease burden, aspirin, and heparin use are associated with HT⁶⁻¹². While more severe hemorrhage is undisputedly associated with worse outcome, there is controversy whether less severe forms of hemorrhage are important^{8, 10, 13-17}. Considering that even small amounts of hemorrhage may be detrimental, it may be desirable to detect patients who are more likely to undergo HT prior to tPA administration. Disruption of blood-brain barrier (BBB) integrity, considered focal to the development of HT has been demonstrated in animal models as increases in PS, but has not yet been fully elucidated in humans^{18, 19}. Recently, a small study using dynamic contrast-enhanced MRI with kinetic

modeling demonstrated the feasibility of measuring BBB disruption²⁰. However, the availability, speed, and accessibility of CT are key reasons that it remains the diagnostic procedure of choice in initiating thrombolysis. CT is also able to provide physiological information regarding the infarct core and tissue at risk, as described in Chapter 1²¹⁻²³. This is achieved with a dynamic contrast enhanced CT, or CT perfusion study with a duration of 70-90 seconds. By extending the acquisition time window, further information relating to the BBB integrity can be calculated²⁴. Techniques for the measurement of the CTP-permeability surface area product (PS) have been shown to be achievable with CTP in animal tumor models and a small human case series, but until recently has not been applied to stroke imaging²⁵⁻²⁸.

The aim of this study was to determine whether admission CT perfusion-derived PS maps differ between patients with HT secondary to ischemic stroke and those without HT. We hypothesize that patients with HT will have an increased BBB-PS compared to those without HT.

5.2 MATERIALS & METHODS

5.2.1 Study design and patient cohort

Patients were prospectively recruited at a regional stroke centre (Sunnybrook Health Sciences Center, Toronto, Canada) between January 2006 and October 2007. All study procedures and medical chart review were approved by the institutional research ethics board⁺. All recruited patients gave signed consent for the study. Inclusion criteria were: less than 3 hours of stroke symptoms, full clinical assessment by the on-call neurology

⁺ Appendix E – Human Ethics Approval form

stroke team, completed CT stroke imaging protocol at admission, as described below; completed follow up CT and MRI study (including MR-diffusion weighted and gradient-echo T2 weighted imaging) 5-7 days after stroke onset to determine final infarct size and detect HT. All patients were included, regardless of whether they underwent thrombolysis. One of two dedicated stroke neurologists, each with more than 5 years stroke experience and certified in National Institutes of Health Stroke Scale (NIHSS) score and modified Rankin score assessments, collected baseline patient data (age; sex; blood pressure; clotting status; NIHSS score; tPA treatment status, dose, route, and administration time; and stroke onset) at presentation and determined the modified Rankin score at the 90-day follow-up stroke clinic visit. Intravenous tPA therapy was administered up to 3 hours after symptom onset, following the admission CT perfusion examination, according to standard clinical practice based on American Heart Association–American Stroke Association guidelines²⁹. TPA treatment was administered in patients with an Alberta Stroke Program Early CT (ASPECT) score of 5 or higher³⁰. A modified Rankin score of 2 or lower was considered a good clinical outcome. The data were maintained in a database. Patients were excluded if they had contraindications to iodinated contrast material injection or MR imaging. Patients who repatriated to a local hospital before completing the CT stroke imaging protocol were also excluded. Seventy-four patients met the study entry criteria. Thirty-three patients were excluded owing to repatriation to another hospital before completion of the imaging protocol (n=26), intraventricular hemorrhage (n=1), or excessive movement during imaging (n=6). Forty-one patients were included in this study.

5.2.2 CT and MR imaging protocols

A CT stroke series was performed at admission using a 64-section scanner (VCT GE Healthcare) which included a non-contrast CT (NCCT), contrast-enhanced CT angiography (CTA) and CT perfusion (CTP). The NCCT was taken at 120 kVp, 300 mA, a 1-second rotation, a 5 mm section thickness. The CTA, from the aortic arch to the vertex, was performed with the administration of iodinated contrast material (300 mg of iodine per kilogram of body weight; iohexol [Omnipaque], GE Healthcare, Piscataway, NJ) to a maximum of 90 mL, a 5–10 second scanning delay, 120 kVp, 270 mA, a gantry speed of 1 second per rotation, a 1.25-mm section thickness, and a table speed of 20.62 mm per rotation. After the CT angiography series, a two-phase CTP examination was performed. The first phase involved a 45-second continuous (cine) acquisition reconstructed at 0.5-second intervals to produce a series of 90 sequential images of eight sections each, encompassing a total of 40 mm from the basal ganglia to the lateral ventricles. In the second phase of the CTP exam, images encompassing the same eight sections were collected at 15-second intervals for an additional 90 seconds immediately after the first phase. The scanning parameters for both phases were 80 kVp, 190 mA, 8x5 mm collimation, and a gantry speed of 1 second per rotation. A 0.5 mL/kg dose (maximal dose, 50 mL) of iohexol was injected at a rate of 4 mL/sec 3–5 seconds before the start of the first phase. Follow-up CT and MR examinations were performed for all patients 5–7 days after stroke onset. NCCT scanning was performed as described above. MR sequences were performed as follows: diffusion-weighted imaging (DWI) parameters were 8125/minimum (repetition time msec/echo time msec), 26-cm field of view, image matrix of 128 x 128 pixels, 5 mm section thickness with no intersection gap; fast low-angle inversion-recovery imaging with scanning parameters of 8000/120/200 (repetition

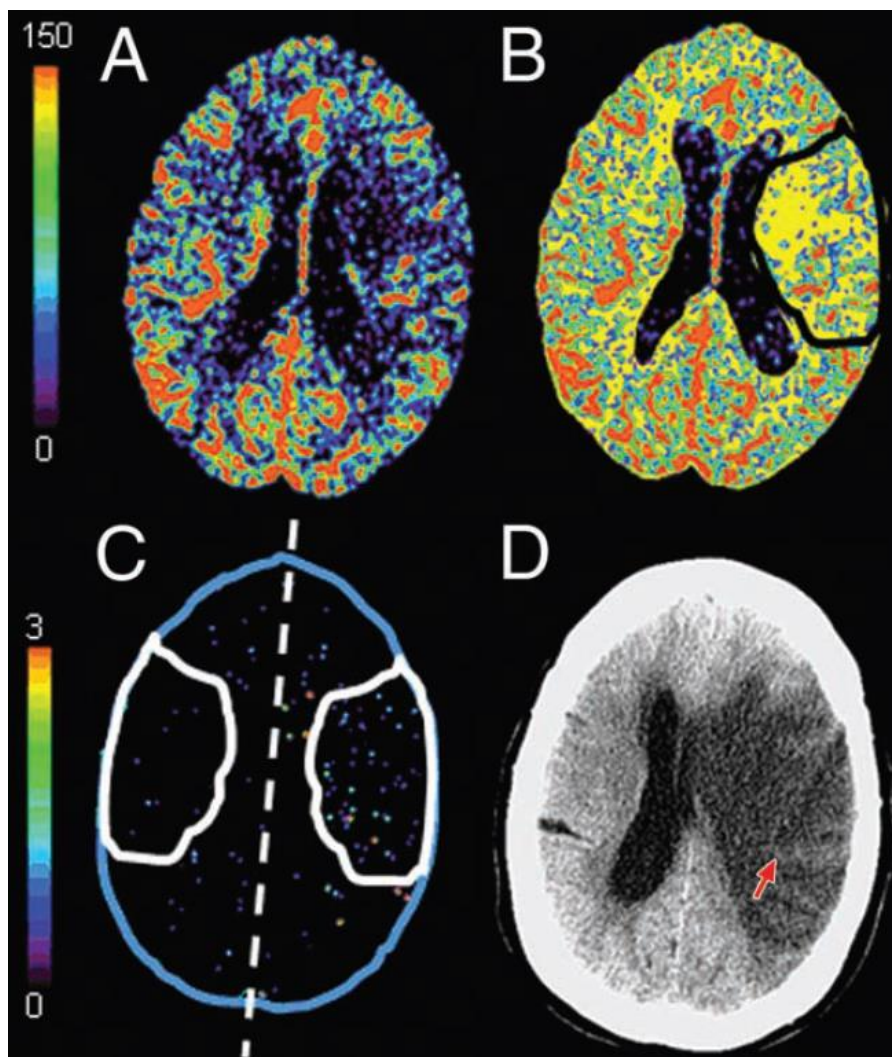
time msec/echo time msec/inversion time msec), 22-cm field of view, image matrix of 320 x 224 pixels, 5-mm section thickness with 1-mm intersection gap); and gradient-echo T2-weighted (1100/35, 20° flip angle, 24 cm field of view, image matrix of 320 x 224 pixels, 5 mm section thickness with 1-mm intersection gap)

5.2.3 Image analysis

Two neuroradiologists with more than 5 years stroke experience and blinded to previous examination results used follow-up NCCT and gradient-echo T2-weighted MR images to determine HT severity in consensus. Any susceptibility effect–induced area of low signal intensity in the ischemic region on a gradient-echo T2-weighted MR image was considered HT, even in the absence of a corresponding area of high attenuation on the NCCT image. The neuroradiologists did not record the size and location of these areas, but they graded the extent of hemorrhage by using an established grading system (6). HT was categorized as hemorrhagic infarction (HI) or parenchymal hematoma (PH) according to the ECASS criteria². HI was defined as blood petechiae within the infarcted area, without space-occupying effect, while PH was defined as blood clot with space-occupying effect. ASPECT scores were assigned by one experienced neuroradiologist with 5 years of experience. One operator with 2 years of experience used commercially available software (CT Perfusion 4; GE Healthcare Waukesha, Wis) to calculate parametric maps of cerebral blood flow (CBF), cerebral blood volume (CBV), mean transit time (MTT), and PS from the first- and second-phase CT perfusion data (Appendix F). Arterial input and venous output functions were derived from the ipsilateral anterior cerebral artery and the superior sagittal sinus, respectively. We corrected partial volume averaging of the arterial input curve by scaling the curve with the ratio of the area under

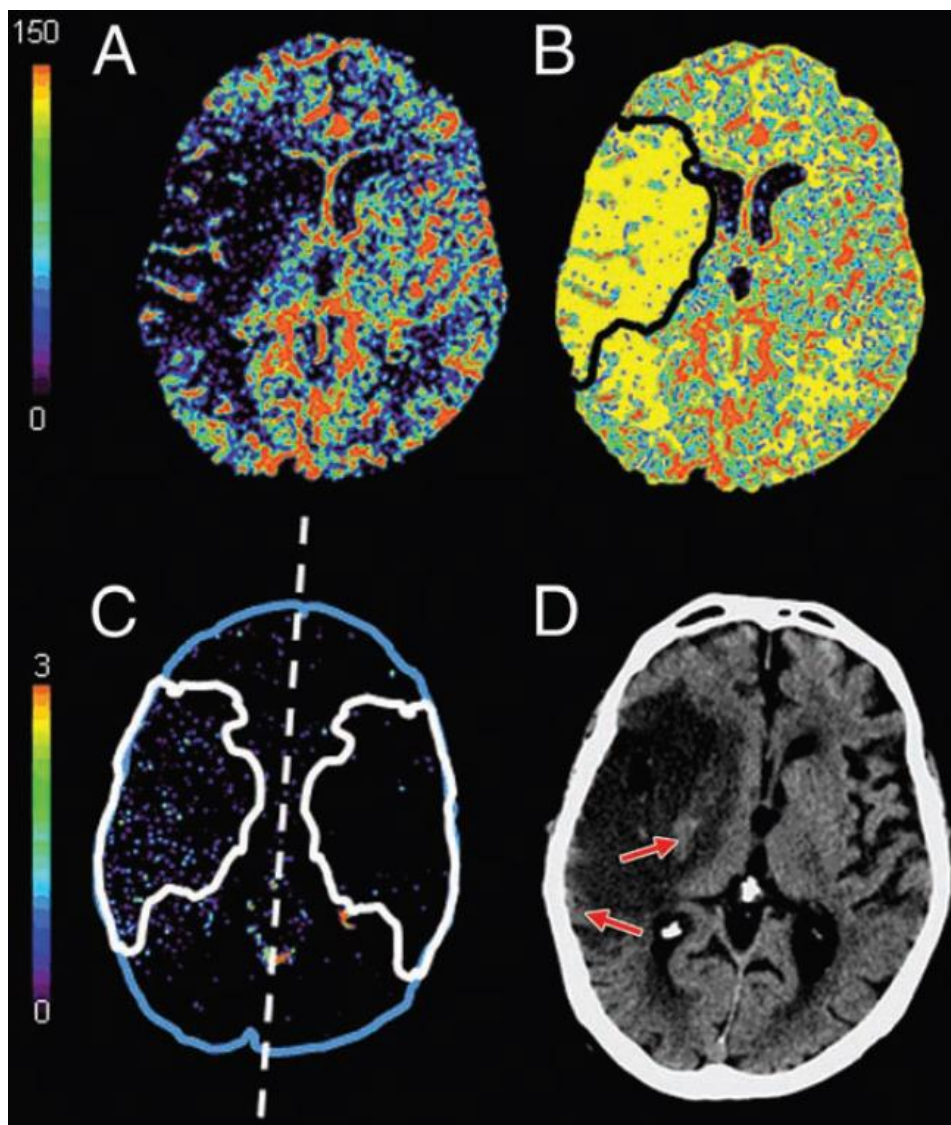
the venous output curve to the area under the arterial input curve. Maps were calculated by means of deconvolution of the arterial input curve and the tissue curves from 3 x 3 pixel blocks of CT images with use of the Johnson-Wilson model³¹. In addition to CBF, CBV, and mean transit time maps, perfusion-weighted and PS maps were calculated. Although we calculated the perfusion-weighted maps by averaging the images acquired over the duration of the first phase, calculation of the PS maps required use of the data from the second phase of the two-phase CT perfusion examination. The PS is used to assess the rate of contrast material extravasation from the intravascular to the extravascular space through a disrupted BBB²⁶. Extravasation of contrast material leads to prolonged enhancement of the tissue beyond the intravascular (first) phase, which can only be properly characterized with a two-phase CTP acquisition. One author with 2 years of experience analyzed the parametric maps by using custom software (IDL v6.1; Research Systems, Boulder, Colorado). To reduce bias, all components of the analysis were performed with the author blinded to the other study data - the HT status in particular. As depicted in figures 5.1 and 5.2, imaging data for all patients was analyzed by: 1) a CBF threshold of $25 \text{ ml}\cdot\text{min}^{-1}\cdot(100\text{g})^{-1}$ was applied to delineate an ischemic region of interest (ROI) on the admission CBF map, 2) this ROI was superimposed onto the admission PS and CBV functional maps, 3) a mirror ROI was created by reflecting the ischemic ROI across the hemispheric midline. To minimize the contribution of large vessels, any pixel with $\text{CBF} > 100 \text{ ml}\cdot\text{min}^{-1}\cdot(100\text{g})^{-1}$ or a $\text{CBV} > 8 \text{ ml}\cdot(100\text{g})^{-1}$ was excluded from the mean ROI value calculations²³. Finally, CBF and CBV defect volumes were calculated by using a CBF threshold of $25 \text{ ml}\cdot\text{min}^{-1}\cdot(100\text{g})^{-1}$ and a CBV threshold of $2 \text{ ml}\cdot(100\text{g})^{-1}$ on the corresponding maps^{22, 23}.

Figure 5.1 CT images for patient with small leakage in ischemic region



(A) Admission CT perfusion– derived CBF map of 5 mm thick brain section displayed with color scale from 0 (dark blue) to 150 (red) $\text{ml}\cdot\text{min}^{-1}\cdot(100\text{g})^{-1}$. (B) Corresponding CBF map shows ischemic ROI outlined with help of a yellow overlay of pixels with CBF of less than $25 \text{ ml}\cdot\text{min}^{-1}\cdot(100\text{g})^{-1}$. (C) PS map corresponding to (A) shows superimposed ischemic ROI and mirrored ROI in contralateral hemisphere. PS values in ischemic and mirrored ROIs are 0.17 and $0.038 \text{ ml}\cdot\text{min}^{-1}\cdot(100\text{g})^{-1}$, respectively. (D) Corresponding delayed (7 day) NCCT scan of same section shows infarct and HT (arrow).

Figure 5.2 CT images for patient with large leakage in ischemic defect



(A) Admission CT perfusion– derived CBF map of 5 mm thick brain section displayed with color scale from 0 (dark blue) to 150 (red) $\text{ml}\cdot\text{min}^{-1}\cdot(100\text{g})^{-1}$. (B) Corresponding CBF map shows ischemic ROI outlined with help of a yellow overlay of pixels with CBF of less than $25\text{ ml}\cdot\text{min}^{-1}\cdot(100\text{g})^{-1}$. (C) PS map corresponding to (A) shows superimposed ischemic ROI and mirrored ROI in contralateral hemisphere. PS values in ischemic and mirrored ROIs are 0.40 and $0.122\text{ ml}\cdot\text{min}^{-1}\cdot(100\text{g})^{-1}$, respectively. (D) Corresponding delayed (5 day) NCCT scan of same section shows infarct (hypoattenuation) and HT (arrows).

5.2.4 Statistical analysis

Quantitative variable results were expressed as mean \pm standard deviation or median with corresponding interquartile ranges, and categorical results were expressed as proportions. All data was checked for normality to determine if parametric or non-parametric tests should be performed. An unpaired Wilcoxon rank sum, or Fisher exact test was used to compare differences in demographic data and CTP variables between the HT and non-HT groups, and between the tPA and non-tPA groups. Age, NIHSS score, time to treatment, HT type were compared between these groups. PS, CBF and CBV values from within ipsilateral and contralateral ROIs, as well as CBF and CBV defect size were compared between groups. Associations between PS and both demographic and CTP parameters were tested at univariate and multivariate logistic regression analyses. The odds ratio for PS-based prediction of hemorrhage extent and the corresponding 95% confidence interval (CI) were estimated at logistic regression analysis. Receiver operating characteristic curve analysis of the PS values for prediction of hemorrhage extent was then performed, and the area under the receiver operating characteristic curve, sensitivity, specificity accuracy, positive and negative predictive values, and positive likelihood ratio were determined. Results were considered significant at $p < 0.05$.

5.3 RESULTS

The 41 patients (26 men, 15 women) included in the study had a mean \pm standard deviation age of 70.3 years \pm 15.4. The median NIHSS score at presentation was 15 (interquartile range, 7–20). The mean \pm standard deviation time from stroke symptom onset to CT scanning was 125 \pm 46 minutes. The MR and CT follow-up examinations were performed a median of 3 days (interquartile range, 2–6 days) after the initial CT

examination. Twenty-two (54%) patients received tPA, which was administered both intravenously (IV) and intra-arterially (IA) in two patients and IV only in 20. The mean \pm standard deviation tPA dose was 61 ± 12 mg. Twenty three (56%) patients had a HT: 15 (37%) with HI and eight (20%) with PH. The data obtained at both baseline and discharge was dichotomized according to presence of HT (Table 5.1). Patients with hemorrhage were more likely to have a higher NIHSS score at presentation ($p < 0.01$), receive tPA ($p < 0.01$), have a lower baseline ASPECT score ($p < 0.05$), and have a worse outcome ($p < 0.01$) compared with patients without HT. There was no significant difference in time to tPA treatment between the two groups ($p = 0.65$). At presentation, defect volumes obtained with CBF and CBV ischemic thresholds were larger for the HT group, but not significant ($p > 0.05$; Table 5.1).

Table 5.1 Baseline and follow-up patient data dichotomized according to presence of HT

Characteristic	HT (n = 23)	No HT (n = 18)	P-value
Female patients	10 (44)	5 (28)	0.30
Age (y) [*]	74 (58-83)	72 (64-81)	0.67
Mean arterial blood pressure > 120mm Hg	7 (30%)	2 (11)	0.25
International normalized ratio [†]	1.04 ± (0.10)	1.02 ± (0.07)	0.99
NIHSS at presentation	19 (13-20)	10 (7-15)	0.005
Time to imaging (min) [†]	124 ± 765	125 ± 118	0.37
ASPECT score [*]	6 (5-7)	10 (8-10)	0.02
Volume with CBF defect (cm ³) [†]	63±31	52±21	0.17
Volume with CBVdefect (cm ³) [†]	48±24	31±13	0.11
TPA given number (%)	17 (74%)	5 (28%)	0.005
Time to TPA (mins)	143 (27)	135 (31)	0.65
TPA dose (mg)	62±13	57±10	0.43
90 day modified Rankin score mRS	4 (2-6)	1 (0-2)	0.001

Unless otherwise noted, data are numbers of patients, with percentages in parentheses. *P* values were obtained with unpaired *t*, Wilcoxon rank sum, or Fisher exact testing. *P* < 0.05 was considered to indicate a significant difference.

* Data are median values, with the interquartile range in parentheses.

† Data are mean values ± the standard deviation.

The mean \pm standard deviation PS within superimposed ischemic ROIs for patients with and without HT was $0.49 \pm 0.3 \text{ ml}\cdot\text{min}^{-1}\cdot(100\text{g})^{-1}$ and $0.09 \pm 0.10 \text{ ml}\cdot\text{min}^{-1}\cdot(100\text{g})^{-1}$. These were significantly different ($p < 0.01$; Figure 3A). No significant differences in CBF within the ischemic ROI were observed between the HT [$15.6 \pm 6.8 \text{ ml}\cdot\text{min}^{-1}\cdot(100\text{g})^{-1}$] and non-HT [$18.0 \pm 5.9 \text{ ml}\cdot\text{min}^{-1}\cdot(100\text{g})^{-1}$] ($p > 0.05$). Similarly, no significant differences in mean CBV were observed between patients with HT [$1.0 \pm 0.38 \text{ ml}\cdot(100\text{g})^{-1}$] and patients without [$1.0 \pm 0.40 \text{ ml}\cdot(100\text{g})^{-1}$] ($p > 0.05$). For patients with HT, mean \pm standard deviation PS values within the contralateral ROI [$0.17 \pm 0.15 \text{ ml}\cdot\text{min}^{-1}\cdot(100\text{g})^{-1}$] was significantly different than ipsilateral values [$0.49 \pm 0.3 \text{ ml}\cdot\text{min}^{-1}\cdot(100\text{g})^{-1}$] ($p < 0.05$). For patients without HT, no significant difference was observed between ipsilateral [$0.09 \pm 0.10 \text{ ml}\cdot\text{min}^{-1}\cdot(100\text{g})^{-1}$] and contralateral ROIs [$0.06 \pm 0.04 \text{ ml}\cdot\text{min}^{-1}\cdot(100\text{g})^{-1}$] ($p > 0.05$). The mean PS for the contralateral ischemic ROI was significantly different for patients with and without HT ($p < 0.05$). Subgroup analysis revealed no significant differences in PS, CBF, or CBV between the patients with HI and those with PH; however, significant differences in PS, but not in CBF or CBV, were observed between patients with HI, PH, and non-HT groups ($p > 0.05$; Table 5.2, Figure 5.3b).

Table 5.2 Mean PS, CBF and CBV values for ischemic ROIs in patients dichotomized according to HT type and presence

	PH (n=8)	HI (n=15)	Any HT (n=23)	No HT(n=18)
PS [ml•min ⁻¹ •(100g) ⁻¹]	0.51 ± 0.39	0.48 ± 0.27	0.49 ± 0.3	0.09 ± 0.10
CBF [ml•min ⁻¹ •(100g) ⁻¹]	15.67 ± 5.6	15.6 ± 7.6	15.62 ± 6.8	18.01 ± 5.9
CBV ml•(100g) ⁻¹	1.00 ± 0.38	0.98 ± 0.39	1.00 ± 0.38	1.00 ± 0.40

Data are mean values ± the standard deviation. $P < 0.0001$ for difference between PS and CBF in parenchymal hematoma (PH), hemorrhagic infarction (HI), and any HT groups compared with those in no HT group. $P = 0.97$ to $P = 0.99$ for PS, CBF, and CBV in PH group compared with those in HI group.

Compared with the patients who were treated with tPA, non-tPA treated patients were older ($p = 0.03$), tended to have a higher baseline NIHSS ($p = 0.06$), arrived at the hospital later ($p = 0.04$), and were less likely to have HT ($p = 0.005$). The patients treated with tPA had smaller CBF and CBV defect volumes, although neither parameter was significantly different between the two groups. Among the patients treated with tPA, PS values were higher in those with HT [$0.47 \pm 0.33 \text{ ml}\cdot\text{min}^{-1}\cdot(100\text{g})^{-1}$] than in those without HT [$0.13 \pm 0.13 \text{ ml}\cdot\text{min}^{-1}\cdot(100\text{g})^{-1}$] ($p < 0.05$). A similar finding was seen for non-tPA patients with and without HT [0.56 ± 0.24 vs. $0.07 \pm 0.07 \text{ ml}\cdot\text{min}^{-1}\cdot(100\text{g})^{-1}$; $p < 0.05$]. No PS difference was found between tPA and non tPA patients with HT (0.47 ± 0.33 vs. $0.56 \pm 0.24 \text{ ml}\cdot\text{min}^{-1}\cdot(100\text{g})^{-1}$; $p=0.49$) and without HT (0.13 ± 0.13 vs. $0.07 \pm 0.07 \text{ ml}\cdot\text{min}^{-1}\cdot(100\text{g})^{-1}$; $p > 0.05$). The PS value of tPA treated patients with HT was not different from that of all hemorrhage patients ($p > 0.05$; Table 5.3).

Table 5.3 Baseline and follow-up patient data dichotomized according to tPA treatment status

Characteristic	tPA (n=22)	No tPA (n=19)	P-value
Age (y)	66.86 ± 14.98	76.56 ± 11.85	0.03
Baseline NIHSS score*	15.8 (13-21)	8.3 (5.25-16.25)	0.06
Baseline ASPECT score*	6 (6-9)	9 (6-19)	0.13
Time to treatment (min)	97 ± 49	159 ± 116	0.04
CBF volume (cm ³)	59.32 ± 33.02	54.66 ± 20.96	0.90
CBV volume (cm ³)	40.52 ± 16.14	45.20 ± 25.75	0.77
PS [ml•min ⁻¹ •(100g) ⁻¹]	0.28 ± 0.28	0.39 ± 0.33	0.10
CBF [ml•min ⁻¹ •(100g) ⁻¹]	16.0 ± 6.48	17.39 ± 6.62	0.77
CBV [ml•(100g) ⁻¹]	0.98 ± 0.32	1.03 ± 0.45	0.77
HT†	17 (77)	6 (31.6)	0.005
PH†	5 (23)	2 (10)	0.42

Unless otherwise noted, data are mean values ± the standard deviation. *P* values were obtained with unpaired *t*, Wilcoxon rank sum, or Fisher exact testing. *P* < 0.05 was considered to indicate a significant difference.

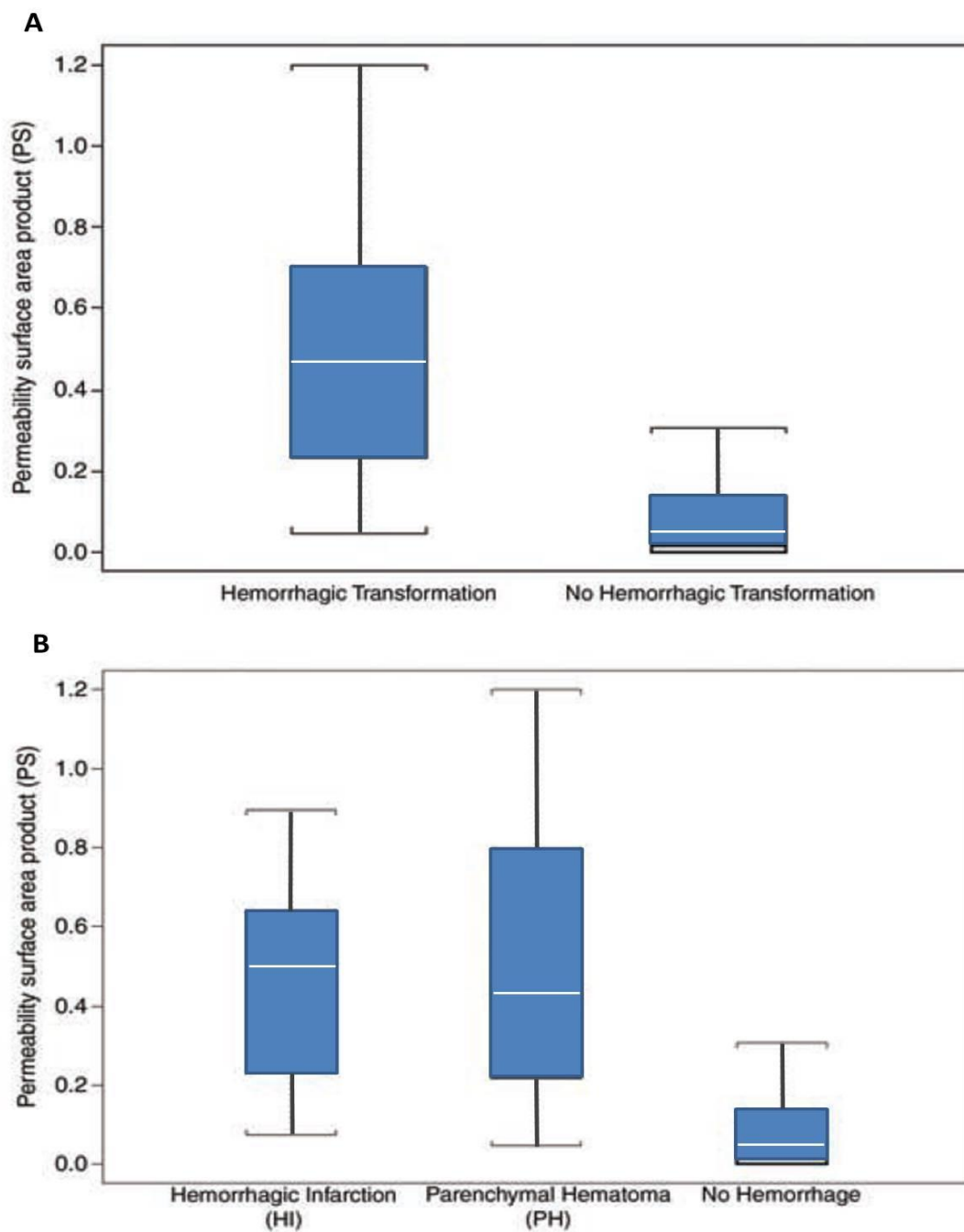
* Data are median values, with the interquartile range in parentheses.

† Data are numbers of patients, with the percentage of patients in parentheses.

The patients were subdivided according to hemorrhage status in addition to tPA treatment status (Figure 5.4). Although there were overlapping mean PS values within the ipsilateral ischemic ROI between the HT and non-HT groups among the patients treated with tPA, there was no such overlap in values among the patients who were not treated with tPA.

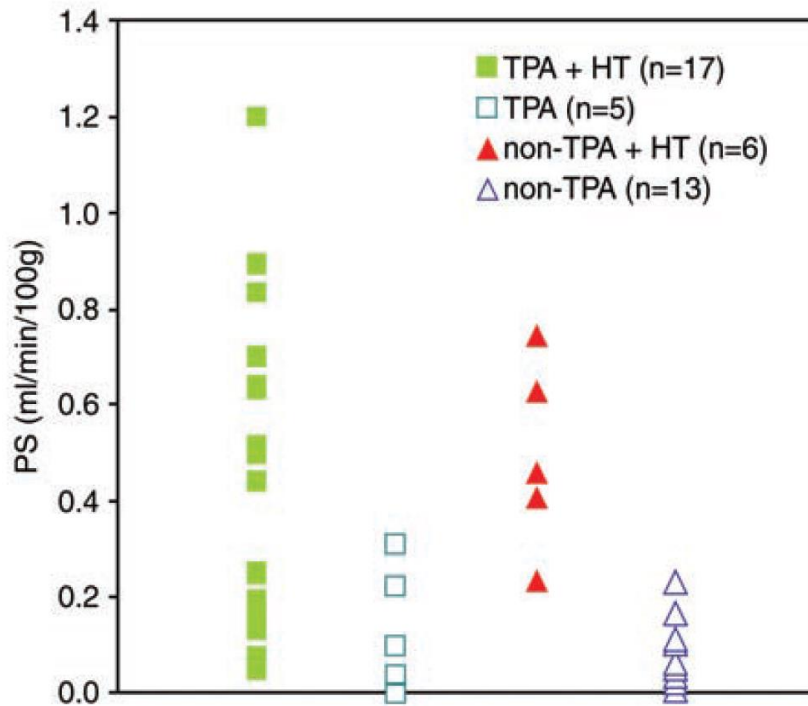
Univariate logistic regression analysis demonstrated significance for HT with PS (OR 3.5; 95% CI 1.69-7.06, $p = 0.001$), baseline NIHSS (OR 1.2; 95% CI 1.0-1.3 $p=0.001$), baseline ASPECTS (OR 0.5; 95% CI 0.3-0.7; $p=0.0007$) and tPA administration (OR 6.8; 95% CI 1.7-27.5, $p=0.007$). PS (OR 3.5; 95% CI 1.69-7.06; $p=0.0007$) and baseline ASPECTS (OR 0.4; 95% CI 0.2-0.7, $p = 0.002$) were the only independent variable associated with HT following a stepwise multivariate analysis. Receiver operator curve (ROC) analysis demonstrated an optimum PS cutoff value of $0.23 \text{ ml}^{-1} \cdot \text{min}^{-1} \cdot (100\text{g})^{-1}$, with an AUC of 0.92 ± 0.05 (Figure 5.4). Sensitivity, specificity, positive and negative predictive value and positive likelihood ratio was 77% (CI 55-92%), 93.8% (CI 70-100%), 94% (CI 84-100%), 75% (CI 60-90%) and 4.1 respectively.

Figure 5.3 PS values for patients with/without HT, and HT sub-types



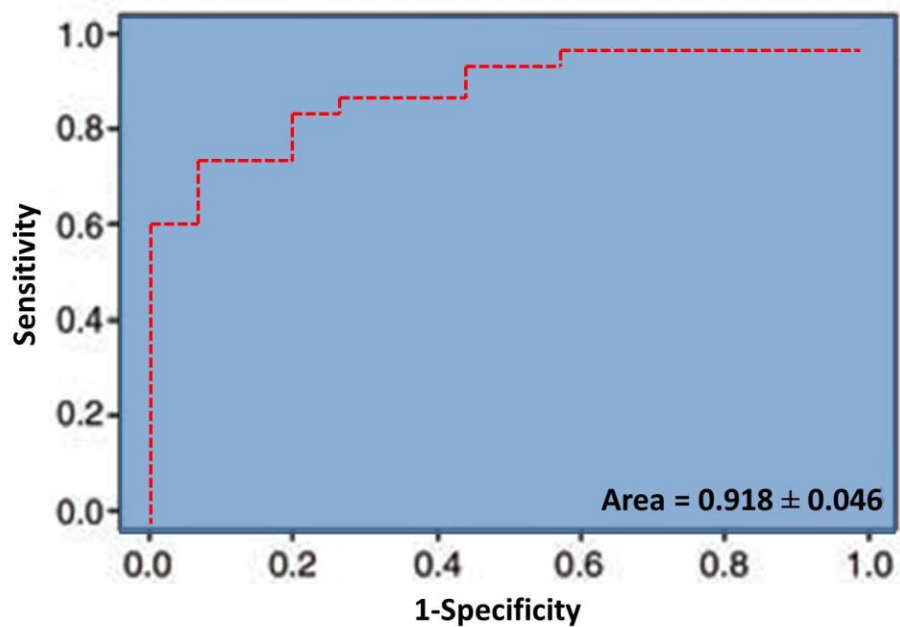
Box plots of PS [$\text{ml}^{-1} \cdot \text{min}^{-1} \cdot (100\text{g})^{-1}$] within ischemic ROIS for (A) patients with HT and those without HT, and (B) patients with either of two hemorrhage subtypes (HI or PH) and those without HT. In each box, median, 95% CI, and first and third quartile values are illustrated.

Figure 5.4 Distribution of PS values for tPA treated/non-treated



Graph illustrates distribution of mean PS values for ischemic ROIs in patients grouped according to tPA treatment status and HT status.

Figure 5.5 Receiver Operator Characteristic Curve for the PS parameter



Receiver operator characteristic curve (true positive rate versus false positive rate) of PS thresholds to determine HT. Area under the curve (AUC) is shown.

5.4 DISCUSSION

Our study results demonstrate the feasibility of a two-phase protocol for measuring hemodynamic parameters and the PS during one CT perfusion examination. The patients with HT had a significantly higher PS than did those without hemorrhage. A PS threshold of $0.23 \text{ ml}^{-1} \cdot \text{min}^{-1} \cdot (100\text{g})^{-1}$ also enabled the differentiation of patients with HT from those without.

It is important that we identify no significant difference in CBF between the patients with and those without hemorrhage. The patients treated with tPA were more likely to have HT. However, we observed no significant differences in PS between the tPA-treated and non-treated patients. Patients with HT were more likely to have higher admission NIHSS scores and poorer clinical outcomes compared with patients without HT. There were no significant differences between the patients with HI and those with PH. The limited number of patients precluded further stratification of the HT sub-types into HI-1, 2 and PH-1,2.

MR imaging has also been used to study BBB breakdown in patients with acute stroke³²⁻³⁴. In particular, Warach et al. (2004) found the hyperintense acute reperfusion marker (HARM) to be a useful early marker of BBB breakdown in their MR-based natural history examination of acute stroke patients³⁵. HARM is the hyperintense signal observed on fast low-angle inversion-recovery images hours to days after gadopentetate dimeglumine administration and is believed to be caused by the accumulation of MR contrast material in the cerebrospinal fluid space or ventricles before BBB breakdown. In some cases, the HARM signal was not just localized to the ischemic hemisphere; rather, it was generalized throughout the brain on the fast low-angle inversion-recovery images, signifying more widespread and remote BBB permeability, including that in the

contralateral hemisphere. Given that HARM was found to be associated with HT and stroke severity, their finding may help to explain our observation that the PS in the contralateral mirror ROI in patients with HT was higher than that in patients without HT.

HT is common in stroke patients, especially following thrombolytic therapy^{9, 36, 37}. In our study, HT was associated with PS, NIHSS score, baseline ASPECT score, and tPA therapy at univariate analysis; however, the association with tPA was weaker. The absence of an independent association between tPA and HT likely reflects the fact that the patients were selected for treatment on the basis of their ASPECT and NIHSS scores, both of which were independently used to predict HT. Therefore, no additional influence of tPA on this outcome could be detected. Our results, like those in most stroke studies, could have been affected by the specific inclusion and exclusion criteria that we adopted for this study, and by whether the studied cohorts had matched clinical data. Nonetheless, our results show that besides the PS parameter and ASPECT score, no other factors (age, sex, or baseline NIHSS score) were associated with HT.

The prevalence of PH in this study is higher than that of previously published randomized studies of thrombolysis^{10, 38}. This may have been due in part to the classification of hemorrhage at 5–7-day post symptom onset, rather than within the 36-hour time window used in many other studies^{14, 39}. Vasogenic edema and mass effect are expected to peak at 3–4 days, which may contribute to the increased number of cases with mass effect in our series. An experienced team of stroke neurologists administered tPA by following standard thrombolysis guidelines. No tPA dosing errors or protocol violations occurred. All patients in this series were classified into hemorrhage and nonhemorrhage groups by using gradient-echo T2-weighted MR imaging rather than CT. The superiority

of this MR sequence for hemorrhage detection may also account for the higher reported prevalence of HT^{40, 41}.

Our sample size was too small for us to make any definitive conclusions about the effect of tPA treatment on HT; however, tPA may act in concert with ischemic effects to render the brain more susceptible to HT as the minimal PS in patients with HT who were treated with tPA [$0.047 \text{ ml}^{-1} \cdot \text{min}^{-1} \cdot (100\text{g})^{-1}$] was lower than that of patients with hemorrhage who were not treated with tPA [$0.23 \text{ ml}^{-1} \cdot \text{min}^{-1} \cdot (100\text{g})^{-1}$]. A lower pre-treatment PS with tPA treatment may be as likely to cause HT as a higher PS without tPA treatment.

CT is the modality of choice for the initial investigation of acute stroke for patients that may require lytic treatment²⁹. CT scanners are widely available, accessible, and less expensive to operate compared with MR units. Occlusion site and perfusion defect size are important considerations in determining the outcome of revascularization procedures and defining a target population for treatment⁴²⁻⁴⁴. Surrogate radiological markers of BBB breakdown, including intra-procedural early venous filling and post-procedural contrast enhancement and extravasation, have been described previously^{45, 46}. These markers are usually associated with larger volumes of contrast material injected over a prolonged period. Until recently, leakage of contrast material volumes used in current acute stroke protocols were not detectable with CT^{47, 48}. The two-phase perfusion CT protocol, described herein, is designed to depict contrast material leakage owing to the extension of the acquisition time window of a conventional perfusion CT examination by 90 seconds, with six additional acquisitions at 15-second intervals. In this study, CT angiography was performed before PS measurement in the two-phase perfusion CT protocol. This particular design raises the question of whether residual contrast material

from the prior CT angiography examination affects the accuracy of the subsequent PS measurement, which itself requires another contrast agent injection. Both the arterial input curve and the tissue curve used to calculate the PS with the Johnson-Wilson model were generated by subtracting the attenuation of the artery and the tissue before the arrival of contrast material from the attenuation after the contrast material arrival. The residual contrast material from prior CT angiography would cause the same increase in attenuation in the artery and the tissue before and after the arrival of contrast material, and the effect of this increase would be eliminated by the subtraction during the generation of the arterial input and tissue curves. Therefore, the residual contrast material from prior CT angiography would not affect the accuracy of the PS parameter.

Our study had several limitations. First, comparisons among the small number of patients with HT did not reveal significant differences in PS between the HI and PH groups. However, the importance of the HT subtypes is being debated^{15, 17-19}. Results of a recent study demonstrated that HI is not necessarily benign and is associated with a worse clinical outcome compared with that of patients without hemorrhage¹⁸. Second, six patients in our study were excluded because of excessive motion during imaging. This number represents 15% (6/41) of the current patient data set, and the exclusion may have resulted in an overestimation of the diagnostic accuracy of the technique. Third, the sensitivity and specificity of our optimal PS threshold for predicting HT needs to be tested prospectively in a larger data set. Fourth, as quantitative permeability measurements are uniquely tracer dependent, our specific quantitative results may not be generalizable to other contrast agents or other acquisition timing protocols - every contrast agent has a different permeability constant, depending on its charge and molecular weight. Fifth, we used one threshold value to delineate ischemia, which may

have led under/overestimation of the ischemic ROI depending on gray/white matter distribution. Sixth, although blood products are easily identified on gradient-echo T2-weighted MR imaging, this sequence is hindered by susceptibility artifacts that can make the area of hemorrhage appear larger than it really is. However, since the PS was evaluated within the entire ischemic ROI, defined on CBF maps, overestimation of the hemorrhage region volume likely had no substantial effect on the PS calculation. Last, although CT perfusion is widely used, it is limited by ionizing radiation, contrast material nephrotoxicity, and limited coverage in the z-direction.

5.5 CONCLUSION

In conclusion, the BBB PS parameter can be measured accurately during the acute stroke CT protocol. PS elevation appears to be a promising marker for predicting the risk of HT in acute stroke patients.

5.6 REFERENCES

1. Tissue plasminogen activator for acute ischemic stroke. The national institute of neurological disorders and stroke rt-pa stroke study group. *The New England journal of medicine*. 1995;333:1581-1587
2. Hacke W, Kaste M, Fieschi C, Toni D, Lesaffre E, von Kummer R, et al. Intravenous thrombolysis with recombinant tissue plasminogen activator for acute hemispheric stroke. The european cooperative acute stroke study (ecass). *JAMA : the journal of the American Medical Association*. 1995;274:1017-1025
3. Larrue V, von Kummer RR, Muller A, Bluhmki E. Risk factors for severe hemorrhagic transformation in ischemic stroke patients treated with recombinant tissue plasminogen activator: A secondary analysis of the european-australasian acute stroke study (ecass ii). *Stroke; a journal of cerebral circulation*. 2001;32:438-441
4. Hacke W, Albers G, Al-Rawi Y, Bogousslavsky J, Davalos A, Eliasziw M, et al. The desmoteplase in acute ischemic stroke trial (dias): A phase ii mri-based 9-hour window acute stroke thrombolysis trial with intravenous desmoteplase. *Stroke; a journal of cerebral circulation*. 2005;36:66-73
5. Fisher M, Adams RD. Observations on brain embolism with special reference to the mechanism of hemorrhagic infarction. *Journal of neuropathology and experimental neurology*. 1951;10:92-94
6. Larrue V, von Kummer R, del Zoppo G, Bluhmki E. Hemorrhagic transformation in acute ischemic stroke. Potential contributing factors in the european cooperative acute stroke study. *Stroke; a journal of cerebral circulation*. 1997;28:957-960
7. Tong DC, Adami A, Moseley ME, Marks MP. Relationship between apparent diffusion coefficient and subsequent hemorrhagic transformation following acute ischemic stroke. *Stroke; a journal of cerebral circulation*. 2000;31:2378-2384
8. Molina CA, Alvarez-Sabin J, Montaner J, Abilleira S, Arenillas JF, Coscojuela P, et al. Thrombolysis-related hemorrhagic infarction: A marker of early reperfusion, reduced infarct size, and improved outcome in patients with proximal middle cerebral artery occlusion. *Stroke; a journal of cerebral circulation*. 2002;33:1551-1556
9. Hacke W, Kaste M, Fieschi C, von Kummer R, Davalos A, Meier D, et al. Randomised double-blind placebo-controlled trial of thrombolytic therapy with intravenous alteplase in acute ischaemic stroke (ecass ii). Second european-australasian acute stroke study investigators. *Lancet*. 1998;352:1245-1251
10. Hacke W, Donnan G, Fieschi C, Kaste M, von Kummer R, Broderick JP, et al. Association of outcome with early stroke treatment: Pooled analysis of atlantis, ecass, and ninds rt-pa stroke trials. *Lancet*. 2004;363:768-774

11. Neumann-Haefelin T, Hoelig S, Berkefeld J, Fiehler J, Gass A, Humpich M, et al. Leukoaraiosis is a risk factor for symptomatic intracerebral hemorrhage after thrombolysis for acute stroke. *Stroke; a journal of cerebral circulation*. 2006;37:2463-2466
12. Kase CS, Furlan AJ, Wechsler LR, Higashida RT, Rowley HA, Hart RG, et al. Cerebral hemorrhage after intra-arterial thrombolysis for ischemic stroke: The proact ii trial. *Neurology*. 2001;57:1603-1610
13. Berger C, Fiorelli M, Steiner T, Schabitz WR, Bozzao L, Bluhmki E, et al. Hemorrhagic transformation of ischemic brain tissue: Asymptomatic or symptomatic? *Stroke; a journal of cerebral circulation*. 2001;32:1330-1335
14. Albers GW, Thijs VN, Wechsler L, Kemp S, Schlaug G, Skalabrin E, et al. Magnetic resonance imaging profiles predict clinical response to early reperfusion: The diffusion and perfusion imaging evaluation for understanding stroke evolution (defuse) study. *Annals of neurology*. 2006;60:508-517
15. von Kummer R. Brain hemorrhage after thrombolysis: Good or bad? *Stroke; a journal of cerebral circulation*. 2002;33:1446-1447
16. Dzialowski I, Pexman JH, Barber PA, Demchuk AM, Buchan AM, Hill MD. Asymptomatic hemorrhage after thrombolysis may not be benign: Prognosis by hemorrhage type in the canadian alteplase for stroke effectiveness study registry. *Stroke; a journal of cerebral circulation*. 2007;38:75-79
17. Fiorelli M, Bastianello S, von Kummer R, del Zoppo GJ, Larrue V, Lesaffre E, et al. Hemorrhagic transformation within 36 hours of a cerebral infarct: Relationships with early clinical deterioration and 3-month outcome in the european cooperative acute stroke study i (ecass i) cohort. *Stroke; a journal of cerebral circulation*. 1999;30:2280-2284
18. Neumann-Haefelin C, Brinker G, Uhlenkuken U, Pillekamp F, Hossmann KA, Hoehn M. Prediction of hemorrhagic transformation after thrombolytic therapy of clot embolism: An mri investigation in rat brain. *Stroke; a journal of cerebral circulation*. 2002;33:1392-1398
19. Hamann GF, Okada Y, Fitridge R, del Zoppo GJ. Microvascular basal lamina antigens disappear during cerebral ischemia and reperfusion. *Stroke; a journal of cerebral circulation*. 1995;26:2120-2126
20. Kassner A, Roberts T, Taylor K, Silver F, Mikulis D. Prediction of hemorrhage in acute ischemic stroke using permeability mr imaging. *AJNR. American journal of neuroradiology*. 2005;26:2213-2217
21. Schaefer PW, Roccatagliata L, Ledezma C, Hoh B, Schwamm LH, Koroshetz W, et al. First-pass quantitative ct perfusion identifies thresholds for salvageable penumbra in acute stroke patients treated with intra-arterial therapy. *AJNR. American journal of neuroradiology*. 2006;27:20-25

22. Wintermark M, Flanders AE, Velthuis B, Meuli R, van Leeuwen M, Goldsher D, et al. Perfusion-ct assessment of infarct core and penumbra: Receiver operating characteristic curve analysis in 130 patients suspected of acute hemispheric stroke. *Stroke; a journal of cerebral circulation*. 2006;37:979-985
23. Murphy BD, Fox AJ, Lee DH, Sahlas DJ, Black SE, Hogan MJ, et al. Identification of penumbra and infarct in acute ischemic stroke using computed tomography perfusion-derived blood flow and blood volume measurements. *Stroke; a journal of cerebral circulation*. 2006;37:1771-1777
24. TY. L. Functional ct: Physiological models. . *Trends in Biotechnology* 2002;20:S3-S10
25. Purdie TG, Henderson E, Lee TY. Functional ct imaging of angiogenesis in rabbit vx2 soft-tissue tumour. *Physics in medicine and biology*. 2001;46:3161-3175
26. Cenic A, Nabavi DG, Craen RA, Gelb AW, Lee TY. A ct method to measure hemodynamics in brain tumors: Validation and application of cerebral blood flow maps. *AJNR. American journal of neuroradiology*. 2000;21:462-470
27. Roberts HC, Roberts TP, Lee TY, Dillon WP. Dynamic, contrast-enhanced ct of human brain tumors: Quantitative assessment of blood volume, blood flow, and microvascular permeability: Report of two cases. *AJNR. American journal of neuroradiology*. 2002;23:828-832
28. Lin K, Kazmi KS, Law M, Babb J, Peccerelli N, Pramanik BK. Measuring elevated microvascular permeability and predicting hemorrhagic transformation in acute ischemic stroke using first-pass dynamic perfusion ct imaging. *AJNR. American journal of neuroradiology*. 2007;28:1292-1298
29. Cenic A, Nabavi DG, Craen RA, Gelb AW, Lee TY. Dynamic ct measurement of cerebral blood flow: A validation study. *AJNR. American journal of neuroradiology*. 1999;20:63-73
30. Murphy BD, Fox AJ, Lee DH, Sahlas DJ, Black SE, Hogan MJ, et al. White matter thresholds for ischemic penumbra and infarct core in patients with acute stroke: Ct perfusion study. *Radiology*. 2008;247:818-825
31. Lee TY, Purdie TG, Stewart E. Ct imaging of angiogenesis. *Q J Nucl Med*. 2003;47:171-187
32. Hemorrhage in the interventional management of stroke study. *Stroke; a journal of cerebral circulation*. 2006;37:847-851
33. Trouillas P, von Kummer R. Classification and pathogenesis of cerebral hemorrhages after thrombolysis in ischemic stroke. *Stroke; a journal of cerebral circulation*. 2006;37:556-561
34. Aoki T, Sumii T, Mori T, Wang X, Lo EH. Blood-brain barrier disruption and matrix metalloproteinase-9 expression during reperfusion injury: Mechanical versus embolic focal ischemia in spontaneously hypertensive rats. *Stroke; a journal of cerebral circulation*. 2002;33:2711-2717

35. Warach S, Latour LL. Evidence of reperfusion injury, exacerbated by thrombolytic therapy, in human focal brain ischemia using a novel imaging marker of early blood-brain barrier disruption. *Stroke; a journal of cerebral circulation*. 2004;35:2659-2661
36. Castellanos M, Leira R, Serena J, Pumar JM, Lizasoain I, Castillo J, et al. Plasma metalloproteinase-9 concentration predicts hemorrhagic transformation in acute ischemic stroke. *Stroke; a journal of cerebral circulation*. 2003;34:40-46
37. Sumii T, Lo EH. Involvement of matrix metalloproteinase in thrombolysis-associated hemorrhagic transformation after embolic focal ischemia in rats. *Stroke; a journal of cerebral circulation*. 2002;33:831-836
38. Montaner J, Molina CA, Monasterio J, Abilleira S, Arenillas JF, Ribo M, et al. Matrix metalloproteinase-9 pretreatment level predicts intracranial hemorrhagic complications after thrombolysis in human stroke. *Circulation*. 2003;107:598-603
39. Horstmann S, Kalb P, Koziol J, Gardner H, Wagner S. Profiles of matrix metalloproteinases, their inhibitors, and laminin in stroke patients: Influence of different therapies. *Stroke; a journal of cerebral circulation*. 2003;34:2165-2170
40. Adams H, Adams R, Del Zoppo G, Goldstein LB. Guidelines for the early management of patients with ischemic stroke: 2005 guidelines update a scientific statement from the stroke council of the american heart association/american stroke association. *Stroke; a journal of cerebral circulation*. 2005;36:916-923
41. Tan JC, Dillon WP, Liu S, Adler F, Smith WS, Wintermark M. Systematic comparison of perfusion-ct and ct-angiography in acute stroke patients. *Annals of neurology*. 2007;61:533-543
42. Lansberg MG, Thijs VN, Hamilton S, Schlaug G, Bammer R, Kemp S, et al. Evaluation of the clinical-diffusion and perfusion-diffusion mismatch models in defuse. *Stroke; a journal of cerebral circulation*. 2007;38:1826-1830
43. Furlan A, Higashida R, Wechsler L, Gent M, Rowley H, Kase C, et al. Intra-arterial prourokinase for acute ischemic stroke. The proact ii study: A randomized controlled trial. Prolyse in acute cerebral thromboembolism. *JAMA : the journal of the American Medical Association*. 1999;282:2003-2011
44. Ohta H, Nakano S, Yokogami K, Iseda T, Yoneyama T, Wakisaka S. Appearance of early venous filling during intra-arterial reperfusion therapy for acute middle cerebral artery occlusion: A predictive sign for hemorrhagic complications. *Stroke; a journal of cerebral circulation*. 2004;35:893-898
45. Yoon W, Seo JJ, Kim JK, Cho KH, Park JG, Kang HK. Contrast enhancement and contrast extravasation on computed tomography after intra-arterial thrombolysis in patients with acute ischemic stroke. *Stroke; a journal of cerebral circulation*. 2004;35:876-881

46. Hayman LA, Evans RA, Bastion FO, Hinck VC. Delayed high dose contrast ct: Identifying patients at risk of massive hemorrhagic infarction. *AJR. American journal of roentgenology*. 1981;136:1151-1159
47. Johnson JA, Wilson TA. A model for capillary exchange. *Am J Physiol*. 1966;210:1299-1303
48. Yeung WT, Lee TY, Del Maestro RF, Kozak R, Brown T. In vivo ct measurement of blood-brain transfer constant of iopamidol in human brain tumors. *Journal of neuro-oncology*. 1992;14:177-187

CHAPTER 6

Early Rate of Contrast Extravasation in ICH Patients

The contents of this chapter have been adapted from the paper entitled “Early rate of contrast extravasation in patients with intracerebral hemorrhage” published in the *American Journal of Neuroradiology*, 2011;32(10):1879-84, by: C.D. d'Este, T. Chia, A. Jairath, T.Y. Lee, S.P. Symons, R.I. Aviv.

6.1 INTRODUCTION

As discussed in Chapter 1, primary intracerebral hemorrhage (ICH) accounts for ~23% of all strokes, and leads to rapid clinical deterioration¹. During the first 3 hours of symptom onset, early hematoma growth is seen in 18% to 38% of intracerebral hemorrhage patients, reducing to 11% thereafter²⁻⁴. Early hematoma expansion is associated with poorer neurological outcome and increased mortality⁵. The cause of early hematoma expansion is unknown, but secondary vessel injury and perihematomal ischemia have been implicated. Prevention or reduction of secondary bleeding is important when dealing with ICH⁶. Recently, administration of recombinant Factor VIIa resulted in the reduction of hematoma expansion, without improvement in clinical outcome⁷; however, post hoc analysis has suggested benefit in a small sub-group of patients⁸.

CT imaging is considered the modality of choice for the acute investigation of ICH. Extravasation is demonstrated on CT angiography (CTA) and post contrast CT (PCCT) in approximately 40-50% of patients^{9, 10}. Several imaging studies have demonstrated an association between early contrast extravasation and hematoma

expansion¹⁰⁻¹³. A recent study demonstrated that foci of contrast-leakage not discernable during the arterial phase of a CTA may be detected on PCCT (PCL)¹⁴. A further study demonstrated that delayed CTA detected other areas of contrast extravasation not seen on an early CTA¹⁵. In both studies, sensitivity to hematoma expansion improved when delayed images were considered - it is reasonable to assume that a slower rate of contrast extravasation in PCL accounts for the lack of CTA detection, although this has not been shown. Further, the etiology and pathophysiological significance of the various manifestations of contrast extravasation remain unknown. However, given the association between risk of hematoma expansion and poor outcome with the number and density of extravasation defects, it is likely that more rapid extravasation, such as that seen on arterial phase CTA, may confirm the highest risk¹³.

CT perfusion (CTP)-derived permeability surface area product (PS) is a novel method of measuring the rate of contrast extravasation from the intra- to extravascular compartment¹⁶. Knowing the rate of contrast extravasation may provide insight into the pathophysiology of hematoma expansion by identifying the contributing target abnormality. A clinical technique that quantifies this rate provides objective assessment of hematoma expansion risk rather than the qualitative approach currently used. Such information may become increasingly important as novel ICH treatments, such as focused ultrasound coagulation, are developed that will target specific defects¹⁷.

Using the CTP-PS parameter we sought to measure the rate of contrast extravasation for CTA-Spot Sign defects and PCCT-PCL defects, respectively. PS values from these two abnormalities will be compared to PS values from hematoma volumes excluding any extravasation, hematoma volumes in patients without extravasation, and contralateral normal tissue. We hypothesize that the rate of contrast extravasation will be

highest in CTA Spot Sign defects compared to PCL defects and hematoma regions without extravasation.

6.2 MATERIALS AND METHODS

6.2.1 Patient cohort

With approval by the local institutional ethics review board⁺, 16 consecutive patients with ICH presenting over a 6-month period at a tertiary stroke centre underwent initial non-contrast CT (NCCT), and CTA upon admission. The imaging was reviewed acutely with the patient on the CT table by an attending neuroradiologist with 5 years experience. If ICH was identified, a PCCT scan and CT Perfusion (CTP) study was performed regardless of the result of contrast extravasation in CTA. Spot Sign and PCL extravasation were identified retrospectively by the presence of contrast extravasation on the CTA or PCCT, respectively. Of 16 screened patients, 7 demonstrated contrast extravasation. Nine foci of contrast extravasation were present on each of the CTA and PCCT, respectively, for a total of 18 regions.

6.2.2 Image acquisition

CT scanning was performed on a 64-slice CT (Lightspeed plus and VCT; GE Healthcare, Waukesha, Wis) scanner at admission and 24 hours after presentation in all patients. The standard ICH protocol includes a NCCT head followed by a CTA and PCCT. Pre- and post-contrast head imaging was acquired from the skull base to vertex with parameters:

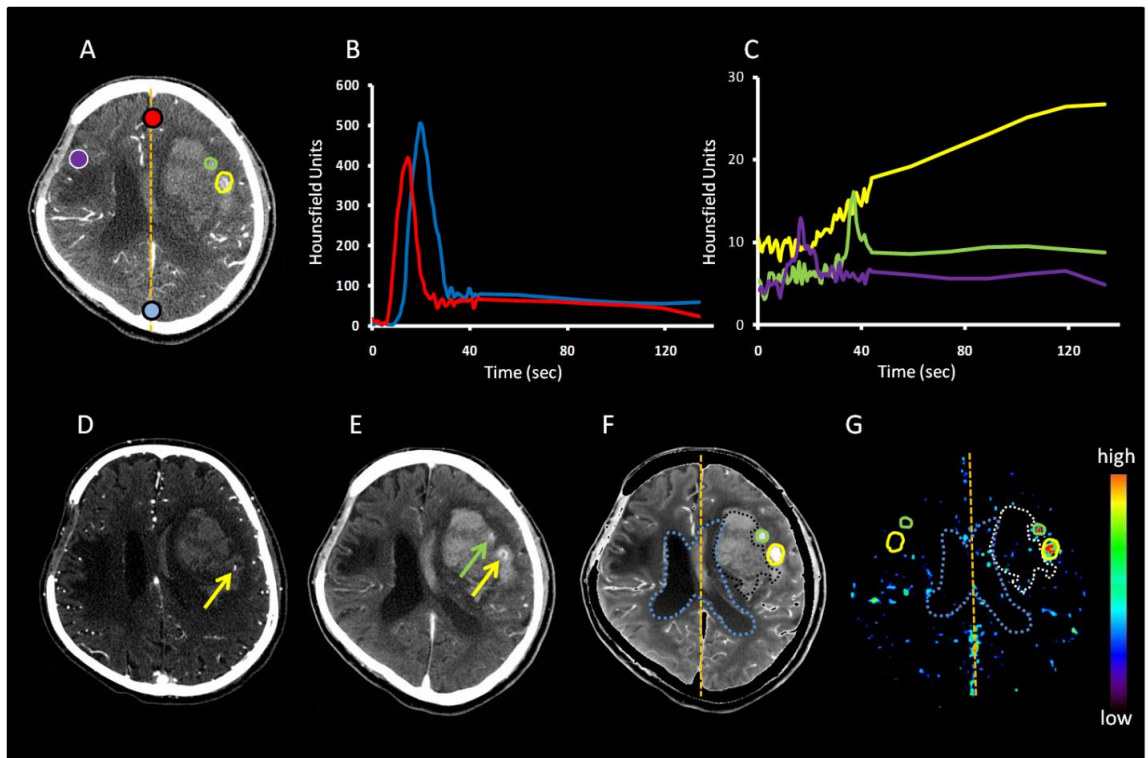
⁺ Appendix G – Human Ethics Approval form

120 kVp; 340 mA; 4 x 5 mm collimation; 1 second/rotation; and a table speed of 15 mm/rotation. CTA studies were acquired from C6 to the vertex in the helical HS mode with parameters: 0.7 ml/kg contrast (to a maximum of 90 ml through an antecubital vein via at least an 18 or 20 gauge angiocatheter); 5 to 10 second delay; 120 kVp; 270 mA; 1 second/rotation; 1.25 mm slice thickness at 0.625 mm intervals, table speed 3.75 mm/rotation. The CTP study was comprised of 2 phases. The first phase was a 45 seconds continuous (cine) scan reconstructed at 0.5 second intervals to produce a series of 90 sequential images for each of the eight slices, covering a total of 40 mm from the basal ganglia to the lateral ventricles. The second phase collected images covering the same 8 slices over an additional 90 seconds immediately after the first phase at intervals of 15 seconds. Scan parameters for both phases were: 80 kVp, 190 mA, 8 x 5 mm collimation and 1 second/rotation. The dose-length products for NCCT, CTA (intracranial only) and CTP components were 1073, 592 and 1804 mGy-cm, respectively. Assuming a conversion factor of 0.0021 mSv per mGy-cm, the effective dose was 7.3 mSV. Iodinated contrast agent at a dose of 0.5 ml/kg (maximum 50 ml) was injected 3-5 seconds prior to the start of the first phase at a rate of $4 \text{ ml}\cdot\text{s}^{-1}$. A 5 minute post processing time is as previously reported¹⁵. The follow up consisted of an NCCT only. All images were viewed on AGFA Impax 4.5 PACS workstation.

6.2.3 Image analysis

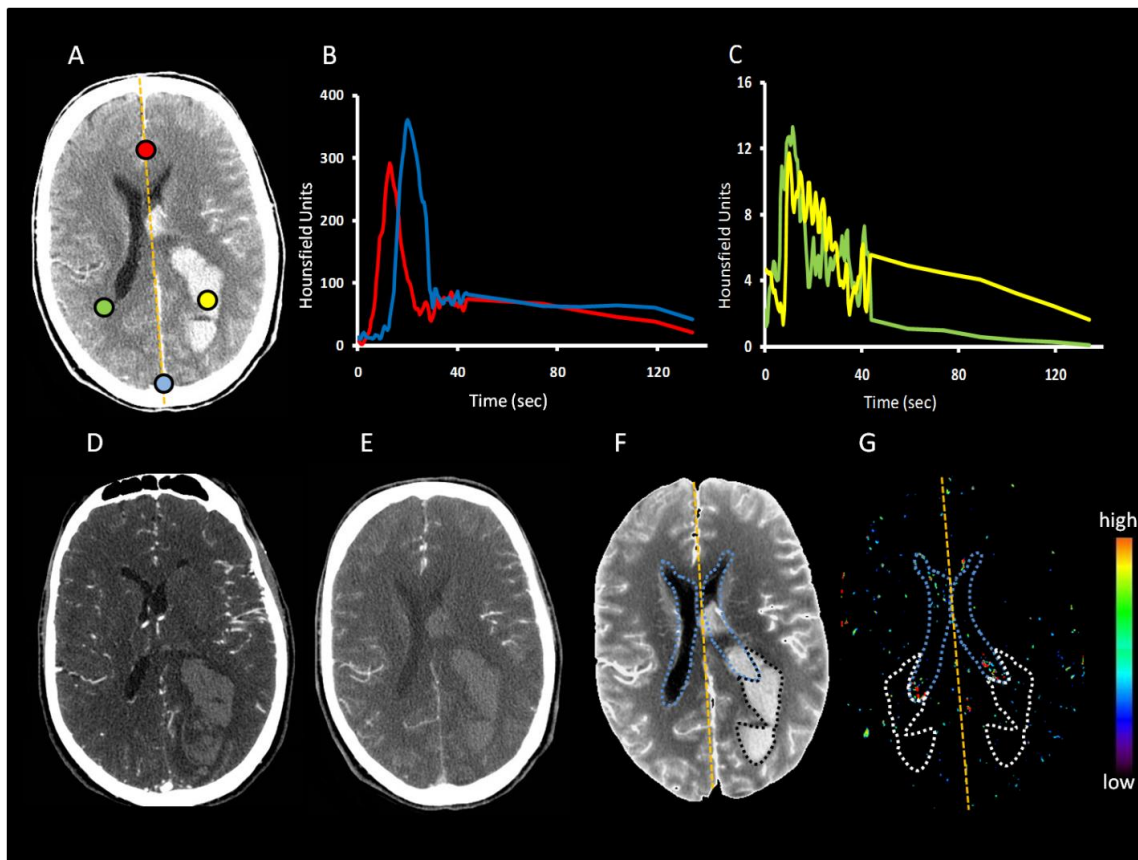
CT Perfusion 4 software (GE Healthcare) was used to calculate parametric maps of PS. Arterial input and venous output functions were obtained from the ipsilateral anterior cerebral artery and from the superior sagittal sinus, respectively (Figures 6.1 and 6.2). Partial volume averaging was corrected by multiplying the arterial input function by

Figure 6.1 Example of patient with a spot sign and post-contrast leakage



(A) Baseline contrast enhanced source CTP image. (B) Corresponding time-density curves (TDC) for the artery (red) and vein (blue; Hounsfield Unit scale: 0-600). (C) TDC for Spot Sign (yellow), post contrast-leakage (PCL; green), and contralateral region of interest (ROI; purple; Hounsfield Unit scale: 0-30). (D) CTA with Spot Sign visible (yellow arrow). (E) Post-contrast enhanced CT (PCCT) showing PCL (green arrow) and Spot Sign with extravasation (yellow arrow). (F) Perfusion weighted image and (G) permeability surface area product (PS) map. ROIs encircle the contrast extravasation (Spot Sign and PCL) on the perfusion weighted image, and entire hematoma excluding extravasation and overlap with ventricles (intraventricular hemorrhage). ROIs are superimposed onto PS map and reflected about the midline.

Figure 6.2 Example of patient without contrast extravasation



(A) Baseline contrast enhanced source CTP image. (B) Corresponding time-density curves (TDC) for the artery (red) and vein (blue; Hounsfield Unit scale: 0-400). (C) TDC for region of interest (ROI) within hematoma (yellow), and contralateral ROI (green; Hounsfield Unit scale: 0-16). (D,E) CTA and PCCT with no visible contrast extravasation within hematoma. (F) Perfusion weighted image (PWI) and (G) permeability surface area product (PS) map. An ROI encircles the hematoma on the PWI. Hematoma ROI is superimposed onto PS map, excluding overlap with ventricles, and is reflected about the midline.

the ratio of the area of venous time attenuation curve to that of the arterial input function¹⁸. Maps were calculated by deconvolution of the arterial input curve and tissue curves from 2 x 2 pixel blocks of CT images using the adiabatic approximation to the Johnson-Wilson (J-W) model¹⁹.

PS, by definition, is the unidirectional rate of contrast extravasation from the intravascular to the extravascular space through a disrupted blood-brain barrier²⁰. Extravasation of contrast material leads to prolonged enhancement of the tissue beyond the intravascular (first) phase which can only be properly characterized by a two-phase CTP study as previously described²¹. Parametric maps were analyzed by one author with 4 years' experience using custom software (IDL v6.1, RSI Inc, Boulder, Colo. USA). Extravasation, observed on CTA and/or PCCT, was located on inherently co-registered perfusion weighted images (PWI) from the CTP protocol. Four regions of interest (ROI) were superimposed onto co-registered PS functional maps for extravasation positive patients: areas of focal contrast extravasation on 1) location of CTA Spot Sign defect and/or 2) location of PCL defect, 3) entire hematoma excluding both extravasation and overlap with ventricles (IVH), and 4) mirror regions contralateral to extravasation regions defined in (1) and (2), (Figure 6.1). For extravasation negative patients, ROIs were placed on: 1) entire hematoma volume excluding overlap with ventricles, and 2) mirror regions contralateral to region defined in (1) (Figure 6.2). ROIs were superimposed onto cerebral blood flow (CBF), cerebral blood volume (CBV) and PS functional maps; pixels with values of $CBF > 100 \text{ ml} \cdot \text{min}^{-1} \cdot (100\text{g})^{-1}$ and $CBV > 8 \text{ ml} \cdot (100\text{g})^{-1}$ were excluded²². Hematoma volumes at presentation and follow up study were calculated blinded to extravasation status using Medical Image Processing, Analysis and Visualization (Center for Information Technology, National Institutes of Health) Hematoma expansion was

defined as an increased volume of $> 6\text{ml}$ or 30% ^{11, 23}. Intraventricular hemorrhage (IVH) was not considered in the definition of hematoma expansion.

6.2.4 Statistical Analysis

All analyses were performed with SPSS for windows (v. 16; SPSS Chicago, Ill), and all data sets were checked for normality with the Shapiro-Wilk calculation to determine whether a parametric or a non-parametric test should be used. The Wilcoxon rank-sum test with bonferroni-correction was used to compare all PS values. Significance was defined as $p < 0.05$. Average PS values were compared for: 1) Spot Sign defects only (9 foci), 2) PCL defects only (9 foci), 3) hematoma excluding extravasation, 4) regions contralateral to extravasation, 5) hematoma in patients without extravasation and 6) an area contralateral to (5). Unpaired t-tests were used to compare differences in age, time to CTA, average arterial pressure, international normalized ratio, partial thromboplastin time, National institute of Health Stroke Scale Score and glucose score, respectively. Using the Wilcoxon rank-sum test with bonferroni-correction, the average hematoma volume at follow-up (24 hours) was compared with admission hematoma volume within extravasation positive and negative groups, respectively.

6.3 RESULTS

Permeability surface area product (PS) data was acquired for 16 ICH patients (9 males and 7 females). Their demographics are listed in Table 6.1. Of the 7 patients with extravasation on the admission CTA and/or PCCT imaging, three patients had both Spot Sign and PCL defects, three patients had only PCL defects, and one patient had only a

Table 6.1 Demographics for extravasation positive and negative groups

	Extravasation Positive	Extravasation Negative	P value
Age	73.83 ± 22.96	63.8 ± 17.13	0.23
Time to CTA, min	234.50 ± 384.95	131.00 ± 46.96	0.74
MAP	142.72 ± 27.12	160.25 ± 51.02	0.69
INR	1.15 ± 0.32	1.05 ± 0.11	0.16
PTT	33.23 ± 4.78	31.54 ± 4.24	0.15
Glucose, mmol/L	6.57 ± 1.78	6.85 ± 1.41	0.31
NIHSS median, range	15 (5 - 23)	11 (2 - 16)	0.37

Patients are dichotomized into contrast extravasation positive (n = 7) and negative (n = 9) groups. MAP = average arterial pressure; INR = international normalized ratio; PTT = partial thromboplastin time; NIHSS = National institute of Health Stroke Scale Score. Unpaired t-tests are used to compare the data.

Spot Sign defect. Nine patients did not present with extravasation on CTA or PCCT. One extravasation positive patient received rFVIIa as an off-label treatment. Average PS was $6.5 \pm 1.60 \text{ ml}\cdot\text{min}^{-1}\cdot(100\text{g})^{-1}$, $0.95 \pm 0.39 \text{ ml}\cdot\text{min}^{-1}\cdot(100\text{g})^{-1}$, $0.12 \pm 0.39 \text{ ml}\cdot\text{min}^{-1}\cdot(100\text{g})^{-1}$, $0.26 \pm 0.09 \text{ ml}\cdot\text{min}^{-1}\cdot(100\text{g})^{-1}$, $0.38 \pm 0.26 \text{ ml}\cdot\text{min}^{-1}\cdot(100\text{g})^{-1}$ and $0.09 \pm 0.32 \text{ ml}\cdot\text{min}^{-1}\cdot(100\text{g})^{-1}$ for 1) Spot Sign defects only (9 foci), 2) PCL defects only (9 foci), 3) hematoma excluding extravasation, 4) regions contralateral to extravasation, 5) hematoma in patients without extravasation and 6) an area contralateral to (5). PS values from Spot Sign defects and PCL defects were significantly different from each other and all other regions of interest ($p < 0.05$; Table 6.2). Average absolute or percent hematoma volume increased from $34.1 \pm 41.0 \text{ ml}$ to $40.2 \pm 46.1 \text{ ml}$ or 27.8% in contrast extravasation positive patients. In extravasation negative patients absolute or percent volume decreased from $19.8 \pm 31.8 \text{ ml}$ to $17.4 \pm 27.3 \text{ ml}$, or -1.5% (Table 6.3).

Table 6.2 PS values for extravasation positive and negative patients

	Extravasation Positive				Extravasation Negative	
	Spot Sign lesions (9 foci)	PCL lesions (9 foci)	Hematoma w/o extravasation	Contralateral to extravasation ROI	Hematoma ROI	Contralateral ROI
Mean PS	6.5±1.6*	0.95±0.39*	0.12±0.39	0.26±0.09	0.38 ± 0.26	0.09±0.32
Median PS	6.69	0.87	0.15	0.29	0.42	0.07
Interquartile range	5.31 - 7.36	0.67 - 0.98	0.06 - 0.34	0.25 - 0.31	0.14 - 0.59	0.03 - 0.40

Permeability surface area product (PS) values ($\text{ml}\cdot\text{min}^{-1}\cdot(100\text{g})^{-1}$) for patients with ($n = 7$) and without ($n = 9$) contrast extravasation. Sub-groups are based on region of interest location. Wilcoxon rank-sum tests with bonferroni-correction were used to compare data.

*Denotes significantly different ($p < 0.05$) from all other sub-group mean PS values.

Table 6.3 Hematoma expansion data for extravasation positive/negative patients

	Initial volume, cm ³	Final volume, cm ³	Volume change, cm ³	Volume change, %	P value
Extravasation Positive	34.10 ± 41.00	40.24 ± 46.15	5.68 ± 13.45	27.84 ± 74.70	0.86
Extravasation Negative	19.89 ± 31.86	17.47 ± 27.31	-2.42 ± 4.70	-1.56 ± 35.23	0.95

Patients are dichotomized into contrast extravasation positive (n = 7) and negative groups (n = 9). Initial and final hematoma volumes were measured at admission and 24 hours, respectively. Wilcoxon rank-sum tests, with a bonferroni-correction, were used to compare initial and final hematoma volumes within both groups, respectively.

6.4 DISCUSSION

Early CT contrast extravasation [CTA Spot Sign and post contrast-leakage (PCL)] is an important predictor for ICH evolution^{10, 12, 14, 15}. Size and density of contrast on admission CTA reflect the rate of contrast accumulation and have recently been shown to be two of three factors associated with hematoma expansion and patient outcome¹⁵. This study utilizes CTP-derived PS measures to quantify the differential rates of contrast leakage in contrast extravasation abnormalities observed on admission CTA or PCCT. A technique such as CTP that quantifies contrast leakage rate may better define which patients with extravasation are at highest risk for expansion. Hematoma volume expansion occurred more frequently in patients with extravasation, who also tended to have worse clinical outcome.

Although the pathophysiological significance of the CTA Spot Sign and PCCT-PCL defect is uncertain, we have previously suggested that the former may represent the primary causative abnormality, whereas the latter may represent secondary vessel injury due to hematoma shearing²⁴. Although PCL appears to be significant for hematoma growth compared to patients with no extravasation, a recent study showed that 40% of patients with only the PCL defect did not demonstrate hematoma expansion¹⁴. As such, the clinical effect of PCL appears overshadowed by the presence of the CTA Spot Sign where only 4% of Spot Sign positive patients did not undergo hematoma expansion¹³.

The rate of contrast extravasation is an important consideration when assessing the sensitivity of modalities being used. Slower rates of contrast accumulation will be more difficult to detect with early scan techniques if insufficient contrast density has accumulated. Two recent studies reported higher rates of extravasation detection using a

delayed CTA acquisition (median 113 seconds delay following initial CTA) or PCCT (typically performed 3-5 minutes following contrast injection)^{14, 15}. Herein, the detection of 9 extravasation defects on PCCT, not present on early CTA, is consistent with these accounts. Importantly, however, all PCL defects could be visualized as increased PS on post processed CTP functional maps. By virtue of a dynamic acquisition lasting 2 minutes after contrast injection, CTP appears more sensitive in assessing different contrast leakage rates than either CTA or PCCT; however this remains to be confirmed in a larger clinical study. CTP has the advantage of not requiring a pre-contrast decision between early and late scanning. Further, the overall dose of CTP is similar to a NCCT and avoids radiosensitive structures such as the thyroid and orbits.

Quantification of the rate of leakage provides a unique opportunity to objectively study the effect of the rate of contrast extravasation on hematoma expansion for which the CTA Spot Sign is currently a surrogate marker. The high PS values obtained in patients with the CTA Spot Sign emphasize the rapid rate of contrast extravasation, reinforcing the need for a rapid and efficient treatment. Herein, we calculated PS with the Johnson-Wilson (J-W) distributed parameter model which accounts for: 1) the ‘gradual’ leakage of contrast as it travels from the arterial input to the venous output and 2) the clearance (backflux) of contrast from the interstitial space into the vascular space. Another tracer kinetic model for the calculation of PS is the Patlak model which, unlike the J-W model, uses compartments to represent the vascular and interstitial spaces²⁵. Therefore, it is required that both contrast arrival and leakage through the brain vasculature are instantaneous, as opposed to gradual, finite transit. Thus, the Patlak model is not valid under conditions when the arterial contrast concentration is changing rapidly, as seen during the vascular (first) phase of our data acquisition. This is exemplified by the initial

region of non-linearity observed in the Patlak plot, when the first pass data is included²⁶. Whereas the J-W model can be used to measure PS, CBV and CBF simultaneously, the Patlak model provides estimates of PS and CBV but not CBF, which has to be estimated separately by using another calculation/model²⁵. The Patlak model also assumes that there is no clearance (backflux) of contrast from the interstitial space into the vascular space. As a result, PS measured with the J-W model, which accounts for backflux, will be higher than that derived from the Patlak model.

Several limitations of this study need to be discussed. First, the case series is limited by a small sample size. For practical reasons, patients were recruited by supervising neuroradiologists during daytime admissions. Although difficult to achieve given the relatively low incidence of ICH admissions and lower incidence of contrast extravasation, these results will require validation from larger patient cohorts. The influence of systemic and local features such as blood pressure, hematoma location, mass effect and shift, respectively, on the rate of extravasation and hematoma growth is currently unknown limiting the prediction of potential hematoma volume. Also, because the CTA, PCCT and CTP imaging are separated by ~10-15 minutes, PS could conceivably change between sequences. The effect of time to scan on presence of extravasation is not yet fully understood. Patients with extravasation in this series demonstrated a non- significant increased time to scan. Conceivably, increased duration from ictus may result in greater opportunity for BBB disruption, re-bleeding and contrast extravasation; however, a retrospective series evaluating a longer time to scan interval in patients with ICH reported a non- significant trend to lower incidence for expansion beyond 3 hours¹⁰. Similarly a prospective ICH study of 268 patients demonstrated no difference in spot sign incidence within the first 3 hours (personal communication: Dr.

Andrew Demchuck). Due to the concurrence of PCCT- PCL and CTA Spot Sign in some patients, we were unable to compare hematoma expansion in patients possessing solely PCL or Spot Sign; within the same hematoma, the interaction of different coexisting patterns of extravasation is uncertain. Finally, PS may be underestimated in the presence of higher BBB disruption where increased amounts of blood, with lower Hounsfield unit than CT contrast, can leak into the extravascular space during the CTP acquisition.

6.5 CONCLUSION

In conclusion, the CTP-PS parameter measures different rates of CT contrast extravasation for ICH patients with/without CTA-Spot Sign and/or PCL defects. This information could be used to guide hemostatic treatment during the acute stroke stage.

6.6 REFERENCES

1. Broderick JP, Brott TG, Tomsick T, Barsan W, Spilker J. Ultra-early evaluation of intracerebral hemorrhage. *Journal of neurosurgery*. 1990;72:195-199
2. Kazui S, Naritomi H, Yamamoto H, Sawada T, Yamaguchi T. Enlargement of spontaneous intracerebral hemorrhage. Incidence and time course. *Stroke; a journal of cerebral circulation*. 1996;27:1783-1787
3. Fujii Y, Takeuchi S, Sasaki O, Minakawa T, Tanaka R. Multivariate analysis of predictors of hematoma enlargement in spontaneous intracerebral hemorrhage. *Stroke; a journal of cerebral circulation*. 1998;29:1160-1166
4. Brott T, Broderick J, Kothari R, Barsan W, Tomsick T, Sauerbeck L, et al. Early hemorrhage growth in patients with intracerebral hemorrhage. *Stroke; a journal of cerebral circulation*. 1997;28:1-5
5. Broderick JP, Brott TG, Duldner JE, Tomsick T, Huster G. Volume of intracerebral hemorrhage. A powerful and easy-to-use predictor of 30-day mortality. *Stroke; a journal of cerebral circulation*. 1993;24:987-993
6. Kidwell CS, Saver JL, Mattiello J, Warach S, Liebeskind DS, Starkman S, et al. Diffusion-perfusion mr evaluation of perihematomal injury in hyperacute intracerebral hemorrhage. *Neurology*. 2001;57:1611-1617
7. Mayer SA, Brun NC, Begtrup K, Broderick J, Davis S, Diringer MN, et al. Efficacy and safety of recombinant activated factor vii for acute intracerebral hemorrhage. *The New England journal of medicine*. 2008;358:2127-2137
8. Mayer SA, Davis SM, Skolnick BE, Brun NC, Begtrup K, Broderick JP, et al. Can a subset of intracerebral hemorrhage patients benefit from hemostatic therapy with recombinant activated factor vii? *Stroke; a journal of cerebral circulation*. 2009;40:833-840
9. Becker KJ, Baxter AB, Bybee HM, Tirschwell DL, Abouelsaad T, Cohen WA. Extravasation of radiographic contrast is an independent predictor of death in primary intracerebral hemorrhage. *Stroke; a journal of cerebral circulation*. 1999;30:2025-2032
10. Goldstein JN, Fazen LE, Snider R, Schwab K, Greenberg SM, Smith EE, et al. Contrast extravasation on ct angiography predicts hematoma expansion in intracerebral hemorrhage. *Neurology*. 2007;68:889-894
11. Wada R, Aviv RI, Fox AJ, Sahlas DJ, Gladstone DJ, Tomlinson G, et al. Ct angiography "spot sign" predicts hematoma expansion in acute intracerebral hemorrhage. *Stroke; a journal of cerebral circulation*. 2007;38:1257-1262
12. Kim J, Smith A, Hemphill JC, 3rd, Smith WS, Lu Y, Dillon WP, et al. Contrast extravasation on ct predicts mortality in primary intracerebral hemorrhage. *AJNR. American journal of neuroradiology*. 2008;29:520-525

13. Delgado Almandoz JE, Yoo AJ, Stone MJ, Schaefer PW, Oleinik A, Brouwers HB, et al. The spot sign score in primary intracerebral hemorrhage identifies patients at highest risk of in-hospital mortality and poor outcome among survivors. *Stroke; a journal of cerebral circulation*. 2009;40:54-60
14. Ederies A, Demchuk A, Chia T, Gladstone DJ, Dowlatshahi D, Bendavit G, et al. Postcontrast ct extravasation is associated with hematoma expansion in cta spot negative patients. *Stroke; a journal of cerebral circulation*. 2009;40:1672-1676
15. Delgado Almandoz JE, Yoo AJ, Stone MJ, Schaefer PW, Goldstein JN, Rosand J, et al. Systematic characterization of the computed tomography angiography spot sign in primary intracerebral hemorrhage identifies patients at highest risk for hematoma expansion: The spot sign score. *Stroke; a journal of cerebral circulation*. 2009;40:2994-3000
16. St Lawrence KS, Lee TY. An adiabatic approximation to the tissue homogeneity model for water exchange in the brain: II. Experimental validation. *Journal of cerebral blood flow and metabolism : official journal of the International Society of Cerebral Blood Flow and Metabolism*. 1998;18:1378-1385
17. Connor CW, Hynynen K. Patterns of thermal deposition in the skull during transcranial focused ultrasound surgery. *IEEE transactions on bio-medical engineering*. 2004;51:1693-1706
18. Cenic A, Nabavi DG, Craen RA, Gelb AW, Lee TY. Dynamic ct measurement of cerebral blood flow: A validation study. *AJNR. American journal of neuroradiology*. 1999;20:63-73
19. Lee TY, Purdie TG, Stewart E. Ct imaging of angiogenesis. *Q J Nucl Med*. 2003;47:171-187
20. St Lawrence KS, Lee TY. An adiabatic approximation to the tissue homogeneity model for water exchange in the brain: I. Theoretical derivation. *Journal of cerebral blood flow and metabolism : official journal of the International Society of Cerebral Blood Flow and Metabolism*. 1998;18:1365-1377
21. Aviv RI, d'Esterre CD, Murphy BD, Hopyan JJ, Buck B, Mallia G, et al. Hemorrhagic transformation of ischemic stroke: Prediction with ct perfusion. *Radiology*. 2009;250:867-877
22. Kudo K, Terae S, Katoh C, Oka M, Shiga T, Tamaki N, et al. Quantitative cerebral blood flow measurement with dynamic perfusion ct using the vascular-pixel elimination method: Comparison with h2(15)o positron emission tomography. *AJNR. American journal of neuroradiology*. 2003;24:419-426
23. Chang EF, Meeker M, Holland MC. Acute traumatic intraparenchymal hemorrhage: Risk factors for progression in the early post-injury period. *Neurosurgery*. 2007;61:222-230

24. Thompson AL, Kosior JC, Gladstone DJ, Hopyan JJ, Symons SP, Romero F, et al. Defining the ct angiography 'spot sign' in primary intracerebral hemorrhage. *The Canadian journal of neurological sciences. Le journal canadien des sciences neurologiques*. 2009;36:456-461
25. Lin K, Kazmi KS, Law M, Babb J, Peccerelli N, Pramanik BK. Measuring elevated microvascular permeability and predicting hemorrhagic transformation in acute ischemic stroke using first-pass dynamic perfusion ct imaging. *AJNR. American journal of neuroradiology*. 2007;28:1292-1298
26. Dankbaar JW, Hom J, Schneider T, Cheng SC, Lau BC, van der Schaaf I, et al. Dynamic perfusion ct assessment of the blood-brain barrier permeability: First pass versus delayed acquisition. *AJNR. American journal of neuroradiology*. 2008;29:1671-1676

CHAPTER 7

Development and Implementation of a Rabbit Model of Middle Cerebral Artery Embolic Occlusion: Pre-morbid Cerebrovascular Conditioning with Dipyridamole

The contents of this chapter have been adapted from the paper entitled “Dipyridamole treatment prior to stroke onset: examining post-stroke cerebral circulation and outcome in rabbits”, published in *Translational Stroke Research*, 2011;2:186-194, by C.D. d’Esterre, K.M. Tichauer, R.I. Aviv, L. Morrison, W. Eisert, T.Y.

7.1 INTRODUCTION

Clinical outcome following embolic stroke depends on a timely maintenance of the ischemic penumbra through endogenous regulation and exogenous intervention. Primary stroke treatment with intravenous tissue plasminogen activator is the most widespread method of restoring blood flow to the ischemic defect; however, it is an aggressive approach that can lead to undesirable complications, primarily hemorrhagic transformation¹. For this reason, there is much interest in uncovering novel methods for cerebrovascular conditioning before stroke onset.

Clinical trials have suggested a combination of extended-release dipyridamole (DIP) and low dose aspirin, both antithrombotic drugs which limit platelet activation, as a cornerstone for reducing stroke incidence in high-risk patients². In addition to its antithrombotic ability, DIP offers many pleiotropic, neuroprotective properties and has a lower propensity for bleeding when compared to aspirin^{3, 4}. DIP conditioning may

ameliorate the effects of stroke, if it were to occur; however, clinical observations are conflicting regarding this issue⁵⁻⁷. Therefore a multi-modal experiment is warranted to verify the possible neuroprotective benefit of pre-stroke DIP administration.

Pre-clinical animal models of focal ischemia are imperative to evaluate vascular changes and outcome throughout the acute ischemic stroke (AIS) setting. Animal models have notable advantages over clinical studies: 1) in animals, final infarct volume from brain tissue staining can be delineated minutes after euthanasia, limiting infarct expansion into penumbral tissue, as opposed to imaging based final infarct delineation in humans; 2) when assessing drug efficacy in humans, inconsistent dosing and different baseline characteristics (ie. other medications and underlying vascular pathologies) can skew clinical results⁸. In comparison, controlled drug administration and baseline homogeneity can be achieved non-clinically; 3) Serial imaging is feasible with animal models, as radiation dose and/or potential toxicity from contrast is not an issue.

Large vessel mechanical- or filament-induced occlusions, thrombotic infusion and endothelin-1 induced vasoconstriction have been used successfully to create focal ischemic territories; however, these techniques do not completely simulate human AIS pathophysiology, posing a problem when establishing neuroprotective treatment efficacies. Thus, an AIS induction method which involves embolic occlusion of a large vessel, usually the middle cerebral artery (MCA), by an autologous blood clot is an appropriate model to investigate the pathophysiology related to thromboembolism. The most common thromboembolic MCA occlusion technique, first described in canines, involves injection of a fibrin rich autologous blood clot into the internal carotid artery (ICA) via a ligated external carotid artery (ECA) in rats^{9,10}. This technique has since been applied to rabbits who, unlike rats, have a complete Circle of Willis with anterior and

middle cerebral arteries arising from the ICA, similar to that in humans¹¹. The rabbit embolic large/small clot stroke models were first developed to investigate the effects of anticoagulants on cerebral perfusion and intracerebral hemorrhage¹². Since then, these model have been used reliably to examine the efficacy of several AIS treatment strategies, including one of the first studies to show benefits of tissue plasminogen activator (tPA) administration¹³⁻¹⁶. The models produce a homogeneous stroke, and clot placement is easily confirmed with hemodynamic measurements from computed tomography perfusion (CTP) or magnetic resonance imaging (MRI). Nonetheless, the ligation of the ECA and its branches may cause damage to muscles involved in mastication, causing accelerated weight loss and misinterpretation of neurological outcome¹⁷.

The purpose of this work was to 1) develop an improved, reproducible rabbit large clot embolic model (RLCEM) of focal cerebral ischemia, assessed with the CT perfusion (CTP) imaging modality, while maintaining adequate perfusion to extra-cranial structures, and 2) implement this modified RLCEM to examine the effect a common secondary stroke anti-thrombotic treatment, dipyridamole, on stroke severity.

7.2 MATERIALS & METHODS

7.2.1 *Surgical procedures*

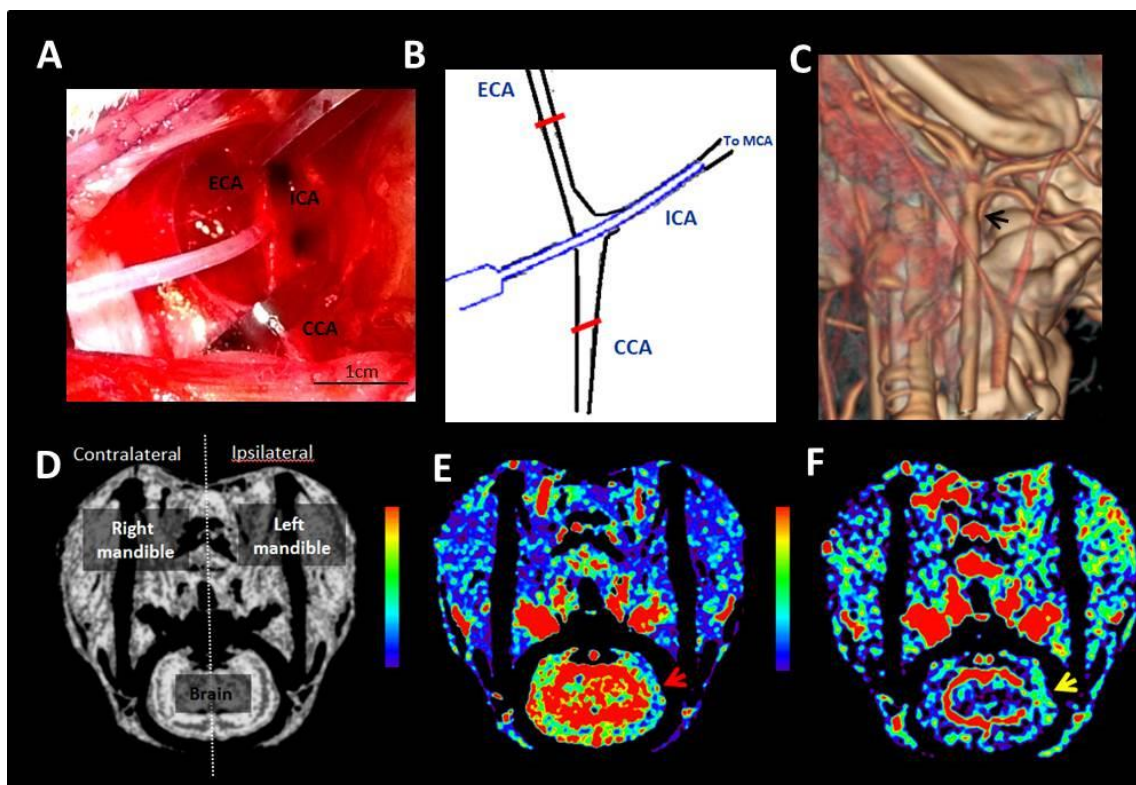
Study procedures were approved by our institutional review board⁺. Twenty male New Zealand white rabbits (2.7-3.6 kg) were randomized to either DIP treatment ($n=10$) or saline treatment ($n=10$). Seven days before stroke onset anesthesia was induced with 5% isoflurane, with subsequent 'pedal reflex' to test for deep pain response. Close monitoring of CO₂ levels and 'pedal reflex' response throughout the entire experiment ensured the animal was properly anesthetized. A cannula was inserted into a saphenous vein, and a single bolus of ketamine/diazepam (3mg/kg, 0.3mg/kg) was administered to maintain anaesthesia during intubation. Subsequently the rabbit was ventilated with 4% isoflurane. The right jugular vein was exposed, tied off and catheterized at 2cm proximal to the heart. The opposite end of the catheter was fed subcutaneously to a battery-powered infusion pump (Med-e-cell, San Diego, CA), fixed behind the head. Pumps were filled with either 5mg/ml pharmaceutical grade DIP (Pharmaceutical Partners Canada, Richmond Hill, ON) or 9mg/ml sterile saline. The infusion was continued for 7 days at 0.08ml•h⁻¹. At 4 and 7 days after insertion of the infusion pump, blood was collected from an ear-artery to determine the plasma concentration of DIP spectrofluorometrically (F-7000, Hitachi High Technologies America, Inc., Santa Clara, CA). Samples were excited with light at a wavelength of 420 nm and fluorescence spectra were recorded in the range of wavelengths from 430-660 nm and compared to standard calibration solutions. The calibration solution was made by dissolving 1 mg of DP into 20 ml of alcohol with subsequent dilution to 100 ml with water¹⁸. Sodium hydroxide solution was added as

⁺Appendix H – Animal Ethics Approval Form

necessary to achieve a physiological pH (Microprocessor pH meter, Hanna Instruments, Ann Arbor, MI).

On the last day of treatment, the left internal carotid artery (ICA) was exposed under 5% isoflurane and tied off at the common carotid bifurcation. An 18 gauge catheter was advanced 1.5cm into the ICA, at which time a baseline CTP scan was acquired under 3% isoflurane. Autologous arterial blood was used to fill 3 thrombin-coated capillary tubes (Thrombostat; Sigma-Aldrich, St Louis, Mo). A 3 mm autologous arterial blood clot was then injected into the left ICA with 2.5ml of saline ¹¹. The catheter was removed and ICA was repaired with 8-0 suture. Microvascular clips were removed and reperfusion was observed in within ICA, ECA and common carotid arteries (Figure 7.1).

Figure 7.1 Methodology for blood clot induction with extracranial perfusion preservation



Gross anatomy (A) and diagram of left common carotid artery (CCA), external carotid artery (ECA), and internal carotid artery (ICA). (B) An 18-gauge catheter was placed into the ICA via an incision in the CCA, for injection of an autologous blood clot into the middle cerebral artery (MCA). After injection, the catheter was removed and the incision was repaired to allow reperfusion of the CCA, ECA and ICA. A small stenosis (black arrow) is observed on the contrast enhanced CT angiography 3D rendered image in (C), which confirmed reperfusion of these major arteries. Coronal slices of perfusion weighted image (D) describing anatomical regions, with corresponding CBF (E), and CBV (F) functional maps. An ischemic defect (red arrow) with hypervolemia (yellow arrow), a CBF/CBV mismatch, is present within the left hemisphere, while complete reperfusion of extracranial vessels is observed. CTP images are coloured according to a rainbow colour scale with red and purple representing high and low values, respectively: CBF, $0\text{-}180\text{ ml}\cdot\text{min}^{-1}\cdot(100\text{g})^{-1}$; CBV, $0\text{-}10\text{ ml}\cdot(100\text{g})^{-1}$.

Additional CTP scans were acquired at 10 and 30 minutes after embolization under 3% isoflurane. Animals were then recovered with fentanyl (12.5 mcg patch) and buprenorphine (0.1ml/kg) and monitored until stable. CTP scans under 3% isoflurane were repeated at 1, 4, 7, 14, 21, and 28 days post-embolization if possible (some animals were sacrificed prior to the end day due to severe neurological deficits). Neurological testing was done on each scanning day blinded to the treatment of the animal¹⁹. During CTP scanning, rectal temperature was maintained between 37°C and 39°C and arterial blood pH, partial pressures of O₂ and CO₂, and mean arterial pressure were monitored. Animals were euthanized with potassium chloride injection either on day 28 post or when the animal was assessed a neurological score greater than 15 (see Neurological Testing section)¹⁹. Following sacrifice, the brain was removed to locate the embolus, and sectioned for histology.

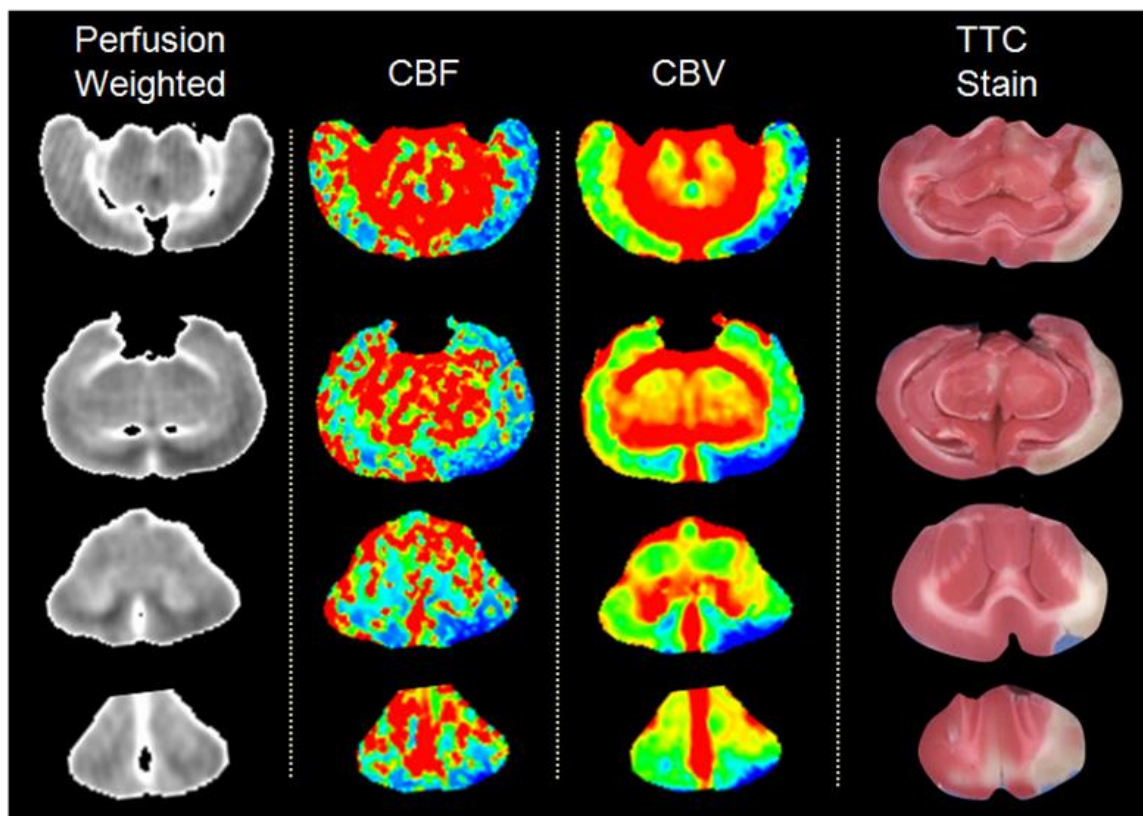
7.2.2 CT perfusion imaging

Each CTP scan was performed with a Lightspeed Plus 4 section CT scanner (GE Healthcare, Waukesha, WI). A preliminary axial CT scan was used to localize four 5 mm-thick slices in the supply territories of the middle cerebral arteries¹¹. Next, a 5ml bolus of 300mg·ml⁻¹ non-ionic, iodinated contrast (Omnipaque, GE Healthcare, Mississauga, Ontario) was injected into a saphenous vein at 0.5 ml·s⁻¹. The head was continuously scanned for 50 seconds using 80kVp, 80mA and 1s rotation period. From the acquired data, 512 x 512 images were reconstructed at 0.5 second intervals.

7.2.3 CTP data analysis

Each CTP study was analyzed by one author for consistency using commercially available CT perfusion software (version 4, GE Healthcare, Milwaukee, Wis; Figure 7.2). For each CTP imaging data set, time density curves (TDC) for the arterial input function (AIF) and venous output functions (VOF) were obtained from the anterior cerebral artery and superior sagittal sinus, respectively. Partial volume averaging of the AIF was corrected using the VOF-TDC. Perfusion weighted maps were created by averaging the cine CT perfusion images over the duration of the first pass of contrast. Parametric maps of cerebral blood flow (CBF; $\text{ml}\cdot\text{min}^{-1}\cdot 100\text{g}^{-1}$) and cerebral blood volume (CBV; $\text{ml}\cdot 100\text{g}^{-1}$) were calculated by deconvolution of tissue TDCs and the AIF. This hemodynamic functional map calculation method has been described previously²⁰. Functional maps were further analysed by custom software developed in our lab using IDL v6.2 (ITT Visual Information Solutions, Boulder, CO). For each slice, regions of interest (ROIs) were manually traced around the ipsilateral and contralateral hemispheres using the perfusion weighted functional map, and superimposed onto hemodynamic maps. For each ROI, mean CBF and CBV were also determined within the ipsilateral and contralateral hemispheres following exclusion of pixels with a $\text{CBF} > 100 \text{ ml}\cdot\text{min}^{-1}\cdot(100\text{g})^{-1}$ or $\text{CBV} > 8 \text{ ml}\cdot(100\text{g})^{-1}$ - a technique used to eliminate large vessel hemodynamic values, focusing on parenchymal perfusion²¹.

Figure 7.2 A typical CT perfusion study and corresponding excised brain slices.



Four contiguous, coronal CTP-derived functional maps acquired 30 minutes post stroke for a saline-treated animal. Infarct region (white) on TTC stained excised brain slices, analysed at 7 days post stroke, corresponds to the initial ischemic defect shown on the CBF [$\text{ml}\cdot\text{min}^{-1}\cdot(100\text{g}^{-1})$] and CBV [$\text{ml}\cdot(100\text{g}^{-1})$] maps. Within tissue that is destined to infarct, CBV in various regions is still within the normal physiological range. CTP images are coloured according to a rainbow colour scale with red and blue representing high and low values, respectively: CBF, 0-180 $\text{ml}\cdot\text{min}^{-1}\cdot(100\text{g}^{-1})$; CBV, 0-10 $\text{ml}\cdot(100\text{g}^{-1})$

7.2.4 Neurological testing

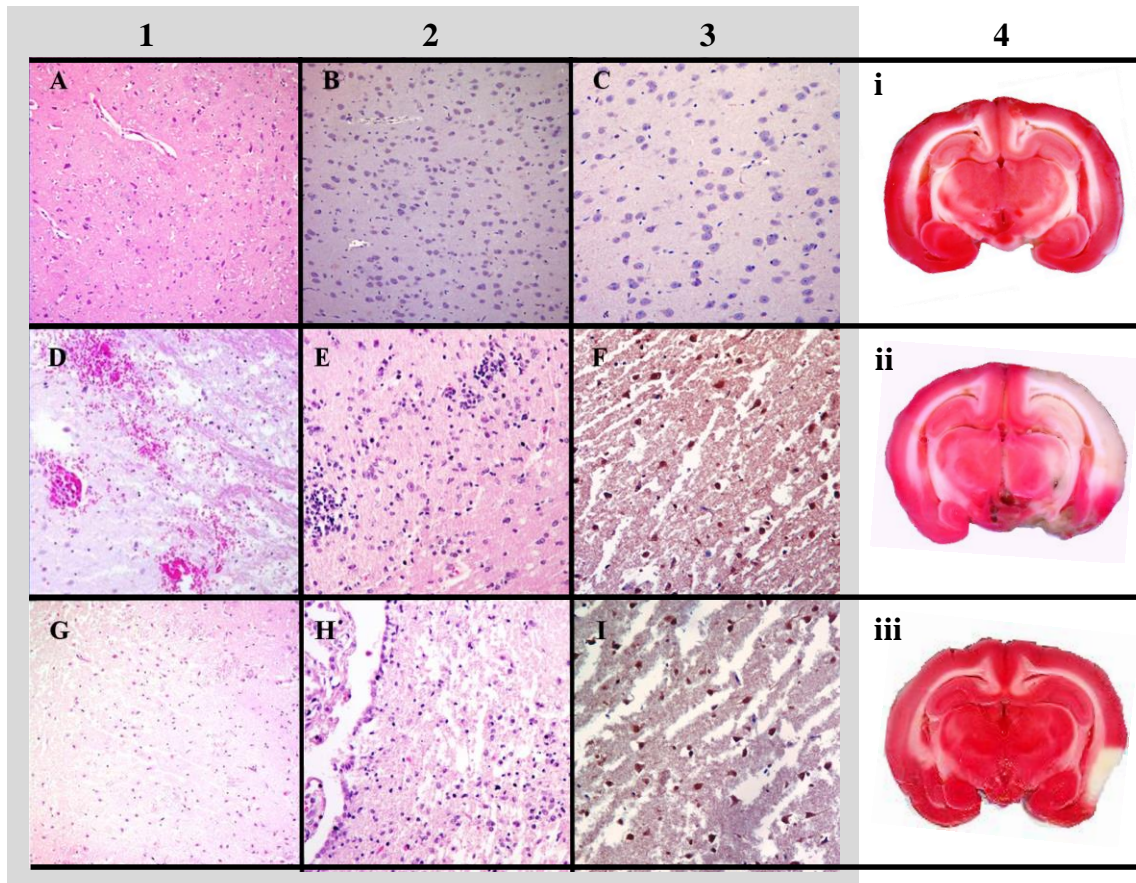
One blinded individual performed all neurological assessments. Spontaneous behaviour, reaction to handling, posture, gait, limb hypertonia, righting reflexes, limb reflexes, and feeding behaviour were scored separately: 0, normal; 1, mild; 2, moderate; and 3, severely impaired, and all scores summed, and averaged for each group¹⁹.

7.2.5 Post-mortem analysis

Brain tissue from up to one week post stroke onset was analysed histopathologically (Figure 7.3). Minutes after brain excision, brain tissue was cut into coronal sections corresponding to the CT scan slice locations and stained with 2,3,5-tetrazolium chloride (TTC) to quantify the extent of infarcted tissue – the entire brain was used for this quantification. Additionally, presence, location, and length of emboli were noted. Brain tissue was fixed in 10% buffered paraformaldehyde solution for 24 hours, then stored in Dulbecco's phosphate buffered saline (1X) for future histopathological staining. Regions of interest from three tissue types were selected from: i) within the TTC-defined infarct, ii) 1.5 mm from the TTC-defined infarct volume (peri-infarct penumbral region), and iii) normal tissue contralateral to the infarct. These tissue fragments were embedded in paraffin, cut into 5µm thick sections and stained (H&E) to quantify hemorrhage; to determine the extent of peri-infarct inflammation with leukocyte quantification; and to quantify the extent of peri-infarct apoptosis with caspase-3 staining. All quantification was performed by a single individual in a blinded manner. To quantify hemorrhage, each section was analysed at a magnification of 100x for the number of visible areas of extravascular red blood cells. One and two points were given for each localized and

confluent area, respectively, to a maximum of 10 (most severe). Scored sections were averaged and used to give an average hemorrhage score for each group. Apoptosis quantification was done using an apoptotic index (AI). Sections at 400x magnification were used to create digital images, on which apoptotic cells were manually counted, using point counting. The AI was calculated, using the entire field of view, as: the total number of apoptotic cells / the total number of nuclei. To quantify inflammation, 3 random 2mm² areas were chosen for each tissue type, from each section. Each area was given a score based on the following criteria: 0 = minimal leukocyte infiltration, 1 = mild, 2 = moderate, and 3 = severe. An average leukocyte infiltration score was calculated from all sections for each group.

Figure 7.3 Examples of histology



Histopathological staining of healthy tissue (A-C), and infarcted tissue from DIP- (D-F) and saline-treated (G-I) animals. Column 1, 2, and 3 show hemorrhage (100x magnification), leukocyte infiltration (200x magnification), and caspase-3 staining (400x magnification), respectively. Column 4 shows excised brain slices for i) normal brain (no stroke), ii) saline- and iii) DIP-treated animals.

7.2.6 Statistical Analysis

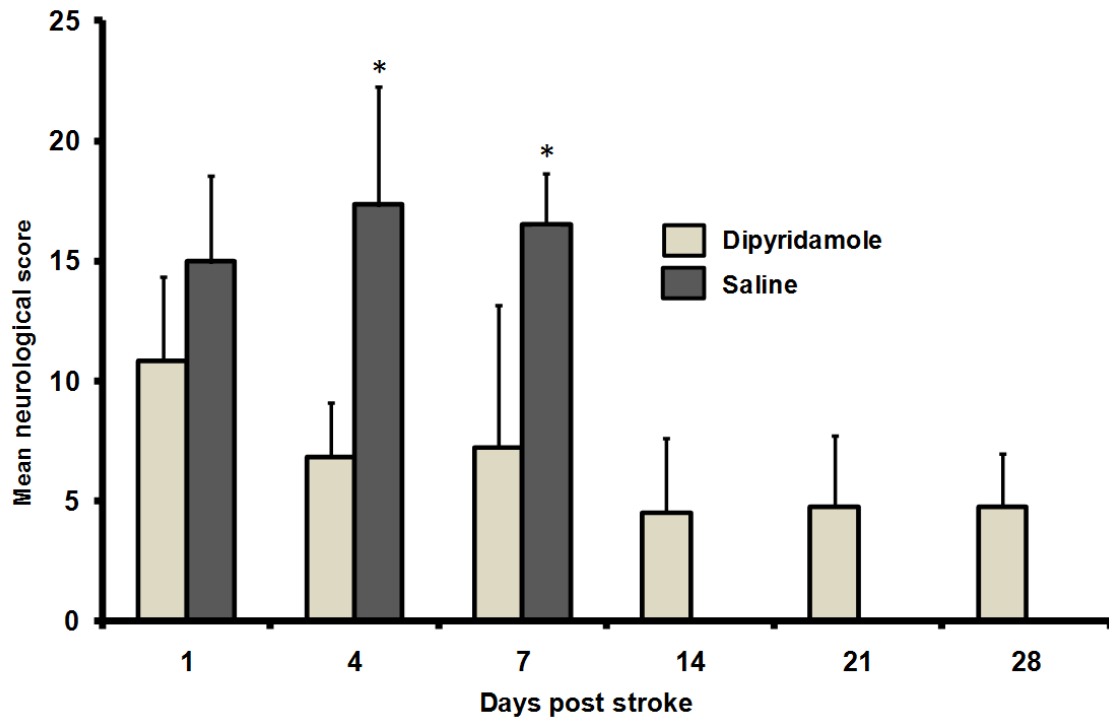
The statistical package, SPSS 15.0 (SPSS Inc., Chicago, IL), was used for all analyses. Differences were considered significant at $p < 0.05$. Repeated measures analysis of variance was used as an omnibus test to identify significant differences between the DIP- and saline- treated groups for all physiological parameters, data collected from CTP imaging, and neurological scoring. Differences in mortality were analysed using Fisher exact test. Mann-Whitney, non-parametric comparison was used to analyse all histopathological data. Linear regression was used to determine the relationship between CTP-defined ischemic defects at time of sacrifice and excised brain infarct volumes for each animal.

7.3 RESULTS

Twelve of the twenty animals studied were included in the results (6 DIP, 6 saline; average weight: 3.1 ± 0.3 kg). Animals were excluded from the study if there were problems in the embolization procedure, or if blood plasma DIP concentrations were not therapeutic ($< 1 \mu\text{g/ml}$ plasma)²². No differences were observed between the physiological parameters of the treated and non-treated groups on any scan day. At 10 minutes post-embolization, mean arterial pressure (MAP) in both groups increased significantly from their respective baseline values ($p < 0.05$); for the remainder of the experiment, average MAP of both groups returned to baseline levels. At 28 days post embolization, 66% of the DIP-treated animals survived compared to 0% of the saline-treated. All saline-treated animals had to be sacrificed on or before day 7 post-

embolization due to severe neurological deficit. The survival times between the groups were significantly different ($p < 0.05$).

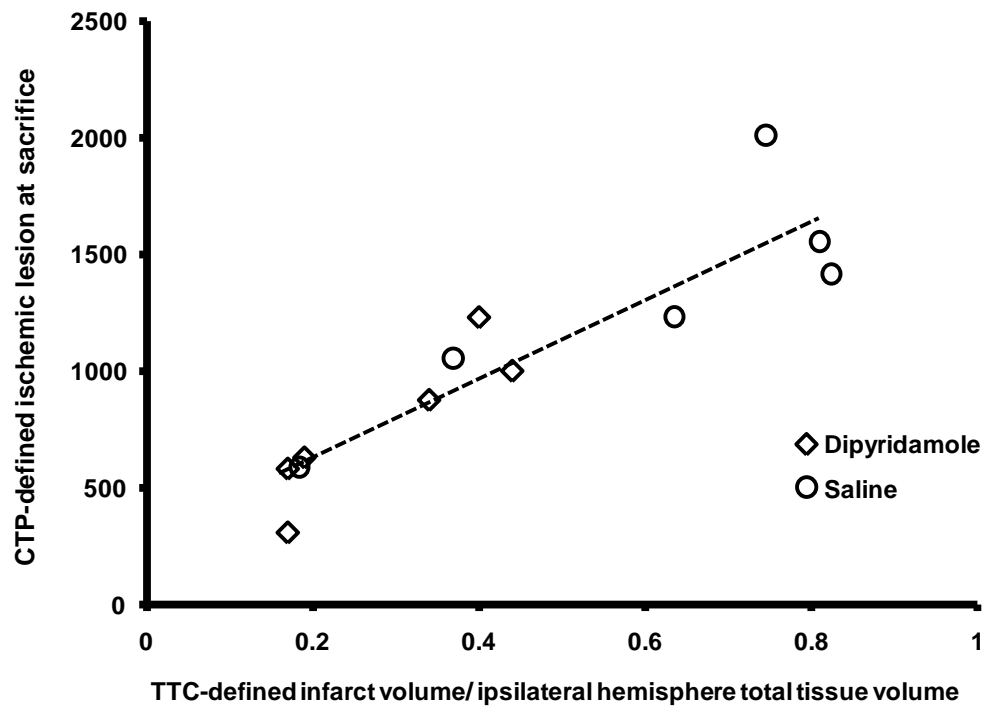
Figure 7.4 compares mean neurological scores collected from DIP- and saline-treated animals before each CTP scan. On days 4 and 7, the average neurological score of the DIP group was significantly lower than the saline-treated ($p < 0.05$). On days 14, 21, and 28, the average neurological score of the DIP-treated group dropped to below 5 and was significantly less than one day post stroke ($p < 0.05$).

Figure 7.4 Neurological Scoring

Mean neurological scores (mean+SD) for dipyridamole- and saline-treated groups. Significant differences were observed between groups on days 4 and 7 ($*p < 0.05$).

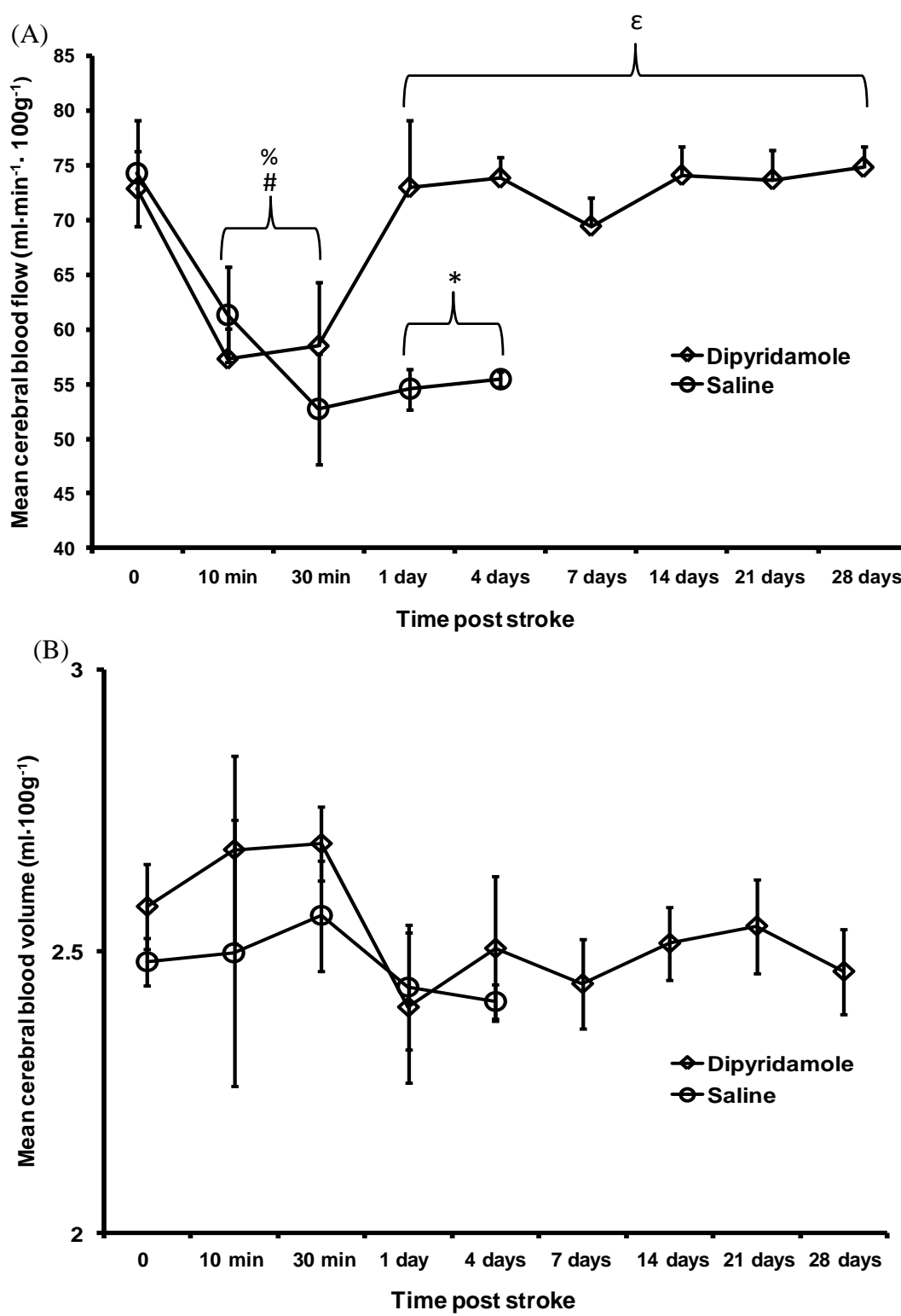
Cerebral emboli were found in 3 of 6 DIP-treated animals and 4 of 6 saline-treated animals. Average length of emboli in DIP and saline treated groups were 1.6 ± 0.5 and 2.3 ± 0.2 mm, respectively. The average percent volumes of infarcted tissue in the hemisphere ipsilateral to the stroke were $31 \pm 7\%$ and $69 \pm 10\%$ for the DIP- and saline-treated groups, respectively ($p < 0.05$).

Average baseline CBF values for both DIP- and saline-treated groups were 72.9 ± 3.6 and 74.32 ± 4.9 $\text{ml}\cdot\text{min}^{-1}\cdot(100\text{g})^{-1}$; these were within the normal CBF physiological range of $45\text{-}75$ $\text{ml}\cdot\text{min}^{-1}\cdot(100\text{g})^{-1}$, and similar to values previously reported in our group^{23, 24}. A significant decrease in average CBF was found at 10 and 30 minutes for both DIP- and saline-treated animals compared to their respective baseline values ($p < 0.05$). Comparing DIP- and saline-treated animals, average CBF was significantly different on days 1 and 4 ($p < 0.05$). For the DIP-treated group, values on days 4 to 28 were significantly higher than values at 10 and 30 minutes post embolus induction ($p < 0.05$). Contralateral hemisphere CBF, averaged over the entire study, for DIP- and saline-treated groups was 67 ± 5.2 and 69 ± 4.1 $\text{ml}\cdot\text{min}^{-1}\cdot(100\text{g})^{-1}$ ($p > 0.05$). There were no significant differences in average CBV within the ipsilateral hemisphere within or between groups throughout the study ($p > 0.05$). For both groups, CBV was slightly elevated at 10 and 30 minutes post stroke. The mean CBV for DIP- and saline-treated, averaged over the entire study was 2.5 ± 0.2 and 2.4 ± 0.2 $\text{ml}\cdot 100\text{g}^{-1}$ within ipsilateral hemisphere, and 2.4 ± 0.7 and 2.3 ± 0.4 $\text{ml}\cdot 100\text{g}^{-1}$ in the contralateral hemisphere, respectively. These values were slightly higher than CBV values previously obtained from our group using a microsphere technique²⁵.

Figure 7.5 CTP-defined ischemia versus TTC-defined infarction

CT perfusion-defined ischemic defect volume (number of pixels with $\text{CBF} < 25 \text{ ml} \cdot \text{min}^{-1} \cdot (100\text{g})^{-1}$ in $4 \times 5\text{-mm}$ slices¹¹) on the day of sacrifice versus the ratio of TTC-defined infarct volume/ ipsilateral hemisphere total tissue volume. A positive correlation was observed ($R^2 = 0.81$)

Figure 7.6 Ipsilateral CBF and CBV values

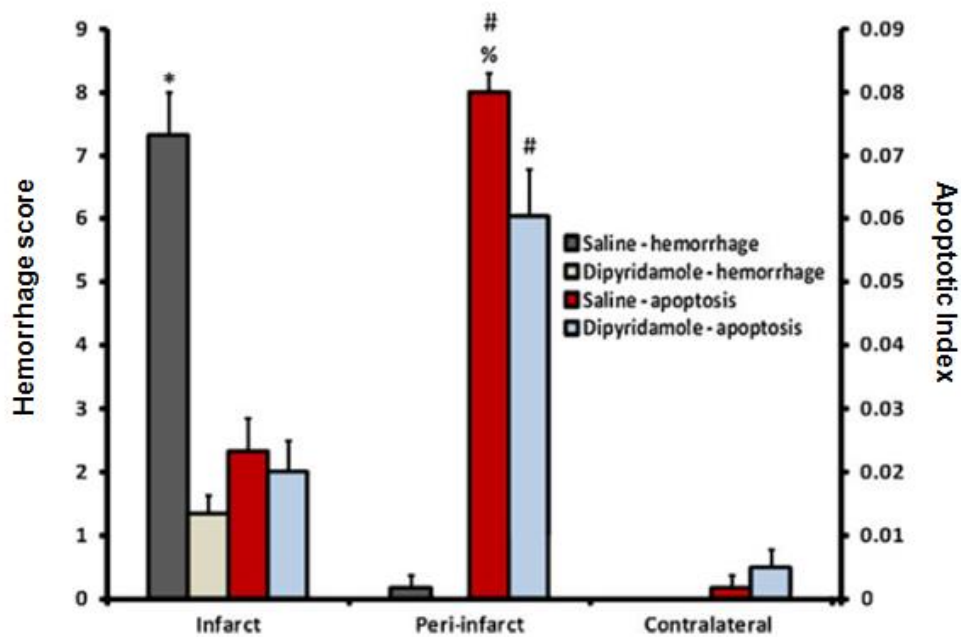


(A) Ipsilateral hemisphere mean CBF ($\text{ml}\cdot\text{min}^{-1}\cdot 100\text{g}^{-1}$). Significant differences ($p < 0.05$) were found at 10 and 30 minutes for both DIP treated (#) and saline treated (%) animals compared to their respective baseline values. Significant differences ($p < 0.05$) occurred between DIP- and saline-treated animals on days 1 and 4 (*). For the DIP-treated group, values on days 4 to 28 were significantly higher ($p < 0.05$) than values at 10 and 30 minutes post embolus (ϵ). (B) Ipsilateral hemisphere mean CBV [$\text{ml}\cdot(100\text{g})^{-1}$]. No significant differences were observed within or between time points for both groups ($p > 0.05$). CBV was slightly elevated at 10 and 30 minutes post stroke. All values are mean \pm standard deviation.

Figure 7.7 depicts the hemorrhage scores and apoptotic indices for infarct, peri-infarct and contralateral hemisphere brain tissue. Hemorrhagic infarction was 5 fold greater in saline-treated animals ($p < 0.05$). For both groups, hemorrhage was minimal in peri-infarct and contralateral tissue regions. For both groups, apoptosis was significantly higher in peri-infarct tissue, compared to infarct and contralateral regions ($p < 0.05$). Within peri-infarct tissue, apoptosis was elevated in saline-treated animals ($p < 0.05$).

Comparing DIP- and saline-treated groups, respectively, inflammatory scores (median [range]) for infarct, peri-infarct and contralateral tissue were: 2[1-3] and 2[2-3]; 2[1-2] and 2[1-2]; 0[0-1] and 0[0-1]. Inflammation was significantly lower in contralateral tissue for both groups ($p < 0.05$). Inflammation, within infarct and peri-infarct regions, was not significantly different within or between groups.

Figure 7.7 Hemorrhage and apoptosis indices



Hemorrhage scores and apoptotic indices for infarct, peri-infarct and contralateral hemisphere brain tissue for DIP- and saline treated animals. Hemorrhagic infarction was fivefold greater ($p < 0.05$) in saline-treated animals (asterisk). For both groups, apoptosis was significantly higher ($p < 0.05$) in peri-infarct tissue (number sign). Within the peri-infarct tissue, apoptosis was elevated ($p < 0.05$) in saline-treated animals (%). All values are mean + standard deviation

7.4 DISCUSSION

This study investigated how dipyridamole (DIP), an antithrombotic drug with antiplatelet (AP) properties, improves cerebral circulation and long-term outcome in a modified rabbit embolic stroke model. The model is an improvement on the RLCEM, allowing reperfusion to the extracranial vasculature. Cerebral hemodynamics were investigated using serial CTP imaging, neurological deficit was determined by repeated neurological testing, and excised brains were analysed with histopathological staining. Animals fared better when treated with a therapeutic dose of DIP before stroke onset: on average, they scored better neurologically, had more favourable cerebral hemodynamics 1 day after embolization, and smaller infarct volume as defined on TTC stained excised brains. Additionally, the DIP-treated group had lower incidence of hemorrhage, and were more likely to recanalize.

Activated platelets in the brain play a central role in accelerating the formation of thrombi, instigating progressive tissue injury²⁶. AP agents are routinely used as a stroke-prevention strategy for at-risk populations, especially post transient ischemic attack (TIA)²⁷. Even with AP therapy, 4–20% of patients with TIA will have a stroke within 90 days of the episode, half of those occurring within the first 48 hours²⁸. As such, exploring the potential of AP agents to minimize stroke severity is necessary. DIP has been shown to have numerous benefits, which could aid with vascular maintenance/recovery during an ischemic episode²⁹. DIP attenuates platelet aggregability through several mechanisms. DIP inhibits thromboxane synthase, limiting the conversion of prostaglandin to thromboxane, an inducer of platelet aggregation and vasoconstrictor^{30, 31}. Also, by limiting adenosine uptake into platelets, DIP initiates the buildup of intraplatelet cyclic

adenosine monophosphate (cAMP), blocking the platelet response to ADP²². Adenosine has also been shown to promote nitric oxide (NO) production by vascular endothelial cells³². NO is a potent vasodilator and inhibitor of platelet activation in its own right³³. The overall reduction in activated platelets limits both platelet/fibrinogen bridging and platelet plugging. These mechanisms may help conserve collateral flow to the ischemic tissue periphery, limiting infarct expansion into the penumbra. In this study, average ipsilateral CBF in the DIP-treated group returned to pre-stroke levels 24 hours post embolus induction. This hemodynamic recovery could be attributed to platelet effects, but may also result from an increase in circulating plasmin - DIP has been shown to promote plasminogen activator release by endothelial cells, which would encourage fibrinolysis of the induced blood clot³⁴. On that note, DIP-treated animals had a relative reduction in clot size within excised brains compared to the saline-treated counterparts. Still, it is not known whether portions of the clot broke off to create downstream microemboli, or the fibrin mesh was disentangled by way of plasmin interaction.

Interestingly, an increased propensity to hemorrhage, which may be expected with the use of antithrombotic therapy, was not observed in the DIP-treated animals. This result is supported by the European Stroke Prevention Study (ESPS-2), which showed no increases in bleeding with the addition of DIP to aspirin treatment compared to aspirin alone². In fact, we showed minimal hemorrhagic infarction in DIP-treated animals. Although not measured in this study, DIP can decrease the expression of matrix-metalloproteinase-9 (MMP-9), an enzyme implicated in blood brain barrier (BBB) breakdown and inflammation³⁵. An increase in reactive oxygen species, especially during ischemia, is also a major culprit of BBB dysfunction; when ROS concentrations get too high, apoptosis is triggered^{36, 37}. DIP can potentially minimize neuronal damage caused

by reactive oxygen species (ROS) through prevention of membrane lipid peroxidation, and by stimulating the vessel wall's ROS scavenging capability^{38, 39}. As such, the DIP ROS scavenging ability could decrease ROS-induced apoptosis throughout the ischemic defect. DIP-treated animals had slightly lower concentrations of cells undergoing apoptosis within the peri-infarct regions. Overall, the neuroprotective benefits offered by DIP could have important implications for BBB stability and the prevention of hemorrhagic transformation, edema and cell death.

Innate inflammation, beginning at stroke onset, can exacerbate the ischemic defect through the interaction of platelets, leukocytes and thrombotic moderators²⁶. Initial neutrophil infiltration can obstruct microvascular blood flow via capillary plugging, as well as increase vascular permeability^{40, 41}. Additionally, ROS and cytokine release from neutrophils can cause extravascular parenchymal damage⁴². An increase in adenosine levels have been shown to inhibit neutrophil activation by reducing the expression of neutrophil adhesion molecules⁴³. Although DIP causes intravascular increases in adenosine, as described herein, we did not observe a difference in leukocyte infiltration between DIP- and saline-treated animals. Given that DIP was administered only prior to stroke onset, we can speculate that DIP blood concentrations, around the time of euthanasia, were too low to cause inter-group differences in adenosine concentrations, and subsequent reductions in neutrophil deactivation.

There are study limitations which warrant discussion. First, it was difficult to obtain accurate cerebral blood volume (CBV) measurements since isoflurane, a potent vasodilator, was used as the anaesthetic during all CT perfusion scanning⁴⁴. For both groups, a slight increase in mean CBV at 30 minutes post stroke was observed; this could be related to the autoregulatory vasodilation phenomenon that occurs during the hyper-

acute stroke phase, causing a mismatch between CBF and CBV in the ischemic tissue¹¹. Nonetheless, we did not observe CBV differences within or between groups. Second, neurological assessment may have been skewed due to variations in the extent of surgical trauma between animals – internal carotid anatomical variability contributed to increased surgery time. Third, our sample size was small relative to other studies using rodents; however, our serial in-vivo imaging procedures and neurological testing allowed comparisons in the same animal to be made over many days of survival eliminating the need to use a larger number of animals to achieve the same statistical power. Lastly, it was uncertain whether the emboli found within excised brains were originally injected or endogenously produced. Even so, this model examines the animal's ability to deal with the injected embolus and its associated pathological manifestations (ie. microemboli, inflammation).

7.5 CONCLUSION

Dipyridamole is given to patients at increased risk of stroke as it decreases the incidence of cerebroembolism. Presumably, if stroke was to occur, the pathways involved in secondary stroke prevention may be neuroprotective during an ischemic episode. We used a novel animal stroke model to demonstrate that pre-morbid treatment with therapeutic concentrations of DIP provides a neurovascular advantage post stroke onset.

7.6 REFERENCES

1. Wang X, Tsuji K, Lee SR, Ning M, Furie KL, Buchan AM, et al. Mechanisms of hemorrhagic transformation after tissue plasminogen activator reperfusion therapy for ischemic stroke. *Stroke*. 2004;35:2726-2730
2. Diener HC, Cunha L, Forbes C, Sivenius J, Smets P, Lowenthal A. European stroke prevention study. 2. Dipyridamole and acetylsalicylic acid in the secondary prevention of stroke. *Journal of the neurological sciences*. 1996;143:1-13
3. Kim HH, Sawada N, Soydan G, Lee HS, Zhou Z, Hwang SK, et al. Additive effects of statin and dipyridamole on cerebral blood flow and stroke protection. *Journal of cerebral blood flow and metabolism : official journal of the International Society of Cerebral Blood Flow and Metabolism*. 2008;28:1285-1293
4. Chakrabarti S, Freedman JE. Dipyridamole, cerebrovascular disease, and the vasculature. *Vascul Pharmacol*. 2008;48:143-149
5. Ovbiagele B, Buck BH, Liebeskind DS, Starkman S, Bang OY, Ali LK, et al. Prior antiplatelet use and infarct volume in ischemic stroke. *Journal of the neurological sciences*. 2008;264:140-144
6. Greisenegger S, Tentschert S, Weber M, Ferrari J, Lang W, Lalouschek W. Prior therapy with antiplatelet agents is not associated with outcome in patients with acute ischemic stroke/tia. *Journal of neurology*. 2006;253:648-652
7. Sivenius J, Cunha L, Diener HC, Forbes C, Laakso M, Lowenthal A, et al. Antiplatelet treatment does not reduce the severity of subsequent stroke. European stroke prevention study 2 working group. *Neurology*. 1999;53:825-829
8. Kim WJ, Ko Y, Yang MH, Im SH, Park JH, Lee J, et al. Differential effect of previous antiplatelet use on stroke severity according to stroke mechanism. *Stroke*. 41:1200-1204
9. Busch E, Kruger K, Hossmann KA. Improved model of thromboembolic stroke and rt-pa induced reperfusion in the rat. *Brain Res*. 1997;778:16-24
10. Hill NC, Millikan CH, Wakim KG, Sayre GP. Studies in cerebrovascular disease. Vii. Experimental production of cerebral infarction by intracarotid injection of homologous blood clot; preliminary report. *Proc Staff Meet Mayo Clin*. 1955;30:625-633
11. Murphy BD, Chen X, Lee TY. Serial changes in ct cerebral blood volume and flow after 4 hours of middle cerebral occlusion in an animal model of embolic cerebral ischemia. *AJNR. American journal of neuroradiology*. 2007;28:743-749
12. Lyden PD, Zivin JA, Soll M, Sitzer M, Rothrock JF, Alksne J. Intracerebral hemorrhage after experimental embolic infarction. Anticoagulation. *Arch Neurol*. 1987;44:848-850

13. Zivin JA, Fisher M, DeGirolami U, Hemenway CC, Stashak JA. Tissue plasminogen activator reduces neurological damage after cerebral embolism. *Science (New York, N.Y.)*. 1985;230:1289-1292
14. Lapchak PA. Translational stroke research using a rabbit embolic stroke model: A correlative analysis hypothesis for novel therapy development. *Transl Stroke Res*.1:96-107
15. Lapchak PA, Araujo DM, Pakola S, Song D, Wei J, Zivin JA. Microplasmin: A novel thrombolytic that improves behavioral outcome after embolic strokes in rabbits. *Stroke; a journal of cerebral circulation*. 2002;33:2279-2284
16. Lapchak PA, Araujo DM, Song D, Wei J, Purdy R, Zivin JA. Effects of the spin trap agent disodium- [tert-butylimino)methyl]benzene-1,3-disulfonate n-oxide (generic nxy-059) on intracerebral hemorrhage in a rabbit large clot embolic stroke model: Combination studies with tissue plasminogen activator. *Stroke; a journal of cerebral circulation*. 2002;33:1665-1670
17. Lapchak PA, Araujo DM, Song D, Wei J, Zivin JA. Neuroprotective effects of the spin trap agent disodium-[(tert-butylimino)methyl]benzene-1,3-disulfonate n-oxide (generic nxy-059) in a rabbit small clot embolic stroke model: Combination studies with the thrombolytic tissue plasminogen activator. *Stroke; a journal of cerebral circulation*. 2002;33:1411-1415
18. Oshrine B, Malinin A, Pokov A, Dragan A, Hanley D, Serebruany V. Criticality of ph for accurate fluorometric measurements of dipyridamole levels in biological fluids. *Methods Find Exp Clin Pharmacol*. 2005;27:95-100
19. Strong MJ, Wolff AV, Wakayama I, Garruto RM. Aluminum-induced chronic myelopathy in rabbits. *Neurotoxicology*. 1991;12:9-21
20. St Lawrence KS, Lee TY. An adiabatic approximation to the tissue homogeneity model for water exchange in the brain: I. Theoretical derivation. *Journal of cerebral blood flow and metabolism : official journal of the International Society of Cerebral Blood Flow and Metabolism*. 1998;18:1365-1377
21. Kudo K, Terae S, Katoh C, Oka M, Shiga T, Tamaki N, et al. Quantitative cerebral blood flow measurement with dynamic perfusion ct using the vascular-pixel elimination method: Comparison with h2(15)o positron emission tomography. *AJNR. American journal of neuroradiology*. 2003;24:419-426
22. Dresse A, Chevolet C, Delapierre D, Masset H, Weisenberger H, Bozler G, et al. Pharmacokinetics of oral dipyridamole (persantine) and its effect on platelet adenosine uptake in man. *Eur J Clin Pharmacol*. 1982;23:229-234
23. Eyre JA, Essex TJ, Flecknell PA, Bartholomew PH, Sinclair JI. A comparison of measurements of cerebral blood flow in the rabbit using laser doppler spectroscopy and radionuclide labelled microspheres. *Clin Phys Physiol Meas*. 1988;9:65-74

24. Cenic A, Nabavi DG, Craen RA, Gelb AW, Lee TY. Dynamic ct measurement of cerebral blood flow: A validation study. *AJNR. American journal of neuroradiology*. 1999;20:63-73
25. Cenic A, Nabavi DG, Craen RA, Gelb AW, Lee TY. A ct method to measure hemodynamics in brain tumors: Validation and application of cerebral blood flow maps. *AJNR. American journal of neuroradiology*. 2000;21:462-470
26. Croce K, Libby P. Intertwining of thrombosis and inflammation in atherosclerosis. *Curr Opin Hematol*. 2007;14:55-61
27. Verro P, Gorelick PB, Nguyen D. Aspirin plus dipyridamole versus aspirin for prevention of vascular events after stroke or tia: A meta-analysis. *Stroke; a journal of cerebral circulation*. 2008;39:1358-1363
28. Johnston SC, Rothwell PM, Nguyen-Huynh MN, Giles MF, Elkins JS, Bernstein AL, et al. Validation and refinement of scores to predict very early stroke risk after transient ischaemic attack. *Lancet*. 2007;369:283-292
29. Green D, Miller V. The role of dipyridamole in the therapy of vascular disease. *Geriatrics*. 1993;48:46, 51-43, 57-48
30. Ally AI, Manku MS, Horrobin DF, Morgan RO, Karmazin M, Karmali RA. Dipyridamole: A possible potent inhibitor of thromboxane a2 synthetase in vascular smooth muscle. *Prostaglandins*. 1977;14:607-609
31. Blann AD, Landray MJ, Lip GY. Abc of antithrombotic therapy: An overview of antithrombotic therapy. *Bmj*. 2002;325:762-765
32. Li JM, Fenton RA, Cutler BS, Dobson JG, Jr. Adenosine enhances nitric oxide production by vascular endothelial cells. *Am J Physiol*. 1995;269:C519-523
33. Wang GR, Zhu Y, Halushka PV, Lincoln TM, Mendelsohn ME. Mechanism of platelet inhibition by nitric oxide: In vivo phosphorylation of thromboxane receptor by cyclic gmp-dependent protein kinase. *Proc Natl Acad Sci U S A*. 1998;95:4888-4893
34. Kim JA, Tran ND, Zhou W, Fisher M. Dipyridamole enhances tissue plasminogen activator release by brain capillary endothelial cells. *Thrombosis research*. 2005;115:435-438
35. Weyrich AS, Denis MM, Kuhlmann-Eyre JR, Spencer ED, Dixon DA, Marathe GK, et al. Dipyridamole selectively inhibits inflammatory gene expression in platelet-monocyte aggregates. *Circulation*. 2005;111:633-642
36. Schreiber G, Kooij G, Reijkerkerk A, van Doorn R, Gringhuis SI, van der Pol S, et al. Reactive oxygen species alter brain endothelial tight junction dynamics via rhoa, pi3 kinase, and pkb signaling. *FASEB J*. 2007;21:3666-3676
37. Nanetti L, Taffi R, Vignini A, Moroni C, Raffaelli F, Bacchetti T, et al. Reactive oxygen species plasmatic levels in ischemic stroke. *Mol Cell Biochem*. 2007;303:19-25

38. Selley ML, Czeti AL, McGuinness JA, Ardlie NG. Dipyridamole inhibits the oxidative modification of low density lipoprotein. *Atherosclerosis*. 1994;111:91-97
39. Kim HH, Liao JK. Translational therapeutics of dipyridamole. *Arterioscler Thromb Vasc Biol*. 2008;28:s39-42
40. Feuerstein GZ, Liu T, Barone FC. Cytokines, inflammation, and brain injury: Role of tumor necrosis factor-alpha. *Cerebrovasc Brain Metab Rev*. 1994;6:341-360
41. Marshall JC, Malam Z, Jia S. Modulating neutrophil apoptosis. *Novartis Found Symp*. 2007;280:53-66; discussion 67-72, 160-164
42. Huang J, Upadhyay UM, Tamargo RJ. Inflammation in stroke and focal cerebral ischemia. *Surgical neurology*. 2006;66:232-245
43. Wollner A, Wollner S, Smith JB. Acting via a2 receptors, adenosine inhibits the upregulation of mac-1 (cd11b/cd18) expression on fmlp-stimulated neutrophils. *Am J Respir Cell Mol Biol*. 1993;9:179-185
44. Iida H, Ohata H, Iida M, Watanabe Y, Dohi S. Isoflurane and sevoflurane induce vasodilation of cerebral vessels via atp-sensitive k+ channel activation. *Anesthesiology*. 1998;89:954-960

CHAPTER 8

Conclusion and Future Work

8.1 SUMMARY

The introduction of this thesis describes the importance of early treatment strategies to promote tissue salvage and maintain neuronal function in the two most common stroke sub-types, cerebral ischemia and intra-cerebral hemorrhage (ICH). As discussed in detail in the previous chapters, the objective of this thesis was to help with the selection of patients who will benefit from acute stroke treatment (thrombolytics, anti-hypertensive/coagulation drugs, surgical techniques), as well as determine if pre-stroke neuroprotection can reduce stroke severity. Specifically, CTP thresholds of hemodynamic parameters including CBF, CBV and PS for cerebral tissue and BBB status, as well as the neuroprotective benefit of a common secondary ischemic stroke preventative drug, dipyridamole, were explored. Patients with thromboembolic cerebral ischemia and primary ICH were studied, along with the development and implementation of two unique animal models of ischemic stroke.

In this final chapter, I will review the major findings of my research and discuss the implications of the six studies. The discussion will encompass experimental and clinical relevance of the methods and results, as well as important areas that require further investigation. Although we were successful in demonstrating the ability of CTP imaging to verify drug efficacy and monitor stroke progression, considerable work is still required before the goal of an individualized stroke treatment is realized. Therefore, an

outline of the possible investigations that should follow this work will be included. Finally, the major conclusions obtained from this work will be summarized.

8.1.1 Prediction of acute tissue viability for ischemic stroke

Although much research has gone into the management of acute ischemic stroke (AIS), treatment remains limited to revascularization with either intravenous tPA or endovascular strategies (including intra-arterial tPA). The use of either treatment depends on time since stroke onset, the amount of brain tissue involved, location and size of the blood clot, and robust collateral circulation. In general, small and more distal clots which are not amenable to mechanical removal, and present less than 4.5 hours from symptom onset, are treated with intravenous tPA, while larger and more proximal clots are treated up to 8 hours with endovascular techniques. For revascularization to proceed, whether the benefit of tissue salvage outweighs the risk of reperfusion injury, particularly intracerebral hemorrhage (ICH), is an important consideration. To address this concern, we need to know if the infarct is too large such that benefits from tissue salvage may be too small in light of possible hemorrhagic transformation, worsening clinical outcome. Chapters 2, 3 and 4 address the importance of predicting infarct volume during the AIS setting. Using both human and animal studies, we determined that the acute CBF/CBV mismatch may, at times, represent tissue that is not salvageable, even upon reperfusion. This goes against the central dogma which asserts that autoregulatory maintenance, as observed by the increase in CBV, represents electrically silent yet viable tissue. Subsequently, we showed that the CBF parameter was optimal for predicting final infarction in a retrospective analysis, and also best delineated the hyper-acute infarct core,

as defined by MR-diffusion weighted imaging and TTC-histology, in a novel porcine model of ischemic stroke.

8.1.2 Role of the CTP-PS parameter in acute stroke

The CTP-blood brain barrier permeability surface area product (BBB-PS), which quantifies the leakage rate of CT contrast dye from the intra- to extra-vascular space, has the ability to predict clinical and radiological outcome for patients with intracerebral hemorrhage (ICH) secondary to cerebral ischemia and for patients with primary ICH.

In the risk versus benefit assessment of revascularization in patients with ischemic stroke, it is important to recognize that some patients with small infarct volumes may still proceed to symptomatic hemorrhagic transformation. On the contrary, patients arriving past the thrombolysis treatment window who still have salvageable tissue, irrespective of infarct core size, may also be a candidate for tPA. Therefore, assessment of the acute infarct core volume, penumbra volume and integrity of the BBB within infarct, penumbra and contralateral normal tissue are necessary in the decision of revascularization. In patients with secondary ICH from prolonged ischemia with or without reperfusion, admission BBB-PS was higher within the ischemic and contralateral regions compared to patients without hemorrhage at follow-up. The patients with secondary hemorrhage had a significantly higher PS than did those without hemorrhage. A PS threshold of $0.23 \text{ ml}^{-1} \cdot \text{min}^{-1} \cdot (100\text{g})^{-1}$ also enabled the differentiation of patients with HT from those without.

For patients with primary ICH, admission BBB-PS was the highest in patients with the CT angiography (CTA)-Spot Sign compared to those with Post-contrast CT Leakage (PCL) and those without CT contrast extravasation. Moreover, increased BBB-

PS was correlated with hematoma expansion. Measuring the rate of leakage provides a quantitative method to study the degree of BBB derangement on hematoma expansion. The high PS values obtained in patients with the CTA Spot Sign emphasize the rapid rate of contrast extravasation, reinforcing the need for a rapid and efficient treatment in this subgroup of patients.

These two acute stroke studies were the first to use quantitative CTP-BBB PS parameter to predict clinical and radiological outcome in patients with primary and secondary ICH. Using the admission BBB-PS parameter can inform treatment decisions for both of these stroke sub-types.

8.1.3 Reducing stroke severity with secondary prevention drugs

Antiplatelet (AP) drugs are universally recognized for their effectiveness in reducing recurrent stroke in high risk patients^{1, 2}. If stroke does occur, extending the tPA therapeutic window and minimizing long term morbidity may be an additional benefit of this treatment. Dipyridamole (DIP) is prescribed clinically in extended-release form as a secondary stroke treatment, and is primarily recognized as an antithrombotic agent with AP properties³. DIP offers both platelet and non-platelet neuroprotective benefits and, unlike aspirin, has a lower propensity for bleeding⁴. Using a novel rabbit large clot embolic model (RLCEM), we found that administration of therapeutic concentrations of DIP improved ipsilateral CBF at 24 hours after stroke induction. The RLCEM mimics the clinical situation in which a patient would take DIP as a secondary treatment and still suffer a stroke thereafter. The antithrombotic action of dipyridamole seems to be mediated by two complementary mechanisms: i) an anti-platelet action, which reduces thrombi formation, and ii) induced tPA release by endothelial cells, which breaks down

established thrombi through plasmin activation, and subsequent fibrinolysis. As such, DIP has implications for both primary and secondary stroke prevention.

Anti-platelet drugs are now emerging as potential treatments of the inflammatory response of ischemic stroke. Adenosine level increases, initiated by DIP, have been shown to inhibit neutrophil activation via reduction in expression of neutrophil adhesion molecules⁵. There was an increase in H&E stained neutrophils throughout the ipsilateral cerebral parenchyma of non-treated animals out to 7 days – DIP treated animals had minimal neutrophil staining at that time. Neutrophils are generally associated with acute inflammation; therefore their presence during the sub-acute stroke stage would suggest acute inflammatory processes are continuing to occur and that DIP may reduce the inflammatory processes initiated by neutrophils during the sub-acute stroke stages.

Dipyridamole (DIP) is given to patients at increased risk of stroke as it decreases the incidence of cerebroembolism. Presumably, if stroke was to occur, the neuroprotective pathways involved in secondary stroke prevention may be of benefit during an ischemic episode. These neuroprotective pathways are linked to suppression of inflammatory processes, which have direct and indirect effects on thrombus formation and vascular endothelium. As such, acute stroke interventions should implement anti-inflammatory mediators, which include anti-platelet drugs, into practice.

8.2 EXPERIMENTAL & CLINICAL RELEVANCE

The studies described in this thesis contribute important information for the advancement of acute stroke diagnosis and treatment. The animal studies described in Chapters 4 and 7 employed two clinically relevant models of acute ischemic stroke that reproduces a

number of important features of the human disease. These models allowed us to monitor infarct expansion by making consecutive CTP measurements over the first few hours following stroke; this information is not readily obtained in the clinical setting.

One of the current problems in acute ischemic stroke care is that the number of patients that receive treatment remains very low. Thrombolysis and mechanical clot removal are the only two treatments approved for clinical use. Treatment using mechanical retrieval is very limited; thrombolysis is more widely available, but it is restricted to a small percentage of patients. One of the major limiting factors for reperfusion therapy is the narrow 4.5 to 8 hour time window that is mandated for thrombolysis and mechanical clot removal, respectively. The use of the admission NCCT/CTA can help clinicians make thrombolytic treatment decisions by providing evidence of early ischemic changes and vessel occlusion status; however, without perfusion data, information on the severity of hypoperfusion is lacking, a critical factor when deciding to reperfuse - the rate of neuronal death differs for tissue with a CBF of $5 \text{ ml}\cdot\text{min}^{-1}\cdot 100\text{g}^{-1}$ versus $12 \text{ ml}\cdot\text{min}^{-1}\cdot 100\text{g}^{-1}$ between 1-3 hours; although both CBF values will ultimately cause infarction sub-acutely. Moreover, we can observe an unremarkable admission NCCT for a patient with infarct core perfusion values because hypoperfusion has not been established long enough. Therefore, to improve the thrombolytic selection criteria, it is important to include only those patients with a substantial volume of penumbra to salvage, for which accurate infarct core delineation is critical. This approach could be implemented using CTP imaging and applying the thresholds derived from this thesis.

A number of important criteria must be satisfied if a technique for improving patient selection will gain widespread clinical use. Among the most important

requirements are: wide availability, minimal cost, rapid and accurate assessment of penumbra and infarcted tissue. As we have shown in this thesis, CTP imaging is one potential candidate that satisfies most of these requirements. CT scanners are widely available around the clock in most hospitals and relatively inexpensive compared with other imaging techniques. CTP imaging requires less than three minutes of scan time and the functional maps can be calculated within 5-7 minutes.

Another important aspect of the work contained within this thesis was the identification of specific thresholds for grey and white matter. Given the different metabolic needs, specific thresholds for each tissue type have the ability to improve classification of penumbra and infarct. Implications of these tissue-specific thresholds extend beyond patient selection for revascularization procedures and may be important in future studies of neuroprotection.

8.3 FUTURE WORK

This thesis addresses many important questions concerning the diagnosis, prognosis, and treatment of acute stroke. However, as is customary in research, for every question answered there are a number of new questions raised. The following section will outline potential new directions of research.

8.3.1 Improved calculation of CTP functional maps

To improve the image quality of the functional maps, we will use a newer iterative CT image reconstruction technique and advanced image processing techniques including: 1) masked smoothing, where smoothing is guided by a tissue mask derived from the average

image of the source CTP images and 2) principal component analysis where the main features (components) of all time-density curves from the raw CTP images are extracted using a statistical procedure and then individual pixel time-density curves are smoothed by reconstituting them with these main components that are not dominated by noise⁶. These improvements in processing will be applied to the future studies described below.

8.3.2 Multi-variate prospective study to determine secondary ICH

To further improve the selection of patients for thrombolytic therapy, a predictive model based on the acute infarct volume and BBB-permeability will be established using the CTP thresholds obtained in this thesis. Further, we will investigate whether a second (higher) BBB-PS threshold would predict symptomatic versus non-symptomatic hemorrhage – it is speculated that less severe forms of hemorrhage may not be clinically relevant and represent different pathogenesis⁷.

8.3.3 Minor stroke and transient ischemic attack

Patients with transient ischemic attack (TIA) and minor strokes are often excluded from revascularization treatment because their neurological deficits are transient or mild; however, these patients can often have subsequent stroke⁸. TIA confers a 10% risk of stroke within 30 days, one half of these occurring within 48 hours; a proportion of these sub-acute episodes are simply due to worsening of initial minor stroke⁹. Further, long term disability has been shown to occur in patients with mild symptoms at presentation and without recurrent events⁸. In these patients, cerebral perfusion pressure (CPP) may have fallen to a level that needs to be corrected promptly to prevent an impending stroke. Knowledge of CPP, along with basic clinical parameters, may be used to guide treatment

and predict clinical outcome. CPP is inversely related to the tissue mean transit time (MTT) which measures the time required for blood/contrast to traverse the tissue vasculature under prevailing CPP. A related parameter to MTT is Tmax which is the sum of MTT and the time blood requires to reach the local tissue distal to an obstruction via collaterals. Determination of the optimal MTT (Tmax) threshold may predict impending disabling stroke in patients with TIA/minor stroke (NIHSS <4).

8.3.4 Voxel based classification

An inherent limitation of the studies described in this thesis is the region of interest analysis that was used to derive the hemodynamic thresholds. The thresholds derived from this method depend on the mean value of the regions; therefore, the true thresholds for infarction and BBB permeability may be different than those identified in this study. To more accurately determine the thresholds, independent of the mean regional values, voxel or pixel based thresholds can be applied. These thresholds could be derived in a similar manner to the region of interest thresholds by obtaining hemodynamic values from all voxels within the ischemic region. Voxels could then be classified, based on delayed imaging.

8.3.5 Comparing AIS therapeutics

Using the RLCEM developed in this thesis, anti-thrombotic therapeutics in the AIS setting can be compared. One treatment regimen, Clopidogrel monotherapy, has been shown to reduce recurrent stroke, but may not improve the functional severity post stroke onset, and has a propensity to cause intracranial bleeding¹⁰. This secondary stroke preventative agent is typically given as an alternative to Aspirin or Dipyridamole^{11, 12}.

Using a similar methodology as described in chapter 7, investigation and comparison of the effect of pre-morbid administration of anti-thrombotic drugs, which have anti-platelet and pleiotropic properties, in the setting of embolic ischemic stroke are possible.

8.3.6 ¹⁸F-Flumazenil imaging in porcine AIS model

To determine the volume of acute infarct core the use of the ¹⁸F-flumazenil tracer, a central benzodiazepine receptor antagonist, could be utilized in the porcine model of AIS developed in this thesis¹³. Using a similar methodology as described in chapter 4, a comparison of infarction volume, as defined by contemporaneous CTP imaging, MR-DWI and PET imaging, is possible. Moreover, an attempt to determine hemodynamic thresholds for penumbral tissue using the CTP-CBF/Tmax mismatch, while comparing the predicted infarct core to final infarct volume, defined using TTC histology can be achieved. Moreover, infarct core and penumbra volumes derived from CTP imaging could be compared with MR-perfusion weighted imaging as well as MR-arterial spin labeling sequences.

8.4 CONCLUSION

In summary, the significant findings in this thesis include:

1. As shown in the clinical studies and study with a novel porcine model of ischemic stroke, very low CBV is indicative of infarct core, while acute and sub-acute hypervolemia may be nutritive or non-nutritive. Moreover, the CBF parameter was optimal for prediction of infarct volume.
2. Blood brain barrier integrity within the first few hours of stroke onset can be measured with the CTP-PS parameter. PS values can predict radiological and clinical outcome in the primary and secondary ICH stroke sub-types.
3. Pre-morbid administration of dipyridamole, a common secondary preventative drug, may extend the tPA treatment window and reduce stroke severity.

8.5 REFERENCES

1. De Schryver EL, Algra A, van Gijn J. Dipyridamole for preventing stroke and other vascular events in patients with vascular disease. An update. *Stroke; a journal of cerebral circulation*. 2008; 15:21-4
2. Diener HC, Cunha L, Forbes C, Sivenius J, Smets P, Lowenthal A. European stroke prevention study. 2. Dipyridamole and acetylsalicylic acid in the secondary prevention of stroke. *Journal of the neurological sciences*. 1996;143:1-13
3. Green D, Miller V. The role of dipyridamole in the therapy of vascular disease. *Geriatrics*. 1993;48:46, 51-43, 57-48
4. Kim HH, Sawada N, Soydan G, Lee HS, Zhou Z, Hwang SK, et al. Additive effects of statin and dipyridamole on cerebral blood flow and stroke protection. *Journal of cerebral blood flow and metabolism : official journal of the International Society of Cerebral Blood Flow and Metabolism*. 2008;28:1285-1293
5. Wollner A, Wollner S, Smith JB. Acting via a2 receptors, adenosine inhibits the upregulation of mac-1 (cd11b/cd18) expression on fmlp-stimulated neutrophils. *Am J Respir Cell Mol Biol*. 1993;9:179-185
6. Konstas AA, Goldmakher GV, Lee TY, Lev MH. Theoretic basis and technical implementations of ct perfusion in acute ischemic stroke, part 2: Technical implementations. *AJNR. American journal of neuroradiology*. 2009;30:885-892
7. Thomalla G, Sobesky J, Kohrmann M, Fiebach JB, Fiehler J, Zaro Weber O, et al. Two tales: Hemorrhagic transformation but not parenchymal hemorrhage after thrombolysis is related to severity and duration of ischemia: Mri study of acute stroke patients treated with intravenous tissue plasminogen activator within 6 hours. *Stroke; a journal of cerebral circulation*. 2007;38:313-318
8. Coutts SB, Modi J, Patel SK, Aram H, Demchuk AM, Goyal M, et al. What causes disability after transient ischemic attack and minor stroke?: Results from the ct and mri in the triage of tia and minor cerebrovascular events to identify high risk patients (catch) study. *Stroke; a journal of cerebral circulation*. 2012;43(11):3018-22
9. Adams H, Adams R, Del Zoppo G, Goldstein LB. Guidelines for the early management of patients with ischemic stroke: 2005 guidelines update a scientific statement from the stroke council of the american heart association/american stroke association. *Stroke; a journal of cerebral circulation*. 2005;36:916-923

10. Hankey GJ, Hacke W, Easton JD, Johnston SC, Mas JL, Brennan DM, et al. Effect of clopidogrel on the rate and functional severity of stroke among high vascular risk patients: A prespecified substudy of the clopidogrel for high atherothrombotic risk and ischemic stabilization, management and avoidance (charisma) trial. *Stroke; a journal of cerebral circulation*. 2010;41:1679-1683
11. Dowlathshahi D, Hakim A, Fang J, Sharma M. Pre admission antithrombotics are associated with improved outcomes following ischaemic stroke: A cohort from the registry of the canadian stroke network. *International journal of stroke : official journal of the International Stroke Society*. 2009;4:328-334
12. Sacco RL, Diener HC, Yusuf S, Cotton D, Ounpuu S, Lawton WA, et al. Aspirin and extended-release dipyridamole versus clopidogrel for recurrent stroke. *The New England journal of medicine*. 2008;359:1238-1251
13. Odano I, Halldin C, Karlsson P, Varrone A, Airaksinen AJ, Krasikova RN, et al. [18f]flumazenil binding to central benzodiazepine receptor studies by pet--quantitative analysis and comparisons with [11c]flumazenil. *NeuroImage*. 2009;45:891-902

Appendix A - Human Ethics Approval Form

Protocol Title: CT based indices of tissue viability and Infarction in Acute Stroke.

Approval Date: 06-Feb-04

End Date: 28-Feb-05

Documents Reviewed and Approved: Revised Study End Date

Documents Received for Information:

This is to notify you that the University of Western Ontario Research Ethics Board for Health Sciences Research Involving Human Subjects (HSREB) which is organized and operates according to the Tri-Council Policy Statement and the Health Canada/CH Good Clinical Practice Practices: Consolidated Guidelines; and the applicable laws and regulations of Ontario has received and granted expedited approval to the above named research study on the date noted above. The membership of this REB also complies with the membership requirements for REB's as defined in Division 5 of the Food and Drug Regulations.

This approval shall remain valid until end date noted above assuming timely and acceptable responses to the HSREB's periodic requests for surveillance and monitoring information. If you require an updated approval notice prior to that time you must request it using the UWO Updated Approval Request Form.

During the course of the research, no deviations from, or changes to, the protocol or consent form may be initiated without prior written approval from the HSREB except when necessary to eliminate immediate hazards to the subject or when the change(s) involve only logistical or administrative aspects of the study (e.g. change of monitor, telephone number). Expedited review of minor change(s) in ongoing studies will be considered. Subjects must receive a copy of the signed information/consent documentation.

Investigators must promptly also report to the HSREB:

- a) changes increasing the risk to the participant(s) and/or affecting significantly the conduct of the study;
- b) all adverse and unexpected experiences or events that are both serious and unexpected;
- c) new information that may adversely affect the safety of the subjects or the conduct of the study.

If these changes/adverse events require a change to the information/consent documentation, and/or recruitment advertisement, the newly revised information/consent documentation, and/or advertisement, must be submitted to this office for approval.

Members of the HSREB who are named as investigators in research studies, or declare a conflict of interest, do not participate in discussion related to, nor vote on, such studies when they are presented to the HSREB.

This is an official document. Please retain the original in your files.

UWO HSREB Ethics Approval

09143E

Page 1 of 1

Appendix B - Human Ethics Approval Form

COMITATO ETICO DELLA PROVINCIA DI FERRARA

irreversibile; ad uno studio CTP con analisi del mismatch CBF/MTT>CBV e del punteggio ASPECTS sulla mappa perfusionale CBV per stabilire l'evoluzione della penombra ischemica; ad una indagine CTA per verificare la presenza di ricanalizzazione del vaso precedentemente occluso.

- Visita 2 (a 7-10 giorni dall'ingresso): in occasione di tale visita verrà eseguito un esame obiettivo neurologico completo con calcolo del punteggio del NIHSS e verranno eseguite, analogamente alla visita successiva, tutte le indagini strumentali già previste dalla visita 1.

- Visita 3 (a 3 mesi dall'ingresso): in occasione di tale visita verrà effettuato il calcolo del punteggio del Rankin Scale modificato (mRS) per misurare l'evoluzione dell'ictus ischemico in senso prognostico.

Modalità di sospensione:

è prevista l'interruzione dello studio qualora si verificano eventi avversi, su decisione del medico sperimentatore e, comunque, per libera scelta e disposizione dell'arruolato.

Si dà atto che durante la discussione della sperimentazione clinica la Prof.ssa Tola si è assentata e quindi astenuta dalla votazione.

Il Comitato Etico esprime parere favorevole allo studio proposto, ove siano soddisfatti i requisiti etici nei termini innanzi richiesti.

Si ricorda al proponente responsabile la necessità di comunicare alla Segreteria Tecnico-Scientifica del Comitato Etico la fine dello studio, nonché di trasmettere copia di eventuale/i pubblicazione/i ovvero del report finale.

Si dà atto che il Comitato Etico ha preso visione della seguente documentazione:

- n. 1 copia di Lettera di intenti;
- n. 1 copia di Protocollo di studio;
- n. 1 copia di Foglio informativo per il paziente;
- n. 1 copia Modulo di Consenso per il paziente;
- n. 1 copia di lettera per il medico di base;
- n. 1 copia di dichiarazione di intenti della Regione Emilia-Romagna per proposta di programma strategico "Nuove conoscenze e problematiche assistenziali nell'ictus cerebrale: un programma strategico di ricerca e sviluppo";
- n. 1 copia di dichiarazione di inizio attività del progetto della Regione Emilia-Romagna: "Nuove conoscenze e problematiche assistenziali nell'ictus cerebrale: un programma strategico di ricerca e sviluppo".

Appendix C – Animal Ethics Approval Form

Official Notification of AUS Approval: A MODIFICATION to Animal Use Protocol 2007-050-06 has been approved.

The holder of this Animal Use Protocol is responsible to ensure that all associated safety components (biosafety, radiation safety, general laboratory safety) comply with institutional safety standards and have received all necessary approvals. Please consult directly with your institutional safety officers.

Submitted by:
on behalf of the Animal Use Subcommittee

Appendix D

Method to determine the optimal CT perfusion hemodynamic thresholds for gray and white matter in the setting of acute stroke

Patients and Imaging

Twenty-one patients, from the analysis in Chapter 5, had CTA confirmed full recanalization at 24 hours, confirmed with the modified TIMI score¹. All imaging was as described in Chapter 5. Briefly, the CTP study scanned eight 5 mm thick sections of the brain in 2 phases together with contrast injection via an antecubital vein at a rate of 2-4 ml/s. The first phase was a 45-second continuous (cine) acquisition reconstructed at 0.5-second intervals to produce a series of 89 sequential images for each section. The second phase followed 15 seconds after the completion of the first phase and scanned the same eight sections at 15-second intervals for an additional 90 seconds. CBF, CBV, Tmax, a special 'Time-density curve (TDC) truncation' functional maps and a perfusion-weighted map were calculated from the acquired 2-phase contrast enhanced dynamic images as described previously².

Image Analysis

CTP functional maps of CBF, CBV, Tmax, and perfusion weighted images (PWI) were calculated with CT Perfusion 4D, delay insensitive software (GE Healthcare), as described in Chapter 1. Using custom software (IDL v6.2, RSI Inc.), follow-up images from 5-7 day post stroke were registered to baseline images to adjust for movement between the scans. The PWIs of the CTP studies were used to segment gray and white

matter based on Hounsfield Unit thresholds. The resulting gray and white matter masks were applied to the admission CBF and CBV maps to obtain average gray and white matter values for infarcted tissue - pixels with $CBF > 100 \text{ ml}\cdot(100\text{g})^{-1}\cdot\text{min}^{-1}$ or $CBV > 8 \text{ ml}\cdot(100\text{g})^{-1}$ were excluded and not used in calculating average CBF and CBV values for regions of interest (ROI) to remove contributions from large vessels. Final infarction was outlined on the registered 5-7 day follow-up imaging. These infarct ROIs were superimposed onto the admission CTP functional maps. The critically hypoperfused tissue (relative $T_{\text{max}} > 2$), if present, was outlined on the admission T_{max} map, and the gray/white matter mask was applied³. The area outside of the infarct ROI and within the area of critical hypoperfusion was operationally defined as penumbra. Logistic regression analysis was performed using all data points. Gray and white matter CBF, CBV, and an interaction term $CBF\cdot CBV$ were included as potential predictors in the regression model. Sensitivity and specificity for infarction were calculated from the resulting regression model.

Statistical Analysis

Logistic regression analysis was performed on functional data of all infarct and penumbra. Gray and white matter CBF, CBV, and an interaction term $CBF\cdot CBV$ were included as potential predictors of infarct vs penumbra in the regression model. Sensitivity and specificity for infarction were calculated from the resulting regression model. All statistical analyses were performed using SPSS 13 for Windows (SPSS for Windows, SPSS Inc.).

Results

Gray matter thresholds

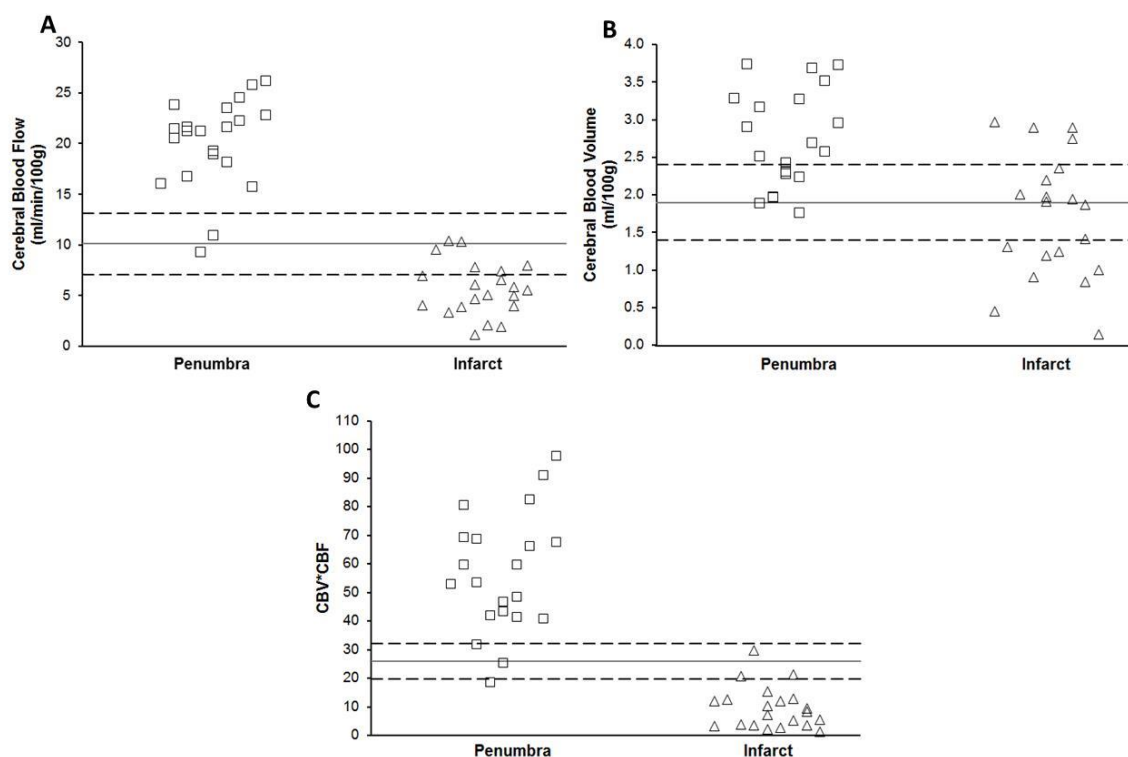
Average CBF and CBV gray matter tissue that was infarcted on the 5-7 day NCCT was $5.60 \pm 2.63 \text{ ml}\cdot(100\text{g})^{-1}\cdot\text{min}^{-1}$ and $1.68 \pm 0.82 \text{ ml}\cdot(100\text{g})^{-1}$, respectively. Average CBF and CBV values for ischemic regions on the admission CTP that were not infarcted on the 5-7 day NCCT (Penumbra) were $20.10 \pm 4.41 \text{ ml}\cdot(100\text{g})^{-1}\cdot\text{min}^{-1}$, and $1.68 \pm 0.82 \text{ ml}\cdot(100\text{g})^{-1}$. Contralateral CBF and CBV values were $29.64 \pm 9.53 \text{ ml}\cdot(100\text{g})^{-1}\cdot\text{min}^{-1}$ and $2.75 \pm 0.63 \text{ ml}\cdot(100\text{g})^{-1}$. Univariate logistic regression using admission CBF, CBV or CBF*CBV as predictor was performed. Optimal gray matter CBF, CBV and CBF•CBV product thresholds to separate penumbra from infarct were $10.1 \text{ ml}\cdot\text{min}^{-1}\cdot(100\text{g})^{-1}$, $1.9 \text{ ml}\cdot(100\text{g})^{-1}$, and 26.0, respectively. The regression model using the CBF parameter resulted in the highest sensitivity (95.2%, 20/21) and specificity (95.2%, 20/21) for infarction, with an overall accuracy of (95.2%, 40/42) of tissue types classified correctly (Figure A1).

White matter thresholds

Average CBF and CBV gray matter tissue that was infarcted on the 5-7 day NCCT was $5.86 \pm 1.32 \text{ ml}\cdot(100\text{g})^{-1}\cdot\text{min}^{-1}$ and $1.04 \pm 0.61 \text{ ml}\cdot(100\text{g})^{-1}$, respectively. Average CBF and CBV values for ischemic regions on the admission CTP that were not infarcted on the 5-7 day NCCT (Penumbra) were $12.27 \pm 3.26 \text{ ml}\cdot(100\text{g})^{-1}\cdot\text{min}^{-1}$, and $1.70 \pm 0.61 \text{ ml}\cdot(100\text{g})^{-1}$. Contralateral CBF and CBV values were $21.18 \pm 6.89 \text{ ml}\cdot(100\text{g})^{-1}\cdot\text{min}^{-1}$ and $1.33 \pm 0.50 \text{ ml}\cdot(100\text{g})^{-1}$. Univariate logistic regression using admission CBF, CBV or CBF*CBV as predictor was performed. Optimal white matter CTP-CBF, CBV and CBF•CBV product thresholds to separate penumbra from infarct were $7.4 \text{ ml}\cdot\text{min}^{-1}\cdot(100\text{g})^{-1}$, $1.25 \text{ ml}\cdot(100\text{g})^{-1}$

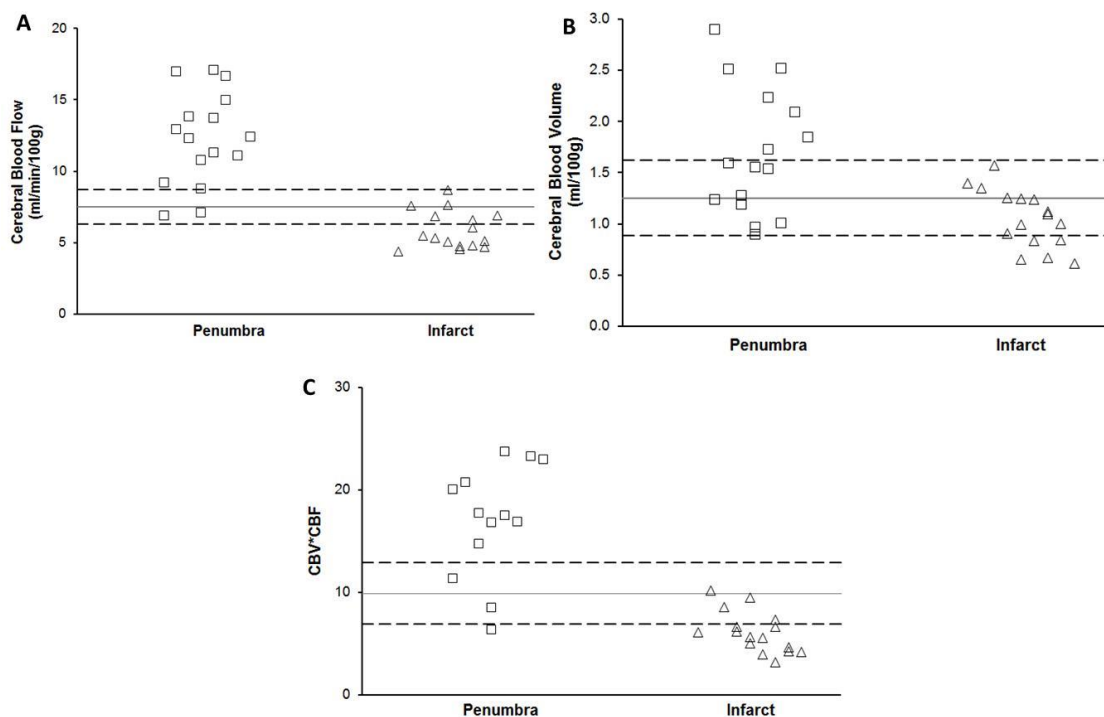
¹, and 9.9, respectively. The regression model using the CBF•CBV product resulted in the highest sensitivity (93.8%, 15/16) and specificity (87.5%, 14/16) for infarction, with an overall accuracy of (90.6%, 29/32) of tissue types classified correctly (Figure A1).

Figure A1 Thresholds for infarction for gray matter CBF, CBV and CBF•CBV



Gray matter values for all Infarct (n=21) and Penumbra (n=21) regions of interest with the solid line representing the optimal threshold to separate infarct from penumbra, the upper and lower dashed lines represent the 5% and 95% probability for infarction, derived from univariate logistic regression with A) CBF, B) CBV, and C) CBF•CBV product as predictor. CBF provided the best classification of penumbra and infarct regions with a sensitivity of 95.2%, (20/21 regions), and specificity of 95.2%, (20/21 regions), and overall accuracy of 95.2% (40/42).

Figure A2 Thresholds for infarction for white matter CBF, CBV and CBF·CBV



White matter values for all Infarct (n=16) and Penumbra (n=16) regions of interest with the solid line representing the optimal threshold to separate infarct from penumbra, the upper and lower dashed lines represent the 5% and 95% probability for infarction, derived from univariate logistic regression with A) CBF, B) CBV, and C) CBF·CBV product as predictor. The CBF·CBV parameter provided the best classification of penumbra and infarct regions with a sensitivity of 93.7%, (15/16 regions), specificity of 87.5%, (14/16 regions), and overall accuracy of 90.6% (29/32 regions).

1. Tan IY, Demchuk AM, Hopyan J, Zhang L, Gladstone D, Wong K, et al. Ct angiography clot burden score and collateral score: Correlation with clinical and radiologic outcomes in acute middle cerebral artery infarct. *AJNR. American journal of neuroradiology*. 2009;30:525-531
2. d'Este CD, Aviv RI, Lee TY. The evolution of the cerebral blood volume abnormality in patients with ischemic stroke: A ct perfusion study. *Acta radiologica*. 2012;53:461-467
3. Bivard A, Spratt N, Levi C, Parsons M. Perfusion computer tomography: Imaging and clinical validation in acute ischaemic stroke. *Brain : a journal of neurology*. 2011;134:3408-3416

Appendix E – Human Ethics Approval Form

MEMORANDUM

To:**From:****Date:** September 5, 2006**Subject:** **Predicting Hemorrhagic Transformation in Stroke Patient
Using CT Permeability**

*Project Identification Number: 341-2006**Approval Date: September 5, 2006*

The Research Ethics Board of Sunnybrook Health Sciences Centre has conducted an expedited review of the research protocol referenced above on the above captioned date and approved the involvement of human subjects as specified in the protocol and the Information sheet/Consent form.

The quorum for approval did not involve any member associated with this project.

Should your study continue for more than one year you must request a renewal on or before one year from the approval date. Please advise the Board of the progress of your research annually and/or any adverse reactions or deviations which may occur in the future.

The above Project Identification Number has been assigned to your project. Please use this number on all future correspondence.

Chair, Research Ethics Board
/cap

Research Ethics Board of Sunnybrook Health Sciences Centre Operates in Compliance with the Tri-Council Policy Statement, the ICH/GCP Guidelines and Division 5 of the Food and Drug Regulations.

Fully affiliated with the University of Toronto

Appendix F

Tracer Kinetic Modeling

The Johnson and Wilson model used in this study is a refinement to compartmental models which have previously been used to measure PS in the context of tumors^{1,2}. Because contrast agents are not metabolized in tissue and excluded from cell entry, the modeling of contrast agent distribution calls for only two compartments, the plasma and interstitial space, with bidirectional exchange via passive diffusion between the compartments. Groothuis et al. were the first to apply compartmental models in CT scanning to measure this parameter^{3,4}. Compartmental models can only measure PS and CBV, not CBF, because when PS is much smaller than CBF, contrast distribution in the brain is only determined by diffusion. The Patlak approach simplifies the compartmental model by assuming the absence of contrast agent backflux from the interstitial to the intravascular space^{4,5}. Under the Patlak assumption, the normalized tissue concentration is linearly related to the normalized integral of the artery input function with the slope and intercept of the linear regression equal to PS and CBV⁵. Notably, the Johnson and Wilson model used in this study does not require us to invoke the Patlak assumption, which is likely not valid for contrast agent behavior in the brain with a ‘leaky’ BBB. Unlike compartmental models, it also allows CBF to be estimated together with CBV and PS. Kinetics of contrast distribution in the brain using the Johnson and Wilson model applies to the entire brain independent of whether the blood-brain barrier is intact.

The model divides the brain into two principal spaces: the intravascular space (IVS) and the extra-vascular space (EVS), separated by a capillary endothelium of

variable permeability and therefore applies to both leaky and non-leaky blood-brain barrier. Three basic assumptions concerning contrast kinetics in the brain were made in the model⁶. First, the permeable capillary endothelium allows bidirectional diffusion of contrast between EVS and IVS. Second, there is an axial contrast concentration gradient in the capillaries but the radial concentration gradient is assumed to be negligible. Third, within the EVS, the tracer concentration is assumed to have a homogeneous spatial distribution. St Lawrence and Lee had derived the adiabatic approximation solution which simplifies the calculation of parametric maps with the Johnson and Wilson model⁷. The adiabatic approximation assumes that the EVS contrast concentration is changing slowly (i.e. in a quasi-steady state) relative to the rate of change of concentration in the IVS (capillaries). Under this approximation, the impulse residue function, $H(t)$, can be represented simply as:

$$H(t) = \begin{cases} 1 & 0 \leq t \leq T_c \\ Ee^{-\left(\frac{EF}{V_c}\right)(t-T_c)} & t > T_c \end{cases} \quad [1]$$

where T_c is the capillary mean transit time (MTT) and F is cerebral blood flow (CBF), so that cerebral blood volume (CBV) is $F \cdot T_c$ according to the Central Volume Principle⁸. E is the contrast extraction fraction and V_c is the EVS contrast distribution volume. E relates to the PS of brain capillaries (blood-brain barrier) via the following relationship:

$$E = 1 - e^{-\left(\frac{PS}{F}\right)} \quad [2]$$

If $Ca(t)$ is the arterial input function to the brain, then the measured brain tissue curve, $Q(t)$, can be calculated as the convolution of $Ca(t)$ and $H(t)$:

$$Q(t) = F \cdot [C_a(t) * H(t - T_o)] \quad [3]$$

where * is the convolution operator and T_o is the appearance time of brain contrast relative to that in the input artery. The validity of Equation 3 assumes that brain blood flow is constant and $Q(t)$ is linear with respect to $C_a(t)$. With $Q(t)$ and $C_a(t)$ measured in a CT Perfusion study, CT Perfusion 4 (GE Healthcare) estimates the parameters: CBF, CBV, MTT, PS and T_o by iteratively changing their values until an optimum fit to $Q(t)$ is achieved via Equations 1-3.

1. Yeung WT, Lee TY, Del Maestro RF, Kozak R, Brown T. In vivo CT measurement of blood-brain transfer constant of iopamidol in human brain tumors. *J Neurooncol* 1992;14:177-187.
2. Yeung WT, Lee TY, Del Maestro RF, Kozak R, Bennett J, Brown T. Effect of steroids on iopamidol blood-brain transfer constant and plasma volume in brain tumors measured with x-ray computed tomography. *J Neurooncol* 1994;18:53-60.
3. Groothuis DR, Vriesendorp FJ, Kupfer B, et al. Quantitative measurements of capillary transport in human brain tumors by computed tomography. *Ann Neurol* 1991;30:581-588.
4. Groothuis DR, Lapin GD, Vriesendorp FJ, Mikhael MA, Patlak CS. A method to quantitatively measure transcapillary transport of iodinated compounds in canine brain tumors with computed tomography. *J Cereb Blood Flow Metab* 1991;11:939-948.
5. Patlak CS, Blasberg RG. Graphical evaluation of blood-to-brain transfer constants from multiple-time uptake data: generalizations. *J Cereb Blood Flow Metab* 1985;5:584-590.
6. Lee TY, Purdie TG, Stewart E. CT imaging of angiogenesis. *Q J Nucl Med* 2003;47:171-187.
7. St Lawrence KS, Lee TY. An adiabatic approximation to the tissue homogeneity model for water exchange in the brain. I. Theoretical derivation. *J Cereb Blood Flow Metab* 1998;18:1365-1377.
8. Meier P, Zieler K. On the theory of the indicator dilution method for measurement of blood flow and volume. *J Appl Physiol* 1954;6:731-744.

Appendix G – Human Ethics Approval Form

20-Jul-2010

To:**From:****Re: NOTICE OF ANNUAL RENEWAL****Study File No: 278-2007****The CT Angiography "Spot Sign" in Primary Intracerebral Hemorrhage**

Please be advised that the above referenced study is due for annual renewal on or before the following date: 24-Aug-2010

Original Approval: 24-Aug-2007**Last Renewal: 24-Aug-2009**

You may obtain a copy of the latest annual renewal form from the Sunnybrook intranet/internet site.

To prevent suspension of approval please complete the renewal form as soon as possible and return the hardcopy with original signatures to:

Thank you in advance for your attention to this

You must submit a close out letter for this study if it is completed/terminated.

Appendix H – Animal Ethics Approval Form

2010-259::2:

AUP Number: 2010-259

AUP Title: Correlation of CT Perfusion Defects and Histopathological Staining in a Survival Ischemia Model of Stroke in Rabbits

Yearly Renewal Date: 02/01/2013

The YEARLY RENEWAL to Animal Use Protocol (AUP) 2010-259 has been approved, and will be approved for one year following the above review date.

1. This AUP number must be indicated when ordering animals for this project.
2. Animals for other projects may not be ordered under this AUP number.
3. Purchases of animals other than through this system must be cleared through the ACVS office.
Health certificates will be required.

REQUIREMENTS/COMMENTS

Please ensure that individual(s) performing procedures on live animals, as described in this protocol, are familiar with the contents of this document.

The holder of this Animal Use Protocol is responsible to ensure that all associated safety components (biosafety, radiation safety, general laboratory safety) comply with institutional safety standards and have received all necessary approvals. Please consult directly with your institutional safety officers.

Appendix I – Copyright Agreements

“The evolution of the cerebral blood volume abnormality in patients with ischemic stroke: a CT perfusion study”, published in *Acta Radiologica* 53(4):461-7, May 2012, by: C.D. d’Esterre, R.I. Aviv, T.Y. Lee.

Dear

Thank you for your email.

Please consider this email as written permission to include the reuse of content from 'The evolution of the cerebral blood volume abnormality in patients with ischemic stroke: a CT perfusion study' from our publication in *Acta Radiologica* for your PhD thesis.

This permission does not cover any 3rd party material found in the work.

Please include a full reference to the original material and inform the author(s) of this reuse.

Best wishes,

“Hemorrhagic transformation of ischemic stroke: prediction with CT perfusion”
 published in *Radiology* 250(3):867-77, in March 2009, by: R.I Aviv, C.D. d’Esterre, B.D.
 Murphy, J.J. Hopyan B. Buck, G. Mallia, V. Li, L. Zhang, S.P. Symons, T.Y. Lee.

March 19, 2013

The Radiological Society of North America (RSNA®) is pleased to grant you permission to reproduce the following article in electronic format for educational use in your dissertation/thesis, provided you give full credit to the authors of the original publication.

. Hemorrhagic transformation of ischemic stroke: prediction
 with CT perfusion. *Radiology* 2009;250:867-877.

This permission is a one-time, non-exclusive grant for English-language use and is exclusively limited to the usage stated and underlined above. The requestor guarantees to reproduce the material as originally published. Permission is granted under the condition that a full credit line is prominently placed (i.e. author name(s), journal name, copyright year, volume #, inclusive pages and copyright holder).

This permission becomes effective upon receipt of this signed contract. Please sign a copy of this agreement, return a signed copy to me and retain a copy for your files. Thank you for your interest in our publication.

[Print Name]:

SIGNATURE: _____

 Date: March 19, 2013

“Early rate of contrast extravasation in patients with intracerebral hemorrhage” published in the *American Journal of Neuroradiology*, 32(10):1879-84, November 2011 by: C.D. d'Esterre, T. Chia, A. Jairath, T.Y. Lee, S.P. Symons, R.I. Aviv.

Could I get permission to use the entire text/figures from “Early rate of contrast extravasation in patients with intracerebral hemorrhage” published in the *American Journal of Neuroradiology*, 32(10):1879-84, November 2011

I am using it for my thesis dissertation.

Thanks so much,

Permission granted by the copyright owner, contingent upon the consent of the author(s). provided complete credit is given to the original source and © owner. Credit line: (initials, last name of author(s), (title of article), (name of journal), (volume #), (issue #), (inclusive pages), (year of publication, © by American Society of Neuroradiology . . . / . . . / . . . / . . . /

“Dipyridamole treatment prior to stroke onset: examining post-stroke cerebral circulation and outcome in rabbits”, published in *Translational Stroke Research*, 2: 186-194, January 2011, by: C.D. d’Esterre, K.M. Tichauer, R.I. Aviv, L. Morrison, W. Eisert, T.Y.. Lee.

**SPRINGER LICENSE
TERMS AND CONDITIONS**

Mar 18, 2013

This is a License Agreement between _____ (“You”) and Springer (“Springer”) provided by Copyright Clearance Center (“CCC”). The license consists of your order details, the terms and conditions provided by Springer, and the payment terms and conditions.

All payments must be made in full to CCC. For payment instructions, please see information listed at the bottom of this form.

License Number	3112081108287
License date	Mar 18, 2013
Licensed content publisher	Springer
Licensed content publication	Translational Stroke Research
Licensed content title	Dipyridamole Treatment Prior to Stroke Onset: Examining Post-stroke Cerebral Circulation and Outcome in Rabbits
Licensed content author	_____
Licensed content date	Jan 1, 2011
Volume number	2
Issue number	2
Type of Use	Thesis/Dissertation
Portion	Full text
Number of copies	1
Author of this Springer article	Yes and you are a contributor of the new work

CURRICULUM VITAE

CHRISTOPHER D. D'ESTERRE

EDUCATION / WORK EXPERIENCE

Graduate Student	09/2006 -	Robarts Research Institute, London Ontario. Faculty of Medicine, Medical Biophysics
Work/Study Student	12/2007 – 12/2008	University of Western Ontario, London Ontario. Supervisor: Dr. Aaron Fenster Data management
Summer Student Placement	05/2006 - 09/2006	Robarts Research Institute, London Ontario. Supervisor: Dr. Ting Yim Lee Data analyst: Acute Stroke Diagnosis with functional imaging
Work/study placement	05/2005 - 09/2005	University of Western Ontario, London Ontario Supervisor: Dr. Kelly Zarnke Data management for Diabetes patients

ACADEMIC SCHOLARSHIPS AND AWARDS

03/2012	Canadian Stroke Network/European Stroke Network Collaborative Grant, \$96,000
05/2010	Junior Investigator Award, European Stroke Conference, Barcelona Spain, \$300
05/2010	Young Investigator Award, Canadian Institutes of Health Research, \$1000
05/2009	Young Investigator Award, Canadian Institutes of Health Research, \$1500
11/2007	Ontario Student Opportunity Trust Fund, University of Western Ontario, \$1000
09/2006 - ongoing	Western Graduate Research Scholarship, University of Western Ontario \$6000 p.a.

09/2006 - 05/2008	CIHR Strategic Training Program in Vascular Research Fellowship , University of Western Ontario, \$10,000 p.a.
09/2002	Academic Entrance Scholarship , University of Western Ontario, \$1000 p.a.
05/2006	Varsity Athletics 'Bronze W' , University of Western Ontario Track & Field and Cross Country
09/2002 - 05/2006	Academic All-Canadian , University of Western Ontario, National Varsity Sport Performer with Academic Honour role (>80% average)
10/02	Ontario University Athletics Bronze Medal , University Cross Country Championships, Guelph Ontario.

PUBLICATIONS AND PRESENTATIONS

MANUSCRIPTS PUBLISHED

1. **d'Esterre CD.**, Fainardi E., Aviv R., Lee TY., *Improving acute stroke management with computed tomography perfusion: a review of imaging basics and applications*. Translational Stroke Research. 2012 3: Number 2: 205-220.
2. **d'Esterre CD.**, Aviv R., Lee TY., *The evolution of the cerebral blood volume abnormality in patients with ischemic stroke: a CT perfusion study*. Acta Radiologica 2012 May 1;53(4):461-7.
3. **d'Esterre CD.**, Lee TY., Aviv R., *Early rate of contrast extravasation in patients with intra-cerebral hemorrhage*. AJNR, 2011, Nov;32(10):1879-84.
4. **d'Esterre CD.**, Tichauer KM., Aviv R., Bertha G., Eisert W., Lee TY. (2010) *Dipyridamole treatment prior to stroke onset: examining post-stroke cerebral circulation and outcome in rabbits*. Trans Stroke Research. 2011 2:186-194
5. **d'Esterre CD.**, Lee TY. (2010) *Effect of Dipyridamole during acute stroke: exploring antithrombosis and neuroprotective benefits*. Annals of the New York Academy of Sciences: Volume 1207, 2010.
6. Aviv R., **d'Esterre CD.**, et al. (2009) *Hemorrhagic transformation of ischemic stroke: prediction with CT perfusion*. Radiology 2009, Mar;250(3):867-77.

MANUSCRIPTS SUBMITTED

1. Eilaghi, A., **d'Esterre CD.**, Lee TY., Jakubovic R., Zhang L., Swartz RH., Aviv R., (2012) *Towards patient-tailored perfusion thresholds for prediction of stroke outcome. Submitted to AJNR.*
2. Fainardi, E. **d'Esterre CD.**, Lee TY. (2012) *Temporal changes in CT perfusion values before and after cranioplasty in patients without symptoms related to external decompression. A pilot study Submitted to Journal of Neurotrauma.*
3. **d'Esterre CD.**, Fainardi E., Lee TY., (2012) *Reliability of the CTP-CBV parameter for acute infarct delineation. Submitted to Neuroradiology*
4. **d'Esterre CD.** Anazodo U., St. Lawrence K., Morrison L., Lee TY., Fainardi E., (2012) *Multi-modality neuroimaging in a porcine model of endothelin-1 induced cerebral ischemia: defining the acute infarct core. Submitted to Radiology*

MANUSCRIPTS IN PROGRESS

1. **d'Esterre CD.**, Fainardi E., Lee TY., (2012) *Optimal CT perfusion parameter for acute infarct delineation*
2. Yang J., **d'Esterre CD.**, Amtul Z., Cechetto D., Lee TY (2012) *Rat model of combined β -amyloid pathology and cerebral ischemia: a CT perfusion study*
3. **d'Esterre CD.**, Morrison L., Lee TY., (2012) *Development and implementation of a novel longitudinal embolic stroke model: the effects of dipyridamole and clopidogrel monotherapies on ischemic stroke severity.*

INVITED CHAPTERS

1. So A., Stewart E., **d'Esterre CD.**, Yeung T., Bauman G., Jensen N., Wong E., Lee TY., (2012) *CT Perfusion: Principles, Implementations and Clinical Applications*

ORAL PRESENTATIONS

1. **d'Esterre CD.**, Lee TY., (10/2012; presenter) *Assessment of acute stroke with CT perfusion: caveats, thresholds and multi-modal comparisons. Invited Speaker, Calgary, AB, Canada.*
2. Eilaghi A., Jakubovic R., **d'Esterre CD.**, Swartz R., Lee., TY., Aviv R., (04/2012; non-presenter) *Gray and white matter CT perfusion thresholding for tissue fate prediction in 114 patients with acute ischemic stroke. ASNR, New York, NY, USA.*
3. **d'Esterre CD.**, Lee TY., Aviv R., (05/2011; presenter) *Rate of contrast extravasation in patients with ICH. 2nd Canadian Stroke Congress, Ottawa, Ontario, Canada.*
4. **d'Esterre CD.**, Lee TY., Chia TL., Symons SP., Aviv RI. (05/2011; non-presenter) *Early Rate of Contrast Extravasation in Intracerebral Hemorrhage: A CT Perfusion Study. American Society of Neuroradiology 49th Annual Meeting. Seattle, Washington, USA.*

5. **d'Esterre CD.**, Lee TY (10/2010); presenter) *Cerebral blood volume reversibility in regions of infarction: an acute ischemic stroke study*. Medical Biophysics Seminar Series. University of Western Ontario, London Ontario, Canada.
6. **d'Esterre CD.**, Tichauer KM., Aviv R., Bertha G., Eisert W., Lee TY. (05/2010; presenter) *Effect of dipyridamole on cerebral circulation and stroke outcome in a rabbit model of middle cerebral artery embolic occlusion*. European Stroke Conference. Barcelona, Spain.
7. **d'Esterre CD.**, Hadway J., Lee TY. (05/2010; presenter) *Examining cerebral hemodynamics, inflammation and outcome in a rabbit model of middle cerebral artery embolic occlusion: A pilot study*. Innate Inflammation as the Common Pathway of Risk Factors Leading to Transient Ischemic Attacks and Stroke: Pathophysiology and Potential Interventions. New Academy of Sciences, New York NY. USA.
8. **d'Esterre CD.**, Aviv R., Symons S., Black S., Lee TY., (02/2010; presenter) *Hemorrhagic transformation of ischemic stroke: A CT perfusion study*. Imaging Network of Ontario. Toronto, Ontario, Canada.
9. **d'Esterre CD.**, Lee TY (12/2009); presenter) *CT perfusion applications in stroke*. Medical Biophysics Seminar Series. University of Western Ontario, London Ontario, Canada.
10. **d'Esterre CD.**, Aviv R., Hogan M., Lee D., Symons S., Black S., Fox A., Lee TY., (11/2009; Multisession course presenter) *Examining cerebral blood volume reversibility within tissue that progresses to infarction in patients with ischemic stroke: A CT perfusion study*. Radiological Society of North America. Chicago, Ill. USA.
11. Lee TY. **d'Esterre CD.**, (07/2009; non-presenter). *CT perfusion methodologies in acute stroke*. Stroke Collaborator Symposium. Sunnybrook Hospital, Toronto Ontario, Canada.
12. **d'Esterre CD.**, Lee TY., (11/2008; presenter). *Effect of pre-morbid intravenous administration of the anti-platelet drug dipyridamole in a rabbit stroke model*. Medical Biophysics Seminars. University of Western Ontario, London Ontario, Canada.
13. **d'Esterre CD.**, Lee TY., (03/2008; presenter). *Increasing cerebrovascular integrity in a rabbit stroke model*. Western Research Forum. University of Western Ontario. London Ontario, Canada.
14. **d'Esterre CD.**, Lee TY., (12/2007; presenter). *CT perfusion applications in acute stroke: salvaging the ischemic penumbra*. Lawson Health Research Institute Invited Speaker. St. Joseph's Hospital, London Ontario, Canada.
15. **d'Esterre CD.**, Lee TY., (11/2007; presenter) *CT-Perfusion derived blood brain barrier permeability surface product: a diagnostic marker for intracerebral hemorrhage in acute stroke*. The Radiological Society of North America. Chicago, Illinois, USA.
16. **d'Esterre CD.**, D Ouimet, TY Lee (03/2007; presenter). *The effect of dipyridamole on the cerebral hemodynamics in a rabbit model of ischemic stroke*. Medical Biophysics Seminar Series, University of Western Ontario, London Ontario, Canada

POSTER PRESENTATIONS

1. **d'Esterre CD.**, Fainardi E., Lee TY (11/2011; presenter) *Pitfalls when using CT perfusion-derived cerebral blood volume to help guide thrombolysis treatment.* Thrombolysis and Acute Stroke Treatment in 2011: Preparing for the Next Decade, New York Academy of Sciences, New York City, USA.
2. **d'Esterre CD.**, Fainardi E., Saletti A., Ceruti S., Lee TY., (05/2011; presenter) *Changes in CT perfusion-derived cerebral blood volume out to 3 months within tissue that progresses to infarction in ischemic stroke.* Brain Conference, Barcelona Spain.
3. **d'Esterre CD.**, Lee TY., Aviv R., (02/2011; presenter) *Early rate of contrast extravasation in intra-cerebral hemorrhage patients.* International Stroke Conference, Los Angeles, California, USA.
4. **d'Esterre CD.**, R., Hogan M., Lee TY., (02/2011; presenter) *Examining cerebral blood volume reversibility within tissue that progresses to infarction in patients with ischemic stroke.* International Stroke Conference, Los Angeles, California, USA
5. **d'Esterre CD.**, Aviv R., Hogan M., Lee TY., (05/2010; presenter) *Examining cerebral blood volume reversibility within tissue that progresses to infarction in patients with ischemic stroke: A CT perfusion study.* Canadian Institutes of Health Research Young Investigators Forum. Vancouver, BC, Canada.
6. **d'Esterre CD.**, Hadway J., Desjardins L., Lee TY., (03/2010; presenter) *Effect of dipyridamole on cerebral circulation and stroke outcome in a rabbit model of middle cerebral artery embolic occlusion.* Lawson Health Research Day. London Ontario, Canada.
7. **d'Esterre CD.**, Hadway J., Desjardins L., Lee TY., (06/2009; presenter) *Effect of dipyridamole on cerebral hemodynamics, inflammation and stroke outcome in a rabbit model of cerebro- embolic occlusion.* 24th International Symposium on Cerebral Blood Flow, Metabolism and Function. Chicago, Ill. USA.
8. **d'Esterre CD.**, Hadway J., Desjardins L., Lee TY., (06/2009; presenter) *The effect of pre-morbid administration of dipyridamole on stroke severity in a rabbit ischemic stroke model.* London Imaging Discovery, London Ontario, Canada.
9. **d'Esterre CD.**, Aviv R., Symons S., Black S., Lee TY., (05/2009; presenter) *Hemorrhagic transformation of ischemic stroke: A CT perfusion study.* Canadian Institutes of Health Research Young Investigators Forum, Ottawa Ontario, Canada.
10. **d'Esterre CD.**, Lee TY., (03/2009; presenter) *CT-Perfusion derived blood brain barrier permeability surface product: a diagnostic marker for intracerebral hemorrhage in acute stroke.* **Lawson research day, London, Ontario, Canada.**
11. **d'Esterre CD.**, Hadway J., Desjardins L., Lee TY., (08/2008; presenter) *The effect of pre-morbid administration of dipyridamole on stroke severity in a rabbit ischemic stroke model.* Imaging Network of Ontario. Toronto Ontario, Canada.
12. Aviv R., **d'Esterre CD.**, Symons S., Black S., Lee TY., (02/2008; co-presenter) *Hemorrhagic transformation of ischemic stroke: A CT perfusion study.* International Stroke Conference, New Orleans, Louisiana, USA.